

NORTHWESTERN UNIVERSITY

The Role of FLICE-Inhibitory Proteins in Primary Effusion Lymphoma

A DISSERTATION

SUBMITTED TO THE GRADUATE SCHOOL
IN PARTIAL FULFILLMENT OF THE REQUIREMENTS

for the degree

DOCTOR OF PHILOSOPHY

Driskill Graduate Training Program in Life Sciences

By

Neil Kuehnle

EVANSTON, ILLINOIS

September 2023

© Copyright by Neil Kuehnle, 2023

All Rights Reserved

Abstract

Kaposi' sarcoma-associated herpesvirus (KSHV) causes primary effusion lymphoma (PEL). PEL cell lines require expression of the cellular FLICE inhibitory protein (cFLIP) for survival, although KSHV encodes a viral homolog of this protein (vFLIP). Cellular and viral FLIP proteins have several functions, including, most importantly, the inhibition of pro-apoptotic caspase 8 (CASP8) and modulation of nuclear factor kappa B (NF- κ B) signaling.

Here I show that knockout (KO) of cFLIP is lethal in PEL cells, while vFLIP expression varies significantly across different PEL cell lines and that vFLIP knockdown (KD) is largely only lethal in the small subset of PEL cell lines where vFLIP levels are detectable. To investigate the essential role of cFLIP and its potential redundancy with vFLIP in PEL cells, I first performed rescue experiments with human or viral FLIP proteins known to affect FLIP target pathways differently. The long and short isoforms of cFLIP and molluscum contagiosum virus (MCV) MC159L, which are all strong CASP8 inhibitors, efficiently rescued the loss of endogenous cFLIP activity in PEL cells. KSHV vFLIP was unable to fully rescue the loss of endogenous cFLIP and is therefore functionally distinct.

Next, I employed genome-wide CRISPR/Cas9 synthetic rescue screens to identify loss of function perturbations that can compensate for cFLIP KO. Results from these screens and my validation experiments implicate the canonical cFLIP target CASP8 and TRAIL receptor 1 (TRAIL-R1 or TNFRSF10A) in promoting constitutive death signaling in PEL cells. However, this process was independent of TRAIL receptor 2 or TRAIL, the latter of which is not detectable in PEL cell cultures. The requirement for cFLIP is also overcome by inactivation of the ER/Golgi resident chondroitin sulfate proteoglycan synthesis and UFMylation pathways,

Jagunal homolog 1 (JAGN1) or CXCR4. UFMylation and JAGN1, but not chondroitin sulfate proteoglycan synthesis or chemokine receptor 4 (CXCR4), contribute to TRAIL-R1 expression.

In sum, my work shows that cFLIP is required in PEL cells to inhibit ligand-independent TRAIL-R1 cell death signaling downstream of a complex set of ER/Golgi-associated processes that have not previously been implicated in cFLIP or TRAIL-R1 function.

Acknowledgment

During the time in which I completed my PhD I was fortunate enough to meet many exceptional individuals. Without the help that their mentorship and/or friendship provided, I would never have been able to grow as a scientist in the manner which I have.

First and foremost, I must thank my advisor, Dr. Eva Gottwein for taking me in as a wayward student transferring labs so many years ago. It goes without saying to any who know her that Eva is a fiercely keen scientist with an eye for detail. By encouraging those around her to take every opportunity for growth and improvement, my written and oral presentation skills have grown substantially. Moreover, under her patient tutelage I was able to grow and develop a wholly new core technical skillset on which I plan to base my future endeavors. It is uncertain that I would have had the confidence to make such a considerable transition without the confidence that her tenacity for trying new and unfamiliar techniques inspired in me.

I cannot thank Eva without also offering specific thanks to the many members of the Gottwein lab who have helped me. Chief among these are Dr. Mark Manzano, Scout Osbourne, and Ziyan Liang who appear as co-authors on my primary research article. Mark's early work on cFLIP was pivotal for finding a footing in my own work, while Scout and Ziyan worked hard alongside me during my paper's revisions to ensure its acceptance and produce the best final manuscript possible. It also goes without saying that Mark, in his role as the senior post-doctoral researcher in the lab through most of my studies, served as a sort of secondary intellectual mentor on top of Eva – always offering valuable insight during lab meetings. Similarly, in his final months in the lab, Scout proved a keen and passionate debate and discussion partner regarding many topics relevant to the projects on which I collaborated.

Several other previous members are highly of note for their companionship and advice throughout the years. First and foremost, Dr. Kylee Morrison, who has been a constant and continued friend and mentor, offering some of the best feedback during some of the most difficult periods of my studies. I must offer substantial thanks in no order to: Haocong “Katherine” Ma, Ajinkya Patil, Jesus Ortega, Shreya Jambardi, Aakaanksha Maddineni, and Jingyi “Anna” Lu. Each of you has been a pillar to lean on for support at various times.

To the many excellent friends I’ve made within the Driskill Graduate, I am more grateful than I can possibly express. Though you are simply too numerous to name directly, my gratitude can be known in the countless hours spent together and memories developed over lunches, birthdays, happy hours, and more.

To the members of my thesis committee, Drs. Richard Longnecker, Derek Walsh, and Daniel Foltz, thank you for your feedback throughout the years throughout the many iterations of this work.

Lastly, to my closest friends, family, and my partner of 13 years—Austin Quinn, I thank you all for your great patience with me, for being the never-ending font of humor I need to make it through each day, occasionally inspiring me to be a better person, and reminding me what it means to live life.

List of Commonly Used Abbreviations

This list includes abbreviations which appear two or more times. Abbreviations are generally defined at first use. Some abbreviations are used and provided only once for convenience/familiarity since they are often more commonly understood than the expanded term. The author apologizes if any abbreviations/acronyms have been left undefined (i.e. for gene names where they serve primarily as references and are not frequently understood as terms beyond their abbreviated form)

Abbreviation	Meaning
7-AAD	7-Amino-Actinomycin D
AAVS1	adeno-associated virus integration site 1
AIDS	Acquired Immunodeficiency Syndrome
bp	base-pair(s)
CASP8	caspase-8
CDK	cyclin dependent kinase
cDNA	complementary DNA
CFLAR	CASP8 and FADD-like apoptosis regulator (gene name for cellular FLIP)
cFLIP	cellular FLIP
cGas	cyclic GMP-AMP (guanosine/adenosine monophosphate) synthase
CRISPR	clustered regularly interspaced short palindromic repeats
CXCR4	Chemokine receptor 4
DNA	deoxyribonucleic acid
EBV	Epstein-Barr virus

EPOCH	etoposide, prednisone, oncovin (vincristine sulfate), cyclophosphamide, and hydroxydaunorubicin (doxorubicin) treatment
ER	endoplasmic reticulum
FACS	fluorescence activated cell sorting
FADD	Fas-associated death domain protein
Fas	FS-7-associated surface antigen
FDR	false-discovery rate
FLIP	FADD (see FADD)-like interleukin-1-β-converting enzyme [FLICE/caspase 8]-inhibitory protein
gB/gH/gL/gM/gM	glycoprotein B/H/L/M/N
HAART	highly-active anti-retroviral therapy
HCMV	human cytomegalovirus
HHV	human herpesvirus
HIV	human immunodeficiency virus
HSV	herpes simplex virus
ICTV	international committee on taxonomy of viruses
IE	immediate-early
hIL-6	human interleukin 6
IL-10	(human) interleukin 6
IMiD	immunomodulatory drug
IRES	internal ribosome entry site
IRF	interferon regulatory factor 4
vIRF	viral IRF 3
JAGN1	Jagunal homolog 1

kb	kilobase-pairs
KD	Knockdown
KICS	KSHV-induced cytokine syndrome
KO	Knockout
KS	Kaposi's Sarcoma
KSHV	Kaposi's sarcoma-associated herpesvirus
LANA	latency-associated nuclear antigen
LCL	lymphoblastoid cell lines
LEC	lymphatic endothelial cells
MCD	multicentric Castleman's disease
MCP	major capsid protein
MCV	molluscum contagiosum virus
miRNA	microRNA
miR	microRNA (as a prefix)
MOI	multiplicity of infection
mRNA	messenger RNA
NF-κB	nuclear factor kappa B
NLR	nucleotide-binding domain, leucine-rich repeat containing
nts	nucleotides
ORF	open reading-frame
PCR	polymerase chain reaction
PEL	primary effusion lymphoma
PSMD1	proteasome 26S subunit, non-ATPase 1
PSOD	PEL-specific oncogenic dependency

Rb	retinoblastoma
R-EPOCH	EPOCH with rituximab
RNA	ribonucleic acid
RTA	replication and transcription activator
TPA	terephthalic acid
TRAIL	TNF-related apoptosis inducing ligand
TRAIL-R1	TRAIL receptor 1
TRAIL-R2	TRAIL receptor 2
UFM	ubiquitin-fold modifier 1
UPR	unfolded protein response
vCyc	KSHV viral cyclin
vFLIP	viral FLIP
vIL-6	viral interleukin-6
vIRF-3	viral IRF 3
VZV	Varicella zoster virus
WT	wild-type

Table of Contents

Abstract.....	3
Acknowledgements.....	5
List of Commonly Used Abbreviations	7
Table of Contents.....	11
List of Tables.....	14
List of Figures.....	15
1. Chapter 1: Introduction.....	18
1.1. History and discovery of KSHV.....	18
1.2. Overview of KSHV.....	18
1.2.1. Classification and Related Viruses.....	18
1.2.2. Structural Overview.....	20
1.3. KSHV Epidemiology & Associated Malignancies.....	23
1.3.1. Kaposi's Sarcoma.....	23
1.3.2. Primary Effusion Lymphoma.....	25
1.3.3. Multicentric Castleman's Disease & KSHV-Induced Cytokine Syndrome.....	27
1.4. KSHV infectious cycle.....	28
1.4.1. Entry and early infection.....	28
1.4.2. Lytic replication.....	31
1.4.3. Latent replication.....	33
1.5. The role of KSHV in disease.....	34

1.6. Host genetic dependencies in PEL.....	37
1.7. FLICE-Inhibitory Proteins (FLIPs)	42
1.7.1. Structure and evolution of FLIPs.....	42
1.7.2. Canonical function: Extrinsic apoptosis.....	45
1.7.3. Non-canonical functions.....	46
1.8. Summary and overview of experimental aims.....	47
2. Chapter 2: Materials and Methods.....	50
2.1. Materials and Methods for Chapter 1.....	50
2.1.1. Phylogenetic analysis.....	50
2.2. Materials and Methods for Chapter 3.....	52
2.2.1. Cloning.....	52
2.2.2. Detailed pLentiGuide SpBsmBI cloning protocol.....	60
2.2.3. Western blotting.....	62
2.2.4. Cell culture.....	64
2.2.5. Cumulative cellular growth curves.....	64
2.2.6. Lentiviral production, infection, and titration.....	66
2.2.7. Concentration of lentiviral vectors.....	67
2.2.8. CRISPR-based single-gene KO.....	67
2.2.9. CRISPR-based synthetic rescue screens with sgRNA challenge.....	68
2.2.10. Synthetic rescue screens with shRNA-based challenge.....	68
2.2.11. CRISPR library preparation and next-generation sequencing	69
2.2.12. CRISPR screen analysis.....	70
2.2.13. Indel sequencing of CRISPR KO pools.....	71

2.2.14. mRNA sequencing.....	73
2.2.15. RNA purification and reverse transcription.....	74
2.2.16. TRAIL-R1 TaqMan assay.....	74
2.2.17. Inducible KO and AMD3100 treatment.....	75
2.2.18. Cellular staining and flow cytometry.....	75
2.2.19. Generation of BCBL-1 cell lines expressing MPZ-Del63-mCherry constructs...	76
2.2.20. Immunofluorescence and colocalization analysis.....	76
2.2.21. Anti-TRAIL ELISA.....	77
2.2.22. <i>In vitro</i> TRAIL Treatment.....	78
2.2.23. Statistical analysis.....	78
3. Chapter 3: Results.....	80
3.1. Viral protein expression is highly variable in PEL cells.....	80
3.2. cFLIP is broadly essential in PEL cell lines.....	84
3.3. Several PEL cell lines may not depend on vFLIP/vCyc.....	86
3.4. cFLIP and vFLIP have distinct roles in PEL cell lines.....	90
3.5. Partial rescue of cFLIP by vFLIP may be mediated by NF- κ B signaling.....	93
3.6. Genome-wide rescue screens uncover an ER/Golgi/CASP8-dependent death signaling program repressed by cFLIP.....	96
3.7. cFLIP protects PEL cells from ligand-independent TRAIL-R1-induced cell death.....	110
3.8. UFMylation and JAGN1 promote TRAIL-R1 expression in PEL cells.....	119
4. Chapter 4: Discussion.....	129
Appendices.....	139
Vita.....	148

References.....	153
-----------------	-----

List of Tables, Illustrations, Figures, and Graphs

List of Tables

Chapter 1: Introduction

Table 1.1 Revised PEL-specific oncogenic dependencies.....	40
---	----

Table 1.2 Sequence similarity of human and human-tropic viral FLIPs.....	43
---	----

Chapter 2: Materials and Methods

Table 2.1 List of viral and host FLIP protein sequences used for phylogenetic analysis.....	52
--	----

Table 2.2 PCR primers used for cloning of lentiviral constructs.....	56
---	----

Table 2.3 Gene fragments used for cloning of lentiviral constructs.....	58
--	----

Table 2.4 Oligonucleotides used for cloning of sgRNA constructs.....	61
---	----

Table 2.5 Antibody sources and conditions.....	63
---	----

Table 2.6 Indexing primers used for NextSeq.....	71
---	----

Table 2.7 Primers used for amplicon-based INDEL sequencing.....	73
--	----

Chapter 3: Results

Table 3.1 cFLIP rescue screen hits.....	100
--	-----

Table 3.2 Output of DAVID pathway analysis.....	105
--	-----

Table 3.3 Characterization of CRISPR target loci by amplicon sequencing.....	120
---	-----

Appendix

Results and descriptions of statistical tests.....	136
--	-----

Electronic Data

Electronic Supplement 1 Full cFLIP rescue screen output

Electronic Supplement 2 Variant-level CRISPR editing results

List of Figures

Chapter 1: Introduction

Figure 1.1 KSHV virion structure.....	19
Figure 1.2 Simplified phylogenetic tree of human herpesviruses.....	22
Figure 1.3 Schematic of KSHV major latency locus.....	34
Figure 1.4 Phylogenetic relationship between host and viral FLIPs.....	45
Figure 1.5 Structural comparison of human and human-tropic viral FLIPs.....	46

Chapter 2: Materials and Methods

Figure 2.1 Diagram of cFLIP resistance screens.....	70
--	----

Chapter 3: Results

Figure 3.1 Expression of viral proteins and their cellular homologs compared to cellular gene dependencies in 8 PEL cell lines.....	81
Figure 3.2 Quantitative titration of vFLIP/vCyc western blot.....	82
Figure 3.3 Expanded, unpublished version of Fig 3.1.....	83
Figure 3.4 Validation of cFLIP dependence in 5 PEL cell lines.....	85
Figure 3.5 Rescue of cFLIP KO by cFLIP re-expression.....	86
Figure 3.6 shRNA KD of vFLIP/vCyc in BC-3.....	88
Figure 3.7 Validation of vFLIP/vCyc shRNA toxicity in 5 PEL cell lines.....	89
Figure 3.8 Validation of vFLIP/vCyc shRNA in alternative BCBL-1 sources.....	90
Figure 3.9 Rescue of cFLIP KO with different viral FLIPs in BCBL-1.....	92

Figure 3.10 Comparison of ectopic FLIP expression levels in BCBL-1.....	93
Figure 3.11 Testing whether a putative IKK-interaction deficient vFLIP rescues cFLIP KO in BCBL-1 cells.....	95
Figure 3.12 Quantification of mRNA levels for selected death signaling genes.....	97
Figure 3.13 Cumulative growth curves of BCBL-1 cFLIP depletion resistance screens.....	98
Figure 3.14 Distribution of statistical outputs of MAGeCK-RRA for cFLIP depletion resistance screen results.....	99
Figure 3.15 Overview of common cFLIP depletion resistance screen results in BCBL-1.....	101
Figure 3.16 DAVID pathway analysis of shared cFLIP depletion resistance screen results in BCBL-1.....	103
Figure 3.17 Schematic of canonical activation of extrinsic apoptosis by TRAIL through TRAIL receptors.....	106
Figure 3.18 Schematic of UFMylation and SRP/SEC61-mediated protein co-translation at the ER.....	107
Figure 3.19 Schematic of the chondroitin sulfate proteoglycan synthesis pathway.....	108
Figure 3.20 Western validation of CASP8/cFLIP double KO in BCBL-1.....	109
Figure 3.21 Validation of resistance to cFLIP KO following CASP8 KO in BCBL-1 cells.....	110
Figure 3.22 Western validation of TRAIL-related double KOs.....	111
Figure 3.23 Validation of resistance to cFLIP KO following KO of canonical TRAIL signaling genes in BCBL-1 cells.....	112
Figure 3.24 Quantification of TRAIL expression and TRAIL insensitivity of PEL cells.....	113
Figure 3.25 Quantification of membrane vs intracellular TRAIL-R1 signal by flow cytometry in BCBL-1 cells.....	114
Figure 3.26 Quantification of TRAIL-R1 co-localization with subcellular markers and/or MPZ mutant proteins by confocal IF.....	116
Figure 3.27 Representative images of TRAIL-R1 co-staining with subcellular markers by confocal IF.....	117
Figure 3.28 Representative images of TRAIL-R1 co-staining with mCherry-tagged MPZ mutant proteins by confocal IF.....	118

Figure 3.29 Validation of disruption of UFMylation following single gene KO.....	121
Figure 3.30 Validation of resistance to cFLIP KO following KO of select ER/Golgi-associated screen hits in BCBL-1 cells.....	122
Figure 3.31 Validation of cFLIP KO in double KO experiments from Fig 3.30.....	123
Figure 3.32 Testing expression of key extrinsic apoptosis pathway components (TRAIL-R1, CASP8) following KO of select ER/Golgi associated screen hits.....	124
Figure 3.33 Quantifying surface and intracellular TRAIL-R1 signal by flow cytometry following KO of select ER/Golgi associated screen hits.....	125
Figure 3.34 RT-qPCR quantification of TRAIL-R1 mRNA levels following KO of select ER/Golgi associated screen hits.....	126
Figure 3.35 mRNA expression level of all screen related hits.....	127
Figure 3.36 Testing resistance to cFLIP KO following pharmacological inhibition of CXCR4.....	128

Chapter 4: Discussion

Figure 4.1 Working model of the role of FLIPs in PEL cells.....	130
Figure 4.2 Work model of TRAIL-related processes in the ER of PEL cells.....	138

Chapter 1: Introduction

1.1 History and Discovery of KSHV

In 1872, Moritz Kaposi first described Kaposi's Sarcoma as a rare tumor occurring primarily in elderly men of Mediterranean or Ashkenazi Jewish origins [1]. KS received little scientific attention until the 1980s, when a significant increase in the occurrence of the disease was observed in homosexual men [2-5]. This observation along with the observation of other opportunistic infections occurring in homosexual men eventually led to the discovery of HIV/AIDS. Due to the increased prevalence observed in individuals with compromised immune systems, such as AIDS patients and transplant recipients, KS was hypothesized to have a pathogenic etiology. Prior to this, in 1972, electron micrographs of KS lesions suggested a possible viral origin due to the presence of herpesviral-like particles within the lesions [6]. In 1994, Patrick Moore and Yuan Chang isolated DNA from KS lesions related to but distinct from known gammaherpesviruses [7]. Two years later, they completed the sequencing of the KSHV genome, revealing a genome containing a 140.5 kb region comprising multiple open reading frames, flanked by 801 bp terminal repeats [8].

1.2 Overview of KSHV

1.2.1 Classification and Related Viruses

In the 2020 Classification by the International Committee on Taxonomy of Viruses (ICTV), KSHV falls within the *Herpesviridae* family, the *Gammaherpesvirinae* sub-family, and the *Radinovirus* genus (Fig 1.1) [9]. Of the eight human herpesviruses, the most closely related to KSHV is the gammaherpesvirus Epstein-Barr virus (EBV). Notably, KSHV and EBV are the only two human herpesviruses known to act as tumor viruses.

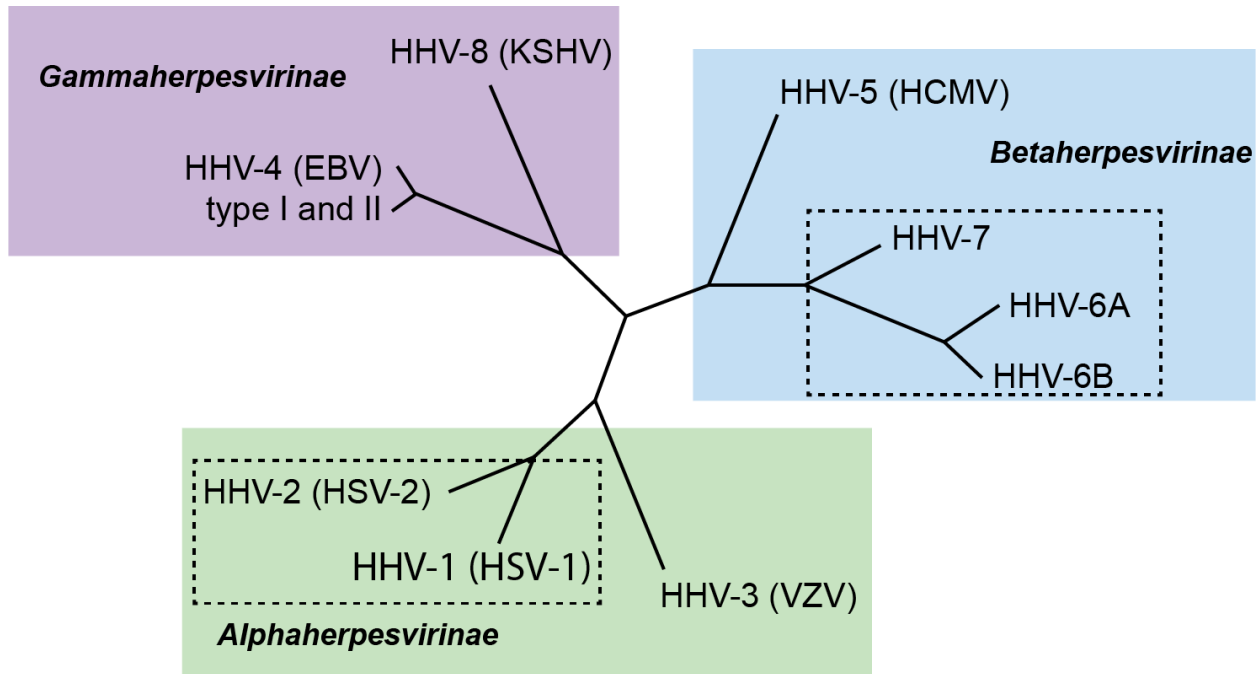


Figure 1.1 Cladogram of known human herpesviruses.

Figure adapted from Kylee Morrison who generated it using figure generated using phyloT (<https://phylot.biobyte.de/>) and Interactive Tree of Life (iTOL) [10]. Tree was updated to include additional subtypes and is now cladistic (branch lengths are not proportionate to similarity). Displayed are the three subfamilies of family herpesvirales and the known examples of human-tropic viruses within each. Colored boxes represent subfamilies indicated in bold. Viruses within the same genus are grouped by dashed boxes.

The *Alphaherpesvirinae* subfamily includes herpes simplex virus 1 and 2 (HHV-1/HSV-1 and HHV-2/HSV-2 respectively) and varicella-zoster virus (VZV/HHV-3). HSV-1 and HSV-2 lie within the genus *Simplexvirus*, while VZV is from the *Varicellovirus* genus. The *Betaherpesvirinae* subfamily includes human cytomegalovirus (HCMV/HHV-5), two types of HHV-6 (A and B are recognized as distinct viral species), and HHV-7. HHV-6A, HHV-6B, and HHV-7 lie within the *Roseolovirus* genus, while HCMV is from the *Cytomegalovirus* genus. The *Gammaherpesvirinae* subfamily includes two distinct types of EBV (HHV-4, a single species which differ only by the EBNA3 gene) and KSHV (HHV-8). EBV is from the *Lymphocryptovirus* genus while KSHV is from the *Radinovirus* genus.

1.2.2 Structural Overview

Herpesviruses are large, enveloped viruses which encode several glycoproteins involved in cellular adhesion and entry (see Fig 1.2 for a schematic overview). The most highly conserved of these is gB, though several others occur, often complexed in pairs such as gH/gL, and gM/gN. KSHV encodes six envelope glycoproteins, i.e., ORF8 (gB), ORF22 (gH), ORF47 (gL), ORF39 (gM), ORF53 (gN), and K8.1 (which encodes several differentially glycated proteins) [11, 12]. ORF28 and ORF68 have also been reported within the viral envelope, with the former having a known homolog in EBV (BDLF3/gp150) but not HSV-1 or HCMV, while the latter has homologs in EBV, HSV-1, and HCMV (BFL1, UL32, and UL52 respectively) [11, 12].

Most herpesviruses encode a single major capsid protein (MCP) that forms the bulk of the capsid. In addition to this, they typically form a “triplex” structure which is formed of two distinct proteins in a 1:1 ratio. Frequently the capsid will be coated by a small protein (one per hexon [13]). Lastly, the presence of a so-called “portal vertex” through which the genome passes and is composed of twelve copies of a single protein. In KSHV, the roles of these proteins are filled by ORF25 (MCP), ORF26/ORF62 (components of triplex), ORF43 (forming the portal vertex), and ORF65 (the small, capsid coating protein) [12, 14, 15].

All herpesviruses contain double stranded genomes, typically between 125-240 kb (165 kb for KSHV), which is packaged into the central capsid in a linear form. However, herpesviral genome replication (either during lytic or latent infection) involves circularization and chromatinization (see section 1.4.3) [16]. The KSHV genome can be divided into three regions of varying sizes: a small locus encoding the major latent genes (see Fig. 1.4 and section 1.4.3), a terminal repeat sequence, and all other genes.

Herpesvirus particles also contain a milieu of proteins between their glycoprotein envelope and the capsid termed the “tegument.” The tegument of herpesviruses can be varied and is traditionally thought to be made up of viral proteins, though evidence for packaging of host proteins into herpesviral teguments, including that of KSHV, has been reported [12]. Tegument proteins are classified into either “inner” or capsid-associated proteins and “outer” or envelope-associated proteins.

KSHV has at least eleven well-established tegument proteins [12, 17, 18]. Where not otherwise specified, tegument proteins are most likely “outer” tegument proteins. ORF19 is an inner tegument protein found at non-portal vertices and conserved in most herpesviruses [19]. ORF21 is the viral thymidine kinase (vTK) involved in herpesviral genome replication, which is not typically seen in the tegument of other herpesviruses. ORF32 is an inner tegument protein conserved in herpesviruses and present at vertexes like ORF19 [19]. ORF33 and OR38 are inner and outer tegument proteins, respectively, which interact and are required for the efficient production of new virions [18]. ORF45 is an inner tegument protein which is specific to the gammaherpesvirus family, though poorly conserved within gammaherpesviruses. ORF45 modulates several post-translational modifications, including phosphorylation, SUMOylation, and ubiquitination to aid in immune evasion and viral replication [20]. ORF50, also known as the replication and transcription activator (RTA), is a key transcription factor in the lytic transcriptional cascade (discussed in section 1.4.2) [21, 22]. ORF52, also known as KicGas (KSHV inhibitor of cGas), is a small protein with homologues in related gammaherpesviruses such as murine gammaherpesvirus-68 (MHV-68) and EBV, which acts as an inhibitor of the innate immune protein cyclic GMP-AMP Synthase (cGAS) [23]. ORF63 is a nucleotide-binding domain, leucine-rich repeat containing (NLR) homolog that inhibits NLR and pyrin domain

containing (NLRP) inflammasome activity [24]. ORF64 encodes a de-ubiquitinase which counteracts RIG-I signaling [25, 26]. Lastly, ORF75 is critical for replication of viral DNA by counteracting an ND10-mediated innate immune response that targets many DNA viruses [27].

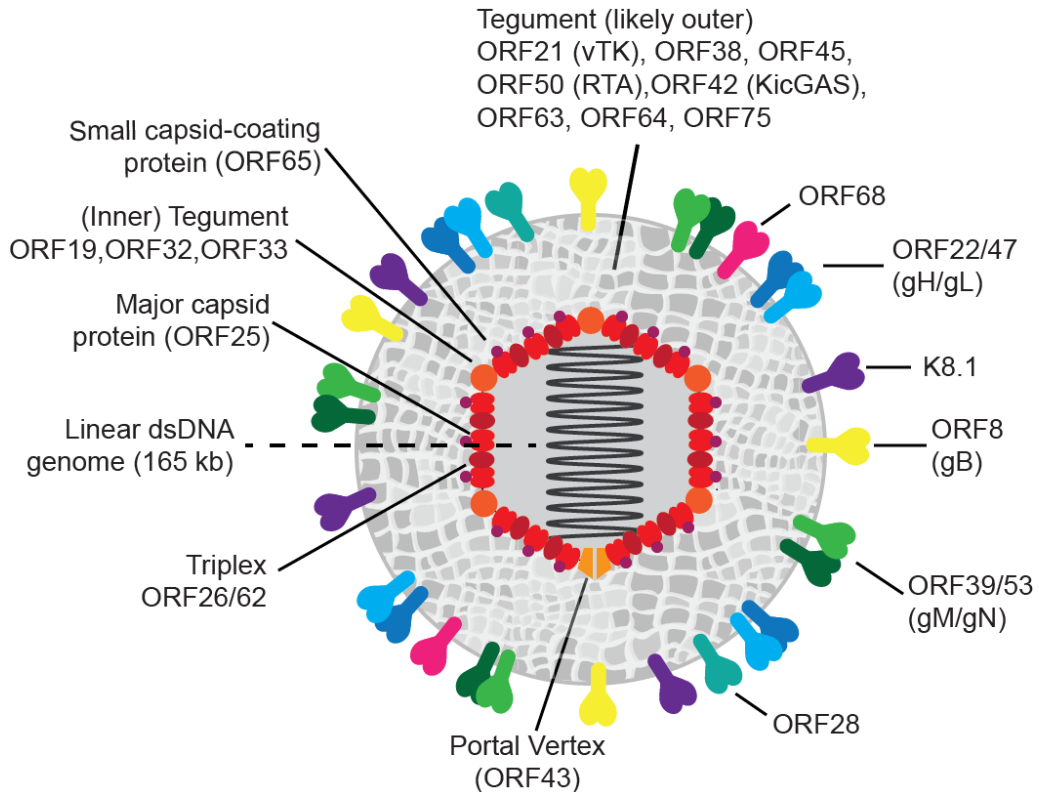


Figure 1.2 KSHV virion structure

A lipid bilayer (containing several glycoproteins, including pairings indicated) surrounds a core, proteinaceous viral capsid. Between these layers is a mixture of proteins known as the tegument. Note that the size, shapes, quantity, and positions of constituent molecules are not necessarily accurate due to the difficulty of representing the full 3D structure of hexons, pentons, and vertices in 2D. The triplex structure (represented as a single dark red molecule) is composed of two separate proteins. A single portal vertex, composed of dodecameric ORF43, is present per capsid. The mosaic textured region represents the outer tegument protein mixture. Dark orange structures at other vertexes are used to represent inner tegument proteins which interact with the capsid, though only ORF19 and ORF32 are present at the 11 remaining vertexes (along with other penton components). The small capsid coating protein (ORF65) is considered a core tegument protein (in hexons).

1.3 KSHV Epidemiology & Associated Malignancies

Seroprevalence of KSHV varies geographically, ranging from less than 10% in North America, Europe, and Asia to approximately 20-30% in the Mediterranean and higher than 50% in parts of sub-Saharan Africa [28]. However, observable disease is almost exclusively in immunocompromised individuals, such as HIV/AIDS patients, transplant recipients, or other groups thought to have compromised immune function [2-5]. KSHV is associated with three malignancies, KS, primary effusion B-cell lymphoma (PEL), and multicentric Castleman's disease (MCD) as well as an often life-threatening condition known as KSHV-induced cytokine syndrome (KICS) [29]. This section will review these diseases, focusing on clinical manifestations such as symptoms, outcomes, and treatment with limited discussion regarding the molecular basis of the disease.

1.3.1 Kaposi's Sarcoma

KS is the most common KSHV-associated disease and remains among the most common AIDS associated malignancies overall [28]. KS is a highly-angiogenic, inflammatory cancer which localizes to the skin or mucous membranes. KS lesions exhibit significant, leaky vascularization giving them a distinctive reddish hue [1, 30]. KS lesions are made up of unique spindle cells purportedly of microvascular origin (hence its designation as sarcoma) and latently infected with KSHV [30-33]. The exact origin of KS spindle cells is a matter of contentious debate, as they share features of lymphatic endothelial cells (LECs), blood vessel endothelial cells, and other cells of mesenchymal origins. Transcriptional reprogramming by the virus likely further adds to this ambiguity, however LECs has emerged as the most likely origin for KS spindle cells [31, 33-36].

Prognosis for patients with KS is complex due to its close association with HIV status but is generally positive [37, 38], although life threatening cases are reported with noteworthy frequency in regions where KS is endemic [39]. Notably, in classical KS patients who are HIV negative, survival time is unchanged from age matched cohorts of the same country of origin [37]. Further, up to 50% of KS cases in the context of HIV/AIDS regress with the administration of highly-active anti-retroviral therapy (HAART) [38]. In light of this, whether KS can truly be considered a form of cancer or simply a neoplasm is debatable [40, 41].

The strongest evidence against its status as a cancer comes from early finding that tumors do not readily arise when KS spindle cells are xenografted nude mice (Beige, BALB/c, Swiss, and NCr) [42]. This may be in part due to paracrine or autocrine signaling from KS-infected spindle cells or the immune infiltrates of KS lesions that are not recapitulated in murine xenograft models. One early study found that KS spindle cells transplanted into mice develop into KS-like lesions only if supplemented conditioned media containing pro-inflammatory cytokines derived from HTLV-II transformed cells [42]. However, as this study predates the discovery of KSHV it lacks proper controls to ensure that outgrowths contained active KSHV infections. Moreover, no care was taken to ensure similar viability of cells across conditions prior to engraftment. Further support for the notion that KS represents an inflammatory neoplasm rather than a true cancer comes from findings that KS lesions are predominantly polyclonal, with only a small number of patients displaying monoclonal lesions, as is common to most cancers [43-46]. Similarly, mutations frequently observed in cancer have been observed relatively late during KS progression [47-50].

Despite the above, KS has been observed in highly disseminated and aggressive forms which are hard to distinguish meaningfully from “true cancer” [51-54]. Collectively these observations point to KS as a complex, atypical malignancy.

1.3.2 Primary Effusion B-Cell Lymphoma

Primary effusion B-cell lymphoma (PEL) is a non-Hodgkin lymphoma which typically manifests as body cavity tumors [55, 56]. Since lymphomas containing KSHV DNA were first detected in 1995, KSHV-associated PEL has gained recognition as a distinct subset of lymphoma [56]. Thus, latent infection with KSHV is considered a diagnostic criterion for PEL and 100% of tumor cells in PEL are KSHV positive, similar to the spindle cells of KS lesions [32, 55, 56]. PEL is primarily seen in HIV/AIDS patients and has a poor prognosis, with an average survival below two years [57].

Treatment options for PEL are limited and typically include HAART (as part of ongoing HIV management) chemotherapy, such as EPOCH/R-EPOCH, a combination of five or six chemotherapeutics: etoposide, prednisone, oncovin (vincristine sulfate), cyclophosphamide, hydroxydaunorubicin (doxorubicin), and more recently rituximab (reviewed in [58]). Recent efforts have focused on characterizing and testing (see NCI clinical trial NCT02911142) targeted therapeutics such as immunomodulatory inhibitors (IMiDs) such as lenalidomide in combination with EPOCH-based treatments. The possibility of combinatorial therapies, such the IMiD pomalidomide and anti- PD-1 immunotherapy has also been investigated in patients with PEL and other non-Hodgkin lymphomas [59].

PEL-derived cell lines grow rapidly in culture and form xenograft tumors into mice, making them a favorable model to study KSHV biology, particularly latency [60]. The

characterization of KSHV latency genes and their function in the context of infection has largely been conducted in PEL-derived cell lines [61].

Co-infection with the related gammaherpesvirus Epstein-Barr Virus (EBV), occurs in a majority of PELs [62]. While EBV is widely known to be associated with several cancers, including B cell lymphomas, whether EBV contributes to KSHV-induced oncogenesis or vice-versa remains unclear; however, co-infection does not appear to be essential for disease progression, given that not all PELs contain EBV.

Although the etiology of PEL is incompletely understood, latently expressed KSHV oncoproteins are thought to play essential roles in the KSHV-mediated transformation of PEL cells, including the latency-associated nuclear antigen (LANA), viral interferon regulatory factor 3 (vIRF3), a KSHV-encoded D type cyclin (vCyc), and viral FLICE-inhibitory protein (vFLIP). Indeed, cultured patient derived PEL cell lines depend on the continued expression of several latency genes [63, 64]. Further discussion of the topic of the role of KSHV proteins in PEL can be found in sections 1.4.3, 1.5.2, and 1.6.2 of this document.

Several modern efforts, including those of my laboratory and that of this dissertation have focused on elucidating the role of host gene dependencies in PEL cells, including a striking dependency on the interferon regulatory factor 4 (IRF4) transcription factor [65, 66]. A thorough review of this topic can be found in Kuehnle & Gottwein, 2022 and the topic is discussed in section 1.5.5 of this document [67].

1.3.3 Multicentric Castleman's Disease & KSHV-Induced Cytokine Syndrome

Castleman's disease is an angiofollicular hyperplasia which impacts the lymph nodes and related tissues [68, 69]. Castleman disease can occur in a unicentric (impacting a single localized site) or multicentric (disseminated) form known as multicentric Castleman's disease which is frequently associated with KSHV infection [68, 70]. While KSHV infection is typically observed in MCD, KSHV negative instances of MCD exist, unlike KS and PEL. When MCD occurs in the absence of KSHV it is known as idiopathic multicentric Castleman's disease (iMCD) [32, 71, 72]. This section will focus on observations made of KSHV positive instances of MCD.

MCD can have a broad set of symptoms, often resembling viremia or sepsis, including fevers, sweats, fatigue, wasting, cytopenias, hypoalbuminemia, and hyponatremia. Outcomes of KSHV_MCD range from relatively to benign to life threatening; however, most patients with MCD recover following treatment with rituximab (a B-cell depleting antibody) given together with doxorubicin (to prevent KS flares following rituximab administration) [73-75]. Further, MCD patients treated with rituximab were found to have a low 5-year relapse rate of 18% and decreased risk of developing lymphoma [76, 77].

MCD is a lymphoproliferative disorder, with confluent cell clusters, referred to as "microlymphomas", predominantly composed of KSHV-infected plasmablasts [78, 79]. Unlike PEL and like KS, the proliferating cells of MCD lesions are polyclonal and rarely, if ever, demonstrate EBV co-infection [32, 80-82]. Unlike both KS and PEL, MCD is co-incident with high rates of lytic KSHV reactivation [70, 83-85]. The pathogenesis of MCD has not been fully elucidated, but likely involves a hyperinflammatory response mediated by elevated levels of cytokines including human and viral interleukin 6 (hIL-6, vIL-6) and human interleukin 10 (IL-

10) [83-85]. Indeed, symptoms following IL-6 dysregulation after ectopic retroviral expression mimic Castleman's disease in mice [86]. Further, concomitant elevation of hIL-6 and vIL-6 levels were observed in 38% of MCD flares and were associated with worse symptoms than cases with elevation of either cytokine alone [87]. At the same time, MCD appears to involve depletion of memory B cells and invariant natural killer T cells which may be involved in the control of KSHV-infected B cells and explain the high KSHV viral loads observed in MCD patients [85, 88].

KSHV-induced cytokine syndrome (KICS) is a newly characterized disease with inflammatory features similar to MCD but lacking the pathological presentation (such as microlymphomas in the lymph node, bone marrow, or spleen) necessary for an MCD diagnosis. Early reports often referred to KICS as "MCD-like syndrome." Indeed, KICS patients display similarly elevated levels of hIL-6, vIL-6, and IL-10 as MCD patients [89, 90]. KICS prognosis is relatively poor with a median survival time of just over a year from diagnosis with a survival rate of less than 50% [91]. Reports of KICS are rarer than for MCD and are confounded by generally poor patient conditions at time of diagnosis, making it difficult to determine whether traditional MCD treatment is as effective for KICS. For instance, in one case report in which the patient appeared to respond to rituximab but ultimately died, rituximab was administered alone due to poor liver function and had to be limited to manage the risk of KS flares [92].

1.4 KSHV infectious cycle

1.4.1 Viral Entry and Early Infection

Overall, the mechanism of infection by KSHV has been poorly characterized, due to several experimental difficulties in working with KSHV. These include reliably titrating KSHV,

as the virus is predominately latent in culture and lacks a standardized plaque assay. As a result, some aspects of our present understanding of KSHV infection draws on studies performed in closely related herpesviruses, such as herpes simplex virus 1 (HSV-1) and EBV.

While the route of KSHV infection has been a matter of debate, current evidence points to transmission being predominantly oral-salivary, as has been observed with EBV [93, 94]. This claim has gained observational and experimental support following reports that mucosa samples taken from KS patients yield higher titers than those from other tissues and that KSHV undergoes increased lytic replication in differentiating oral epithelial cells, as robust lytic replication would likely be needed to support initial acute infection [95, 96].

In terms of tropism, KSHV can infect several adherent cell lines of epithelial, endothelial, or mesenchymal origins *in vitro* [97]. Although B cells from chronically infected patients, such as those taken from PEL patients typically exhibit high degrees of latency, infection of activated primary B cells reportedly produces robust lytic infection [98]. Conversely, existing transformed B cell lines such as the EBV-/KSHV- cell line BJAB, EBV-transformed LCLs, and the human lymphoma line, MC116 can reportedly be latently infected with KSHV to differing extents [99, 100].

Cell surface molecules which have been reported to be used for host cell binding and entry by KSHV include 1) heparan sulfates which are bound by gB (ORF8), gH (OREF22) and K8.1; 2) multiple integrins bound by gB (ORF8); and 3) and Ephrin A2/A4 bound by gH-gL (OREF22/47) complexes [12, 101, 102]. Internalization of viral particles occurs via either clathrin-mediated endocytosis or macropinocytosis. In cells which KSHV enters via micropinocytosis, such as dermal human microvascular endothelial cells (HMVEC-d), entry has been shown to

require the macropinocytosis mediator, c-Cbl [103, 104]. Conversely, in other cells, such as human foreskin fibroblasts, entry is blocked by inhibitors of clathrin-dependent endocytosis [105].

Initial trafficking of KSHV in endosomes utilizes cellular actin and microtubule networks [104, 106]. Cellular signaling events at the cell membrane initiated by gB (ORF8) interactions likely promote trafficking through activation of signaling axis involving focal-adhesion kinase (FAK), Src, phosphoinositide 3-kinases (PI3Ks), and Rho GTPases [107, 108]. Fusion between the viral membrane and the endocytic membrane occurs in a pH-dependent fashion as the endosome matures, as with other herpesviruses [104, 105, 107]. Viral capsids are released into the cytosol, from where they traffic toward the perinuclear region to release their genomic cargo, likely via an interaction between the conserved herpesviral capsid protein pUL25 (ORF43, encoding the portal vertex) and the CAN/Nup214 nuclear pore complex [15, 109].

Upon reaching the nucleus, the naked, linear KSHV genome undergoes both circularization and chromatinization to establish episomes, which is particularly key for establishment of gammaherpesvirus latency as reviewed in [110]). Circularization is thought to protect the ends of viral DNA and underlies both latent and lytic replication, as circularization is necessary to establish the intact episomal maintenance element which LANA binds to and for the rolling circle amplification process by which herpesviruses engage in robust production of viral progeny [111-114]. Chromatinization is necessary for the proper transcriptional regulation of both KSHV and other herpesviruses, via both activating or silencing chromatin markers [115-117]. Through this regulation, KSHV can take on two broad patterns of expression and replication: lytic replication or latency.

1.4.2 Lytic replication

Lytic replication of KSHV is a complex, multi-stage process involving an ordered cascade of around 90 genes. Due to this complexity and the overall focus of this dissertation on disease that occurs in the context of latency, this section will stop short of a truly thorough review of KSHV lytic replication and make limited mention of the functional characterization of specific lytic gene products beyond what has been described above (for a general review see [114, 118]). In brief, lytic gene expression follows temporal patterns which have historically been characterized by a combination of cycloheximide treatment following infection, inhibition of viral polymerase, and time course analyses following treatment with the lytic inducer terephthalic acid (TPA) or *de novo* infection [114, 119]. These groupings are referred to immediate-early, early (sometimes referred to as delayed early), and late genes (sometimes also referred to alpha, beta, and gamma genes, respectively). It is worth noting that the possibility for situational and/or cell line specific behavior to be present within this process exists, as studies of KSHV lytic behavior rely on many artificial systems, including the above pharmacological methodologies as well as a varied mix of physiological and non-physiological cell types.

Immediate-early (IE) gene expression is resistant to cycloheximide and they are amongst the first set of genes expressed after TPA treatment or *de novo* infection [114, 119-121]. Thus, IE gene expression does not require *de novo* protein synthesis in the cell to establish expression, thus the designation of “immediate” and the use of cycloheximide in their profiling. The prototype (and only gene meeting this requirement) for an IE gene is RTA (ORF50), which has been observed as a KSHV tegument protein and serves as the primary initiating transcription factor which begins the lytic gene cascade. RTA exhibits this behavior in part to its presence in the tegument, though not all tegument proteins (i.e. ORF33/ORF38) are of relevance to the early

stages of infection and inclusion in the tegument is not sufficient to earn an IE classification. The strictness of the definition of IE genes has drawn criticism, including by the authors of the earliest papers identifying RTA as the sole IE gene [120, 121]. These same authors have also proposed that K8 (KSHV basic leucine zipper domain, K-bZIP) has IE functions and the homolog of this protein (BRLF1) in EBV is designated as an IE gene, sometimes alongside its homolog of RTA (BZLF1), though this designation has not gained widespread acceptance [122, 123].

Early gene expression begins to involve a more complex set of functions and occurs downstream of the introduction of RTA. A key transcription factor expressed early in the lytic cascade and has substantial interplay with RTA is K-bZIP, which itself is a homolog of the BRLF1 transcription factor which promotes lytic replication of EBV. Though K-bZIP is one of the most abundant products expressed after TPA induction of PEL cells, its expression is thought to modulate RTA activity [114, 124]. Notably, constitutive activation of K-bZIP appears to impede production of virions [124].

The function of other early genes is broad and includes modulators of cellular signaling pathways such as viral interleukin-6 (vIL-6), macrophage inflammatory proteins (vMIP-I/II), and G-protein coupled receptor (vGPCR); enzymes like viral thymidylate synthase (vTS); transcription factors like a subset of the viral interferon regulator factors (vIRFs); and the long non-coding RNA known as PAN [114, 119]. Notably, some of these genes have been proposed to have latent expression in some settings. These include vIL-6 and members of the vIRFs (vIRF-1 and vIRF-2), which bear functional similarities and genomic proximity to a key latency gene in B cells, vIRF-3 (see section 1.4.3 for discussion) [63, 125, 126].

Eventually, lytic gene expression moves towards production of new virions. This final stage, referred to as late gene expression is detectable only after viral DNA replication has been initiated and depends on expression of ORF34 [127, 128]. Late gene expression includes expression of multiple genes required for the production and egress of newly produced virions: i.e. capsid, viral envelope, and tegument proteins, among others.

1.4.3 Latent replication

Latency in KSHV is classically defined by the restricted expression of viral miRNAs from twelve stem-loop precursors and three viral proteins: Latency Associated Nuclear Antigen-1 (LANA-1 or LANA) alongside viral homologs of cellular cyclin D2 (vCyc) and FLICE Inhibitory Factor (vFLIP), all of which come from a genomic region referred to as the “major latency locus” (see Fig 1.4) [61, 129]. In contrast to this, latency in EBV takes on several different forms which may be associated with distinct stages of cellular differentiation (especially in B cells) [130]. However, at least one KSHV gene has been shown to have cell line specific latent expression—vIRF3—and the possibility of other instances of lineage-specific latency genes remains [63].

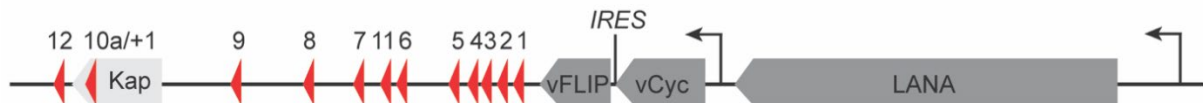


Figure 1.3 KSHV major latency locus

The KSHV latency locus encodes LANA, vCyclin, vFLIP, the kaposins (discussed towards the end of this section) and 12 miRNA precursors (indicated with numbered arrows). Black arrows indicate primary defined promoters, although others may exist. vCyclin and vFLIP are driven from a single promoter and form a dicistronic transcript (vFLIP translation initiation occurs through an IRES).

Core to latency maintenance is expression of the LANA protein, which enables episome persistence in dividing cells during latency [111]. LANA binds to distinct LANA binding site (LBS) motifs [131]. LANA tethers the LBS in the terminal repeats of viral episomes to nucleosomes within the host chromosomes in a process that may depend on interaction between LANA and the DNA damage-associated epigenetic modification, γ H2AX, amongst other factors (reviewed in [132]) [111, 133, 134]. LANA may also be necessary for the transcriptional repression of lytic genes during latency through an interaction with the cellular polycomb repressive complexes (PRC1/2) [135]. Due to their critical role in latency associated diseases such as KS and PEL, deeper discussion of the functions ascribed to LANA and the other latency proteins can be found in section 1.5.

1.5 Role of KSHV in Disease

As described above, KS and PEL are intrinsically linked to the latent stage of KSHV infection. Below I will briefly discuss some of the functions which have been described for the main viral latency proteins and how these are thought to impact KS/PEL.

Beyond its role in the maintenance of latency, LANA interacts with several cellular factors, including tumor suppressors such as p53, von Hippel-Lindau (VHL), and retinoblastoma (RB) [136-139]. Specifically, LANA promotes degradation of p53 and VHL by triggering their ubiquitination and proteasomal degradation [138]. Further LANA has been shown to modulate the Wnt signaling pathway through an interaction with glycogen synthase kinase (GSK-3 β) and TGF- β signaling through epigenetic modification of genes that participate in this pathway [140-142]. However, disruption of LANA in the context of PEL cells or other physiologically relevant cell types has proven elusive, making a true assessment of these functions difficult. In an early

study, targeting of LANA by shRNAs in PEL cell lines failed to demonstrate observable reductions in LANA protein levels and was tolerated over the course of several weeks, although a reduction in viral genome copies per cell was observed over time [64].

Viral cyclin (vCyc) is a homolog of cellular D-type cyclins [143, 144]. The exact role of vCyc in transformation by KSHV is unclear. Several cell-cycle regulatory properties have been proposed for vCyc, including inhibition of the negative cell cycle regulators RB, p53, and p27Kip1 [145-148]. While these functions have not been shown to affect cellular viability in any context thus far, recent work in rodent cells? has suggested that they may enable cells to overcome contact inhibition [148]. vCyc interacts with several cyclin-dependent kinases (CDKs), including CDK2, CDK4, CDK6, and CDK9 and these interactions are resistant to CDK inhibitor proteins [144-147, 149]. However, most of the work performed on vCyc to-date has relied on ectopic assays outside of the context of viral infection and which interactions are relevant to vCyc function in the context of KSHV-transformed cells is unclear. Exogenous expression of vCyc has only been shown to have transformative potential in mice on a p53-null background [150]. This may in part be due to the ability of ectopic vCyc expression to induce the cellular oncogene-induced senescence pathway, via ATM-dependent phosphorylation of p53 [151, 152].

Viral FLIP (vFLIP) is a homolog of cellular FLIP (FLICE-like inhibitory protein) [153, 154]. vFLIP is capable of transforming RAT-1 and 3T3 cells and depletion of vFLIP leads to spontaneous cell death in PEL cells [64, 155]. The function of vFLIP (and FLIP proteins in general) is discussed in greater depth in section 1.7, but studies have focused primarily on NF- κ B activation. Interestingly, vCyc and vFLIP are expressed from a single transcript, with vFLIP translation driven by an internal ribosome entry site (IRES, see Fig 1.3 for schematic of dicistron

and promoter). One interpretation of these findings is that vCyc and vFLIP are tightly co-regulated to promote complementary functions [156].

Reports exist of other possible latency proteins with oncogenic potential, including three putative kaposin proteins (KapA-C), vIRF-3 (in B cells/PEL), and vIL-6 (in PEL) [129]. While Kaposin proteins were initially thought to be oncogenic, more recent evidence has suggested that this is due to a miRNA that is processed from the coding sequence of KapA [157, 158]. The vIRF3 gene is clearly expressed during latency in all PEL cell lines that have been examined so far, where it appears to be essential for cellular viability [61, 63]. The role of vIRF3 has only recently begun to be adequately explored. Early studies found that vIRF3 was required for PEL cell survival and that it antagonized cellular interferon signaling mediated by IRF5/IRF7, promoted Myc-regulated gene expression, and modulated MHC Class II antigen presentation [63, 159-163]. More recently, vIRF3 has been shown to interact with cellular interferon regulatory factor 4 (IRF4) to drive gene expression via super-enhancers in PEL cell lines [66]. Lastly, a KSHV encoded viral cytokine, vIL-6 is also reportedly latently expressed (possibly under the direction of NOTCH) and required for cellular survival at least in a subset of PELs [125, 164]. Although these findings have not been confirmed across multiple cell lines, vIL-6 clearly exhibits broad activity across a number of IL-6 pathways and is likely a key protein in the pathogenesis of MCD and KICS (as described in section 1.3) [165].

Beyond these proteins, the KSHV latency locus encodes for >20 viral miRNAs from 12 pre-miRNA precursors. Several of these miRNAs function to mimic cellular miRNAs [166-169]. One such mimic likely to play a role in PEL is miR-K11, which shares its entire seed sequence with cellular miR-155, a miRNA that is essential in EBV-transformed lymphoblastoid cell lines (LCLs) [168, 170]. While there are over 3,000 detectable mRNA binding sites of the KSHV

miRNAs, functional validation has only been performed for a relative small subset and their regulatory importance is not well established, with a few exceptions [171]. For a review of viral miRNAs and their targets, see [172].

In sum, despite the limited number of proteins expressed by KSHV in PEL cell lines, there remain many questions about the function of these proteins, particularly in physiological contexts and in cells naturally infected with KSHV. A particular barrier to this study is the difficulty of viral genome manipulation in PEL cell lines since RNAi in these settings often of limited effectiveness and may interfere with viral miRNA function. In addition, the potential for CRISPR-mediated editing is limited by the high copy number of KSHV episomes in latent cells, which leads to DNA damage induced cell death.

1.6 Host Genetic Dependencies in PEL

Our group has recently turned much of its attention to understanding the role of host genes in PEL [65, 66, 173, 174]. This understanding has been mediated in large part by the advent of CRISPR-mediated screening technologies. To this end, our lab conducted genome-wide CRISPR-mediated KO screens in 8 PEL cell lines [65]. In that work we originally identified 210 PEL-specific oncogenic dependencies (PSODs), which were designated as essential in PEL cell lines but not 52 published screens conducted in 15 non-PEL cell lines. In the intervening time, the DepMap Project has greatly expanded the number and type of cell lines which have been screened [175].

Using a median FDR-adjusted p-value of less than 0.05 as a cutoff for an essential gene in our 8 PEL screens, I annotated each gene using data obtained from the Cancer Dependency Map (DepMap, Q4 2022), which pools data from 1,070 CRISPR screens representing 34

different tissue lineages [175]. This annotated information includes “commonly essential” gene status based on their inclusion in the top X depleted genes in 90% or more of the screened cell lines using a previously described empirical approach to determine the value of X [176]. I then broadened this definition of gene essentiality, by additionally filtering on genes for which there is a measured sgRNA depletion effect in all screened cell lines (compared to the CRISPR library), as this captures several important housekeeping genes missed by the empirical cutoff above.

Cross-referencing this analysis with our original screens across the 8 PEL cell lines yielded 76 updated PSODs, i.e. genes that are preferentially essential in PEL cell lines compared to other cancer cell lines. In this analysis, 146 of the 210 previously defined PSODs are now designated pan-essential, while 58 still meet our criteria for PSODs (median FDR-adj. $p \leq 0,05$ cutoff in the 8 PEL screens, not pan-essential), 6 genes have unknown status, and 18 genes are newly classified as PSODs. A full listing of all current and former PSODs can be found in Table 1.1.

Amongst both the original and updated PSODs are IRF4, BATF, CCND2, and CFLAR (caspase-8 and FADD-like apoptosis regulator). Meanwhile, previous PSODs MDM2 and MCL1 are now considered to be pan-essential, they belong to a subset of 86 pan-essential genes with highly skewed gene-effect distributions in DepMap, meaning they are likely more essential in PEL cells than other contexts, based on their validated essentiality in PEL cell lines.

Notably, IRF4 and BATF form a transcriptional axis which is essential for several other virally transformed lymphomas [177, 178]. KSHV appears to modulate this transcriptional program through vIRF3 and similar viral proteins have been observed in other IRF4-dependent

virally-associated cancers [66, 177-184]. IRF4 plays a key role in B cell/plasma cell differentiation and class-switch recombination, thus modulation of this pathway could grant these lymphotrophic viruses critical control over the precise cellular identity of the lymphoid compartment [185-188]. Notably all these IRF4/BATF-dependent cancers similarly depend on CFLAR and CCND2 [65, 177, 178], both of which are likely regulated by IRF4/BATF/vIRF3-bound super-enhancers (CFLAR is detected in ChIP-Seq data, but only CCND2 is confirmed) [66, 184]. Thus, one of the distinguishing features of PEL and related lymphoid cancers seems to be a dependence on IRF4/BATF and their transcriptional targets, particularly CCND2 and CFLAR, which encode the cyclin D2 and cFLIP, respectively. In PEL this comes as a surprise, given that KSHV encodes homologs of both proteins. This dissertation focuses on this peculiarity with respect to the role of FLIPs in PEL cells, a family of proteins whose function is outlined in section 1.7 below.

Gene Symbol	Panessential	Updated PSODs	New Status	Gene Symbol	Panessential	Updated PSODs	New Status
ABCF1	X			MIS18BP1	X		
ABHD17A	X			MMS19	X		
AFG3L2	X			MRPL15			X
AK2	X		Skewed PE	MRPL17			X
ALAS1		X		MRPL41	X		
ALG13	X			MRPL44			X
ANAPC1	X			MRPS34	X		
AQR	X			MRPS7	X		
ARPC4	X			MTHFD1			X
ATIC		X		MVD	X		
ATP1B3		X		MYB			X
ATP5F1D	X			MYBBP1A	X		
ATP5F1E	X			N6AMT1			X
ATP5PD	X			NAPA	X		
ATP6V1A	X			NAT10	X		
BATF		X		NCAPD2	X		
BRIX1	X			NDC1	X		
BTF3	X			NDUFA1			X
CAMLG		X		NDUFB10	X		
CCND2		X		NDUFB4	X		
CCT7	X			NDUFB7	X		
CDC73	X			NDUFS1			X
CDK12	X			NDUFS2			X
CDRT15P3			No DM Data	NDUFS1			X
CENPA	X			NHP2	X		
CENPO		X		NSL1	X		
CEP85		X		OGT	X		
CFLAR		X		PAFAH1B1	X		
CHCHD1	X			PGK1	X		
CHD4	X			PHF5A	X		
CLNS1A	X			PLK4	X		
CLP1	X			PMF1-BGLAP			No DM Data
CLTC	X			PNPT1	X		
CNOT1	X			POP1	X		
COA6		X		POT1			X
COPS2	X			PPCS	X		Skewed PE
COQ2	X			PPP1R15B	X		
CTC1		X		PRMT5	X		
CTR9	X			PRORP			X
CYC1		X		PSMG3	X		
DDX23	X			PTCD3	X		
DDX54	X			QRSL1			X
DHX37	X			RABGGTA	X		
DNAJC17	X			RAD1	X		
DNTTIP2	X			RAD51C	X		
DOHH	X			RBFA			X
DOLK		X		RBM17	X		

Gene Symbol	Panessential	Updated PSODs	New Status	Gene Symbol	Panessential	Updated PSODs	New Status
FDXR	X			SMG5	X		
FNBP4	X			SNRPD2	X		
FTSJ3	X			SRBD1	X		
G6PD		X		STX4			X
GART		X		SUPT4H1	X		
GBF1	X			SUPT5H	X		
GEMIN8	X			TAF6	X		
GFPT1	X		Skewed PE	TAF6L			X
GLRX5	X		Skewed PE	TAF7	X		
GNG5		X		TAFAZZIN			X
GNL3L	X			TBCD	X		
GOSR2	X			TBCE	X		
GPN1	X			TELO2	X		
GTF2H1	X			THOC6			X
HIRA	X			TIMELESS	X		
HMGCR	X			TOMM20	X		
HSPA14		X		TOP3A	X		
IDH3A		X		TPR	X		
ILF2	X			TRAPPC11	X		
INTS1	X			TRIM43			X
INTS11	X			TRRAP	X		
INTS14	X			TTI1	X		
INTS5	X			TUFM			X
IPPK		X		UBAP1	X		
IRF4		X		UBE2T			X
ISY1	X			URI1	X		
ITPK1		X		USP39	X		
LIN52	X			VMP1	X		
LIPT1		X		VPS13D	X		
LOC105376839			No DM Data	VPS52			X
LRRC37A3	X			WDR36	X		
LSM12	X			XPO1	X		
LUC7L3	X			YJU2	X		
MARCHF5		X		YRDC	X		
MAU2		X		ZBTB8OS	X		
MCL1	X		Skewed PE	ZCRB1	X		
MDM2	X		Skewed PE	ZNF626			No DM Data
MEN1		X		ZRSR2	X		

Table 1.1 Updated designations for the 210 original PEL-specific oncogenic dependencies

Two sets of four columns are presented side-by-side to minimize space. Each gene was designated as a PSOD in our original 2018 paper (based on median FDR-adjusted p-value < 0.05) [65]. New designations are specified, "pan-essential (in DepMap)" and "updated PSOD" are mutually exclusive designations, where DepMap data is available. Skewed PE designates skewed pan-essential genes; No DM Data designates genes for which no DepMap data were available. The 18 new PSODs are not shown, they are: ASH2L, C7orf26, COX15, DNAJC11, DNLZ, EMC6, ENO1, GFM1, HSD17B10, LARS2, MED12, MRPS2, NIPBL, RPUSD4, SDHA, TEDC1, TWNK, and UQCRC1. Full data and code at https://github.com/Gottwein-Lab/DepMap_Mining

1.7 FLICE-Inhibitory Proteins (FLIPs)

A partial version of this section has been published in Cell Death and Differentiation. CDD 30, 1221–1234 (2023).

CRISPR screens identify novel regulators of cFLIP dependency and ligand-independent, TRAIL-R1-mediated cell death

Neil Kuehnle, Scout Mask Osborne, Ziyan Liang, Mark Manzano & Eva Gottwein

1.7.1 Structure and Evolution of FLIPs

FLIPs, also known as FLICE (FADD-like interleukin-1 β converting enzyme)-inhibitory proteins, are a family of death-effector domain (DED) containing proteins that have evolved from the caspase-8 (CASP8) protein. FLIP and CASP8 are two examples of the many proteins which contain DED motifs, a bundle of 6 alpha helices that mediate protein-protein interactions. DEDs are members of the larger death domain superfamily, which include the caspase-recruitment domain (CARD) and pyrin domain (PYD). The best-known DED-containing proteins are CASP8 and FADD (Fas (FS-7-associated surface antigen)-associated death domain protein), of which several forms of apoptosis (discussed further in section 1.7.2 and 1.7.3).

DEDS are widespread throughout the animal kingdom, occurring from mammals to cnidarians, such as species of the genus *Hydra* [189, 190]. FLIPs are similarly ancient, occurring in both viruses (see Table 2.1 for listing of known viral FLIPs and the isoforms encoded by their hosts) and vertebrate and invertebrate animals (like the feather star crinoid *Anneissia japonica*, NCBI XP_033098588.1). In fact, the first FLIPs were discovered in viral genomes, including that of KSHV, while searching for homologs of FADD/CASP8 [154]. It has been suggested that

viruses may have acquired copies of cellular caspases to regulate the host cell death machinery [154]. Interestingly, phylogenetic analysis of all available host and viral FLIP proteins indicates that there is a clear separation between viral and host FLIPs (Fig 1.4), suggesting that viral FLIPs may not have been acquired directly from their hosts, but are instead related through a common viral ancestor. Related to this, conservation between viral and host FLIPs is typically quite poor at 30% identity at the protein level between KSHV vFLIP and cFLIP-L/S (see Table 1.2).

	CASP8	cFLIP-L	cFLIP-S	KSHV vFLIP	MC159L	MC160L
CASP8	100	27.29	26.26	25.45	24.87	27.59
cFLIP-L	27.29	100	99.51	34.12	30.08	30.34
cFLIP-S	26.26	99.51	100	33.72	32.37	30.34
KSHV vFLIP	25.45	34.12	33.72	100	30.97	25.29
MC159L	24.87	30.08	32.37	30.97	100	42.59
MC160L	27.59	30.34	30.34	25.29	42.59	100

Table 1.2 Protein sequence identity of human-associated FLIPs and CASP8

Pairwise protein alignments were generated with NCBI's protein BLAST (BLOSUM 80 matrix).

Cell values indicate identity (exact amino acid matches).

Despite their divergence, all known viral and cellular FLIP (cFLIP) proteins contain two DEDs, as do CASP8, FADD, and death receptor proteins (see Fig 1.5) [153, 154]. Below I'll discuss some of the broad findings that have been made regarding human cFLIP isoforms and three viral FLIPs from two human viruses. Human cFLIP isoforms that derive by alternative splicing of CFLAR mRNAs include the major isoforms of cFLIP (long/L and short/S). The viral FLIPs include KSHV vFLIP, MC159L from MCV, and MC160L from MCV. The activity of these proteins with respect to two targets, CASP8 activity and NF-κB signaling, are summarized in Fig. 1.5.

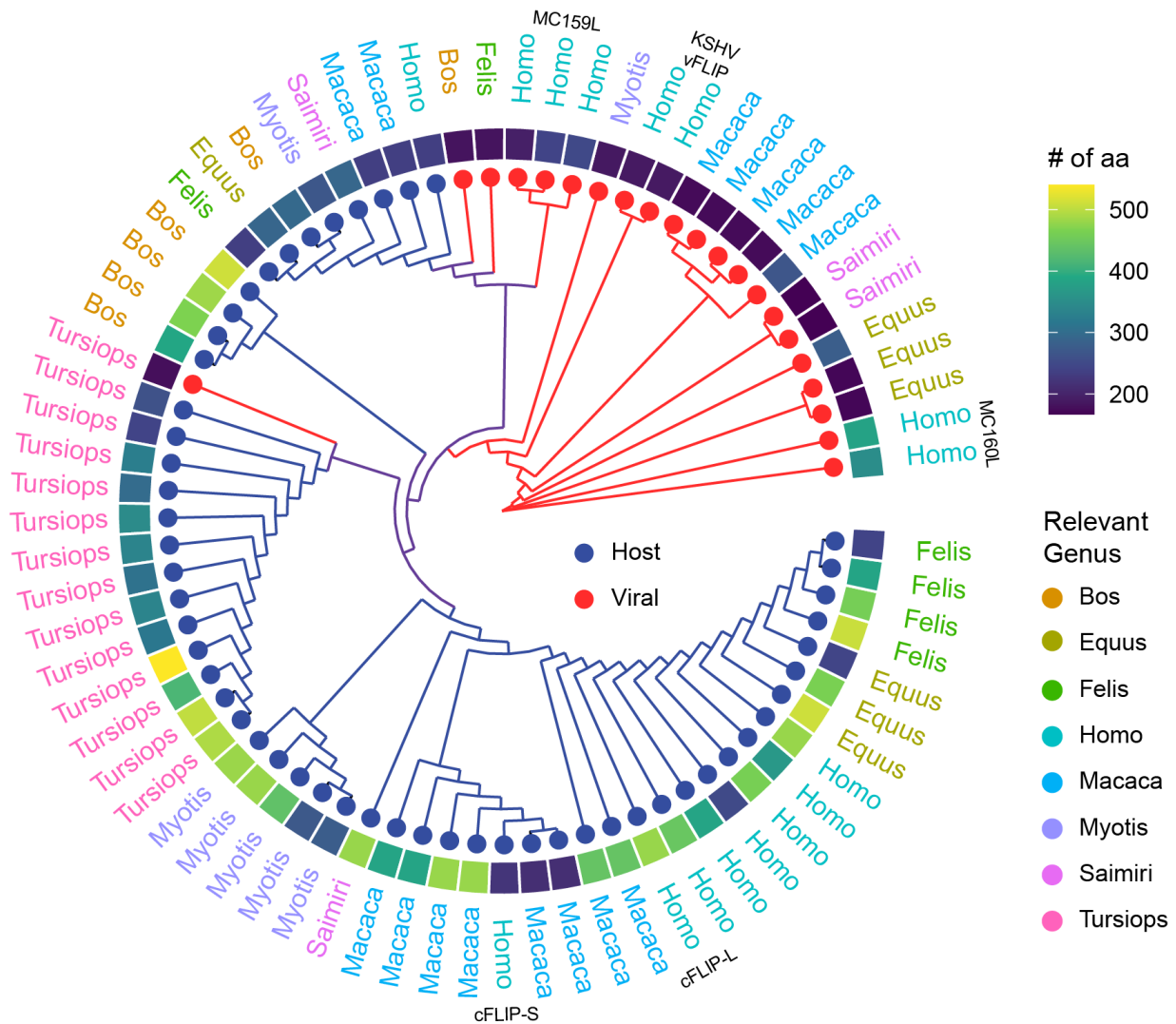


Figure 1.4 Viral and cellular FLIPs form distinct clades.

Nodes and branches in red indicate all known viral FLIPs, nodes and branches in blue represent FLIPs derived from these same viruses' host species/genus. Colored for each node indicates the relevant genus (either of the isoform in question or of the virus' host). The heatmap aligned with each node indicates the length (in amino acids) of each protein/isoform. Multiple isoforms of each viral/host species are included where present. Small text orthogonal to certain nodes indicates the location of the human-tropic viral FLIPs and the two major isoforms of human cFLIP (discussed throughout this document).

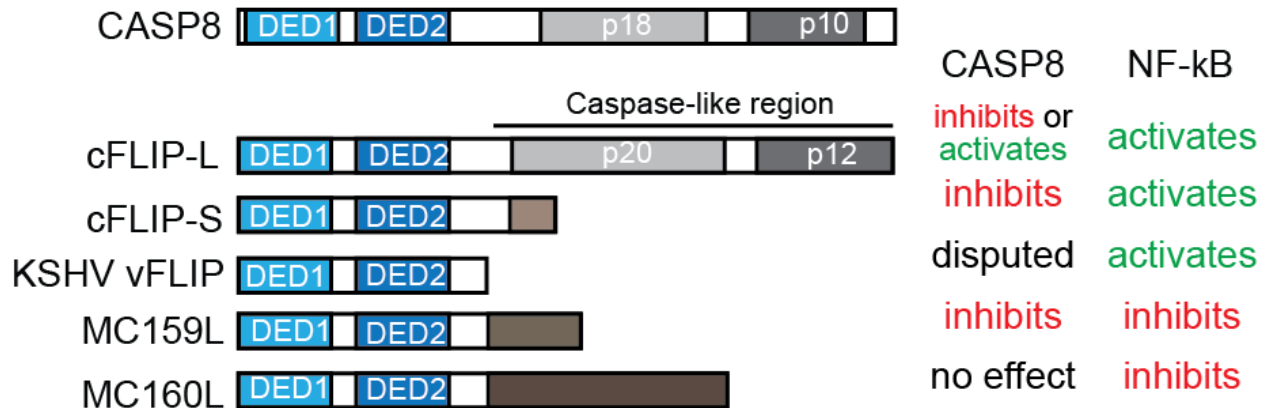


Figure 1.5 Domain organization and function of human-associated FLIPs

Schematic representation of human CASP8, the cFLIP-L/S splice variants, KSHV vFLIP, and the MCV FLIP proteins MC159L and MC160L. Also shown are the characterized activities of each protein towards CASP8/the extrinsic apoptosis pathway and the NF-κB pathway.

1.7.2 Canonical function: Inhibiting extrinsic apoptosis

Canonically, FLIP proteins act as dominant-negative inhibitors of CASP8-induced apoptosis by preventing formation of the death-inducing signaling complex (DISC) or directly inhibiting active CASP8 [153, 154, 191, 192]. Several FLIPs, including both major cFLIP isoforms and MC159L can disrupt CASP8-mediated cell death by directly binding and inhibiting pro-CASP8 or active CASP8 [153, 191-197]. In contrast, MC160L lacks this ability altogether, while reports of KSHV vFLIP's activity with respect to CASP8 have reached opposing conclusions [191, 195, 198, 199].

CASP8 is a pro-apoptotic protein in the cysteine protease (caspase) family that typically acts as the initiator caspase in the extrinsic apoptotic pathway induced by the death ligands tumor necrosis factor α (TNF α), Fas ligand, or TNF-related apoptosis-inducing ligand (TRAIL) (as

reviewed in [200]). The binding of these ligands to specific death receptors initiates the formation of the DISC, containing FADD protein and inactive pro-CASP8.

Autocatalytic cleavage of pro-CASP8 in DISC generates active CASP8, which initiates apoptosis following cleavage of targets. Cleavage by CASP8 occurs at a Leu–Glu–Thr–Asp motif (specifically after Asp) with the death effectors caspases-3 and -7 being the best-known of these targets [201, 202]. CASP8 autocatalytic and substrate-specific activities occur within the context of CASP8 dimers [203]. While FLIPs share homology with CASP8, they lack its primary catalytic (caspase) activity, resulting in a dominant negative mechanism of FLIP action. Interestingly, certain FLIPs, including the long isoform of cFLIP may retain trace levels of enzymatic activity which can result in CASP8 activation and pro-apoptotic activity when expressed beyond normal physiological levels and may possibly mediate inhibition of RIPK3-dependent necrosis [194, 204].

In contrast to this canonical method of CASP8 activation, additional cellular processes can converge on CASP8 to regulate cell death, including necroptosis, pyroptosis, autophagy-dependent cell death, and hyperactivation of the ER stress pathway/the unfolded protein response (UPR) [205-210].

1.7.3 Non-canonical cFLIP functions

Non-canonical cFLIP activities have been identified, including the regulation of NF-κB signaling [211, 212]. KSHV vFLIP is particularly noteworthy as a strong activator of NF-κB signaling, though both cellular FLIP isoforms possess this capacity too [198, 211-216]. The mechanism underlying this is best characterized for KSHV vFLIP, where its direct interaction with the inhibitor of kappa B kinase (IKK) complex modulator NEMO mediates its pro- NF-κB

signaling activity [199, 213, 217]. Conversely, both MC159L and MC160L can inhibit NF-κB signaling through IKK-dependent and IKK-independent mechanisms [195, 196, 218, 219]. It is finally worth noting that NF-κB can be activated downstream of several death receptors when DISC is complexed with certain proteins, such as tumor necrosis factor receptor type 1-associated DEATH domain proteins (TRADDs), and that this context can shift the behavior of FLIPs with respect to NF-κB [220, 221].

Though NF-κB modulation is the best known non-canonical function of FLIP proteins, regulation of several other signaling pathways has been documented as well. For cFLIP, these include the AKT, JNK, and Wnt signaling pathways, all of which are purported to be through direct interactions with elements of the respective pathways [222-227]. cFLIP and KSHV vFLIP have further been proposed to modulate cellular autophagy through direct interaction with ATG3 [228]. A final role for FLIPs (including cFLIP-L, KSHV vFLIP, MC159L, and MC160L) in regulating IRF3 signaling has also been noted, though these effects appear to be mediated through TBK1 and/or the epsilon subunit of IKK which have dual roles in IRF3 and NF-κB signaling [229].

1.8 Summary and Overview of Experimental Aims

A version of this sub-section was submitted as part of R01 CA247619-01A1S1 in Spring 2020 and outlines the most recent formal conception of this study's specific aims. Final research diverged from this plan, for reasons I discuss in chapter 4.

We have previously confirmed that cFLIP is essential for the survival and proliferation of the PEL cell line BCBL-1 [65]. This finding was puzzling, since KSHV encodes a viral cFLIP homolog, called vFLIP, which is thought to similarly be essential in PEL cells. The canonical

function of FLIP proteins is to inhibit the pro-apoptotic protein CASP8. CASP8 is typically activated by the extrinsic arm of the apoptosis pathway, following binding of death ligands to death receptors. However, these pathways are unlikely to be active in cultured cell lines. cFLIP also has non-canonical roles in other signaling pathways that can promote cellular survival. The specific function that underlies the essentiality of cFLIP in PEL cells is unknown. KSHV vFLIP strongly activates NF-κB signaling and it is this activity, rather than direct CASP8 inhibition, that is thought to underlie the essential role of vFLIP in PEL cells. Importantly, the role of cFLIP been not yet been distinguished from the role of KSHV vFlip, nor has the exact role of cFLIP in PEL been elucidated. The studies I propose here (i) seek to distinguish the roles of cFLIP from those of vFLIP, and (ii) involve in-depth mechanistic studies of cFLIP's activity in PEL. Based on my preliminary work, I hypothesize that cFLIP and vFLIP act via distinct mechanisms to promote cellular survival in PEL cells, with cFLIP acting to inhibit a ligand-independent TRAIL-R1 signal mediated by ER/Golgi-derived processes. I have developed two **Specific Aims** to test this hypothesis:

Specific Aim 1: Determine if human cFLIP and KSHV FLIP have non-redundant roles in PEL cells. I hypothesize that human cFLIP and KSHV vFLIP have distinct essential roles in PEL cells. To test this hypothesis, I have generated PEL cell lines that ectopically express one of five human or viral FLIP proteins with distinct positive, negative, or neutral activities towards NF-κB signaling or CASP8-mediated apoptosis. I will challenge these cell lines by KD of endogenous human cFLIP or KSHV vFLIP and measure rescue from this normally lethal challenge by the exogenous FLIP proteins. The distinct functions of the exogenous FLIP proteins will allow me to delineate the essential function(s) of cFLIP and KSHV vFLIP in PEL.

Specific Aim 2: Investigate the role of cFLIP in PEL cells. Based on my preliminary findings, I hypothesize that cFLIP inhibits a ligand-independent, endogenous cell death pathway in PEL cells. This cell death pathway is mediated by TRAIL receptor 1 (TRAIL-R1) and CASP8, but not TRAIL ligand. In Sub-aim 2.1, I will extend my preliminary results to additional PEL cell lines. In Sub-aim 2.2, I will identify endogenous triggers of TRAIL-R1-dependent CASP8 activation in PEL cells.

Collectively, these studies will improve our understanding of the essential roles of human and KSHV FLIP proteins in PEL cells.

Chapter 2: Materials and Methods

2.1 Materials and Methods for Chapter 2

2.1.1 Phylogenetic analysis

All known viral FLIP proteins (20 total) were obtained from UniProt in March 2019. FLIPs (54 total) from the host genus of each virus were collected from NCBI in March of 2019. A detailed listing of these proteins can be found in Table 2.1. The tree was built using Phylogeny.fr pipeline, using the following algorithms and settings. Multiple sequence alignment of available protein sequences was performed using the MUSCLE algorithm with Gblock correction [230]. This alignment was passed into PhyML to generate a neighbor-joining tree with the following settings WAG substitution model, SH-like approximate likelihood ratio test, 4 substitution rate categories, estimated gamma parameter and proportion of invariable sites, and gaps removal enabled [231]. The resulting tree was separately visualized using the R package ggtree [232].

species	relevant genus	accession	gene name	viral	amino acids
Bovine gammaherpesvirus 4	<i>Bos</i>	Q1XBS0	V-FLIP-like protein	Y	182
Equid gammaherpesvirus 2	<i>Equus</i>	A0A0B4Q5Z8	Apoptosis regulator E8	Y	171
Equid gammaherpesvirus 5	<i>Equus</i>	A0A2I4PC65	Apoptosis regulator E8	Y	279
Equid herpesvirus type 2 strain 86/87	<i>Equus</i>	Q66674	Viral CFLAR	Y	171
<i>Felis catus</i> gammaherpesvirus 1	<i>Felis</i>	A0A0M4MD83	F7	Y	182
Human gammaherpesvirus 8	<i>Homo</i>	A0A0N9SMH2	ORF71	Y	188
Human herpesvirus 8 strain GK18	<i>Homo</i>	F5HEZ4	Viral FLICE protein	Y	188
Molluscum contagiosum virus subtype 1	<i>Homo</i>	UPI0000697600	Viral CFLAR	Y	195
Molluscum contagiosum virus subtype 1	<i>Homo</i>	Q98325	Viral CFLAR	Y	241
Molluscum contagiosum virus subtype 1	<i>Homo</i>	A0A1S7DN05	MC160	Y	382
Molluscum contagiosum virus subtype 2	<i>Homo</i>	A0A1S7DM02	MC159	Y	249
Molluscum contagiosum virus subtype 2	<i>Homo</i>	A0A1S7DLZ8	MC160	Y	350

species	relevant genus	accession	gene name	viral	amino acids
<i>Macaca fuscata</i> rhadinovirus	<i>Macaca</i>	Q53CR9	JM151	Y	174
<i>Macaca mulatta</i> rhadinovirus 17577	<i>Macaca</i>	Q9WRM4	FLIP	Y	174
<i>Macaca nemestrina</i> rhadinovirus 2	<i>Macaca</i>	A0A0B5D6J7	N13	Y	174
Retroperitoneal fibromatosis-associated herpesvirus	<i>Macaca</i>	U5NM89	RF13	Y	267
<i>Rhesus</i> monkey rhadinovirus H26-95	<i>Macaca</i>	Q9J2H2	FLIP homolog	Y	174
<i>Myotis</i> gammaherpesvirus 8	<i>Myotis</i>	A0A0X9Y7F7	V-FLIP	Y	187
Herpesvirus saimiri (strain 11)	<i>Saimiri</i>	Q01044	Uncharacterized gene 71 protein	Y	167
Saimiriine gammaherpesvirus 2	<i>Saimiri</i>	O56959	FLIP protein	Y	167
Common bottlenose dolphin gammaherpesvirus 1 strain Sarasota	<i>Tursiops</i>	A0A1Z1NDY8	Apoptosis inhibitor FLIP De1	Y	177
<i>Bos taurus</i>	<i>Bos</i>	XP_015313874.1	CFLAR isoform X4	N	295
<i>Bos taurus</i>	<i>Bos</i>	XP_010800467.1	CFLAR isoform X3	N	388
<i>Bos taurus</i>	<i>Bos</i>	XP_024855306.1	CFLAR isoform X2	N	467
<i>Bos taurus</i>	<i>Bos</i>	NP_001012281.1	CFLAR	N	484
<i>Bos taurus</i>	<i>Bos</i>	XP_005202659.1	CFLAR isoform X1	N	511
<i>Equus caballus</i>	<i>Equus</i>	XP_023478116.1	CFLAR isoform X4	N	243
<i>Equus caballus</i>	<i>Equus</i>	XP_005601737.1	CFLAR isoform X2	N	464
<i>Equus caballus</i>	<i>Equus</i>	XP_005601736.1	CFLAR isoform X1	N	510
<i>Equus przewalskii</i>	<i>Equus</i>	XP_008540432.1	CFLAR isoform X3	N	290
<i>Felis catus</i>	<i>Felis</i>	XP_011283768.1	CFLAR isoform X5	N	235
<i>Felis catus</i>	<i>Felis</i>	XP_023115368.1	CFLAR isoform X4	N	241
<i>Felis catus</i>	<i>Felis</i>	XP_019694015.2	CFLAR isoform X3	N	385
<i>Felis catus</i>	<i>Felis</i>	XP_019694014.1	CFLAR isoform X2	N	460
<i>Felis catus</i>	<i>Felis</i>	XP_011283765.2	CFLAR isoform X1	N	508
<i>Homo sapiens</i>	<i>Homo</i>	NP_001120656.1	CFLAR isoform 2	N	221
<i>Homo sapiens</i>	<i>Homo</i>	NP_001189444.1	CFLAR isoform 3	N	235
<i>Homo sapiens</i>	<i>Homo</i>	NP_001294972.1	CFLAR isoform 8	N	250
<i>Homo sapiens</i>	<i>Homo</i>	NP_001189447.1	CFLAR isoform 6	N	366
<i>Homo sapiens</i>	<i>Homo</i>	NP_001189446.1	CFLAR isoform 5	N	384
<i>Homo sapiens</i>	<i>Homo</i>	NP_001189445.1	CFLAR isoform 4	N	445
<i>Homo sapiens</i>	<i>Homo</i>	NP_001294971.1	CFLAR isoform 7	N	462
<i>Homo sapiens</i>	<i>Homo</i>	NP_001120655.1	CFLAR isoform 1	N	480
<i>Homo sapiens</i>	<i>Homo</i>	XP_016860678.1	CFLAR isoform X2	N	480
<i>Macaca fascicularis</i>	<i>Macaca</i>	XP_005573957.1	CFLAR isoform X1	N	480
<i>Macaca mulatta</i>	<i>Macaca</i>	XP_014966203.1	CFLAR isoform X5	N	213
<i>Macaca mulatta</i>	<i>Macaca</i>	XP_014966202.1	CFLAR isoform X4	N	235
<i>Macaca mulatta</i>	<i>Macaca</i>	XP_014966201.1	CFLAR isoform X3	N	384
<i>Macaca mulatta</i>	<i>Macaca</i>	XP_014966200.1	CFLAR isoform X2	N	441
<i>Macaca nemestrina</i>	<i>Macaca</i>	XP_011716398.1	CFLAR isoform X5	N	213
<i>Macaca nemestrina</i>	<i>Macaca</i>	XP_011716397.1	CFLAR isoform X4	N	235
<i>Macaca nemestrina</i>	<i>Macaca</i>	XP_011716393.1	CFLAR isoform X3	N	384
<i>Macaca nemestrina</i>	<i>Macaca</i>	XP_011716392.1	CFLAR isoform X2	N	441
<i>Macaca nemestrina</i>	<i>Macaca</i>	XP_011716387.1	CFLAR isoform X1	N	480

species	relevant genus	accession	gene name	viral	amino acids
<i>Myotis myotis</i>	<i>Myotis</i>	XP_036175772.1	CFLAR isoform X6	N	268
<i>Myotis myotis</i>	<i>Myotis</i>	XP_036175771.1	CFLAR isoform X5	N	271
<i>Myotis myotis</i>	<i>Myotis</i>	XP_036175770.1	CFLAR isoform X4	N	277
<i>Myotis myotis</i>	<i>Myotis</i>	XP_036175769.1	CFLAR isoform X3	N	436
<i>Myotis myotis</i>	<i>Myotis</i>	XP_036175768.1	CFLAR isoform X2	N	481
<i>Myotis myotis</i>	<i>Myotis</i>	XP_036175758.1	CFLAR isoform X1	N	482
<i>Saimiri boliviensis boliviensis</i>	<i>Saimiri</i>	XP_010334747.1	CFLAR isoform X2	N	292
<i>Saimiri boliviensis boliviensis</i>	<i>Saimiri</i>	XP_003925710.1	CFLAR isoform X1	N	480
<i>Tarsiops truncatus</i>	<i>Tarsiops</i>	XP_019794718.1	CFLAR isoform X13	N	241
<i>Tarsiops truncatus</i>	<i>Tarsiops</i>	XP_019794717.1	CFLAR isoform X12	N	261
<i>Tarsiops truncatus</i>	<i>Tarsiops</i>	XP_019794716.1	CFLAR isoform X11	N	299
<i>Tarsiops truncatus</i>	<i>Tarsiops</i>	XP_019794715.1	CFLAR isoform X10	N	308
<i>Tarsiops truncatus</i>	<i>Tarsiops</i>	XP_019794714.1	CFLAR isoform X9	N	315
<i>Tarsiops truncatus</i>	<i>Tarsiops</i>	XP_019794713.1	CFLAR isoform X8	N	326
<i>Tarsiops truncatus</i>	<i>Tarsiops</i>	XP_019794711.1	CFLAR isoform X6	N	335
<i>Tarsiops truncatus</i>	<i>Tarsiops</i>	XP_019794712.1	CFLAR isoform X7	N	335
<i>Tarsiops truncatus</i>	<i>Tarsiops</i>	XP_019794710.1	CFLAR isoform X5	N	346
<i>Tarsiops truncatus</i>	<i>Tarsiops</i>	XP_019794709.1	CFLAR isoform X4	N	416
<i>Tarsiops truncatus</i>	<i>Tarsiops</i>	XP_019794708.1	CFLAR isoform X3	N	492
<i>Tarsiops truncatus</i>	<i>Tarsiops</i>	XP_019794707.1	CFLAR isoform X2	N	503
<i>Tarsiops truncatus</i>	<i>Tarsiops</i>	XP_019794701.1	CFLAR isoform X1	N	540

Table 2.1 Listing of FLIP proteins used for phylogenetic analysis.

Each row represents a unique protein sequence (no exact duplicates). Viral accessions are for UniProt, all others are NCBI accession numbers.

2.2 Materials and Methods for Chapter 3

A version of this section has been published as part of Cell Death and Differentiation. CDD 30, 1221–1234 (2023).

CRISPR screens identify novel regulators of cFLIP dependency and ligand-independent,

TRAIL-R1-mediated cell death

Neil Kuehnle, Scout Mask Osborne, Ziyan Liang, Mark Manzano & Eva Gottwein

2.2.1 Cloning

Cloning of lentiviral vectors was performed via either annealing and ligation or PCR and Gibson, as described below. Sequences for oligonucleotides and synthetic DNA fragments used for PCR and Gibson cloning can be found in Table 2.2 and Table 2.3, respectively, while sequences of annealed oligonucleotide pairs used for ligation into sgRNA expression vectors are listed in Table 2.4. All restriction enzymes were purchased from New England Biolabs. To limit recombination in lentiviral vectors, cloning reactions were transformed into chemically-competent Stbl3 bacteria and a single colony selected for outgrowth in liquid culture overnight. The insert sequence of all new vectors described below was confirmed by Sanger sequencing (ACGT, Inc.) and general vector integrity was confirmed by visual inspection of band patterns following a restriction test digest.

For rescue experiments, human C-terminally 3X-FLAG tagged FLIP long and short isoforms and KSHV vFLIP were ordered as codon-altered dsDNA gene fragment blocks (Integrated DNA Technologies). This initial codon alteration introduced resistance to cFLIP sg1, while cFLIP sg2 resistance was introduced by two overlapping PCRs centered on the sg2 target site using the synthetic gene fragment as a template (primers 4672/4673 and 4674/4323). PCR products were then inserted between the AgeI and BamHI sites of vector pLC-IRES-HYG using Gibson assembly [66]. KSHV vFLIP was cloned from a codon-optimized gene fragment block containing the entire vCyc/vFLIP locus using primers 4317/4318 and Gibson assembled with 3X-FLAG PCR products amplified from the cFLIP-S gene fragment (primers 4319/4323). PCR products containing MC159L (primers 4338/4339) and MC160L (primers 4340/4341) were amplified from pBabe-based vectors kindly provided by Dr. Joanna Shisler (UIUC) and Gibson

assembled with 3X-FLAG PCR products amplified from the cFLIP-S gene fragment (primers 4342/4323 for MC159L or 4343/4323 for MC160L).

vCyc and vFLIP expression constructs for transfection into 293T in Fig. 3.2 were cloned into pMSCVpuro (Takara, Catalog # 631461) by PCR, using primers 3646/3647 (vCyc) and 3648/3649 (vFLIP), followed by Gibson assembly with the EcoRI/XhoI digested vector. The NEMO interaction mutant used in Fig 3.11 cloned by Gibson assembly into EcoRI/XhoI digested vector from two independent PCR products. The mutant region was amplified using 4480/4482 from the C-terminally tagged MC159L described in the previous paragraph and primers 4481/4323 to amplify un-changed C-terminus vFLfrom the wild-type (WT) control vector.

The parental shR-miR expression vector pZIP-ZsGreen-T2A-Hyg-shNT4 was cloned by replacing the EcoRI-IRES-PuroR-NotI cassette of shERWOOD-UltramiR Lentiviral shRNA NT control #4 in pZIP-hCMV-ZsGreen-Puro (Transomic) with a PCR product containing a T2A-Hygr cassette that was amplified using primers 3551/3552 and template lenti MS2-P65-HSF1_Hygro (Addgene Plasmid #61426). The initial control insert shRNA NT control #4 was replaced by digesting pZIP-ZsGreen-T2A-Hyg-shNT4 with NotI and MluI and inserting miR-30-based shRNAs for cFLIP (sh1, shM, shN) or negative control shRNAs targeting Renilla Luciferase (REN.308 and Ren.713) using Gibson Assembly. These shRNAs were designed using SplashRNA and/or previously published [233]. dsDNA fragments specified in Table 2.3 were ordered and used for Gibson Assembly, either directly (shM, N) or after PCR-amplification with primers 4594/4607 (sh1, Ren.308, Ren.713).

The pZIP-based shRNAs used to target vCyc/vFLIP were designed using shERWOOD (Transomic [234]) and ordered as gene fragments (Epoch Life Science) inserted into pZIP-hCMV-ZsGreen-P2A-Puro-NT4 as previously described [173].

LentiGuide-Puro expressing cFLIP sg2 was cloned by ligation of annealed oligos 4532/4533 with BsmBI-linearized vector as previously described [65]. pLenti SpBsmBI sgRNA Hygro (Addgene, 62205) constructs were cloned by ligating annealed oligonucleotides specified in Table 2.4 with BsmBI digested vector [235]. Ligation and/or restriction digest efficiency of pLentiGuide SpBsmBI was generally poor, a few key steps were taken to improve performance which are described in greater detail below.

To clone sgRNA constructs (cFLIP sg1, CXCR4 sg1 and sg2, TRAILR sg1) for DOX-inducible gene inactivation, the sgAAVS1 sequence within pLX-sgAAVS1 [66] was replaced using overlap PCR. PCR fragment 1 was amplified using the shared forward primer 2430 and an sgRNA-specific reverse primer. PCR fragment 2 was amplified using an sgRNA-specific forward primer and shared reverse primer 2431. Fragments 1 and 2 were joined using overlap PCR with primers 2430 and 2431, cut with XhoI and NheI and ligated with XhoI/NheI-digested pLX-sgRNA vector using T4 DNA ligase (New England Biolabs).

To clone the parental DOX-inducible lentiviral vector pCW-MCS-ZeoR, Gibson assembly of a PCR fragment allowing for zeocin resistance (generated using primers 5327 and 5328) and SbfI/BamHI-digested pCW-MCS-PGK-P2A [173] was used. To clone pCW-ZeoR-mCherry, pCW-ZeoR-MPZ-S63Del-mCherry, and pCW-ZeoR-MPZ-S63Del-EctoYtoE-mCherry, Gibson Assembly of the AgeI-MluI vector fragment of pCW-MCS-ZeoR with a PCR product containing mCherry (primers 5320/5321), gBlocks 5324 and 5322 (DelS63), or gBlocks 5326 and 5322 (DelS63/EctoYtoE) was performed.

ID	Name	Sequence	Final Construct(s)	Primer Direction
pZIP-based shRNA Vectors				
3551	T2A_Hygro_F	CACGCCATCGCCTCCGGCTCCGCCTTGCCCCGGAG TGGAGAGGGCAGAGG	pZIP-ZsGreen-T2A-Hyg-shNT4	Forward
3552	T2A_Hygro_R	CCTCATTCAAACAGGATCCATTGCGGCCGCTCA TTCCTTGCCTAGGACGAGTGC	pZIP-ZsGreen-T2A-Hyg-shNT4	Reverse
4594	ZIP_Hygro_sh_F	CTCGTCCTAGGGCAAAGGAATGAGCGGCCGCTGT TTGAATGAGGCTTCAGT	pZIP-ZsGreen-T2A-Hyg-[cFLIP-sh1, cFLIP-shM, cFLIP-shN, shRen308, shRen713]	Forward
4607	mir30_Mlu_F	GAGGTTGATTGTCAGGCGGCCACGCGTAAGA TGATTTAATTATACC	pZIP-ZsGreen-T2A-Hyg-[cFLIP-sh1, cFLIP-shM, cFLIP-shN, shRen308, shRen713]	Reverse
MSCV vCyc/vFLIP Vectors				
3646	MSCV_vCyc_F	CCGGAATTAGATCTCTCGAGATGGCTACTGCAA ATAATCC	pMSCV-vCyclin	Forward
3647	MSCV_vCyc_R	TCCCCTACCGGTAGAATTCTTAATATGAGTCC AGTATCC	pMSCV-vCyclin	Reverse
3648	MSCV_vFLIP_F	CCGGAATTAGATCTCTCGAGATGGCAACGTACG AAGTACT	pMSCV-vFLIP	Forward
3649	MSCV_vFLIP_R	TCCCCTACCGGTAGAATTCTATGGGTATGCC GAATGT	pMSCV-vFLIP	Reverse
pLX-based inducible sgRNA vectors				
2430	pLX_F1	AAAAACTCGAGTGACAAAAAGCAGGTTT AAAG	pLX sgRNAs	Forward
2431	pLX_R2	AAAAAGCTAGCTAATGCCAACTTGTACAAGA AAGCTG	pLX sgRNAs	Reverse
5312	LXflipSGlf	GATTACCTATAGTCGAAACAGTTTAGAGCTA GAAATAGCAA	pLX-sgRNA-cFLIP sg1	Forward
5313	LXflipSGlr	TGTTTCGGACTATAGGTAATCGGTGTTCGTCCT TTCC	pLX-sgRNA-cFLIP sg1	Reverse
pCW-based inducible expression vectors				
5320	pCWmCherryF	ATCGCCTGGAGAATTGGCTAGCGAACCCGGTGC ACCA TGGTGA GCAAGGGCGA G	pCW-Zeo-mCherry	Forward
5321	pCWmCherryR	TGGAAAAGGCGCAACC	pCW-Zeo-mCherry	Reverse
5327	zeoF4cw	CCGACCTCTCCCCAGCAATTCCCTGCAGGGCC ACCA TGGCCAAGTTGACCAAG	pCW-MCS-Zeo	Forward
5328	zeoR4cw	CAGCAGAGAGAAGTTGTTGCGCCGGATCCGCC TGCTCCTCGGC	pCW-MCS-Zeo	Reverse
pLC-based FLIP Expression Vectors				
4317	VFLIP_F	CGTCAGATCCGCTAGCGCTACCGGTGCCACCAT GGCAACGTACGAAGTA	pLC-[VFLIP]-3XFLAG-IRES-HYG	Forward
4318	VFLIP_R	CCGTCAATGGCTTTGAGTCTGGGTATGCCGAT AGTGCT	pLC-[VFLIP]-3XFLAG-IRES-HYG	Reverse
4319	VFLIP-C-FLAG-F	AGCACTATCGGCATACCCCAGACTACAAAGAC CATGACGG	pLC-[VFLIP]-3XFLAG-IRES-HYG	Forward
4323	FLAG_R	GGGGGGGGAGGGAGAGGGCGGATCCCTACTTGT CATCGTCATCCTTGT A	pLC-[CFLIP-S, CFLIP-L, VFLIP, MC159L, MC160L]-3XFLAG-IRES-HYG	Reverse
4338	MC159L_F	CGTCAAGATCCGCTAGCGCTACCGGTGCCACCAT GTCCGACTCCAAGGAG	pLC-[MC159L]-3XFLAG-IRES-HYG	Forward
4339	MC159L_R	CCGTCAATGGCTTTGAGTCAAGTCAGTCGTTGCTCGGG GCTGT	pLC-[MC159L]-3XFLAG-IRES-HYG	Reverse

ID	Name	Sequence	Final Construct(s)	Primer Direction
4340	MC160L_F	CGTCAGATCCGCTAGCGCTACCGGTCGCCACCATGGCGACGAGCCAATC	pLC-[MC160L]-3XFLAG-IRES-HYG	Forward
4341	MC160L_R	CCGTCACTGGTCTTGATGCGTAGGAAGCTTCGTTCGCA	pLC-[MC160L]-3XFLAG-IRES-HYG	Reverse
4342	MC159L-C-FLAG_F	ACAGCCCCGAGCAAACGACTGACTACAAAGACCATGACGG	pLC-[MC159L]-3XFLAG-IRES-HYG	Forward
4343	MC160L-C-FLAG_F	TGCGAACGAAAGCTTCCTACGACTACAAAGACCATGACGG	pLC-[MC160L]-3XFLAG-IRES-HYG	Forward
4672	CFLIP_F	CGTCAGATCCGCTAGCGCTACCGGTCGCCACCATGTCTGCTGAAGTCATC	pLC-[CFLIP-S, CFLIP-L]-3XFLAG-IRES-HYG	Forward
4673	cFLIP_sgMut_R	TTCTCTTACTTATCTTACCCGACCCATGTAATCCTTCA	pLC-[CFLIP-S, CFLIP-L]-3XFLAG-IRES-HYG	Reverse
4674	cFLIP_sgMut_F	ATGGGTCGGGTAAGATAAGTAAGAGAGAAGAGTTTCTTGG	pLC-[CFLIP-S, CFLIP-L]-3XFLAG-IRES-HYG	Forward
4480	K13MutF1	TTTAGTGAACCGTCAGATCCGCTAGCGCTACCGGTCGCCACCATGTCGAGCTCAAGGAG	pLC-[vFLIP-Mut]-3XFLAG-IRES-HYG	Forward
4481	K13MutF2	TCCTTGAACGCCACCTTGCATGAGTTATTTCTCCCCTA	pLC-[vFLIP-Mut]-3XFLAG-IRES-HYG	Forward
4482	K13MutR	TAGGGGAGAAATAACTCATCGAACGGTGGCGTTCAAGGA	pLC-[vFLIP-Mut]-3XFLAG-IRES-HYG	Forward

Table 2.2 Primers used for cloning vectors

ID/number indicates internal inventory numbers, grouped by similar purpose/parent vector. Final construct indicates the final construct it was used to clone, brackets [] can include multiple variations of the vector that share a common primer. For clearer pairings, see Materials and Methods section 2.2.1.

Name	Sequence
cFLIP-sh1	ACGAGCTGTACAAGTAGCGACACCGGTGCAGTCGACACCGGAATTCAACTCTAGATGTTGAATGAGGCTTCAGTACTTTACAGAAATCGTGTGCCACATCTGGAAACACTTCTGCTGGGATTACTCTTCAGGTTAACCCAACAGAAGGCTCGAGAAGGTATATTGCTGTGACAGTGAGCAGTCGAGCTGCTGACTTGCTGGGACTTCAAGGGGCTACTTCAAGGGGACTTTAGGAGCAATTATCTGTTACTAAACTGAATACTTCGACACTACCGCTCGGGTTATCTCTTGATACATTITACAAAGCTGAATTAAAATGGTATAAAATTAACACTTCAATTGACACTACCGCTCGGGTTGGGGTTGCGCCTTTCAGGCAAGGCAGCCCTGGGTT
cFLIP-shM	CTCGTCCTAGGGCAAAGGAATGAGCGGCCGCTGTTGAATGAGGCTTCAGTACTTACAGAACATCGTGTGCCACATCTTGGAAACACTTCTGCTGGGATTACTCTTCAGGTTAACCCAACAGAAGGCTAAAGAAGGTATATTGCTGTGACAGTGAGCGAAGGGACCTCTGGATATTITATAGTGAAGGCCAGATGTATAAAATATCAGAAGGTCCTGTGCCACTTCAAGGGGCTACTTAGGAGCAATTATCTGTTACTAAACTGAATACTTCGCTATCTCTTGATACATTITACAAAGCTGAATTAAAATGGTATAAAATTAACACTTACITACCGCTGGCGCCTGGAAACAATCACCTC
cFLIP-shN	CTCGTCCTAGGGCAAAGGAATGAGCGGCCGCTGTTGAATGAGGCTTCAGTACTTACAGAACATCGTGTGCCACATCTTGGAAACACTTCTGCTGGGATTACTCTTCAGGTTAACCCAACAGAAGGCTAAAGAAGGTATATTGCTGTGACAGTGAGCGCGGTGAGTGGAGAAACTAAATAGTGAAGGCCAGATGTATAATTAGTCTGTTACTAAACTGAATACTTCGCTATCTCTTGATACATTITACAAAGCTGAATTAAAATGGTATAAAATTAACACTTACITACCGCTGGCGCCTGGAAACAATCACCTC
shRen308	TGTTGAATGAGGCTTCAGTACTTACAGAACATCGTGTGCCACATCTGGAAACACTGCTGGGATTACTCTCAGGTTAACCCAACAGAAGGCTAAAGAAGGTATATTGCTGTGACAGTGAGCGCTGGTTGAACCTCTTAATTATAGTGAAGGCCAGATGTATAAAATTAAGAGTCAAACCATGCTACTGCCTCGGACTCAAGGGGCTACTTAGGAGCAATTATCTGTTACTAAACTGAATACTTCGCTATCTCTTGATACATTITACAAAGCTGAATTAAAATGGTATAAAATTAACACTTAA
shRen713	TGTTGAATGAGGCTTCAGTACTTACAGAACATCGTGTGCCACATCTGGAAACACTGCTGGGATTACTCTCAGGTTAACCCAACAGAAGGCTAAAGAAGGTATATTGCTGTGACAGTGAGCGCAGGAATTATAATGCTTATCTATAGTGAAGGCCACAGATGTATAGATAAGCATTATAATTCCATGCCTACTGCCTCGGACTCAAGGGGCTACTTAGGAGCAATTATCTGTTACTAAACTGAATACTTCGCTATCTCTTGATACATTITACAAAGCTGAATTAAAATGGTATAAAATTAACACTTAA
sh1_vCyc 294	CCTGGAGAATTGGCTAGCGACACCGGTGCAGTCGACACCGGAATTCAACTCTAGATGTTGAATGAGGCTTCAGTACTTACAGAACATCGTGTGCCACATCTGGAAACACTTCTGCTGGGATTACTCTTCAGGTTAACCCAACAGAAGGCTCGAGAAAGTACTGCCTACTGCCTCGGACTTCAGGGGCTACTTAGGAGCAATTATCTGTTACTAAACTGAATACTTCGCTATCTCTTGATACATTITACAAAGCTGAATTAAAATGGTATAAAATTAACACTTCAATTGACACTACCGCTGGGTTGGGGCTTTCCAAGGCAGCCCTGGGTT
sh2_vCyc_224	CCTGGAGAATTGGCTAGCGACACCGGTGCAGTCGACACCGGAATTCAACTCTAGATGTTGAATGAGGCTTCAGTACTTACAGAACATCGTGTGCCACATCTGGAAACACTTCTGCTGGGATTACTCTTCAGGTTAACCCAACAGAAGGCTCGAGAAAGTACTGCCTACTGCCTCGGACTTCAGGGGCTACTTAGGAGCAATTATCTGTTACTAAACTGAATACTTCGCTATCTCTTGATACATTITACAAAGCTGAATTAAAATGGTATAAAATTAACACTTCAATTGACACTACCGCTGGGTTGGGGCTTTCCAAGGCAGCCCTGGGTT
CFLIP-L	CGTCAGATCGCTACCGCTACCGGTGCCACCATGTCGAGTCAGTCATCCATCAGGTTGAAGAACAGCACTTGATACAGAAGAAGGAGATGCTGCTCTTTGTGCCGGGATGTTGCTATAGATGTGTTCCACCTAATGTCAGGGACCTCTGGATATTITACGGGAAAGAGGTAAAGCTGTCGAGGACTTCAAGGGGACTTCAAGGGGCTACTTAGGAGCAATTATCTGTTACTAAACTGAATACTTCGCTATCTCTTGATACATTITACAGGAGATTGGGAGATTGGATAAAATCTGATGTGCTCTTAATTTTCCTCATGAAGGATTACATGGGGCGAGGCAAGATAAGCAAGGAGAAGAGTTCTGGACCTTGTGGTGAAGTTGGAGAAACTAAATCTGGTTGCCAGATCAACTGGATTATTAGAAAAATGCCATAAGAACATCCACAGAATAGACCTGAAGACAAAATCCAGAAGTACAAGCAGTCTGTTCAAGGAGCAGGGACAAGTTACAGGAATGTTCTCCAAGCAGCAATCCAAAAGAGTCTCAAGGATCCTTAAATAACTTCAGGCTCCATAATGGGAGAAGTAAAGAACAAAGACTTAAGGAACAGCTGGCCTCAACAAAGAACAGTGAAGAAATCCATTCAAGGAATCAGAAGCTTTCAGGATACCTGAAGAGAGATAACAGATGAAGAGCAAGCCCTAGGAATCTGTTTGATCATGACTGTATTGGCAATGAGAGACAGACTCTCTCGAGACACCTTCACCTCCCTGGGATGAGTCCAGGAAATCTTGATCTCAGTATGGTGTGCTGAGTGGATGAGCTACACTCAGGGCTCCCCCTGCATCACATCAGGAGGAGATGTTACGGGAGATTCTGAGCCCTTACATGGGCTTATCTAGCAGGGAAAGCCAAGAGTGTGTTATTCAAGAACTATGTTGTCAGAGGGCCAGCTGGAGGGACAGCAGCTCTGGAGGTGGATGGGCCAGCGATGAAGAATGTGGAATTCAAGGCTCAGTCTCACAGCTACCACATCCCTGTACCTGCACTGCCTCTCCCAGAAACTGAGACAAGAAAGAAAACGCCACTCCTGGATCTTCACATTGAACACTCAATGGCTACATGTATGATTGGAAACAGCAGAGTTCTGCCAAGGAGAAATATTATGCTGGCTGAGCACACTCTGAGAAGAAAGAACAGCCACTCCTGGATGGGATCCGCCCTCCCTCCCCCCCC

Name	Sequence
5326MPZ-N-S63Del-EctoYtoE	ATCGCCTGGAGAATTGGCTAGGCACACCGGTGCCACCATGGCTCTGGGCTCCCTATCCAGCCCCAGCCCTATCCTG GCTGTGCTGCTTCTCTTGTGCTGCTCCCCGGCCCAGGCCATCGTTACACCGACAGGGAGGTCCATGGTC TGTGGGCTCCGGGTGACCCCTGCACTGCTCCTCTGGTCCAGTGAGTGGTCTCAGATGACATCTCACCTGGCGGAGC AGCCCGAAGGGGGCAGAGATGCCATTTCGATCTCACGAGGCAAGGGACAACCCATATTGACGAGGTGGGACCT TCAAAGAGGCCATCCAGTGGTAGGGGACCCCTCGCTGGAAGGATGGCTCATTGTCATAACACAACCTAGACTACAGTGA CAATGGCACGTTACTTGTGACGTAAAACCCCTCAGACATAGTGGGCAAGACCTCTCAGGTACGCTGTATGTCTTIG AAAAAGTGCCAACTAGGTACGGGG

Table 2.3 List of gene fragments utilized for cloning vectors

Numeric prefixes for a subset of rows represent internal inventory numbers.

2.2.2. Detailed pLentiGuide SpBsmBI cloning protocol

Prior to digestion, column-prepped base vector was re-purified via phenol:chloroform (PC) extraction. This step is recommended for standard pLentiGuide Puro as well but is especially critical for pLentiGuide SpBsmBi due to the negligible insert size between BsmBI digestion sites. Briefly, 1:1 mixture of vector to PC was mixed by vortex and incubated for 5 minutes at room temp. Samples were then centrifuged at 14000 x g for 5 minutes. Next, the top aqueous layer was removed, 1/10th volume sodium acetate and 2.5 volumes 100% ethanol were added and the solution was incubated at -80 °C for 15 minutes, then allowed to warm briefly at room temperature for 2 minutes. The sample was centrifuged for 10 minutes at 4°C and then the supernatant was decanted, and the pellet washed and pelleted once more in 70% ethanol at 4°C.

Finally, a ratio of 2 uL of BsmBI per 1 mg of the purified, uncut vector with 1 mM DTT supplemented was incubated at 55 C for 1.5 hours in a thermocycler. Cut vector was then purified by gel extraction and a 20-fold excess of T4 PNK phosphorylated, annealed oligonucleotides added to 0.01-0.02 pmol of cut vector and ligated together using T4 ligase.

Nickname	Target	Vector	Forward Oligo	Reverse Oligo	Forward ID	Reverse ID
cFLIP #2	CFLAR	LentiGuide-Puro	<u>CACCGGGGGCCACTAGGGACAGGAT</u>	<u>AAACTGCTTATCTTGCCTCGGCC</u>	4532	4533
AAVS1	AAVS1	pLenti SpBsmBI Guide Hygro	ACACCGGGCCACTAGGGACAGGATG	<u>AAAACATCCTGTCCCTAGTGGCCCCG</u>	3455	3455
cFLIP	CFLAR	pLenti SpBsmBI Guide Hygro	ACACCGATTACCTATA <i>GTCGAAACAG</i>	<u>AAAACTGTTCGGACTATAGGTAATCG</u>	3469	3470
CASP8 #1	CASP8	pLenti SpBsmBI Guide Hygro	<u>ACACCGTCACTGTGCA</u> GTCATCGTGG	<u>AAAACCACGATGACTGCACAGTAGACG</u>	3743	3744
CASP8 #2	CASP8	pLenti SpBsmBI Guide Hygro	<u>ACACCGCCTGGACTACATCCGCAA</u> G	<u>AAAAC</u> <i>TGCGGAATGTAGTCCAGGCG</i>	3745	3746
TRAIL-R1 #1	TNFRSF10A	pLenti SpBsmBI Guide Hygro	<u>ACACCGAGCCTGTAACCGGTGACAGG</u>	<u>AAAAC</u> <i>CTGTGACCGGTTACAGGCTCG</i>	3745	4148
TRAIL-R1 #2	TNFRSF10A	pLenti SpBsmBI Guide Hygro	<u>ACACCGGGGTCCGTGCTGTCCC</u> ATGG	<u>AAAAC</u> <i>CCATGGGACAGCACGGACCCCCG</i>	3745	4523
TRAIL-R2	TNFRSF10B	pLenti SpBsmBI Guide Hygro	<u>ACACCGAGGTGGACACA</u> A <i>TCCCTCTG</i> G	<u>AAAAC</u> <i>AGAGGGATTGTGTCACCTCG</i>	3745	4150
TRAIL	TNFSF10	pLenti SpBsmBI Guide Hygro	<u>ACACCGCCTGGGAATCATCA</u> AGGAGTG	<u>AAAAC</u> <i>ACTCCTGATGATTCCCAGGCG</i>	3745	4164
UFM1 #1	UFM1	pLenti SpBsmBI Guide Hygro	<u>ACACCGACACTITG</u> <i>TACGGCAGCGTG</i>	<u>AAAAC</u> <i>ACGGCTGCCGTACAAAGTGTG</i>	3745	4953
UFM1 #2	UFM1	pLenti SpBsmBI Guide Hygro	<u>ACACCGTTAAGATC</u> <i>ACGCTGACGTG</i>	<u>AAAAC</u> <i>ACGTCAGCGTACCTAAAGCG</i>	3745	4952
DDRGK1 #1	DDRGK1	pLenti SpBsmBI Guide Hygro	<u>ACACCGAAATTGGAGCTA</u> AGAACTGG	<u>AAAAC</u> <i>CCAGTTCTAGCTCCAATT</i> CG	3745	4947
DDRGK1 #2	DDRGK1	pLenti SpBsmBI Guide Hygro	<u>ACACCGGGAGTAC</u> CTGAAACTGAAGGG	<u>AAAAC</u> <i>CCCTTCAGTTCAAGGTACT</i> CCG	3745	4946
JAGN1 #1	JAGN1	pLenti SpBsmBI Guide Hygro	<u>ACACCGAGGTAGCTA</u> <i>ATGTTG</i> TCGG	<u>AAAAC</u> <i>CGCAACACATTAGCTACCTCG</i>	3745	4995
JAGN1 #2	JAGN1	pLenti SpBsmBI Guide Hygro	<u>ACACCGTCGCCATG</u> <i>CACTACCAGAT</i> GG	<u>AAAAC</u> <i>CCATCTGGTAGTGCATGGCGACG</i>	3745	4996
CXCR4 #1	CXCR4	pLenti SpBsmBI Guide Hygro	<u>ACACCGC</u> <i>ATCTTGCCAAC</i> GTCAGT <i>CG</i>	<u>AAAAC</u> <i>CACTGACGTTGGCAAAGATGCG</i>	3745	5005
CXCR4 #2	CXCR4	pLenti SpBsmBI Guide Hygro	<u>ACACCGACACG</u> <i>GAGGAATGGG</i> CTCA <i>G</i>	<u>AAAAC</u> <i>TGAGCCCATTCTCGGTGTCG</i>	3745	5006
UGDH #1	UGDH	pLenti SpBsmBI Guide Hygro	<u>ACACCGGA</u> <i>ACTGGTAGA</i> ATCCTGT <i>CG</i> G	<u>AAAAC</u> <i>CGACAGGATTCTACCA</i> CTCCG	3745	4999
UGDH #2	UGDH	pLenti SpBsmBI Guide Hygro	<u>ACACCGTAGACATG</u> <i>AA</i> GACTACCAGG	<u>AAAAC</u> <i>CTGGTAGTCATT</i> CATGTCTACG	3745	5000
CHST15 #1	CHST15	pLenti SpBsmBI Guide Hygro	<u>ACACCGT</u> <i>GCCCTATG</i> ATGTAAG <i>GTG</i> G	<u>AAAAC</u> <i>CCACTCTACATCATAGGG</i> ACG	3745	5001
CHST15 #2	CHST15	pLenti SpBsmBI Guide Hygro	<u>ACACCGGGC</u> <i>ATTATTATCCCAC</i> ATCG <i>G</i>	<u>AAAAC</u> <i>CGATGTGGATAATA</i> ATGCCG	3745	5002

Table 2.4 Oligos used for cloning sgRNAs.

Underline nucleotides form sticky ends for ligation. Bolded nucleotides are important for context of vector surrounding sgRNA sequence. Actual transcribed sgRNA is indicated in italics. The bolded G upstream of the sgRNA is optional if already present in the first position.

2.2.3 Western blotting

Cells were pelleted, washed in ice-cold PBS, in some cases stored at -80°C, and lysed for 30 minutes in ice-cold RIPA buffer containing 1X protease inhibitor cocktail (Sigma-Aldrich, catalog P8340). Lysates were then subjected to five cycles (30 seconds on/30 seconds off) of sonication at 4 °C on high intensity in a Bioruptor Sonication System (Diagenode) and subsequently cleared by centrifugation at 14,000g for 15 minutes. Lysates were diluted 5 to 10-fold and quantified by Pierce BCA Protein Assay (ThermoFisher Scientific, 23225). Lysates were denatured by heating at 70°C for 10 minutes 1X LDS buffer (ThermoFisher, NP0008) containing a final concentration of 2.5% beta mercaptoethanol and loaded onto Bolt 4-12% Bis-Tris gels (ThermoFisher Scientific; NW0412) at equivalent concentrations (15-20 µg for cFLIP KO validation based on available lysates; 50 µg for vCyc/vFLIP, and 20-30 µg for all other proteins). SDS-PAGE was performed in 1X MES buffer and proteins were transferred onto 0.2 µm nitrocellulose membranes (Bio-Rad, 1620112).

Membranes were blocked at room temperature for 1 hour and probed overnight at 4 °C with primary antibodies at the concentrations indicated in Table 2.5. Images were captured on an Odyssey FC (LI-COR Biosciences) after incubation with IRDye 800CW secondary antibodies (LI-COR Biosciences) at a 1:15000 concentration. In some cases, anti-rat HRP (Santa Cruz) at a 1:5000 concentration was used for detection and developed using SuperSignal West Femto Maximum Sensitivity Substrate (ThermoFisher Scientific, 34094) following manufacturer protocol. Contrast/brightness was dynamically adjusted as needed using ImageStudio. Bands were quantified in ImageStudio Lite version 5.2 (LI-COR Biosciences).

Target Gene/Protein	Vendor/Source	Catalog Number	Dilution	Source Species	Buffer	Application
CFLAR (cFLIP)	Cell Signaling Technology	56343	1:2000	Rabbit	Odyssey or Intercept (TBST)	Western (IRDye 800CW)
CASP8	Cell Signaling Technology	9746S	1:2000	Mouse	Odyssey or Intercept (TBST)	Western (IRDye 800CW)
K13 (vFLIP)	Sander et al. 2008 JVI 4:1908-1922	4C1	1:1000	Rat	5% milk (TBST)	Western (HRP)
ORF72 (vCyclin)	Abcam	ab12208	1:500	Rat	5% milk (TBST)	Western (HRP)
GAPDH	Santa Cruz	SC-47724	1:5000	Mouse	Odyssey or Intercept (TBST)	Western (IRDye 800CW)
FLAG	Sigma-Aldrich	F1804	1:2000	Mouse	Odyssey or Intercept (TBST)	Western (IRDye 800CW)
TNFRSF10A (TRAIL-R1)	Cell Signaling Technology	42533	1:1000	Rabbit	Intercept (TBST)	Western (IRDye 800CW)
TNFRSF10A (TRAIL-R1)	Cell Signaling Technology	42533	1:500	Rabbit	0.1% saponin-3% BSA (PBS)	Immunofluorescence
TNFRSF10A (TRAIL-R1)	Abcam	ab59047	1:100	Mouse	1% BSA (PBS)	Flow Cytometry
TNFRSF10A (TRAIL-R1)	Abcam	ab59047	1:100	Mouse	0.1% saponin-3% BSA (PBS)	Immunofluorescence
anti-Mouse IgG (H + L)	LI-COR	926-32210	1:15000	Goat	Same as primary	IRDYE 800CW Secondary
anti-Rabbit IgG (H + L)	LI-COR	926-32211	1:15000	Goat	Same as primary	IRDYE 800CW Secondary
anti-rat IgG	Santa Cruz	SC-2032	1:5000	Goat	Same as primary	HRP Secondary
ERGIC53	Proteintech	13364-1-AP	1:50	Rabbit	0.1% saponin-3% BSA (PBS)	Immunofluorescence
ERGIC53	Santa Cruz	sc-365158	1:50	Mouse	0.1% saponin-3% BSA (PBS)	Immunofluorescence
ERp72	CST	5033S	1:50	Rabbit	0.1% saponin-3% BSA (PBS)	Immunofluorescence
Giantin	Abcam	ab37266	1:500	Mouse	0.1% saponin-3% BSA (PBS)	Immunofluorescence
anti-Rabbit IgG (H + L)	Thermo Fisher	A11036	1:1000	Goat	0.1% saponin-3% BSA (PBS)	Immunofluorescence (Alexa Fluor 568)
anti-Rabbit IgG (H + L)	Thermo Fisher	PIA32731TR	1:1000	Goat	0.1% saponin-3% BSA (PBS)	Immunofluorescence (Alexa Fluor 488)
anti-Mouse IgG (H + L)	Thermo Fisher	PIA32723TR	1:1000	Goat	0.1% saponin-3% BSA (PBS)	Immunofluorescence (Alexa Fluor 488)
anti-Mouse IgG (H + L)	Thermo Fisher	A11031	1:1000	Goat	0.1% saponin-3% BSA (PBS)	Immunofluorescence (Alexa Fluor 568)

Table 2.5 Antibodies and conditions for immunoassays.

Schema for each antibody and application. Antibodies used for multiple applications (i.e mouse anti-TRAIL-R1 #42533) have separate entries for each application. Anti-TRAIL enzyme-linked immunoassay (ELISA) was performed using a proprietary kit and is described separately in Section 2.2.20

2.2.4 Cell culture

PEL and/or BJAB cell lines were maintained in Roswell Park Memorial Institute (RPMI) 1640 with L-glutamine (Corning, MT10040CM) supplemented with 10% (BC-1, BCBL-1) or 20% (BC-2, BC-3, BC-5, BJAB) Serum Plus-II (Sigma-Aldrich, catalog number 14009C, lots 15H243 and 21C421), 10 µg/mL gentamycin (ThermoFisher, 15710064) and 0.05 mM β-mercaptoethanol (Sigma-Aldrich, M3148-25ML). HEK293T cells were maintained in Dulbecco's modified Eagle medium (DMEM; Sigma-Aldrich, D5796) supplemented with 10% Serum Plus-II and 10 mg/mL gentamycin. PEL cells were counted by trypan exclusion and split every second day to approximately 2×10^5 cells/mL (or 3×10^5 for BC-5). 293T cells were maintained at visually sub-confluent densities and split every 2 days. PEL cell lines expressing lentiCas9-Blast (Addgene, 52962) were previously generated and validated by STR profiling [65]. The BC-1/Cas9 clonal cell line utilized in Fig. 3.4 was subcloned and selected for editing efficiency compared to the parental Cas9 BC-1 pool utilized in our previously published screens [65]. This BC-1/Cas9 clone was re-confirmed by short tandem repeat (STR) profiling. A stable BCBL-1 cell clone allowing for DOX-inducible Cas9 (BCBL-1/pCW-Cas9) was reported previously [66].

For cellular growth curves and functional titration of lentivirus other than pZIP-based vectors (see below), cells were counted by flow cytometry using spike-in of a known amount of AccuCount Blank Particles 5-5.9 µm (Spherotech, ACBP-50-10) as previously described [65].

2.2.5 Cumulative cellular growth curves

Importantly, all lentiviral vectors used for growth curves analyses were titrated in naïve parental cell lines to ensure comparable titers between control sgRNAs and toxic sgRNAs. For growth curves, cells were plated at a density of 3×10^5 cells/mL and transduced at the MOIs indicated in the text or figure legends. Medium was exchanged one day after transduction and

cells were selected with 1.2 µg /ml puromycin for 2 days; 200 µg /ml hygromycin for 3 days (titrations) or 5-7 days (stable cell line production). Every second day, cells were counted by flow cytometry as described above and then split to a density of 2×10^5 cells/ml. This process was repeated until cells that had received toxic sgRNAs were too sparse to split or for up to 10 days. Cumulative cell counts were calculated by taking the measured cell concentration at a given timepoint multiplied by the product of all previous dilution factors and normalized to cumulative cell counts obtained for the sgAAVS1 control.

Statistical testing for reduced cellular viability was performed using one-sided, one-sample t-testing ($H_0: P(\mu=1)$ with $H_A: P(\mu<1)$). For rescue growth curve experiments (i.e. in the context of ectopic FLIP expression or a KO cell pool) an additional one-sided, independent two-sample t-test was performed, comparing the relative cumulative cell counts for each guide between the experimental cell line and the control line (i.e. sgAAVS1-Hygro or ZsGreen-Hygro). In the case of ZsGreen or KSHV vFLIP expression for rescue experiments, where $n=3-6$ was obtained for up to day 10 (Fig. 3.9B), ordinary least squares regression lines were fit. Cumulative cell counts relative to cell-line matched sgAAVS1 were used as the singular dependent variable with one or two predictor variables. To measure depletion, data was subset on the indicated cell line (ZsGreen or vFLIP expression) and sgRNA (sgPSM1 or cFLIP sg1) with the timepoint (>0 days after transduction) as a singular predictor variable. To measure rescue, data was subset on a particular sgRNA (sgPSMD1 or cFLIP sg1) with the cell line (ZsGreen or vFLIP) as an additional categorical predictor variable besides the timepoint (2-8 days post-transduction). A one-sided t-test was then used to determine whether the coefficients for day (depletion) or cell line (rescue) were $<$ or > 0 , respectively.

2.2.6 Lentiviral production, titration, and transduction

Except for pZIP-based vectors, lentivirus was produced using packaging plasmids psPAX2, pMD2.G, and transfer vectors at 1.3:0.72:1.64 molar ratios. HEK293T cells were seeded at a density of 1.25×10^7 per 15-cm dish and transfected with 30 µg of DNA using a 1:3 to 1:3.5 ratio of µg of DNA to µL PEI. Media were replaced after ~6 hours and cell supernatants containing viral vectors were collected 48-72 hours later and filtered through 450nm pore size filters. Viral vector preparations were used as is or concentrated by ultracentrifugation or using Amicon Ultra Centrifugal Filter Units (Millipore, UFC910024) following the protocols described below. In some cases, lentivirus was stored at -80°C.

Lentiviral vector titers were measured using functional titration of serially diluted viral stocks. The multiplicity of infection (MOI) of each dilution point was estimated using the percentage of live cells relative to an untreated control and a resulting viral concentration (transducing units/mL) was calculated from the average of multiple dilution points assuming a Poisson distribution, $P(x) = \frac{\lambda^x e^{-\lambda}}{x!}$, to estimate the mean event rate λ (MOI) assuming $P(x=0)$ is the percentage of uninfected cells.

Transductions were carried out at 3×10^5 cells/ml and the indicated MOIs under normal culture conditions supplemented with 5 µg/mL polybrene (Sigma-Aldrich, TR-1003-G). Culture medium was replaced ~24 hours after transduction and antibiotic resistance selection was carried out using 1.2 µg/ml puromycin for 2 days; 200 µg /ml hygromycin for 3 days (titrations) or 5-7 days (stable cell line production and CRISPR screens).

Procedures for pZIP-ZsGreen-T2A-Hygro shRNA vectors are described below.

2.2.7 Concentration of lentiviral vectors

Filtered viral supernatants were concentrated by either 1) ultracentrifugation (Beckman SW32Ti, 25,000 rpm, 90 min at 4°C) or 2) centrifugation (Eppendorf 5810, 3000 x g, 60 min at 4°C) in Amicon Ultra Centrifugal Filter Units. Following ultracentrifugation, pellets were resuspended in OptiMEM on a platform shaker for at least 60 min at 4°C and followed by pipetting up and down 20 times. Similarly, Amicon concentrated samples were diluted between 1:2 to 1:5 in OptiMem. If samples were not to be used within the next several days, samples were aliquoted and snap frozen at -80°C. Virus aliquots were thawed at 37°C and cleared by centrifugation at 400 g for 5 min before use.

2.2.8 CRISPR-based single-gene KO

CRISPR KO was achieved by transduction of published Cas9-expressing cell pools or clones and published lentiviral single guide RNA constructs targeting the AAVS1 (adeno-associated virus integration site 1) safe harbor locus, PSMD1 (proteasome 26S subunit, non-ATPase 1; using the published sgRNA sg1, IRF4 (using sg1), cFLIP (using the published sg1). A new cFLIP sg2 was cloned for this paper since sg2 from the previous study performed sub-optimally. The new cFLIP sg2 corresponds to sgRNA 2 (by rule set 2 score, on target activity) from the Brunello library. sgRNAs in pLentiGuide-Puro (Addgene, 52963) were used for cumulative growth curve KO, while long-term single-gene KO cell lines were generated using sgRNAs in pLenti SpBsmBI sgRNA Hygro (Addgene, 62205) containing a hygromycin resistance cassette. Sequences of all sgRNAs can be found in Table 2.4 above.

2.2.9 CRISPR-based synthetic rescue screens with sgRNA challenge

Library virus was generated and titrated as described above using the Brunello sgRNA pool library in lentiGuide-Puro (Addgene, 73178). In all cases, approximately 9.2×10^7 to 1.5×10^8 cells were transduced at an MOI of 0.3 to result in a single sgRNA per cell at a coverage of 300-500X cells per guide. Transduced cells were selected using 1.2 mg/ml puromycin, and dropout was allowed to proceed for 12 days with at least 3.6×10^7 cells maintained to preserve library complexity.

The resulting cell pool was then challenged with either cFLIP sg1 or the negative control sgAAVS1 in pLenti SpBsmBI sgRNA Hygro at an MOI < 0.5. Cells were selected with hygromycin and cultured until resistance to cFLIP KO was apparent by cellular proliferation, i.e. until day 12 after sgRNA transduction. At this point, approximately $3-7 \times 10^8$ cells (500-1000X coverage) were harvested, washed in ice-cold PBS, and snap frozen.

2.2.10 Synthetic rescue screens with shRNA-based challenge

pZIP transfer vectors were packaged in Lenti-X 293T cells (Takara) using molar ratios of 0.2 transfer vector to 0.51 psPax2 to 0.29 pMD2.G. Briefly, 2.1×10^7 pLenti-X 293T cells/15 cm dish were transfected with ~48.5 mg total plasmid and supernatant was harvested 48 hours later without replacing media. Supernatants were filtered through 450nm pore size filters and concentrated by ultracentrifugation and frozen prior to use as described above. Titration of the negative control vectors was performed based on ZsGreen expression and flow cytometry in BCBL1/Cas9 clone C2 [65]. Titration of the toxic cFLIP shRNAs was performed in 293T cells lacking Dicer (293T/NoDice) [236], relative to a negative control with known titer in BCBL1/Cas9.

BCBL1/Cas9 Brunello library transduction was performed at MOI 0.3 in eleven 15 cm dishes at 5×10^5 cells/ml and 50ml/dish, ~920x theoretical sgRNA coverage. Cells were selected using 1.2 mg/ml puromycin from days 1 to 4 after transduction and expanded. On day 9 after Brunello transduction, seven 15 cm dishes of cells (3×10^5 cells/ml and 50 ml/dish) were challenged with each shRNA vector at MOI 0.5. The next day, cells were collected by centrifugation and resuspended in fresh medium containing 200mg/ml Hygromycin. Cell pools were maintained at coverage and optimal cell density with hygromycin for one week and at least 4×10^7 cells/condition were harvested on day 12 into the shRNA challenge.

2.2.11 CRISPR library preparation and next-generation sequencing

Genomic DNA isolation and library preparation were performed as previously described for sgRNA and shRNA screens in BCBL-1 [65]. Resulting libraries were quantified by Qubit (ThermoFisher Scientific, Q33231) prior to further QC and quantification by Bioanalyzer (Agilent) and Kapa qPCR (Roche). Multiplexing of sgRNA challenge screens in BCBL-1 was performed utilizing 6-bp indexes and libraries were sequenced on a single lane of a HiSeq4000 (Illumina) using 50bp single-end (SE) reads with 10% PhiX spike-in as previously described [65]. For sgRNA challenge screens in BC-2, sequencing was performed on a single flow-cell of an NextSeq 500 (Illumina) using 75bp SE reads with 10% PhiX spike-in. For these runs, library preparation was modified slightly to combine genomic amplification and addition of adapters/barcode into a single PCR step with custom 8bp indexes (sequences can be found in Table 2.6). Genomic DNA for the shRNA-based screens were prepped and sequenced twice as a quality control using both approaches/platforms and reads were subsequently merged for further analysis. Demultiplexed reads have been deposited on GEO (accession GSE210445).

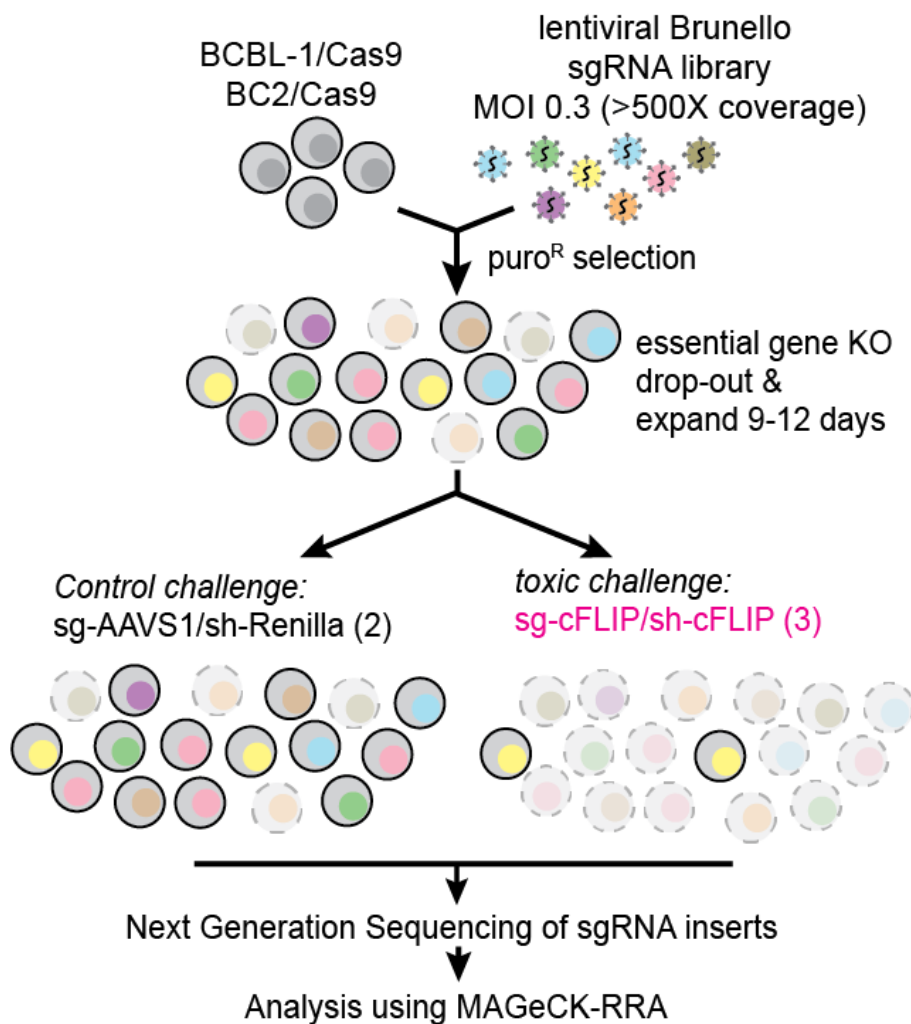


Figure 2.1 Schematic of CRISPR-based genome-wide synthetic rescue screens

BCBL-1/Cas9 (clonal) or BC-2/Cas9 (pool) cells were independently transduced with the Brunello CRISPR sgRNA library (containing 77,441 sgRNAs and 4 guides per gene) at low MOI to ensure single copy infection and high (>300X) coverage per guide. Cells were selected with puromycin and then allowed to propagate for 9-12 days. Cells were then transduced with a second lentiviral vector providing either an sgRNA (2.2.9) or shRNA (2.2.10) challenge or a negative control challenge. Details on sequencing and analysis can be found in 2.2.11.

2.2.12 CRISPR screen analysis

5' adapters were trimmed from raw CRISPR sequencing reads and trimmed to length (20 bp) from the 3' end using Cutadapt v4. 1 [237]. Reads were then aligned using Bowtie v1.1.2 9

[238]. Guide-level counts were obtained using MAGeCK v0.5.9 and statistical testing was performed using MAGeCK's robust rank aggregation (RRA) algorithm using median normalization [239]. The pipeline for analysis of 1:1 (treatment vs. control, any major sgRNA library) experiments with MAGeCK and/or DrugZ ([240], not utilized for this study) can be found at https://github.com/Gottwein-Lab/CRISPR_Screen_Processing.

Index	Index	Index Sequence (Primer/Reverse Complement)	Full Primer Sequence
GWI0	ATCCTTGG	ccaaggat	CAAGCAGAAGACGGCATACGAGATccaaggat GTGACTGGAGTTCAGACGTGTGCTCTTCG
GWI1	GCGGCATT	aatgccgc	CAAGCAGAAGACGGCATACGAGATAatgccgc GTGACTGGAGTTCAGACGTGTGCTCTTCG
GWI3	GTGGCTCC	ggagccac	CAAGCAGAAGACGGCATACGAGATggagccac GTGACTGGAGTTCAGACGTGTGCTCTTCG
GWI4	TGGTCTGC	gcagacca	CAAGCAGAAGACGGCATACGAGATgcagacca GTGACTGGAGTTCAGACGTGTGCTCTTCG
GWI5	GTGTCCCT	agggacac	CAAGCAGAAGACGGCATACGAGATagggacac GTGACTGGAGTTCAGACGTGTGCTCTTCG
GWI9	TGTCCCCG	ccgggacac	CAAGCAGAAGACGGCATACGAGATccgggacac GTGACTGGAGTTCAGACGTGTGCTCTTCG

Table 2.6 Custom indexing primers for NextSeq

The forward primers used for NextSeq 500 are used. These differ from the previously defined scheme only by the indexes indicated, while reverse primers remain the same [65].

2.2.13 Indel sequencing of CRISPR KO pools

A 200-300 bp region around each indicated sgRNA target was amplified from genomic DNA using the primers indicated in Table 2.7 and sent to Massachusetts General Hospital CCIB DNA Core for low depth sequencing. Raw FASTQ files were assembled into contigs by MGH.

The resulting effect on the coding sequence was determined using custom alignment and classification script using Biopython to estimate indel, frameshift, and early stopping incidence

[241]. Briefly, assembled contigs were aligned to the coding sequences targeted by each amplicon to determine optimal positioning of the contig in reference to the full coding sequence. All alignments utilized a simple pairwise scoring matrix (+1 for matches, +0 for mismatches, -.99 for gap opening, and -0 for gap extensions) chosen by iterative manual assessment of the collective results for the most abundant contig for each gene. The resulting, fully assembled coding sequence was then classified as an indel or non-indel for all sequences. Indels were further characterized as in-frame or frameshifted based on the number of nucleotides lost or gained across all alignment gaps. Early stopping events for all variants were predicted by *in silico* translation of predicting coding sequences. Raw FASTQ output was also analyzed using CRISPResso2 to obtain estimates of the number of modified and frameshifted reads [242].

ID	Gene	sgRNA Locus	Sequence	Primer Direction
5186	TNFRSF10B	1	ATGCCCATCCCTGCTTG	Forward
5187	TNFRSF10B	1	GGAAACAGACTGGAAGCTCAT	Reverse
5188	TNFSF10	1	AGCTCCTGCTTGCTACA	Forward
5189	TNFSF10	1	TCGAAAGTATGTTGGAAATAGATG	Reverse
5218	UFM1	1	AGGAAGTCGTGCTACCC	Forward
5219	UFM1	1	GCCGAGCTACTCACACTT	Reverse
5192	UFM1	2	TTGCTTACCGACTGCCATAAT	Forward
5193	UFM1	2	AGATGAAGTGAAGAGATGAAGACTG	Reverse
5194	DDRGK1	1	GAGGAGGAAGGTGTCGAGAAG	Forward
5195	DDRGK1	1	CAAACACCAGCCCAGCAG	Reverse
5196	DDRGK1	2	CTATGTCCACAGGAGGAGGAG	Forward
5197	DDRGK1	2	TGGCTAGCCTTGCCTG	Reverse
5198	JAGN1	1	CATGCCCTATCAGTGGAAATAC	Forward
5199	JAGN1	1	AACCAAAGAGGAAACGGTAGG	Reverse
5200	JAGN1	2	TCTGGGCAGGCACAATGG	Forward
5201	JAGN1	2	GGGACTTGGCAGGTGAGC	Forward
5202	CXCR4	1	AGGAAGCTGTTGGCTGAAA	Forward
5203	CXCR4	1	TGACAATACCAGGCAGGATAAG	Reverse
5204	CXCR4	2	TGTCCATTCCCTTGCCCTTT	Forward
5205	CXCR4	2	CCATGACCAGGATGACCAATC	Reverse
5206	UGDH	1	ACCATGCCCTTAACAAATGTA	Forward
5207	UGDH	1	ACAAGATCAGCTCTTGATGG	Reverse
5208	UGDH	2	TCTGAGTAATGTGTGTCATAGGC	Forward
5209	UGDH	2	CCTTGTATCACCAGTGTCTTT	Reverse
5210	CHST15	1	TCCTACGTGCTACTCCAA	Forward
5211	CHST15	1	CTTGATGGCGGAGAACTTGA	Reverse
5212	CHST15	2	CCTGCTCACTGGAGTGTGTT	Forward
5213	CHST15	2	GAAACTGCTCACCTCTCCAC	Reverse

Table 2.7 Primers for amplicon-based INDEL sequencing.

Primer ID numbers represent internal inventory numbers. Each pair amplifies the locus targeted by the sgRNA targeted by the gene + locus number (i.e. UFM1 locus 1 is targeted by UFM1 sg1)

2.2.14 mRNA sequencing

A frozen BC1 lysate in Trizol was submitted to BGI Group (Shenzhen, China) for single-ended, polyA-enriched RNA sequencing. Un-trimmed reads were aligned to the Gencode 41 annotation of GRCh38.p13 with STAR v2.7.10. Raw sequencing data has been made available on GEO (accession GSE210446).

2.2.15 RNA purification and reverse transcription

5×10^6 Cells were washed in ice-cold PBS, pelleted, and resuspended in 300 uL TRIzol (Invitrogen, 15596026). RNA was isolated using the Zymo Research Direct-zol RNA Miniprep Kit (Fisher Scientific, NC1057004) following the manufacturer's protocol. Purified RNA was treated with RQ1 RNase-free DNase (Promega, M6101) using 1 μ L RQ1 per 5 μ L RNA in a final volume of 10 μ L volume. Poly-dT primed reverse transcription was performed using the SuperScript First-Strand Synthesis System (Invitrogen, 11904018) using 1 μ g of RNA as template in a 10 μ L reaction, including water-only reactions as non-template controls, following manufacturer protocols including optional RNase digestion after transcription. Samples were then diluted to 100 ng input RNA/4.5 μ L prior to TaqMan assay.

2.2.16 TRAIL-R1 TaqMan assay

Real-time PCR was performed by standard TaqMan Assay on either the QuantStudio 7 or Quantstudio 5 Real-Time PCR platform (Applied Biosystems). Briefly, a mastermix of 1 μ L TaqMan probe (Applied Biosystems, Hs00269492_m1 or Hs00984230_m1) to 10 μ L TaqMan Universal Master Mix II (Applied Biosystems, 4440043) was prepared for each probe. 5.5 μ L of mastermix was added per well, followed by 4.5 μ L (equivalent to 100 ng input RNA) cDNA template. Three technical replicates were included, and $2^{-\Delta\Delta CT}$ was calculated relative to the endogenous B2M control and sgAAVS1-transduced cell line for each biological replicate [243]. Biological replicates represent independently harvested cell pellets of the indicated cell lines. Statistical testing for differences between samples was performed using one-way analysis of variance. Post-hoc testing was performed using Dunnett's method and sgAAVS1 as the control group.

2.2.17 Inducible KO and ADM3100 treatment

For data shown in Fig. 3.36, BCBL-1 were transduced with stably integrated DOX-inducible Cas9 with pLX-sgRNA-lentiviral vectors expressing sgRNAs targeting AAVS1, PSMD1, or cFLIP sg1 at ~MOI 2 and selected transduced cells with 7.5 mg/ml Blasticidin S (Sigma-Aldrich, SBR00022) [66]. Cas 9 expression was induced by treatment with 1 mg/ml Doxycycline hyclate (DOX, Sigma-Aldrich, D9891-1G) or cultures were left uninduced. At the same time, DMSO or 25 µM AMD3100 (Selleckchem, S8030) was added to each cell line and Dox-treatment group. Cells were counted by trypan exclusion every 2-3 days, pelleted, and re-suspended to 2×10^5 cells/mL in fresh medium containing the desired treatment regimen.

2.2.18 Cellular staining and flow cytometry

Cells were washed twice in ice-cold PBS and APC Annexin V (BD Biosciences, 550475) and 7-AAD (7-Amino-Actinomycin D; BD Biosciences, 559925) staining was performed on 1×10^5 in 100 mL of 1X Annexin V binding buffer (BD Biosciences, 556454) following manufacturer recommended guidelines, using 5 mL of each stain for 15 minutes at room temperature in the dark. Necrotic cells were generated for Annexin V and 7-AAD compensation controls using a 30-minute heat shock at 95°C. Stained cells were diluted with 400 mL 1x Annexin V binding buffer and flow cytometry was performed on a BD FACSCanto II (BD Biosciences) within 1 hour.

For TRAIL-R1 staining, cells were harvested and washed twice in ice-cold PBS and resuspended in PBS at a concentration of 1×10^6 cells/mL. 500 mL of cells were then fixed in PBS containing 4% w/v PFA for 10 minutes followed by two more PBS washes. On the final wash, cells were split into two and each resuspended in 250 mL PBS containing 1% w/v bovine serum albumin (Sigma, 10735078001) with or without the addition of 0.1% w/v saponin (Sigma-

Aldrich, 47036). Cells were pre-incubated for 15 minutes at room temperature with 250 mL PBS/1% BSA with or without 0.1% w/v saponin, containing 1:400 of Human BD Fc Block (ThermoFisher Scientific, BDB564219) per condition, followed by addition of 1:100 (2.5 mL in 250 mL) of FITC-conjugated Anti-TRAIL receptor 1 (Abcam, ab59047; specific to the extracellular domain of TRAIL-R1) for 30 minutes at room temperature in the dark. Cells were then washed 3X with PBS/1% BSA with or without 0.1% w/v saponin followed by a final re-suspension in 500 mL PBS containing .01% PFA.

Stained cells were stored for up to 2 days at 4 °C in the dark (TRAIL-R1) and flow cytometry was performed on a BD FACSCanto II (BD Biosciences). Raw data were exported to FlowJo v10.8.1 for analysis and plotting.

2.2.19 Generation of BCBL-1 cell lines expressing MPZ-Del63-mCherry constructs

To allow for inducible expression of mCherry, MPZ-Del63-mCherry, or MPZ-Del63-EctoYtoE, BCBL-1 cells were transduced at MOI <1. Cells were selected with 175 mg/ml zeocin (Life Technologies, R25005) and protein expression induced by treatment with 1 mg/ml DOX. Results in Figs. 3.26-3.28 are from day 3 after induction and three independent inductions.

2.2.20 Immunofluorescence and colocalization analysis

Cells were collected by centrifugation, washed with PBS, and resuspended in PBS at 1x10⁶ cells/mL. 650 µL/24 well or 3ml/6 well were spun onto 1.5mm thick, uncoated glass coverslips in swing bucket rotors at 650 g for 5 minutes. Coverslips were fixed for 15 minutes with 4% formaldehyde-PBS, rinsed three times with PBS, and blocked for 1 hour in PBS containing 0.1% w/v saponin-3% bovine serum albumin (BSA, Sigma Aldrich, A7906). Samples were again rinsed three times with PBS and incubated with primary antibodies as indicated in Table 2.5,

diluted in PBS containing 0.1% w/v saponin-3% BSA for 1 hour at 37°C in a humidified chamber. Coverslips were rinsed three times and incubated with the appropriate species IgG (H+L) highly cross-adsorbed secondary antibody conjugated to Alexa Fluor 488 (TRAIL-R1 staining) or 568 (all others) diluted 1:1000 in PBS containing 0.1% w/v saponin-3% BSA for 1 hour at 37°C in a humidified chamber. Coverslips were washed with PBS, incubated with 4',6-diamidino-2-phenylindole (DAPI) as directed (Invitrogen, D1306), and washed with PBS. Finally, coverslips were mounted onto glass slides using ProLong Gold antifade mountant (Invitrogen, P36934), and incubated at room temperature for 24 hours.

Confocal images were acquired on a Nikon W1 Dual Cam Spinning Disk Confocal microscope with Plan Apo λ 60x Oil objective. Widefield images were acquired in Z-stacks on a Nikon Ti-2 Widefield microscope with S Plan Fluor ELWD 40x Ph2 ADM air objective and analyzed with Imaris software for 3D colocalization of the top 10% brightest voxels per channel.

2.2.21 Anti-TRAIL ELISA

Anti-TRAIL ELISA was performed using a Human TRAIL/TNFSF10 Quantikine ELISA Kit (R&D Systems, DTRL00) following manufacturer-provided protocols. Briefly, 50 mL of cell supernatant or cellular lysate obtained using manufacturer provided buffers and instructions were added to each well. Cell densities at time of harvesting were 8×10^6 to 1.2×10^7 PEL cells, while cells were lysed at a concentration of 1×10^7 cells/mL as per manufacturer guidelines. The included recombinant human TRAIL standard (R&D Systems, 892375) was serially diluted in 2-fold steps from 1000 to 15.6 pg/mL. Absorbance was read on a VICTOR Nivo Plate reader at 450 nm. A blank measurement taken from a well containing clean dilution buffer was subtracted from all other wells and least squares regression was performed on the measured values across all replicates to determine effective concentrations.

2.2.21 In vitro TRAIL treatment

BCBL-1/Cas9 cells transduced with pLenti SpBsmBI Guide Hygro (AAVS1 or TRAIL-R1 #1/2) were treated with the indicated serial dilutions of recombinant human TRAIL (Sigma-Aldrich, T9701) and absolute cell numbers were measured 24 hours later by flow cytometry as described above for cumulative growth curves.

2.2.22 Statistical analysis

Statistical testing/modeling was conducted in Python using SciPy 1.6.0 (simple t tests, one-way ANOVA) or Statsmodels 0.13.2 (ordinary least squares) unless otherwise indicated [244, 245]. Vertical bar graphs were generated using Prism 9.4.1 (GraphPad), all other figures were generated using Seaborn 0.11.2 [246]. For groups of tests with similar hypotheses, i.e. similar comparisons in the same figure panel, false-discovery rate (FDR)-adjusted p-values were calculated using the Benjamini-Hochberg procedure implemented in Statsmodels. For two-sample t-tests, equal variances were assumed. Specific tests are indicated in the figure legends. Full code for computational and statistical analyses was made available online on GitHub (<https://github.com/Gottwein-Lab>). A statement regarding sample sizes, handling outliers, justification of statistical test choices, and handling of multiple-hypotheses testing is included below.

A sample size of 3 was standard for all experiments as the phenotype associated with CFLAR is generally considered to be complete loss of viability. A few experiments include larger numbers of replicates. For instance, in Fig 3.4 all cell lines were tested in parallel, but BC-1 required a repeat as editing was incomplete. Similarly, for Fig 3.6 and 3.7 the initial establishment of vFLIP/vCyc shRNA depletion was performed in BC-3 2x on its own before extending to BCBL-1 for a third replicate. The experiment was later performed 3x in parallel for

all cell lines. A single replicate was excluded from Fig 3.4A for the BC-5 cell line on the basis of outlier status ($> 1.5 \times$ Tukey IQR). Further, the BC-5 cells were growing poorly in general during this replicate and no phenotype was observed for the positive control PSMD1. For the unique case of MAGeCK-RRA and the synthetic rescue screens, the library itself provides per-gene replication in the form of multiple sgRNAs, while biological replication was performed using orthogonal methods (sgRNA vs shRNAs) and systems (BCBL-1 vs BC-2).

Tests used for each figure are justified as appropriate for the data and question at hand. Continuous variables appear generally normal as needed for most tests. Standard deviation is shown for all figures alongside individual data points. The standard deviations generally appear similar. In cases where the variance may differ or the distribution is skewed, the resulting test statistics are already insignificant. Alternative testing methodologies using lower-powered tests would result in identical conclusions with similar p values. Visually shown through figures, with information related to tests reported in figure legends. Of relevance, the type I error rate (relating to significance) of the frequently used t-test is robust to distortions in the assumed distribution, though such distortions may lead to lower power (higher type II error) than expected for small effect sizes.

Further, multiple-hypothesis correction was performed on p-values on a per-experiment basis so that where multiple tests are performed relating to a single axis of experimentation, FDR-adjusted p-values are reported.

Chapter 3: Results

A partial version of this chapter has been published in Cell Death and Differentiation. CDD 30, 1221–1234 (2023).

CRISPR screens identify novel regulators of cFLIP dependency and ligand-independent, TRAIL-R1-mediated cell death

Neil Kuehnle, Scout Mask Osborne, Ziyuan Liang, Mark Manzano & Eva Gottwein

3.1 Viral protein expression is highly variable in PEL cells

I first examined the expression of human cFLIP and cyclin D2 and their viral homologs vFLIP and vCyc across 8 PEL cell lines and the KSHV-negative B cell line BJAB. As a control, I analyzed KSHV vIRF3, which is latently expressed in PEL cell lines from a distinct KSHV locus [63]. I observed comparable expression of the major isoforms of cFLIP, cyclin D2, and KSHV vIRF3 across the PEL cell lines (Fig. 3.1A). In contrast, vFLIP and vCyc expression varied greatly, with vFLIP expression detected only in BC-1 and BC-3. Importantly, these are the same two PEL cell lines shown to depend on NF-κB signaling genes in my previous study of cellular gene dependency in PEL cells (Fig. 3.1B) [65]. vCyc expression mirrored the expression of vFLIP, as expected due to their bicistronic expression [247], with the surprising exception of BC-2. Serial dilution of BC-3 lysates suggested that my Western protocol is sensitive enough to detect vFLIP and vCyc expression levels that are ~20-50 fold below those of BC-3 (Fig. 3.2). The observed patterns of vFLIP expression and NF-κB dependency are consistent with the published role of vFLIP in the activation of NF-κB survival signaling [199, 211, 213, 217, 248, 249], in the subset of PEL cell lines where vFLIP is expressed.

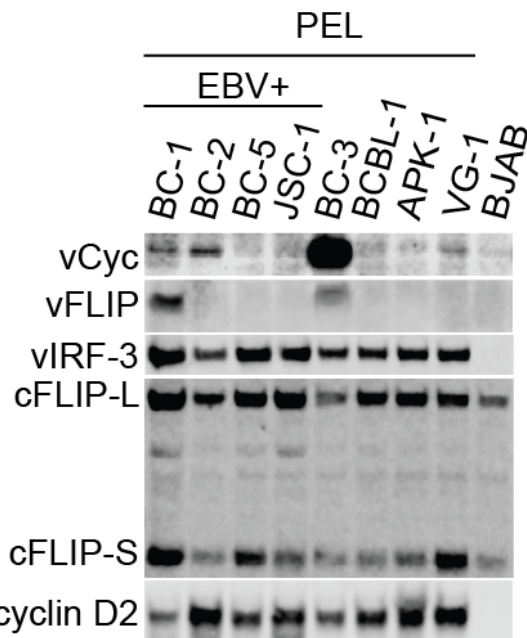
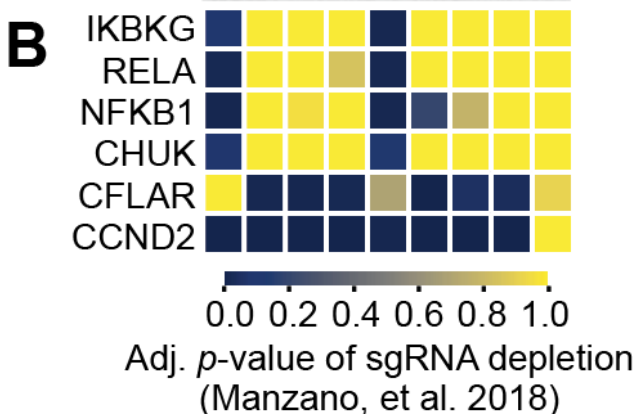
A**B**

Figure 3.1 Cellular and viral protein expression compared to cellular gene dependencies

A. Cell lysates from the indicated PEL cell lines or KSHV-negative BJAB cells were analyzed by western blotting for the indicated proteins. The cFLIP splice variants cFLIP-L and cFLIP-S are marked. **B.** Heatmap of depletion for sgRNAs targeting the indicated genes, using data from Manzano et al. (2018) [65]. Lower FDR-adjusted *p* values of depletion indicate significant sgRNA depletion in the screens, suggesting essential or fitness roles.

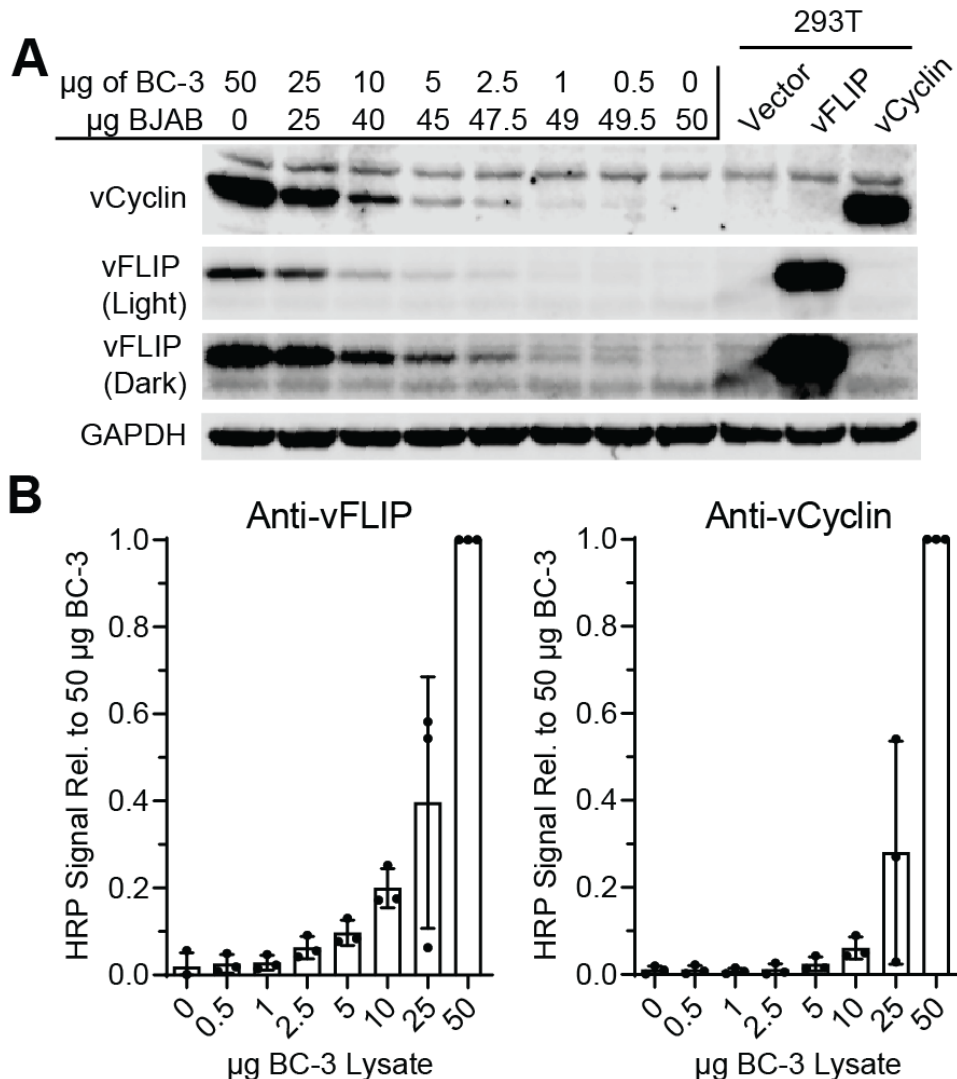


Figure 3.2 Quantitative titration of vCyc and vFLIP Western sensitivity

A. BC-3 and BJAB lysates were harvested, and the indicated amounts of proteins were mixed to achieve a total of 50 μg per lane. Lysates from 293T cells transfected with vCyc or vFLIP expression vectors were included as additional controls (n=3). **B.** Band intensity was quantified for independently harvested lysates, as in panel (A), via densitometry. Error bars indicate SD (n=3).

Further, I observed that vIL-6 levels were similarly varied in different PEL cell lines (Fig 3.3, unpublished), though in a manner that only corresponded weakly with genetic dependence on its purported target pathway (JAK-STAT signaling through IL6ST/STAT3) [165]. I noted that there is a weak, inverse association between vFLIP/NF-κB signatures and vIL-6/JAK-STAT signatures. While vIL-6 has been proposed as a potentially important gene in latently infected

PEL cells and significant functional redundancies between the NF-κB and JAK-STAT signaling pathways has been reported in the literatures, I chose to defer any examination of any potential cross-talk between these proteins and pathways to future studies due to the complex nature and the modest functional importance of some proteins and pathways involved (see section 3.3).

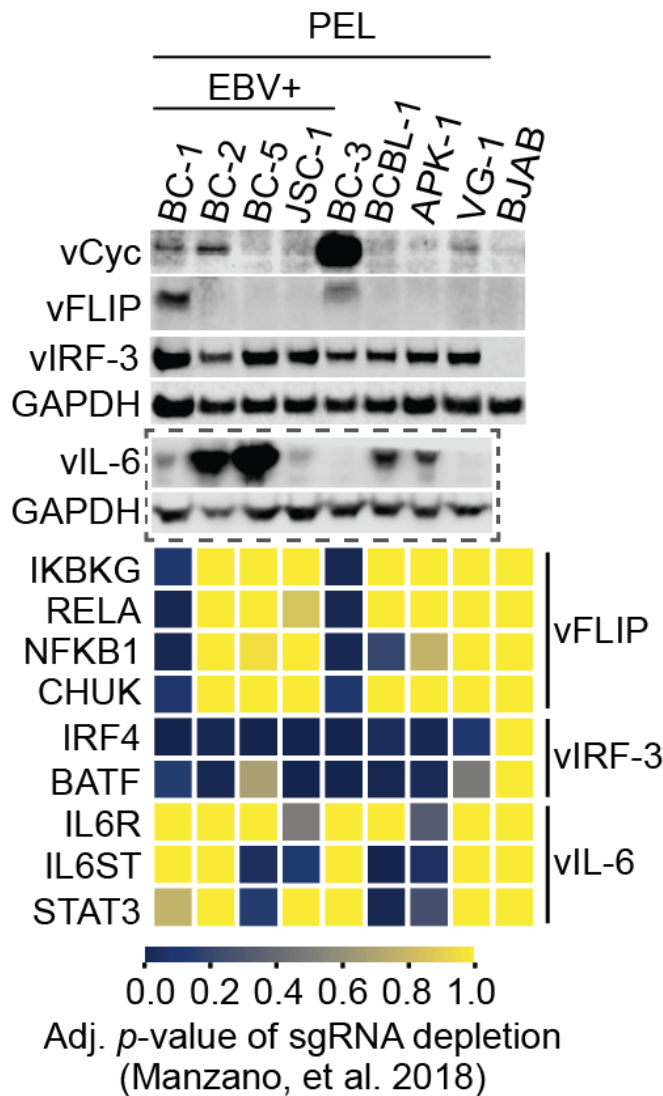


Figure 3.3 A broader view of viral protein expression and host gene dependencies associated with them.

A. Whole-cell lysates were prepared and plotted against **B.** gene-level sgRNA depletion data from Manzano et al. (2018) [65] as in Fig 3.1 but for an alternative set of genes. Westerns for vIL-6 (inside dashed box) represent distinct lysates and membranes from samples prepared for other viral proteins. Host genes associated with select viral genes are indicated at right in B.

3.2 cFLIP is broadly essential in PEL cell lines

We previously validated cFLIP dependency of the PEL cell line BCBL-1 [65]. To establish cFLIP dependency more broadly across PEL cell lines, I performed single guide RNA (sgRNA)-induced functional inactivation (KO) of cFLIP followed by cumulative growth curve analysis relative to an sgRNA that targets a safe harbor locus (sgAAVS1) in BCBL-1/Cas9 and 4 additional Cas9-expressing PEL cell lines (Fig. 3.4, A and B). sgRNAs against the proteasomal subunit PSMD1 and the transcription factor IRF4 served as positive controls for well-established essential genes in PEL cells. The cFLIP sgRNAs lack homology to vFLIP and did not affect vFLIP expression in BC-3 cells (Fig. 3.4C). For BC-1, which did not show significant depletion of cFLIP-specific sgRNAs in the published CRISPR KO screens (Fig. 3.1B, [65]), the experiment was done in a Cas9 cell clone with improved gene editing compared to the original cell pool [65]. Results showed that in addition to BCBL-1, BC-1, BC-2, and BC-5 require cFLIP for viability (Fig. 3.4, A and B). Thus, BC-1 was false negative for cFLIP dependency in the published original CRISPR screens [65]. In contrast, cFLIP single gene KO did not significantly affect the viability of BC-3 cells. Cell death following cFLIP KO in BCBL-1/Cas9 cells was rescued by lentiviral re-expression of either major cFLIP isoform (cFLIP-L and S; Fig. 3.5). These data collectively confirm that cFLIP is essential in the majority of PEL cell lines. The essentiality of cFLIP in BC-I furthermore suggests that expression of vFLIP may not be sufficient to overcome the requirement for cFLIP.

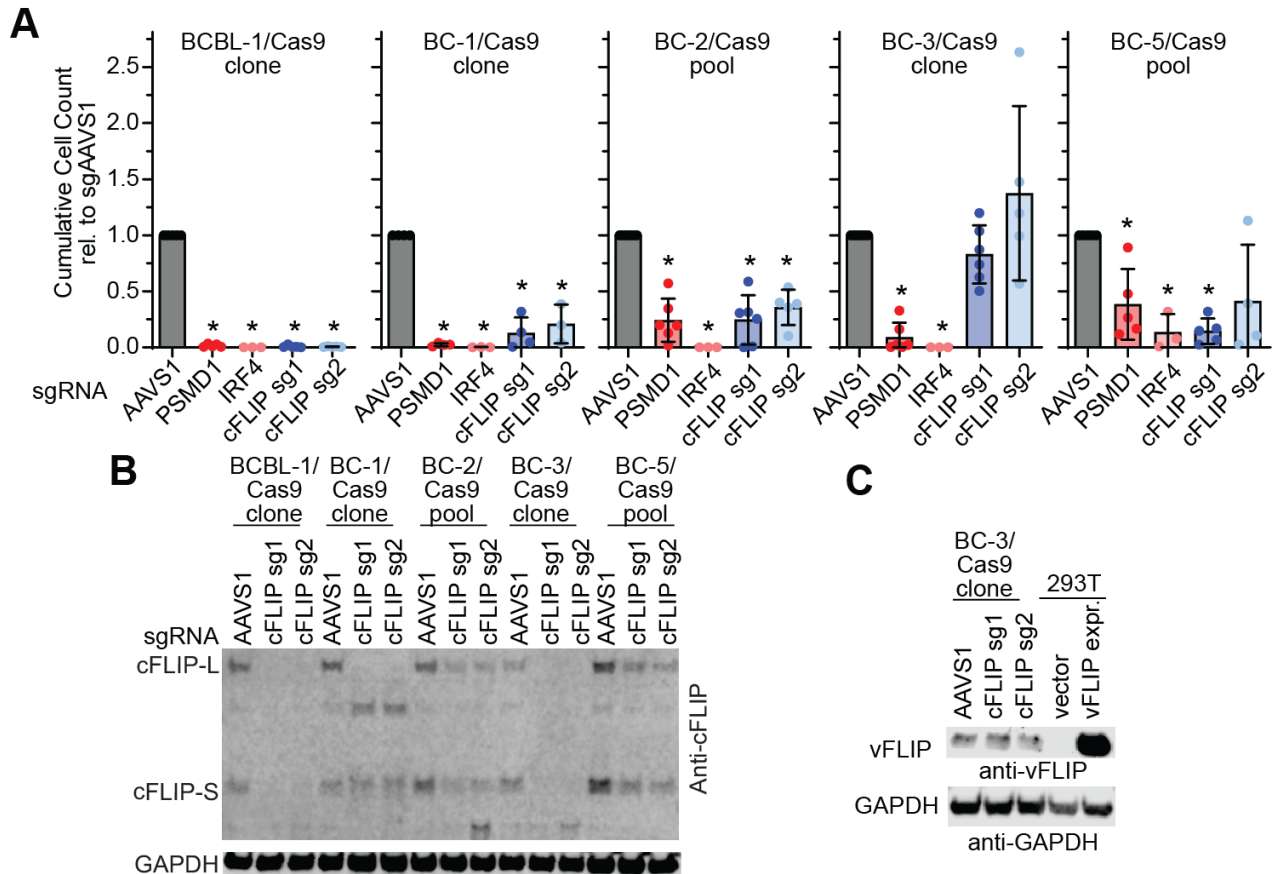


Figure 3.4 Validation of cFLIP dependence in PEL cell lines.

A. Cas9-expressing PEL cell lines were transduced with the indicated sgRNAs at MOI 3 and selected with puromycin. Graphs show the endpoints (days 8–10) of cumulative cell growth curves relative to an sgRNA targeting the safe harbor locus AA VS1 (see Material and methods). sgRNAs targeting PSMD1 and IRF4 are controls for other essential genes. Error bars represent SD ($n = 4$ –6 independent repeats). Statistical significance for loss of cell viability compared to sgAAVS1 was analyzed using one-sided, one-sample t-testing (* denotes FDR-adjusted $p \leq 0.05$), FDR-adjusted p values are listed in Appendix. **B.** Lysates were harvested on day 3 after transduction with the indicated sgRNAs during the cumulative growth curves in panel A and cFLIP Western blotting was performed to confirm KO efficiency ($n=3$). **C.** The lysates from BC-3 in panel B were also probed for vFLIP expression via Western blots ($n=2$).

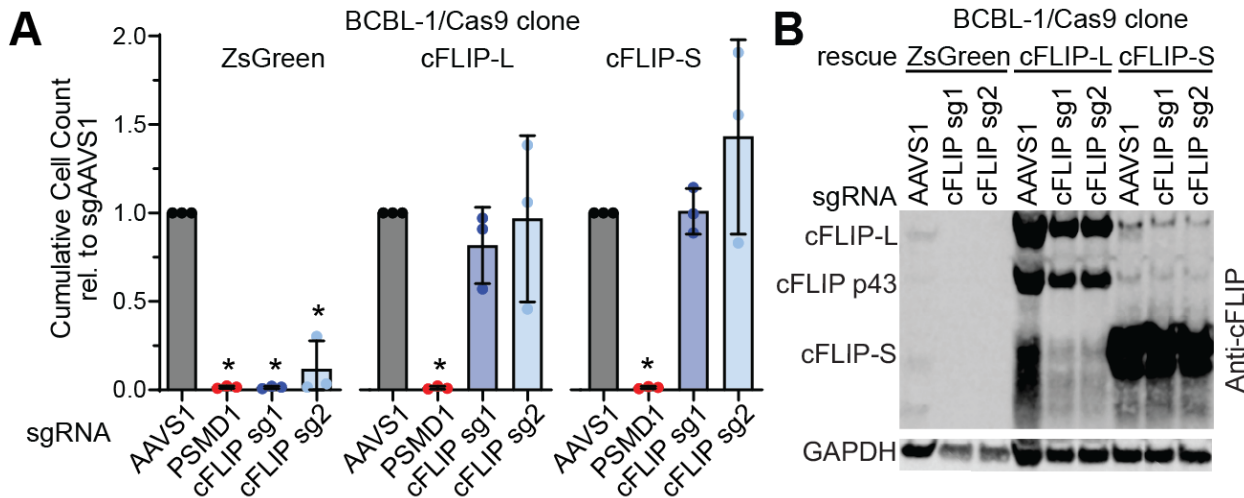


Figure 3.5 cFLIP KO is highly specific

BCBL-1/Cas9 expressing ZsGreen, sgRNA-resistant cFLIP-L, or sgRNA-resistant cFLIP-S were challenged with the indicated sgRNAs. Error bars represent SD ($n = 3$ independent repeats). Statistical significance for loss of cell viability compared to sgAAVS1 was analyzed using one-sided, one-sample t-testing (* denotes FDR-adjusted $p \leq 0.05$), FDR-adjusted p values are listed in Appendix. Rescue was significant as determined using a one-sided, independent two-sample t-test, with FDR-adjusted p values listed in Appendix.

3.3 Several PEL cell lines may not depend on vFLIP/vCyc

I next sought to determine whether vFLIP is similarly required for cellular proliferation and/or survival in PEL cells. As vFLIP is expressed from a single, bi-cistronic locus that also expresses vCyc, I targeted this transcript using lentiviral shRNAs, starting with BC-3 cells, where most studies involving vFLIP in the context of natural KSHV infection have been performed and both vFLIP and vCyc protein is detectable (Fig 3.1A). As expected and complementary to my screen observations that these cells depend on NF- κ B signaling, the known target pathway of vFLIP (Fig 3.1B), BC-3 cells depended on expression of vFLIP/vCyc (Fig 3.6A), though I note that KD was incomplete and apparently more efficient for vCyc (Fig 3.6B). Next, I extended my KD experiments to naïve parents of the cell lines shown in Fig 3.4.

Consistent with my observations of little to no expression of vFLIP and vCyc in BCBL-1, BC-2, and BC-5 (Fig 3.1A), none of these cell lines displayed strong reductions in cumulative cell counts following transduction with lentiviral vectors expressing vFLIP/vCyc shRNAs, compared to our sh-NT4 control (Fig 3.7). To my surprise, BC-1, which expresses detectable levels of vFLIP/vCyc approximately comparable to that of BC-3 (Fig 3.1A) also did not display a strong response to vFLIP/vCyc RNA interference (Fig 3.7), though confirmation of protein levels by Western blot was not performed in this case.

Lastly, to determine whether advanced passage impacted the response to vFLIP/vCyc shRNAs, I re-obtained BCBL-1 cell stocks from the AIDS Reagent Resource Center, which is ostensibly earlier passage than my existing BCBL-1 stocks (denoted BCBL-1 and BCBL-1 AIDS, respectively). Toxicity in response to vCyc/vFLIP shRNA transduction in BCBL-1 AIDS was not significant (Fig 3.8), nor were vFLIP or vCyc detectable in this alternative stock (data not shown).

Overall, these results serve as preliminary evidence that several human cultured PEL cell lines not only lack expression of vFLIP/vCyc but may not require their expression. However, several major technical and conceptual limitations remain, which lead us to urge caution in taking these results at face value (see Chapter 4: Discussion), which is why these data have not been submitted for formal publication as of the time of this dissertation.

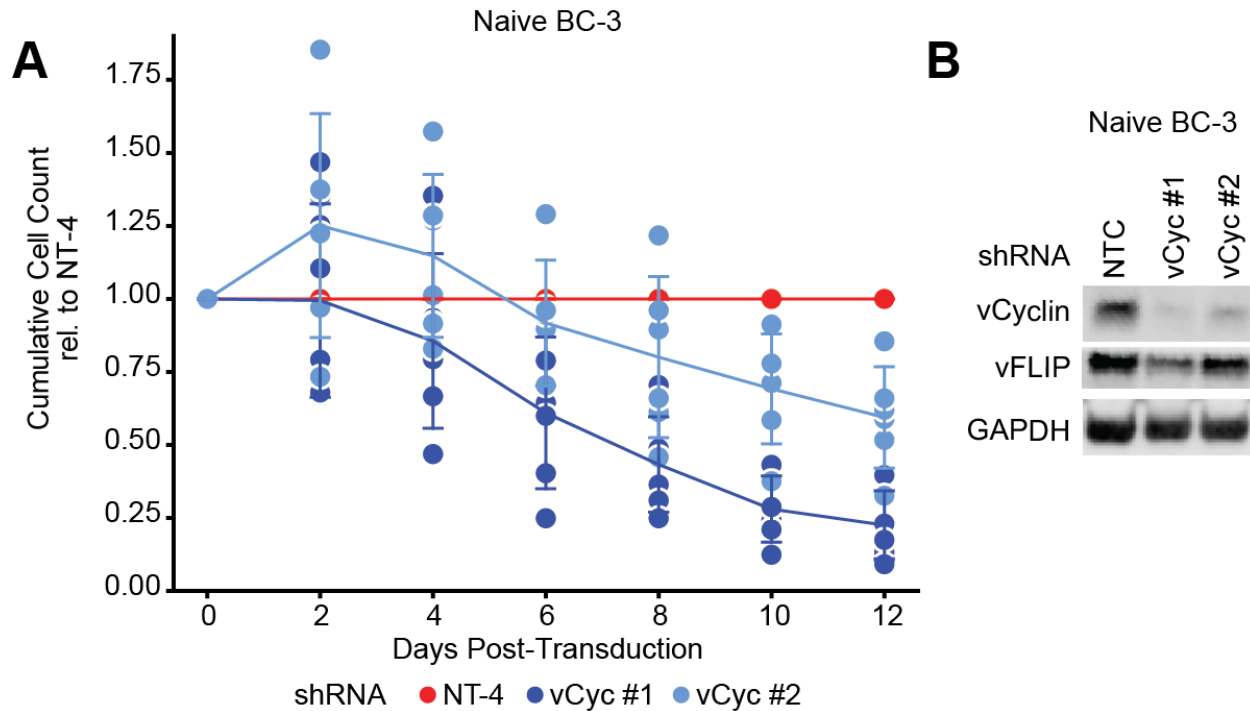


Figure 3.6 shRNAs targeting vFLIP/vCyc are toxic in BC-3 cells.

Naïve BC-3 cells were transduced with one of three shRNAs: NT-4 (non-targeting control) or one of two shRNAs directed against the vCyc portion of the vFLIP/vCyc transcript. **A.** Cumulative growth curve analysis following shRNA transduction. Error bars represent SD ($n=6$ independent repeats). **B.** Western blot confirmation of vCyc/vFLIP expression (vCyc $n=2$, vFLIP $n=1$; vCyc and vFLIP come from separate membranes, GAPDH matches to anti-vCyc; vFLIP antibody differs from that used throughout the rest of this paper). Both vCyc-directed shRNAs result in significant reductions in cell counts (see end-point statistics associated with Fig 3.7)

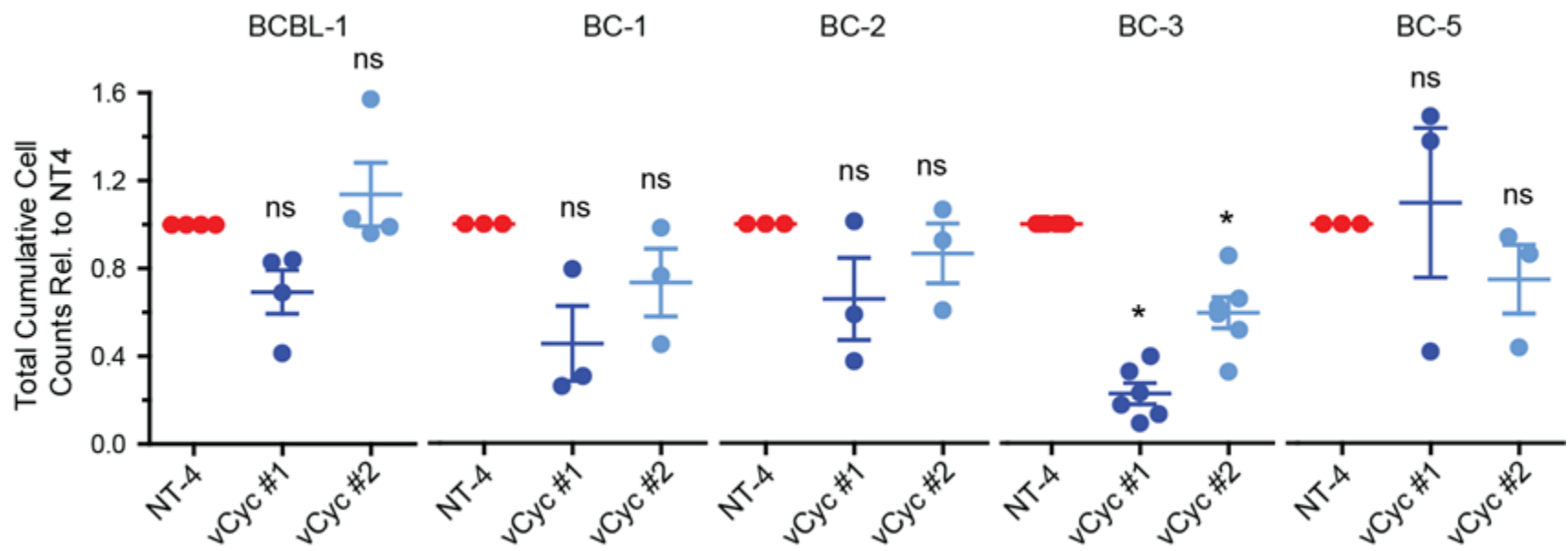


Figure 3.7 Most PEL cell lines have limited response to vFLIP/vCyc shRNAs

Naïve PEL cells were transduced with lentiviral vectors expressing the indicated shRNAs as in Fig 3.6 for BC-3. Data represent endpoints of cumulative growth curve analyses (12-14 days after transduction). Full time-course shown for BC-3 in Fig 3.6 and BCBL-1 in Fig. 3.8. Error bars represent SD ($n = 3-6$ independent repeats). Statistical significance for loss of cell viability compared to shNT-4 was analyzed using one-sided, one-sample t-testing (* denotes FDR-adjusted $p \leq 0.05$, ns $< .05$), FDR-adjusted p values are listed in Appendix.

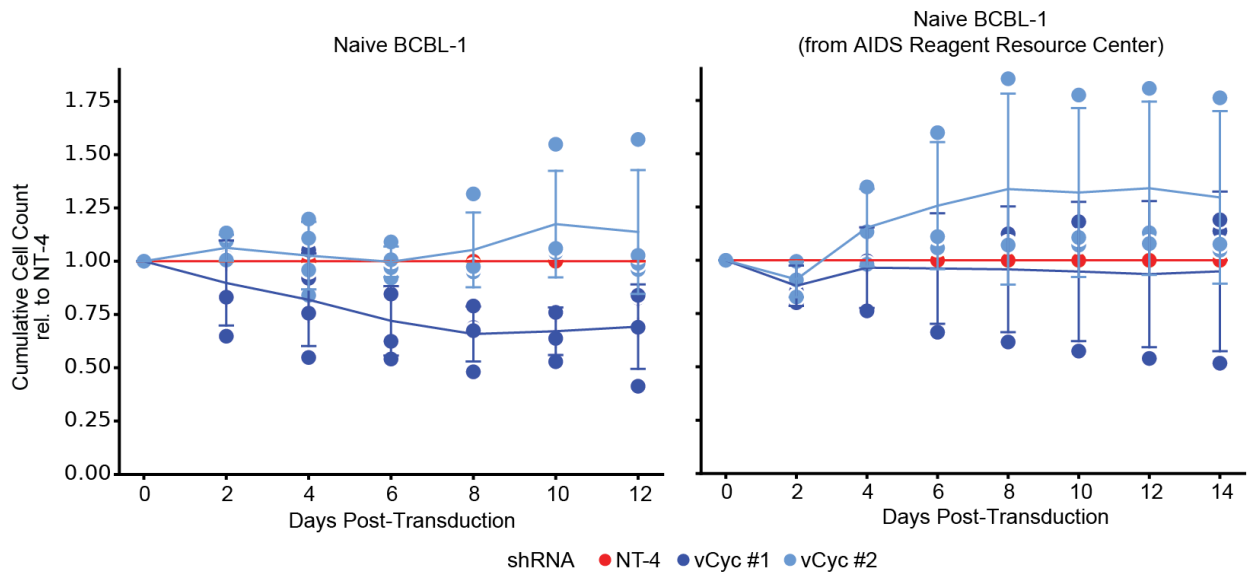


Figure 3.8 Putative early passage BCBL-1 are no more sensitive than previously tested stocks

Naïve BCBL-1 cells of differing provenance were transduced with lentiviruses expressing the indicated shRNAs as in previous figures. Naïve BCBL-1 at left represent the full time-course analysis of data presented in Fig 3.6. At right are Naïve BCBL-1 which were re-obtained from the NIH's AIDS Reagent Resource Center, likely representing the earliest passage of BCBL-1 cells available. Only vCyc sh-1 demonstrated significant toxicity in my exiting BCBL-1 stocks, while neither shRNA demonstrated toxicity in BCBL-1 from the AIDS Reagent Resource Center, when compared to sh-NT4.

3.4 cFLIP and vFLIP have distinct roles in PEL cell lines

To further investigate whether vFLIP and cFLIP are redundant, I tested if KSHV vFLIP can rescue cells from cell death after cFLIP KO. I additionally tested the viral FLIP proteins encoded by molluscum contagiosum virus (MCV), MC159L or MC160L, given that KSHV vFLIP and MCV MC159L and MC160L each have distinct functional activities (Fig. 1.5). While either major isoform of cFLIP can inhibit CASP8 and activate NF-κB signaling in ectopic contexts [212, 214-216], reports of KSHV vFLIP's ability to strongly inhibit CASP8 are mixed or ambiguous. Conversely, MCV MC159L and MC160L both repress NF-κB signaling and only

MC159L inhibits CASP8 [191, 195, 218, 219]. Thus, this approach allows us to assess the redundancy of vFLIP with cFLIP and the importance of NF- κ B activation and CASP8 inhibition for cFLIP dependency.

Interestingly, I observed only partial rescue of cFLIP dependency after overexpression of KSHV vFLIP (Fig 3.9, A & B). In contrast, overexpression of MC159L conferred complete rescue, while overexpression of MC160L had no effect (Fig 3.9, A). Expression of each of the viral FLIP proteins was comparable to overexpressed cFLIP and did not affect the expression of endogenous cFLIP (Fig 3.10 A & B). KSHV vFLIP was furthermore overexpressed well above levels of the endogenous viral protein in BC-3 (Fig 3.10, C). Thus, the inability of vFLIP to efficiently rescue cFLIP expression is not due to lower expression relative to cFLIP or endogenous vFLIP. Collectively, these results suggest that FLIP proteins that are known potent inhibitors of CASP8 (cFLIP and MC159L), but not KSHV vFLIP, can efficiently rescue cFLIP dependency in PEL cells. Therefore, the essential role of cFLIP in PEL cells is substantially distinct from that of vFLIP.

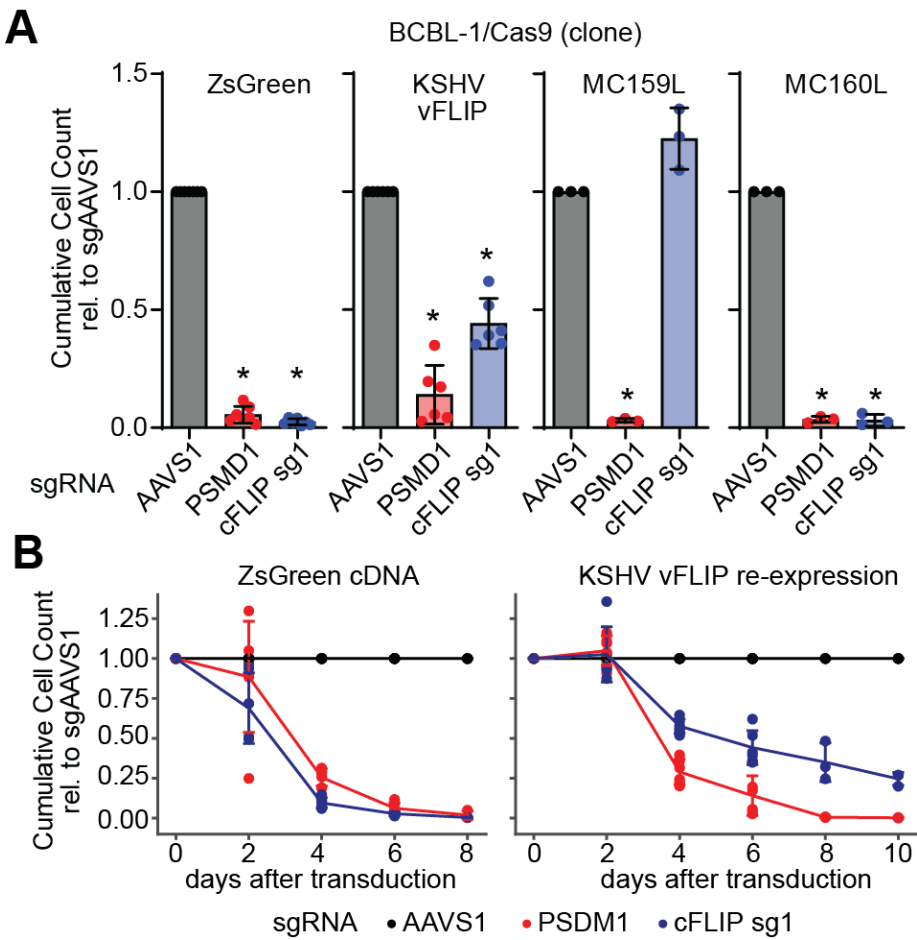


Figure 3.9 cFLIP and KSHV vFLIP are functionally distinct in PEL cell lines.

A. BCBL-1/Cas9 expressing ZsGreen, KSHV vFLIP, MCV MC159L, or MCV MC160L were challenged with the indicated sgRNAs. Analyses of cumulative growth curve experiments on day 6 after sgRNA transduction are shown. Error bars represent SD ($n = 3$ independent repeats). Statistical significance for loss of cell viability compared to sgAAVS1 was analyzed using one-sided, one-sample t-testing (* denotes FDR-adjusted $p \leq 0.05$). Rescue by expression of KSHV vFLIP and MCL159L was significant as determined using a one-sided, independent two-sample t-test. FDR-adjusted p values are listed in Appendix. **B.** Extended growth curves for the ZsGreen and KSHV vFLIP data in panel B show that vFLIP rescue is significant, but not efficient. For details on statistical analysis see Appendix and the Material and methods section.

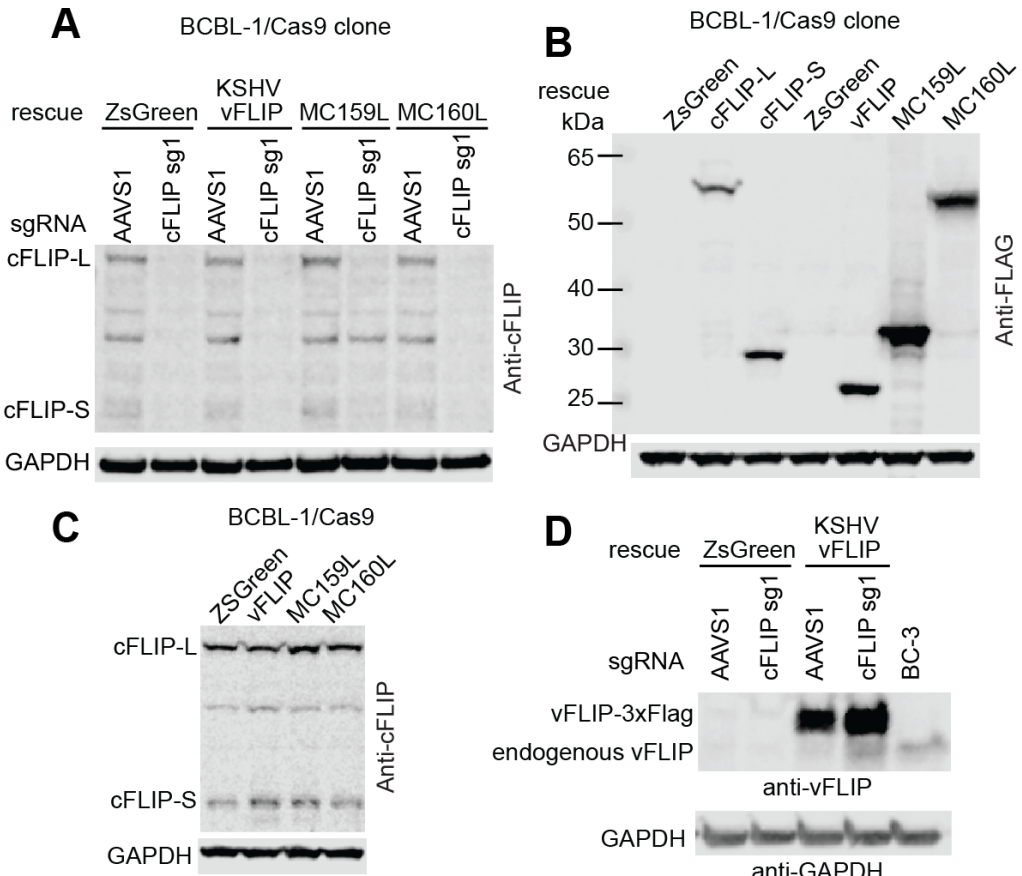


Figure 3.10 Viral FLIP ectopic expression

BCBL1/Cas9 cells were transduced with lentiviral vectors encoding the indicated viral or cellular FLIPs or the ZsGreen control. Lysates were harvested and subjected to Western blot analysis of **A.** total FLAG epitope levels to facilitate comparison of overall expression levels of the various FLIP proteins and **B.** endogenous cellular FLIP levels (n=1).

3.5 Partial rescue of cFLIP requirement by vFLIP may be mediated by NF- κ B signaling

As mentioned above, vFLIP has primarily been linked to activation of the NF- κ B signaling pathway, with conflicting reports on its ability to directly inhibit CASP8 activity. The partial rescue of the requirement for cFLIP by overexpression of vFLIP suggests that either vFLIP is not able to inhibit CASP8 in PEL cells or that it does so very inefficiently. An alternative mechanism by which vFLIP might promote survival in the absence of cFLIP is

through the creation of a pro-survival milieu of proteins. Such activity has been well-established for NF-κB and includes several anti-apoptotic targets, including cFLIP itself [250-252]. If this were the case, then a vFLIP lacking pro-NF-κB activity would fail to rescue cFLIP activity.

To test this, I generated a mutant vFLIP construct based on the published crystal structures of vFLIP with NEMO and that of MC159L. In these crystal structures, a short, N-terminal region outside of the DEDS required for mediate CASP8 interactions of vFLIP and MC159L distinguishes their capacity to interact with NEMO. Therefore, the matching region in MC159L was substituted for the corresponding portion of vFLIP and the resulting protein was expressed in BCBL-1 as previously. Compared to expression of WT vFLIP, the mutant vFLIP demonstrated no detectable rescue of subsequent cFLIP KO (Fig. 3.11A).

This finding is consistent with the idea that vFLIP mediates partial rescue of cFLIP activity by activating NF-κB signaling, though we note that this result is preliminary, due to unequal expression of WT and mutant vFLIP and validation of the expected activities of these proteins (Fig 3.11B). Further discussion of these limitations and potential follow-up experiments are described in Chapter 4: Discussion.

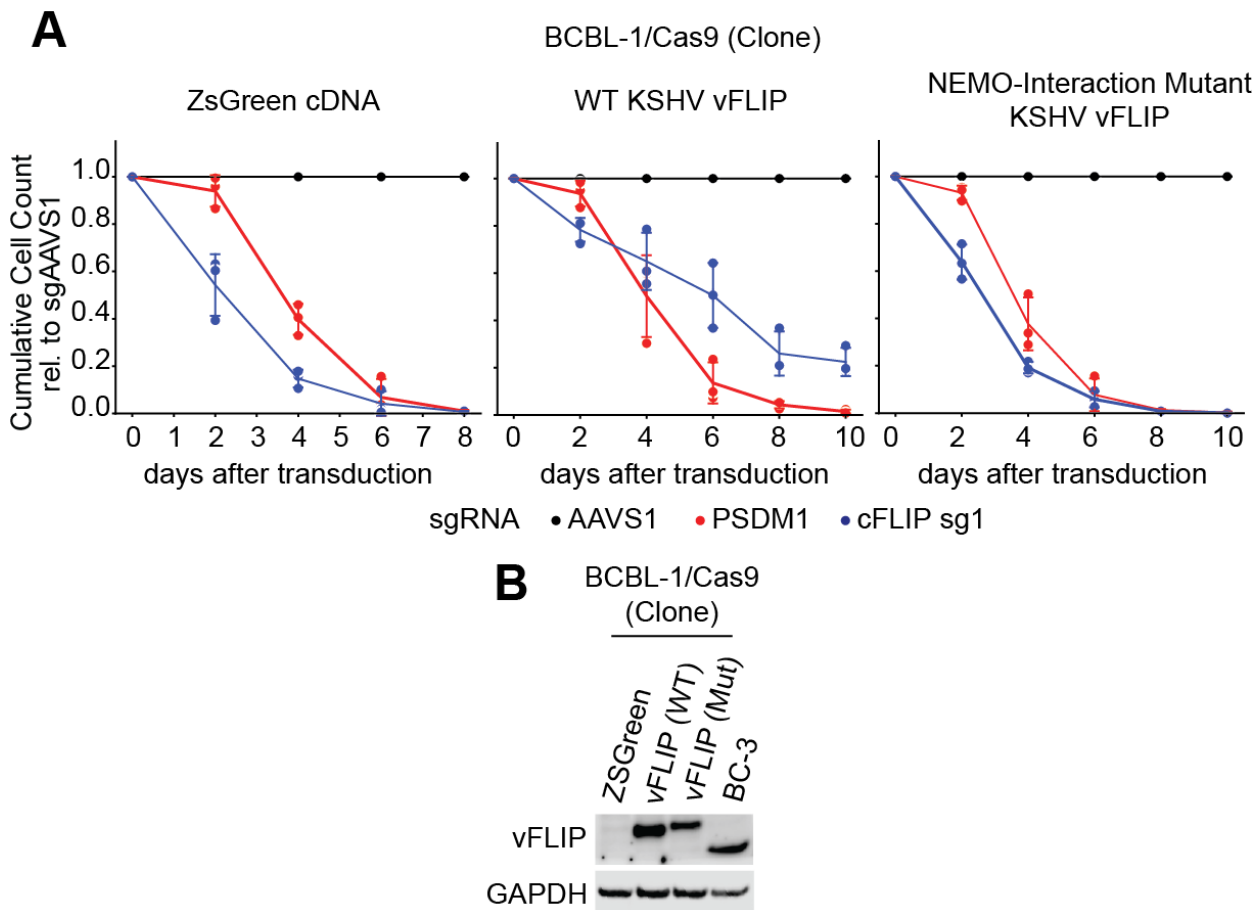


Figure 3.11 Partial rescue of cFLIP by vFLIP may be mediated by NF-κB signaling

BCBL-1/Cas9 cells were transduced with ZsGreen, WT KSHV vFLIP or a vFLIP construct in which the IKK-interacting region was swapped with the equivalent region of MC159L and growth curve analysis was performed as previously. **A.** Extended growth curves for these cell lines shows that WT vFLIP rescue is significant, but not efficient as in Fig 3.9B, while IKK-interaction mutant vFLIP lacks cFLIP rescue altogether (PSMD1 and cFLIP sg1 in all cell lines are significantly depleted relative to AAVS1). For details on statistical analysis see Appendix and the Material and methods section (n=3). **B.** Cell lysates were harvested from each cell line indicated in panel A and a Western blot for vFLIP was performed (n=1). Confirmation of cFLIP levels after sgRNA transduction was not conducted for this experiment.

3.6 Genome-wide rescue screens uncover an ER/Golgi/CASP8-dependent death signaling program repressed by cFLIP

cFLIP has a well-characterized role in protecting cells from the effects of cell death ligands of the extrinsic apoptosis pathway [153, 192]. Indeed, EBV-immortalized LCLs depend on cFLIP expression for protection from autocrine TNF α signaling [177]. However, TNF α is not expressed in PEL cell lines (Fig. 3.12).

I therefore sought to identify mechanisms underlying cFLIP dependency of PEL cell lines in genome-wide CRISPR/Cas9 rescue screens, outlined in Fig. 2.1. In these screens, sgRNAs targeting genes whose inactivation overcomes cFLIP dependency should be enriched after toxic cFLIP inactivation and may represent putative components of the cell death process that is inhibited by cFLIP in PEL cells. I initially chose the background of BCBL-1/Cas9, which has strong cFLIP dependency and excellent CRISPR/Cas9 editing efficiency. Briefly, I transduced BCBL-1/Cas9 with the genome-wide Brunello sgRNA library [253] and passaged the cell population to allow dropout of sgRNAs targeting essential genes. I next challenged the resulting cell pool with another sgRNA vector targeting either cFLIP or the AAVS1 safe harbor locus and further passaged the culture until a cFLIP-sgRNA resistant population was obtained (Fig. 3.13A). In an independent experiment performed with Eva Gottwein, we used three separate shRNAs for toxic cFLIP knock-down alongside two negative control shRNAs targeting Renilla luciferase (RLuc) (Fig. 3.13B). I finally repeated the sg-cFLIP resistance screen in BC-2, which has robust cFLIP dependency (Fig. 3.1B, 3.4). In each case, resulting cell pools were subjected to next generation sequencing of the Brunello sgRNA inserts and sgRNA composition was analyzed using MAGeCK's robust ranked aggregation (RRA), see Electronic Supplement Table 1 for full output (Supplementary Table 1 in [174]). Independent shRNAs targeting either cFLIP or RLuc were treated as replicates in this analysis.

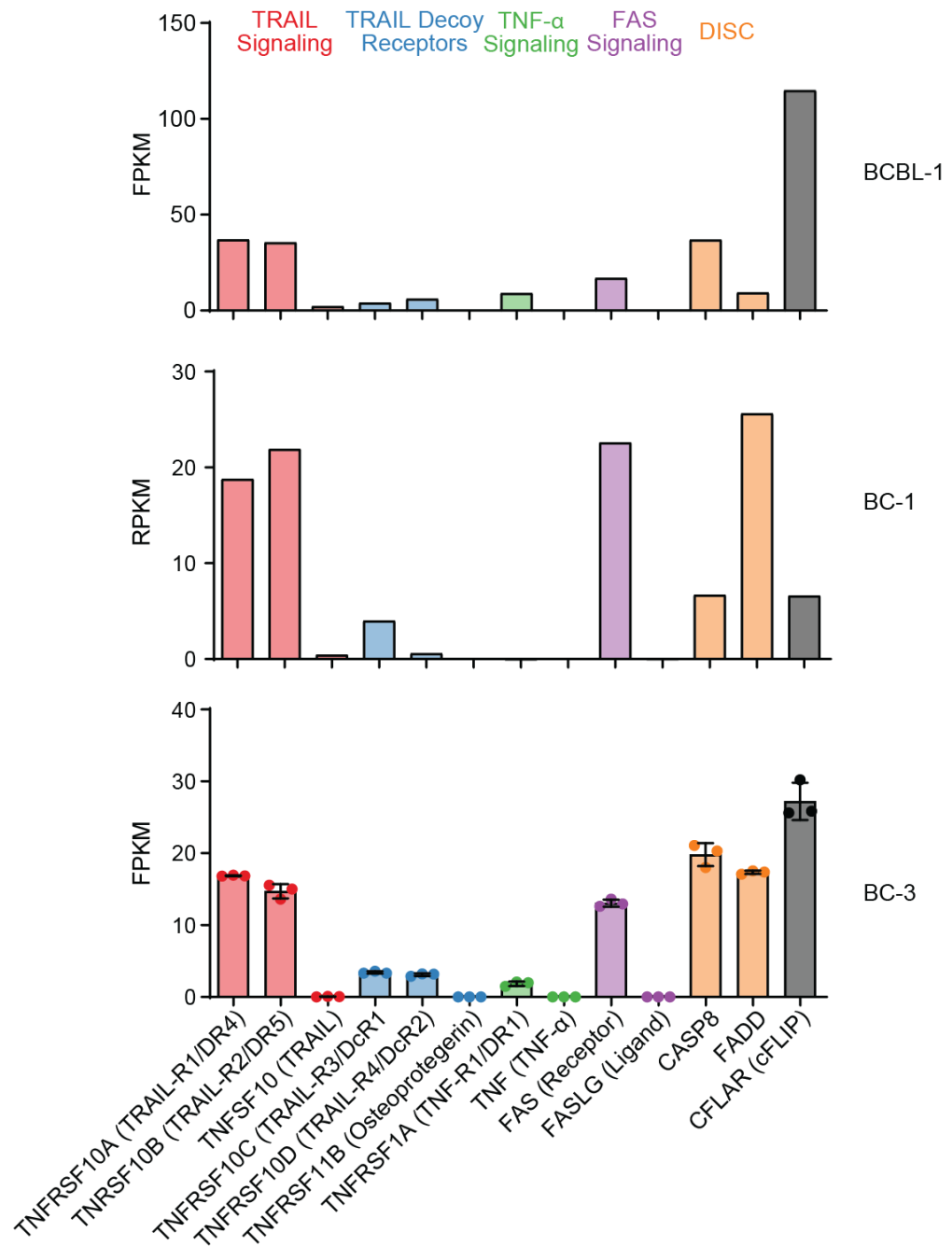


Figure 3.12 Quantification of mRNA levels for selected death signaling genes.

Reads or fragments per kilobase per million were calculated for the three PEL cell lines indicated. Data for BC-3 and BCBL-1 were obtained from datasets previously published by us and others, while my BC-1 data represent new data. RPKM is shown for single-ended sequencing data, while FPKM is shown for paired-end data. For BC-3, error bars indicate SD ($n=3$, samples harvested side-by-side). I note that BCBL-1 represented a DMSO treated control.

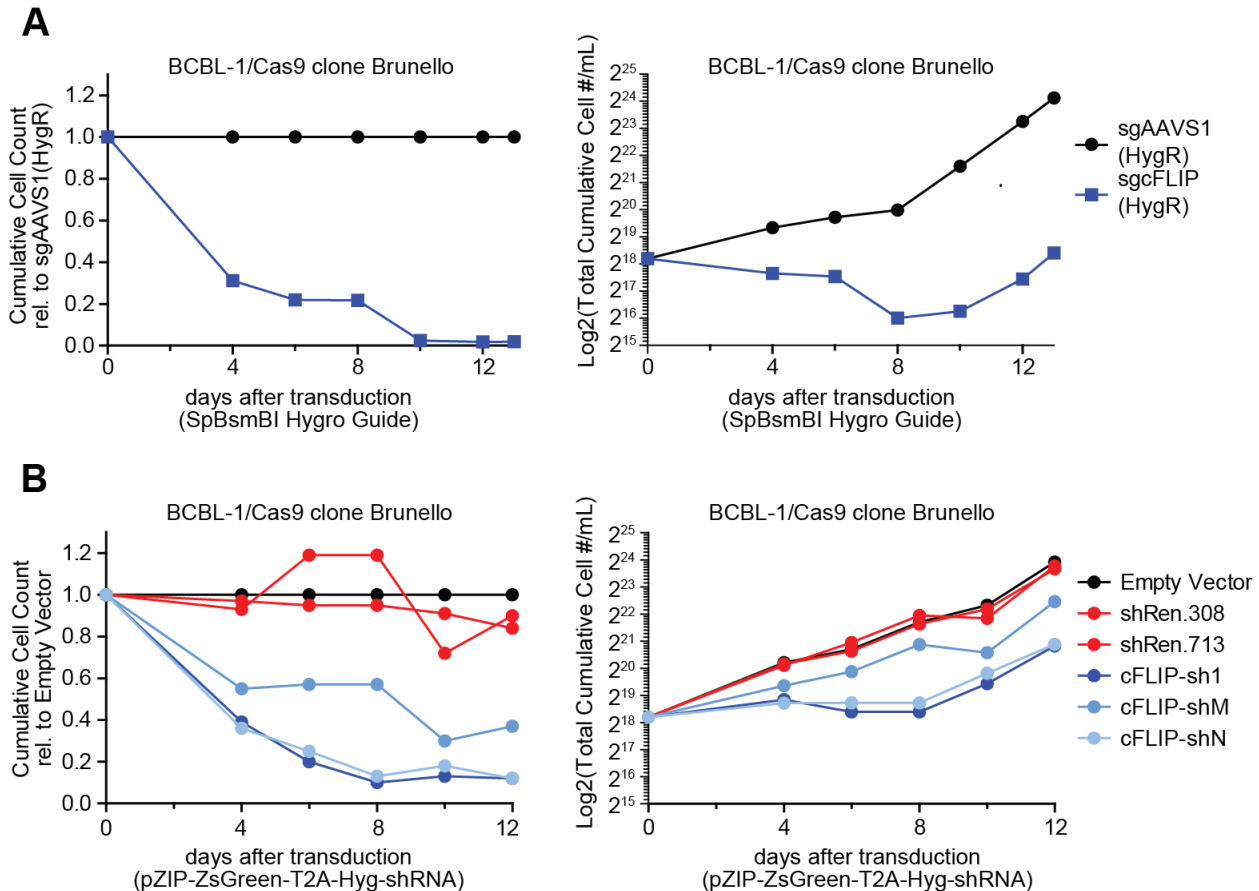


Figure 3.13 Cumulative growth curve analysis of genome-wide synthetic rescue screens.

BCBL-1/Cas9 cells were transduced with the lentiviral sgRNA library Brunello, followed by the indicated **A.** sgRNA or **B.** shRNA constructs. Cumulative cell counts relative to the appropriate control (left) or log₂-transformed raw cumulative counts (right) are shown starting on the day of the secondary transduction (sgRNA/shRNA challenge).

Results from the BCBL-1/Cas9 screens were more robust than those from the BC-2 screen, which was noisy, most likely due to relatively poor editing in the BC-2 Cas9 cell pool (Fig. 3.14). Within BCBL-1, top hits from the shRNA-based challenge were statistically more significant but had less dramatic sgRNA fold-changes (Fig. 3.14). This is likely due to the inclusion of three different shRNAs targeting cFLIP, each resulting in less complete toxicity than the single highly efficient cFLIP sgRNA (Fig. 3.13).

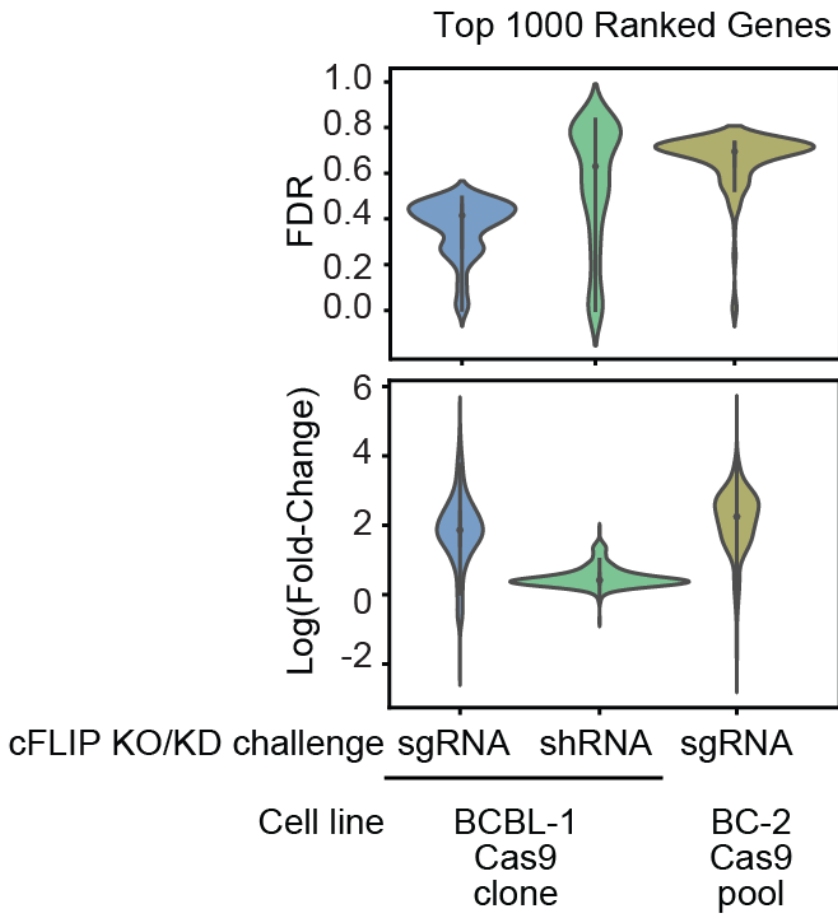


Figure 3.14 Distribution of statistical outputs of MAGeCK-RRA analysis by cell line and challenge mode.

The top 1000 ranked genes for each screen were selected by MAGeCK/RRA-rank. The FDR and log₂-transformed fold-change values for these genes were then plotted with inter-quartile range (solid line) and Gaussian kernel density estimates (colored contours)

To account for these differences, I initially compared the BCBL-1 sgRNA and shRNA screens using a rank-based filtering approach. Intersecting the top 150 hits by RRA score from the sgRNA and shRNA challenge in BCBL-1 yielded 23 high-confidence hits (Fig. 3.15, Table 3.1).

		BCBL1 sgCFLIP Resistance			BCBL1 shCFLIP Resistance			BC2 sgCFLIP Resistance			Manzano NatComm 2018	DepMap Achilles+SCORE 2022 Q2			
		Gene Symbol	Function	pos fdr	pos ra nk	pos lfc	pos fdr	pos r ank	pos lfc	pos fdr	pos ra nk	pos lfc	median_neg fdr (8 PEL)	common_essential	strongly_selective
B3GAT3	chondroitin sulfate proteoglycan synthesis	0.03795	20	3.409	0.00017	9	1.36	0.8054	1157	1.7195	0.9999995				0.10589319
B4GALT7	chondroitin sulfate proteoglycan synthesis	0.02444	14	4.178	0.00017	23	1.2107	0.63328	107	3.0463	0.9999995				0.02117864
C1orf27	UFMylation	0.14731	42	3.503	0.00017	27	1.1024	0.97036	6000	0.3512	1				0.32320442
CASP8	extrinsic apoptosis	0.02094	12	4.226	0.00017	17	1.3963	0.56323	67	2.5001	0.9999995				0.00184162
CHST15	chondroitin sulfate proteoglycan synthesis	0.27567	99	2.745	0.00017	12	1.1222	0.24105	13	3.6511	0.999999		X	0	
CSGALN ACT1	chondroitin sulfate proteoglycan synthesis	0.00495	9	3.528	0.00017	1	1.3095	0.54821	59	2.1474	0.9999995				0
CXCR4	chemokine receptor	0.00495	6	3.564	0.00017	5	1.4739	0.76581	689	1.2947	0.9999995				0
DDRGK1	UFMylation	0.02592	17	3.418	0.00017	15	0.9595	0.74286	577	2.2294	0.9999985				0.11970534
EHMT2	histone methyltransferase	0.34285	148	2.103	0.07912	56	0.7498	1	17528	-0.58684	0.2617265		X		0.58839779
FADD	extrinsic apoptosis	0.00165	1	4.414	0.00017	13	1.5083	0.98429	6895	0.84003	0.940138			X	0.14640884
JAGN1	secretory pathway	0.11634	35	3.12	0.00017	10	1.1634	0.7346	472	1.2025	0.9999995			X	0.00184162
PAPSS1	chondroitin sulfate proteoglycan synthesis	0.09947	33	3.192	0.00017	16	1.3388	0.69491	274	1.482	0.9999985				0
SLC35B2	chondroitin sulfate proteoglycan synthesis	0.21834	61	3.155	0.00017	28	1.1418	1	17126	-0.84156	0.9999985			X	0.18600368
SRP68	signal recognition particle	0.19707	44	2.604	0.13224	65	0.7029	0.93245	4450	0.62116	0.9017535		X		0.97513812
SRP72	signal recognition particle	0.27322	98	2.989	0.0043	38	0.8396	1	8266	-0.07394	0.267373		X		0.99723757
TNFRSF1 0A	extrinsic apoptosis	0.00495	5	3.67	0.00017	4	1.303	0.63328	137	0.37977	0.9999985				0
UBA5	UFMylation	0.00165	2	4.385	0.00017	8	1.4911	0.00495	5	3.8924	0.999998				0.50276243
UFC1	UFMylation	0.00165	3	3.711	0.00017	29	1.1558	0.97468	6388	-1.101	0.9999985				0.38489871
UFL1	UFMylation	0.41513	249	2.801	0.00077	32	0.9737	0.91289	3762	1.1216	0.9999985				0.38581952
UFM1	UFMylation	0.00495	8	3.855	0.00017	20	1.3525	0.78231	992	0.90844	0.999998				0.52854512
UFSP2	UFMylation	0.00495	4	4.01	0.00017	19	1.2999	0.47842	39	2.7552	0.999999				0.09668508
UGDH	chondroitin sulfate proteoglycan synthesis	0.13963	39	3.207	0.00017	25	1.0046	0.82426	1490	1.6431	0.9999995				0.0092081
UXS1	chondroitin sulfate proteoglycan synthesis	0.04435	22	3.602	0.00017	2	1.3216	0.56323	66	2.2005	0.9999955		X		0.23756906
XYLT2	chondroitin sulfate proteoglycan synthesis	0.00545	10	3.715	0.00017	7	1.3272	0.69491	197	1.7435	0.85343			X	0.24217311

Table 3.1 cFLIP Rescue Screen Hits

Data for the intersection of the top 150 ranked genes in both BCBL-1 screens (plus UFL1, which narrowly misses this cutoff in our BCBL-1 sg-cFLIP resistance screen) are shown. Rows in blue, yellow, and green are key metrics for the indicated synthetic rescue screens. The red-orange column represents median FDR in our original PEL genes as an indication of PEL cell dependencies. Rows in grey are data from the Q2 2022 DepMap release indicating how frequently cells depend on each target.

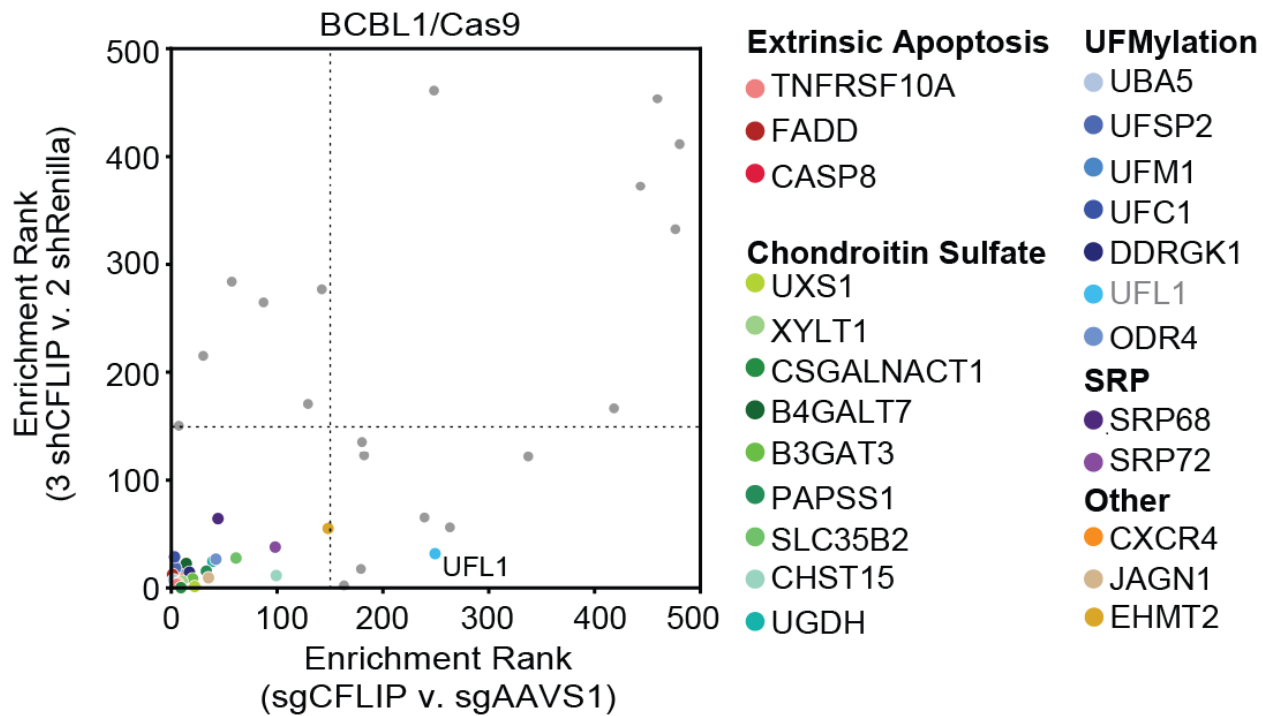


Figure 3.15 Genome-wide synthetic rescue screens implicate 23 common genes in cFLIP dependency in BCBL-1 cells.

Results of the BCBL-1 resistance screens. Shown are the gene-level ranks output by MAGeCK-RRA based on library sgRNA enrichment after the toxic cFLIP shRNA challenge (y-axis) or the toxic cFLIP sgRNA challenge (x-axis) relative to matched negative control perturbations. For clarity, only the top 500 hits in each screen are displayed. Gene names are indicated at the right and grouped/colored by common pathway/complex where possible. UFL1 was highlighted as a UFMylation pathway gene but does not pass my analysis cutoff. Schematics of known biological processes represented can be found in Figs. 3.17 to 3.19.

DAVID pathway analysis [254] shows that these high confidence hits function in three main pathways (Table S3, Fig. 3.16): the extrinsic apoptosis pathway (including CASP8, FADD, and TNFRSF10A, encoding TRAIL receptor 1, Fig. 3.17), protein modification by the ubiquitin-like modifier UFM1 (UFMylation, Fig. 3.18), and chondroitin sulfate proteoglycan synthesis (Fig. 3.19). Hits were furthermore enriched for genes associated with the ER and Golgi cellular compartments (Fig. 3.16). Specifically, TRAIL-R1 and CXCR4 are transmembrane

receptors which traffic through the ER-Golgi network. The UFMylation pathway mediates ubiquitin-fold modified 1 (UFM1) conjugation to lysine residues of target proteins at the cytoplasmic surface of the membrane [255-261]. SRP68 and SRP72 are components of the signal recognition peptide (SRP) complex, which cooperates with the SEC61A translocon to aid insertion of nascent transmembrane proteins into the ER (3.18) [262-264]. The SRP is involved in translational halting during membrane insertion [264, 265]. ER translocation of translationally paused nascent peptides requires UFMylation of the 60S ribosomal protein L26 (RPL26), which has been proposed as the primary target of UFM1 modification [266, 267]. Nine of the 23 high confidence hits participate in the chondroitin sulfate proteoglycan synthesis pathway (Fig. 3.15 and 3.19), a process that occurs in the Golgi apparatus and involves the addition of chondroitin sulfate moieties to transmembrane proteins [268]. Jagunal homolog 1 (JAGN1) is required for vesicular transport from the ER or Golgi, although the exact step JAGN1 participates in is unclear [269]. Lastly, EHMT2 is a histone methyltransferase which has been implicated in the epigenetic regulation of the UPR and/or ER homeostasis [270, 271]. A subset of these genes also scored in the top 150 hits of the BC-2 screen, including CASP8 and TNFRSF10A (extrinsic apoptosis), UBA5 and UFSP2 (UFMylation), and UXS1, B4GALT7, CHST15, CSGALNACT1 (chondroitin sulfate proteoglycan synthesis), thereby confirming these genetic interactions of cFLIP in a second PEL cell line (Tables S1 and S2).

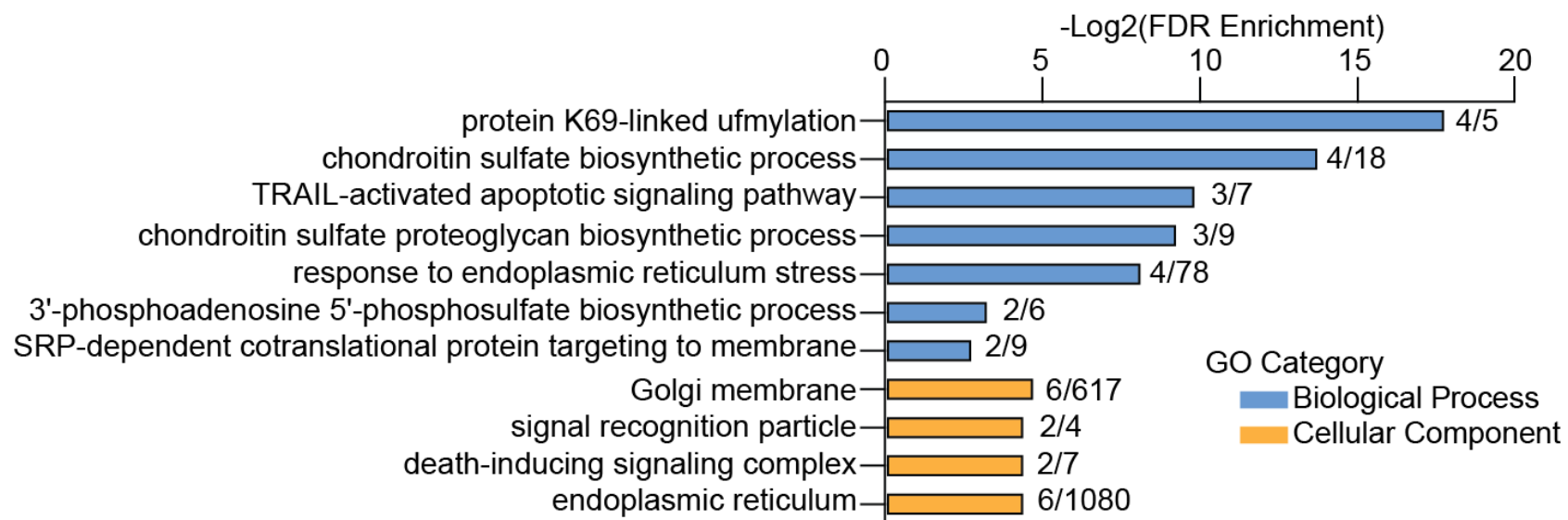


Figure 3.16 cFLIP synthetic rescue screens are enriched for ER/Golgi-associated processes and components.

DAVID pathway analysis of the 23 high confidence hits obtained by intersecting the top 150 hits each from the BCBL-1 sgRNA and shRNA screens. Numbers at right show number of hits from each pathway. For complete DAVID output, see Supplementary Table S3.

Term	Count	%	PValue	Genes	List Total	Pop Hits	Pop Total	Fold Enrichment	FDR	neglog2FDR
GO:1990592~protein K69-linked ufmylation	4	17.39	2.20E-08	UFM1, UFC1, UBA5, DDRGK1	23	5	16129	561.0086957	4.37E-06	17.803935
GO:0071569~protein ufmylation	4	17.39	4.39E-08	UFM1, UFC1, UBA5, DDRGK1	23	6	16129	467.5072464	4.37E-06	17.803935
GO:0033146~regulation of intracellular estrogen receptor signaling pathway	4	17.39	1.23E-07	UFM1, UFSP2, UBA5, DDRGK1	23	8	16129	350.6304348	8.15E-06	16.904769
GO:0061709~reticulophagy	4	17.39	6.24E-07	UFM1, UFC1, UBA5, DDRGK1	23	13	16129	215.7725753	3.11E-05	14.972726
GO:0030206~chondroitin sulfate biosynthetic process	4	17.39	1.77E-06	CSGALNACT1, UGDH, CHST15, XYLT2	23	18	16129	155.8357488	7.06E-05	13.789972
GO:0006024~glycosaminoglycan biosynthetic process	4	17.39	5.61E-06	FADD, B3GAT3, UGDH, XYLT2	23	26	16129	107.8862876	1.86E-04	12.392410
GO:0036462~TRAIL-activated apoptotic signaling pathway	3	13.04	3.71E-05	TNFRSF10A, CASP8, FADD	23	7	16129	300.5403727	0.001055924	9.887278
GO:0050650~chondroitin sulfate proteoglycan biosynthetic process	3	13.04	6.36E-05	CSGALNACT1, B3GAT3, XYLT2	23	9	16129	233.7536232	0.001581268	9.304702
GO:0034976~response to endoplasmic reticulum stress	4	17.39	1.57E-04	UFM1, UFC1, UBA5, DDRGK1	23	78	16129	35.96209588	0.003467397	8.171931
GO:0015012~heparan sulfate proteoglycan biosynthetic process	3	13.04	2.11E-04	B3GAT3, UGDH, XYLT2	23	16	16129	131.486413	0.004192386	7.898013
GO:0030166~proteoglycan biosynthetic process	3	13.04	3.67E-04	FADD, CSGALNACT1, XYLT2	23	21	16129	100.1801242	0.006642204	7.234122
GO:0008625~extrinsic apoptotic signaling pathway via death domain receptors	3	13.04	0.00108791	TNFRSF10A, CASP8, FADD	23	36	16129	58.4384058	0.018041174	5.792563
GO:0097191~extrinsic apoptotic signaling pathway	3	13.04	0.00225976	TNFRSF10A, CASP8, FADD	23	52	16129	40.45735786	0.034591712	4.853430
GO:0050651~dermatan sulfate proteoglycan biosynthetic process	2	8.696	0.004086682	CSGALNACT1, B3GAT3	23	3	16129	467.5072464	0.058089269	4.105585
GO:0071260~cellular response to mechanical stimulus	3	13.04	0.005920775	TNFRSF10A, CASP8, FADD	23	85	16129	24.75038363	0.078548951	3.670264
GO:0050428~3'-phosphoadenosine 5'-phosphosulfate biosynthetic process	2	8.696	0.00815742	SLC35B2, PAPSS1	23	6	16129	233.7536232	0.101457908	3.301047
GO:0006614~SRP-dependent cotranslational protein targeting to membrane	2	8.696	0.012212272	SRP68, SRP72	23	9	16129	155.8357488	0.142955415	2.806363
GO:0030203~glycosaminoglycan metabolic process	2	8.696	0.013560369	FADD, XYLT2	23	10	16129	140.2521739	0.149917413	2.737760
GO:0030210~heparin biosynthetic process	2	8.696	0.01490671	CSGALNACT1, XYLT2	23	11	16129	127.5019763	0.156128174	2.679197
GO:0048148~behavioral response to cocaine	2	8.696	0.020274555	EHMT2, FADD	23	15	16129	93.50144928	0.175665049	2.509101
GO:0060546~negative regulation of necroptotic process	2	8.696	0.020274555	CASP8, FADD	23	15	16129	93.50144928	0.175665049	2.509101
GO:0045651~positive regulation of macrophage differentiation	2	8.696	0.020274555	CASP8, FADD	23	15	16129	93.50144928	0.175665049	2.509101
GO:0005975~carbohydrate metabolic process	3	13.04	0.020302996	FADD, B3GAT3, UGDH	23	162	16129	12.9863124	0.175665049	2.509101
GO:0097202~activation of cysteine-type endopeptidase activity	2	8.696	0.025614472	CASP8, FADD	23	19	16129	73.81693364	0.206233683	2.277648
GO:0043123~positive regulation of I-kappaB kinase/NF-kappaB signaling	3	13.04	0.026790199	CASP8, SLC35B2, FADD	23	188	16129	11.19033302	0.206233683	2.277648
GO:0045862~positive regulation of proteolysis	2	8.696	0.026945104	CASP8, FADD	23	20	16129	70.12608696	0.206233683	2.277648
GO:0043278~response to morphine	2	8.696	0.041468043	CXCR4, FADD	23	31	16129	45.24263675	0.305634835	1.710119
GO:0006915~apoptotic process	4	17.39	0.045493806	TNFRSF10A, CASP8, CXCR4, FADD	23	594	16129	4.722295418	0.323330977	1.628916
GO:0007420~brain development	3	13.04	0.048054662	UFM1, CXCR4, UFC1	23	259	16129	8.122712775	0.329754408	1.600536
GO:0043065~positive regulation of apoptotic process	3	13.04	0.063494062	TNFRSF10A, CASP8, FADD	23	303	16129	6.943176926	0.42117728	1.247500
GO:0071466~cellular response to xenobiotic stimulus	2	8.696	0.085060478	CXCR4, EHMT2	23	65	16129	21.57725753	0.536762128	0.897645
GO:0035690~cellular response to drug	2	8.696	0.086313508	CXCR4, EHMT2	23	66	16129	21.25032938	0.536762128	0.897645
GO:0097190~apoptotic signaling pathway	2	8.696	0.096278943	CASP8, FADD	23	74	16129	18.95299647	0.580591205	0.784405

Term	Count	%	PValue	Genes	List Total	Pop Hits	Pop Total	Fold Enrichment	FDR	neglog2FDR
GO:0000139~Golgi membrane	6	26.09	9.62E-04	FADD, CSGALNACT1, B3GAT3, SLC35B2, CHST15, XYLT2	23	617	17055	7.210908322	0.036561221	4.773542
GO:0048500~signal recognition particle	2	8.696	0.005150254	SRP68, SRP72	23	4	17055	370.7608696	0.045393354	4.461375
GO:0032580~ Golgi cisterna membrane	3	13.04	0.005314967	FADD, CSGALNACT1, UXS1	23	85	17055	26.1713555	0.045393354	4.461375
GO:0005786~signal recognition particle, endoplasmic reticulum targeting	2	8.696	0.007715877	SRP68, SRP72	23	6	17055	247.173913	0.045393354	4.461375
GO:0097342~riboptosome	2	8.696	0.007715877	CASP8, FADD	23	6	17055	247.173913	0.045393354	4.461375
GO:0031265~CD95 death-inducing signaling complex	2	8.696	0.007715877	CASP8, FADD	23	6	17055	247.173913	0.045393354	4.461375
GO:0031264~death-inducing signaling complex	2	8.696	0.008996318	CASP8, FADD	23	7	17055	211.863354	0.045393354	4.461375
GO:0005794~Golgi apparatus	6	26.09	0.010309761	FADD, B3GAT3, TNFRSF10A, SLC35B2, XYLT2, UBA5	23	1069	17055	4.161955505	0.045393354	4.461375
GO:0005783~endoplasmic reticulum	6	26.09	0.010751058	UFM1, SRP68, SRP72, JAGN1, UFSP2, DDRGK1	23	1080	17055	4.119565217	0.045393354	4.461375
GO:0045121~membrane raft	3	13.04	0.038440462	TNFRSF10A, CASP8, FADD	23	242	17055	9.192418254	0.146073757	2.775231
GO:0030173~integral component of Golgi membrane	2	8.696	0.078237073	CSGALNACT1, SLC35B2	23	63	17055	23.54037267	0.270273526	1.887508
GO:0035877~death effector domain binding	2	8.696	0.00505171	CASP8, FADD	22	4	16598	377.2272727	0.258852955	1.949795
GO:0005047~signal recognition particle binding	2	8.696	0.007568442	SRP68, SRP72	22	6	16598	251.4848485	0.258852955	1.949795
GO:008312~7S RNA binding	2	8.696	0.008824533	SRP68, SRP72	22	7	16598	215.5584416	0.258852955	1.949795
GO:0005123~death receptor binding	2	8.696	0.018818896	CASP8, FADD	22	15	16598	100.5939394	0.414015708	1.272243
GO:0015020~glucuronosyltransferase activity	2	8.696	0.032404535	CSGALNACT1, B3GAT3	22	26	16598	58.03496503	0.564966271	0.823763
GO:0005164~tumor necrosis factor receptor binding	2	8.696	0.038520428	CASP8, FADD	22	31	16598	48.6744868	0.564966271	0.823763
GO:0043022~ribosome binding	2	8.696	0.076799	SRP68, SRP72	22	63	16598	23.95093795	0.857686458	0.221478
GO:0030145~manganese ion binding	2	8.696	0.077971496	FADD, XYLT2	22	64	16598	23.57670455	0.857686458	0.221478

Table 3.2 Output of DAVID pathway analysis.

DAVID pathway analysis of high-confidence enrichment targets from cFLIP depletion resistance screens. Data for the intersection of the top 150 ranked genes in both BCBL-1 screens (23 in total—UFL1 not included in this case) were input into the DAVID pathway analysis tool, utilizing all guides detected in either BCBL-1 screen as a background list. Full output for the three broadest categories of gene ontology terms (biological processes in blue, cellular components in green, and molecular functions in yellow) is provided, including which of our enriched genes occur within the indicated pathways. Pathways selected for inclusion into Fig. 3.16 are bolded were considered representative, significant hits (FDR-adjusted p-value < 0.25) as certain terms have major conceptual overlap.

TRAIL-mediated extrinsic apoptosis

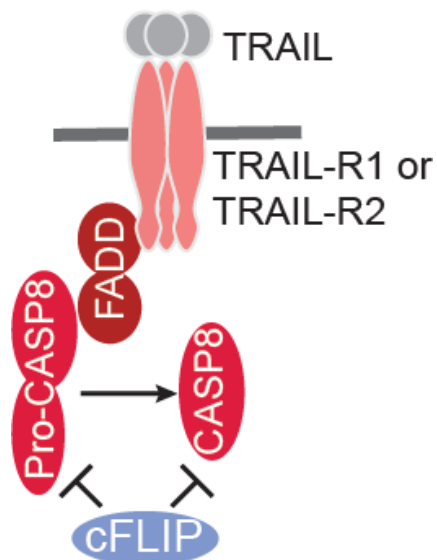


Figure 3.17 TRAIL-mediated extrinsic apoptosis

Hits are colored as in Fig 3.15. TRAIL receptors (1 or 2) signal as homotrimers (though some debate exists as to whether meaningful heterotrimers form) which are induced by interactions with trimers of TRAIL. The intracellular domain of TRAIL receptor complexes interact with two sets of death-inducing signaling complexes (DISC, one complex shown) of pro-CASP8 and FADD. This complex may optionally include other components not shown (such as TRADDs discussed in section 1.7) to mediate signaling events that culminate in transcriptional outcomes, such as promoting NF- κ B activity. In the canonical case, the DISC leads to proteolytic cleavage of pro-CASP8 into active CASP8 by neighboring CASP8 molecules. Cellular FLIP acts as a catalytically-deficient dominant negative which prevents this activation or sequesters active CASP8 from interacting with its downstream substrates, which include CASP10 and culminate in programmed cell death.

UFMylation & ER-associated translation

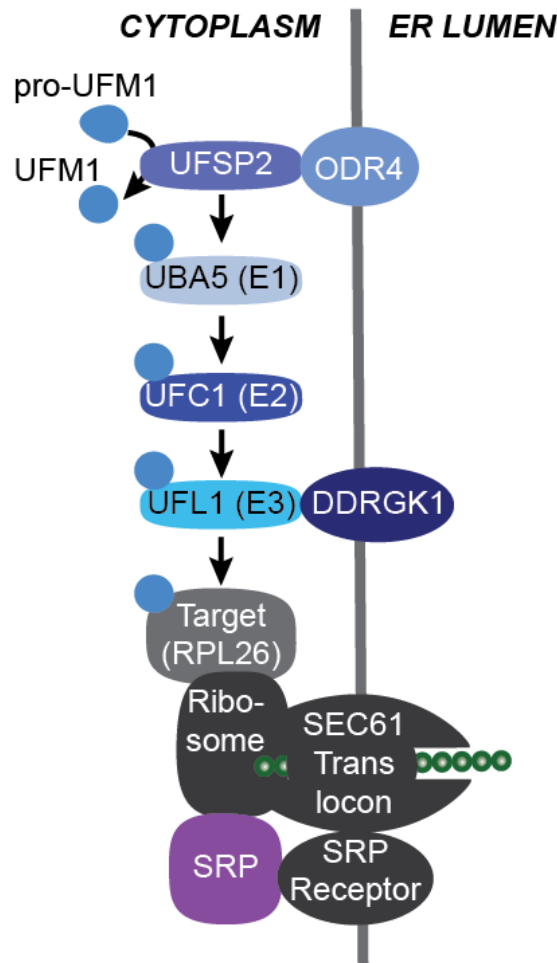


Figure 3.18 UFMylation and SEC61- mediated protein co-translation

Screen hits are colored as in Fig 3.15. free UFM1 is cytoplasmic, but the UFM1 conjugation machinery is anchored on the cytoplasmic face of the ER membrane by adaptors ODR4 and DDRGK1 (UFBP1). UFM1-specific peptidase 2 (UFSP2) cleaves the C-terminal end of pro-UFM1 to produce mature UFM1 containing a C-terminal glycine. UBA5 (E1) activates mature UFM1 via adenylation and the formation of a UFM1-UBA5 thioester bond. UFM1 is then transferred to UFC1 (E2) which forms a complex with the target conjugating enzyme UFL1 (E3). RPL26 is the main characterized substrate for UFMylation and impacts translational pausing during ER-associated degradation (ERAD). The SRP complex is involved in protein translocation and initiates translational pausing of membrane-bound (type I transmembrane and other) proteins until insertion into the ER membrane has begun.

Chondroitin Sulfate (CS) Proteoglycan Synthesis Pathway

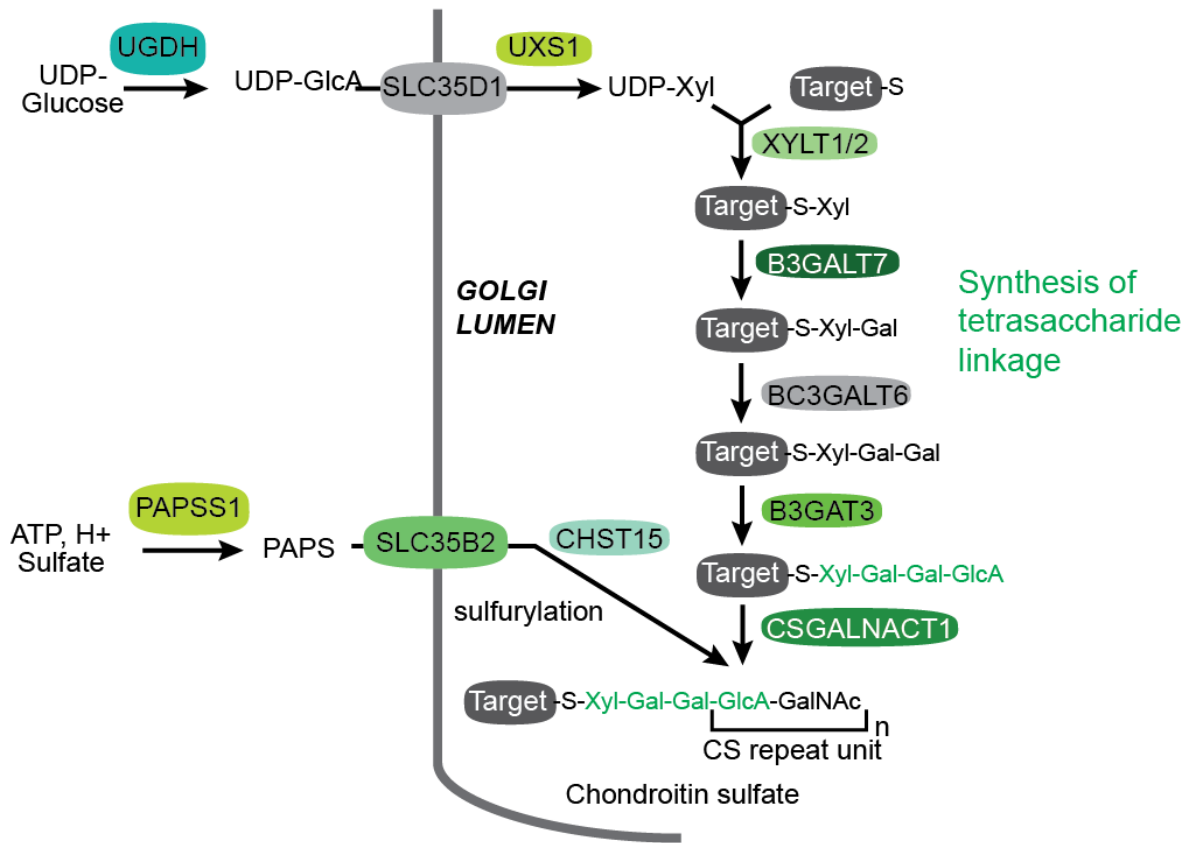


Figure 3.19 Chondroitin sulfate proteoglycan synthesis

Screen hits are colored as in Fig 3.15. CS proteoglycan synthesis begins with UDP-Glucose which is converted into UDP-glucuronic acid (UDP-GlcA) by UDP-glucose dehydrogenase (UGDH) in the cytoplasm and pumped into the lumen of the Golgi by the SLC35D1 transporter. UDP-GlcA is converted into UDP-Xylose (UDP-Xyl) by UDP-glucuronate decarboxylase 1 (UXS1). Xylose is transferred onto target proteins at serine residues by xylose transferase 1/2 (XYLT1/2). This marks the first of four sugars in a chain common to all proteoglycans (Xyl-Gal-Gal-GlcA). Galactose (Gal) linkages are added by beta-1,3-galactosyltransferase 7 (B3GALT7) and beta-1,3-galactosyltransferase 6 (BC3GALT6). Finally, glucuronic acid is added to the chain by beta-1,3-glucuronyltransferase 3 (B3GAT3). Addition of an N-acetyl galactosamine subunit to GlcA by chondroitin sulfate N-acetylgalactosaminyltransferase 1 (CSGALNACT1) defines the chondroitin glucose amino glycan, which can be repeated in varying numbers. These chondroitin repeats are variably sulfated. In this case, carbohydrate sulfotransferase 15 mediates the production of CS-E (chondroitin-4,6-sulfate). Sulfate groups are provided by phosphoadenosine phosphosulfate (PAPS) which is transported into the Golgi lumen by transporter SLC35B2 from the cytoplasm where it is synthesized from ATP, H⁺ and sulfate by the PAPS synthase 1 (PAPSS1) enzyme.

Consistent with my screening results, BCBL-1 CASP8 KO pools derived using two different sgRNAs were completely protected from cell death after subsequent cFLIP sgRNA challenge (Fig. 3.20; Fig. 3.21). These results confirm that my screens capture CASP8 as a key component of the cell death pathway that necessitates cFLIP expression in PEL cells.

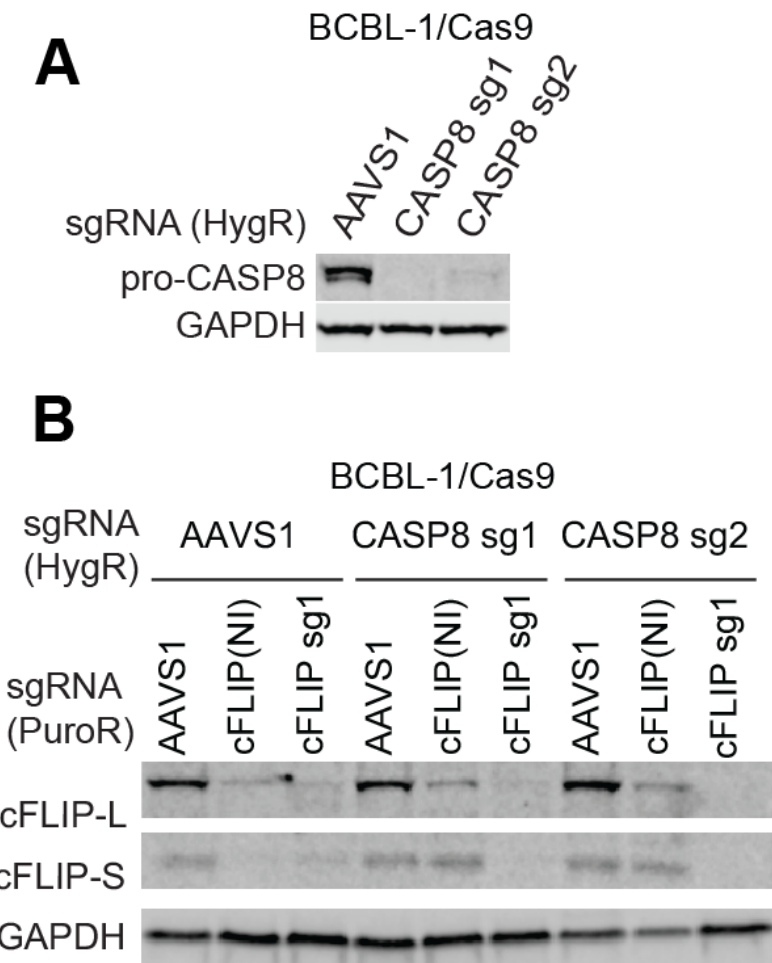


Figure 3.20 Double KO of CASP8/cFLIP is highly efficient.

BCBL-1/Cas9 cells were transduced with the indicated sgRNAs, selected with hygromycin, and KO of CASP8 was confirmed by western blot. Lysates harvested 3 days after transduction with the indicated sgRNA during the cumulative growth curves displayed in Fig 3.21. Lanes marked cFLIP (NI, not included) represent a third, cFLIP sgRNA not included elsewhere in my study, since this guide resulted in only inefficient editing.

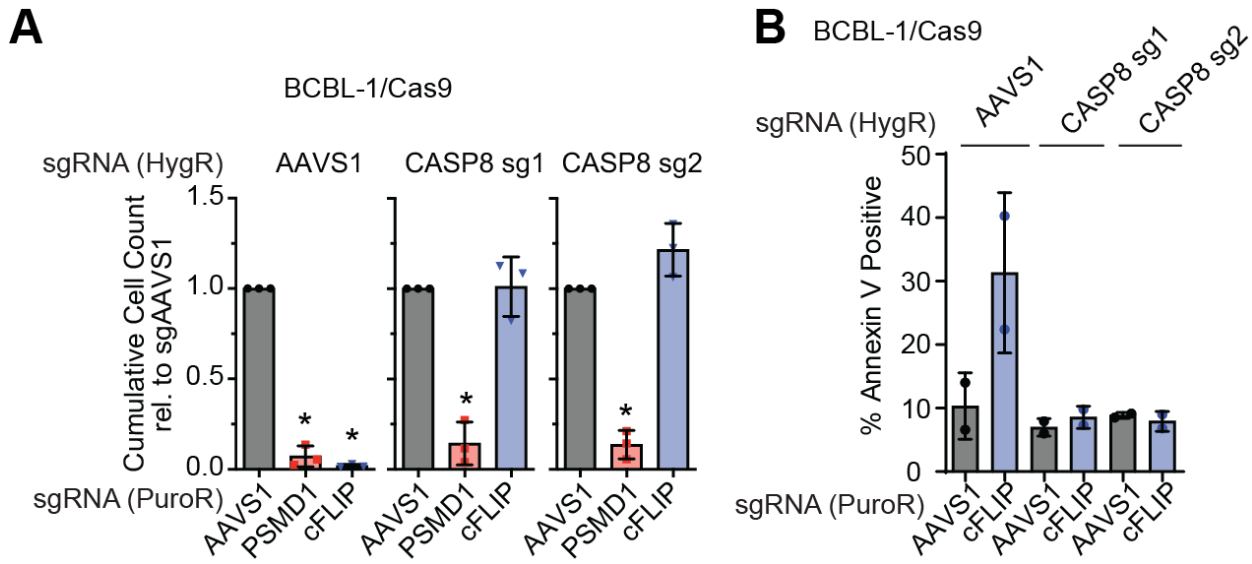


Figure 3.21 CASP8 KO cells lack dependence on cFLIP

A. The cell lines from Figure 3.20 panel A were challenged with puromycin-resistant lentiviral sgRNA vectors at equal MOI and cumulative growth curve analyses were performed as previously. Error bars represent SD from 3 independent repeats. For western blot controls, see Fig 3.20 panel B. Statistical significance for loss of cell viability compared to sgAAVS1 was analyzed using one-sided, one-sample *t*-testing (* denotes FDR-adjusted $p \leq 0.05$). Rescue by CASP8 KO was significant as determined using a one-sided, independent two-sample *t*-test. FDR-adjusted p values are listed in Appendix. **B.** Cells were challenged with control or cFLIP sgRNAs as in panel A, but not selected with puromycin, and stained with Annexin V 48 h after transduction ($n = 2$ independent repeats, error bars indicate range).

3.7 cFLIP protects PEL cells from ligand-independent TRAIL-R1-induced cell death

In addition to *CASP8*, *TNFRSF10A*, encoding TRAIL receptor 1 (TRAIL-R1/DR4) scored highly in my screens. Interestingly, neither the ligand for TRAIL-R1 (i.e. *TNFSF10* encoding TRAIL) nor *TNFRSF10B*, encoding TRAIL receptor 2 (TRAIL-R2/DR5) or other death receptors were hits in my screens (Electronic Supplement Table 1). As for CASP8, I generated TRAIL-R1 KO pools using two independent sgRNAs in which to perform cFLIP KO experiments (Fig 3.22).

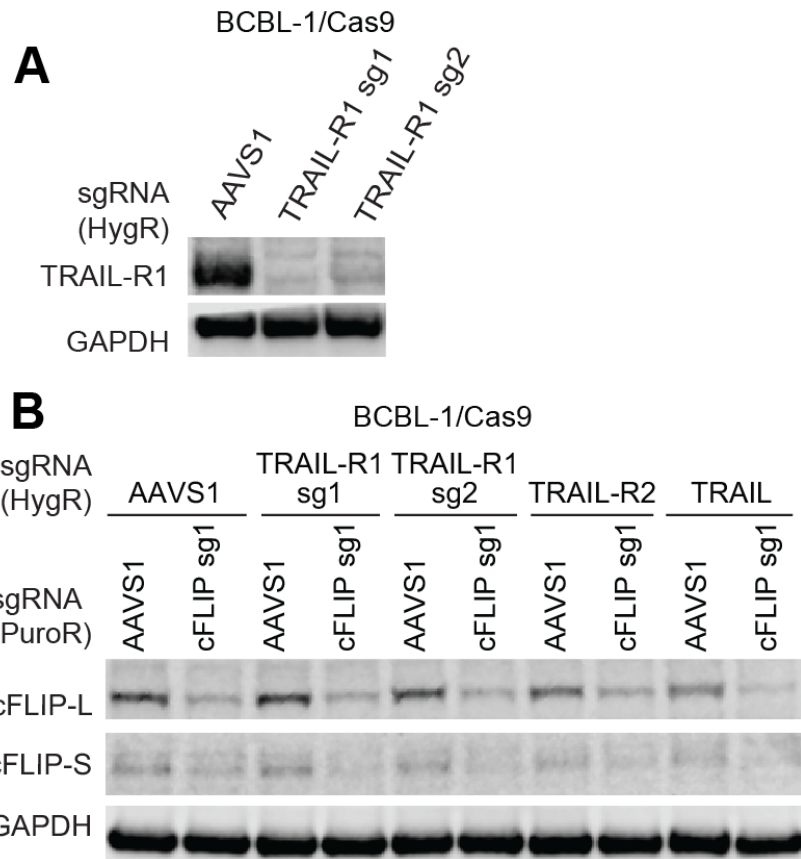


Figure 3.22 Double KO of TRAIL signaling components and cFLIP

A. BCBL-1/Cas9 cells were transduced with the indicated sgRNAs, selected with hygromycin, and KO of TRAIL-R1 was confirmed by western blot. Neither TRAIL-R2 (not shown) nor TRAIL (Fig 3.23) were successfully detected in PEL cells. Targeting of these loci was instead confirmed by sequencing (see Table 3.3) **B.** Lysates were collected 2 days after sgRNA transduction during the cumulative growth curves shown in Fig. 3.18 and cFLIP KO efficiency was established by Western blot.

Cumulative growth curve analyses following subsequent cFLIP KO confirmed that TRAIL-R1-deficient cells no longer require cFLIP expression for viability (Fig. 3.23, cFLIP Western expression controls in Fig. 3.22). TRAIL (ligand) mRNA is not well expressed in RNA-seq data from three different PEL cell lines, including BCBL-1 (Fig 3.12). Indeed, TRAIL ELISA on cellular supernatants or lysates of BCBL-1 and BC-3 cells failed to detect secreted or

intracellular TRAIL [272, 273] in either cell line (Fig. 3.24, panel A). This assay detected levels of recombinant TRAIL well below the IC₅₀ of “TRAIL-sensitive” cell lines within the literature [274]. BCBL-1 cells are furthermore TRAIL-resistant, even to hyper-physiological concentrations as high as 10 mg/mL (Fig. 3.24, panel B). As additional controls, I generated TRAIL and TRAIL-R2 KO pools. While NGS-based sequencing of the targeted loci to characterize indel rates within my KO pools showed that >95% of each locus contains inactivating indels after editing (Table 3.3), genetic disruption of neither locus affected BCBL-1 dependency on cFLIP (Fig. 3.23, cFLIP Western expression controls in Fig 3.22).

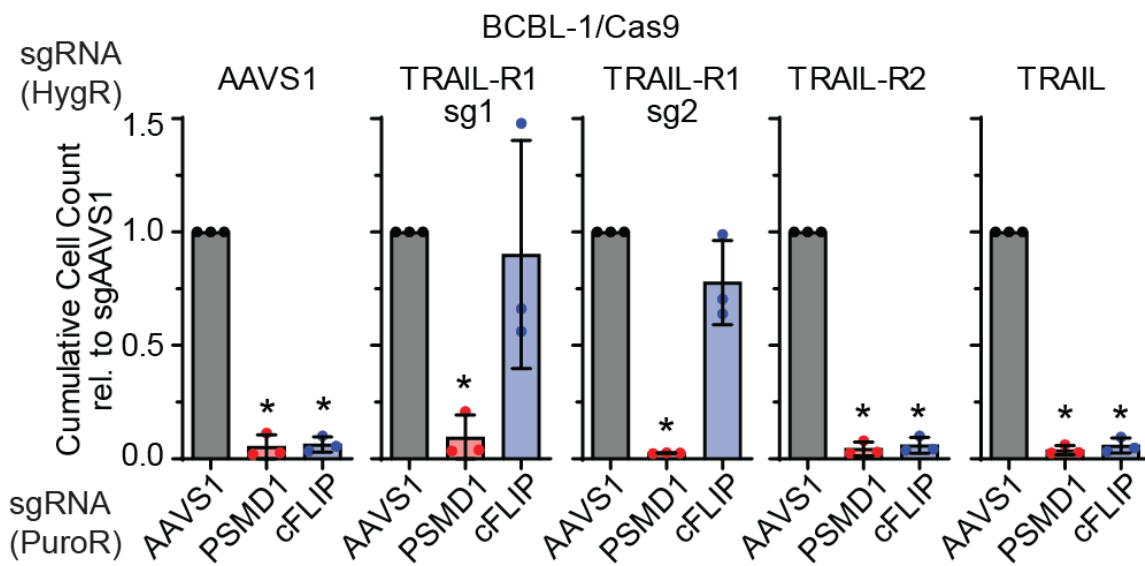


Figure 3.23 TRAIL-R1, but not TRAIL or TRAIL-R2 KO confers resistance to cFLIP loss.

Cell lines depicted in Fig 3.22 panel A were challenged with puromycin-resistant lentiviral sgRNA vectors at equal MOI and cumulative growth curve analyses were performed as previously. Error bars represent SD from 3 independent repeats. For cFLIP Western blot control, see Fig 3.22 panel B. Statistical significance for loss of cell viability compared to sgAAVS1 was analyzed using one-sided, one-sample t-testing (* denotes $p \leq 0.05$). Rescue by TRAIL-R1 KO, but not TRAIL-R2 or TRAIL KO, was significant as determined using one-sided, independent two-sample t-tests. FDR-adjusted p values are listed in Appendix.

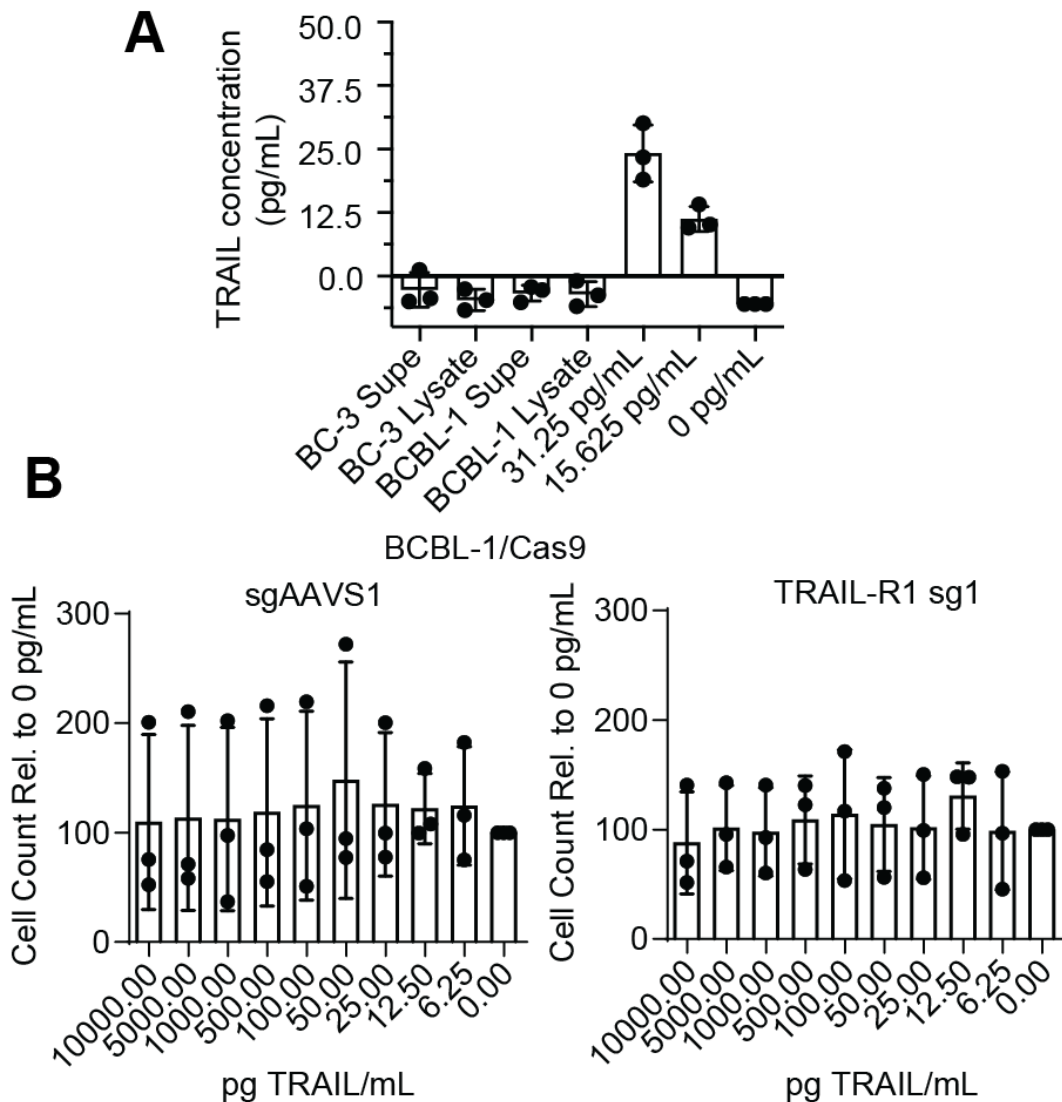


Figure 3.24 PEL cells do not express and are insensitive to TRAIL

A. BC-3 or BCBL-1 cells were plated at 2×10^5 cells/mL, and supernatants or lysates were harvested 3 days later and used for anti-TRAIL ELISA assay. Known concentrations of recombinant human TRAIL confirm sensitivity down to the ~10 pg/mL range. **B.** BCBL-1/Cas9 cells transduced with control (AAVS1) or TRAIL-R1 (sg1) sgRNAs were treated with the indicated concentrations of TRAIL ligand and total cell counts were quantified 24 hours 7 later. Error bars indicate SD (n=3 independent repeats). There were no significant differences between doses for both cell lines, tested by one-way ANOVA ($p=.99$ for both).

Ligand-independent activation of TRAIL-R2, and in some cases TRAIL-R1, has previously been described within the context of Golgi and ER stress-induced cell death [210, 275-279]. Ligand-independent signaling of TRAIL receptor was proposed to follow the intracellular accumulation of TRAIL-R1 in the Golgi or TRAIL-R2 in the ER-Golgi intermediary compartment (ERGIC) [279, 280]. Similarly, TRAIL-R1 in BCBL-1 is exclusively expressed intracellularly in PEL cells (Fig. 3.25)

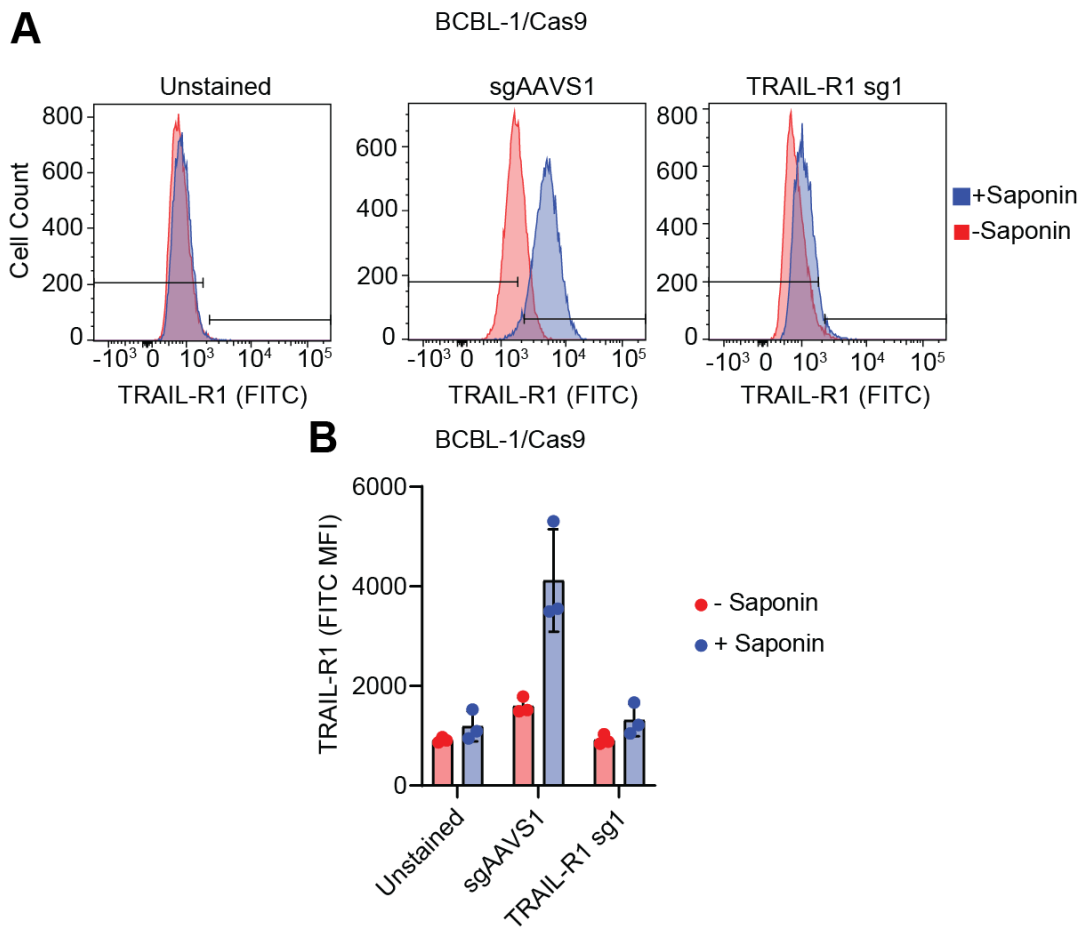


Figure 3.25 TRAIL-R1 is expressed intracellularly in BCBL-1 cells.

A. KO cell lines were fixed in 4% PFA and stained for TRAIL-R1 with or without permeabilization by saponin. Shown at left are unstained control cells. **B.** Mean fluorescence intensity (MFI) across 3 independent repeats, error bars indicate SD.

Next, in collaboration with co-author Scout Osbourne, we probed the subcellular localization of TRAIL-R1 to see if it behaved similarly to that of TRAIL-R2. In contrast, TRAIL-R1 in BCBL-1/Cas9-sgAAVS1 colocalized with the ER marker ERp72 and the cis-Golgi marker Giantin, but much less extensively with the ERGIC marker ERGIC53 (quantification of co-localization in Fig 3.26, representative images in Fig. 3.27). Further, a recent study in HCT116 cells demonstrated that a misfolded mutant of myelin protein zero (MPZ-DelS63) binds to TRAIL-R2 in the ERGIC and consequently triggers TRAIL-independent cell death, while MPZ-DelS63-EctoYtoE misfolds but does not interact with TRAIL-R2) [280]. TRAIL-R1 did not colocalize with either form of MPZ in BCBL-1 after their doxycycline (DOX)-inducible expression with a C-terminal mCherry tag (quantification of co-localization in Fig 3.26, representative images in Fig. 3.28). Neither protein furthermore impaired the viability of BCBL-1 cells over the course of several days (not shown). Based on these findings, I conclude that cFLIP protects PEL cells from an intracellular, ligand-independent, TRAIL-R1-mediated cell death program originating within the Golgi or ER.

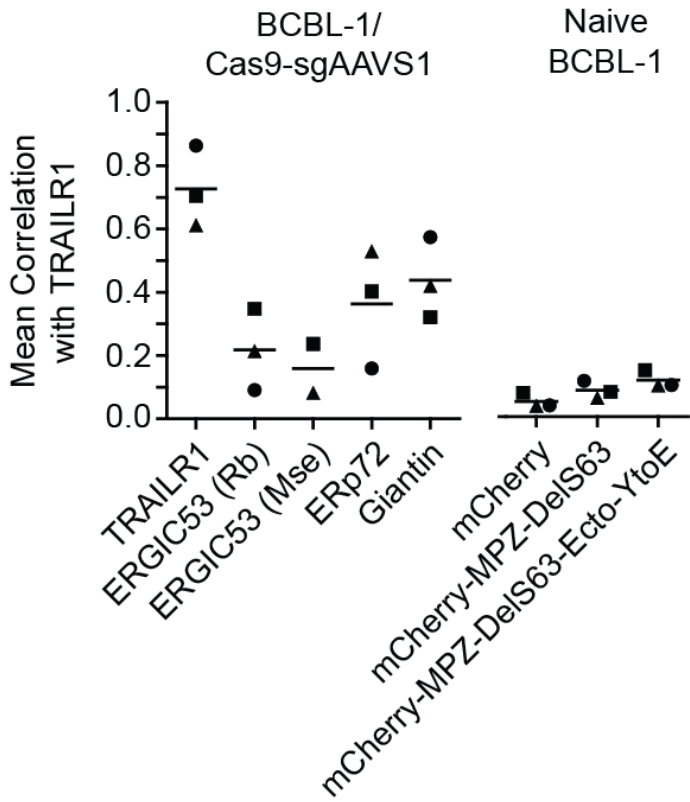


Figure 3.26 Subcellular localization of TRAIL-R1 in BCBL-1 is distinct from previously published reports for TRAIL-R2.

3D colocalization of TRAIL-R1 with the indicated proteins was quantified using Pearson's correlation coefficients (PCCs, $n = 3$ independent repeats, except $n = 2$ for mouse anti-ERGIC53). Representative images are shown in Fig 3.27 and Fig 3.28. I quantified an average of ~1800 cells per replicate. Statistical significance of the difference from TRAIL-R1 self-colocalization detected with two different TRAIL-R1-specific antibodies was determined by two-sided, independent two-sample t -test ($* \leq 0.05$). All markers other than ERp72 and Giantin (indicated by ns) were significantly less colocalized with TRAIL-R1 than TRAIL-R1 self-colocalization.

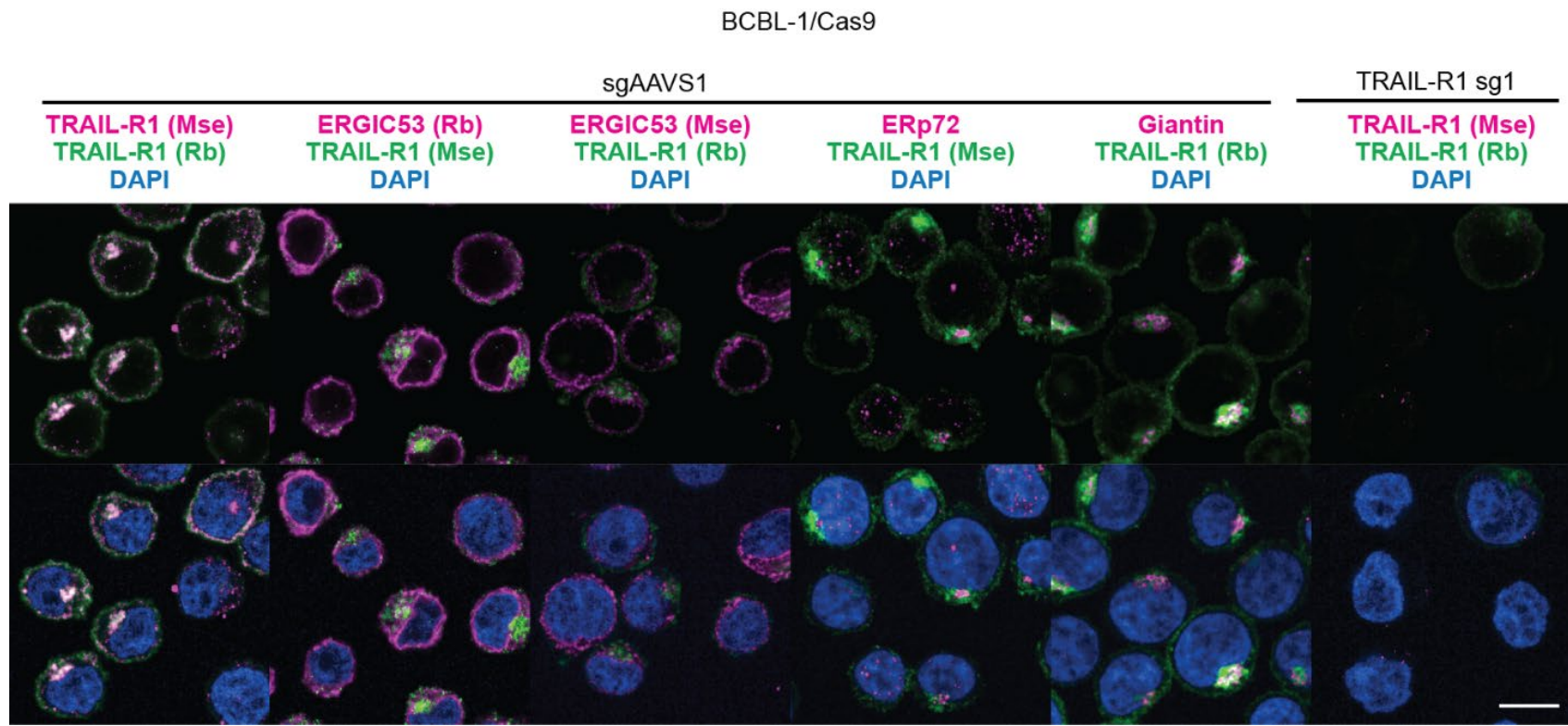


Figure 3.27 TRAIL-R1 signal is predominantly correlated with the ER and Golgi in BCBL-1 cells.

BCBL-1/Cas9 cells expressing either sgAAVS1 or TRAIL-R1 sg1 were permeabilized with saponin and stained with the indicated antibodies. Representative images of TRAIL-R1 and three compartment markers are shown: ERGIC53 (two antibodies, marker of the ER-Golgi intermediate compartment or ERGIC), ERp72 (marker of the ER), and Giantin (marker of the cis- Golgi). TRAIL-R1 is shown in green with all other markers in magenta to depict overlapping signal as white. Mouse anti-TRAIL-R1 is included as a positive control for co-localization with rabbit anti-TRAIL-R1, while TRAIL-R1 sg1 serves as a negative control for TRAIL-R1 signal. Scale bar = 10 μ m. Quantification of co-localization can be found in Fig 3.26.

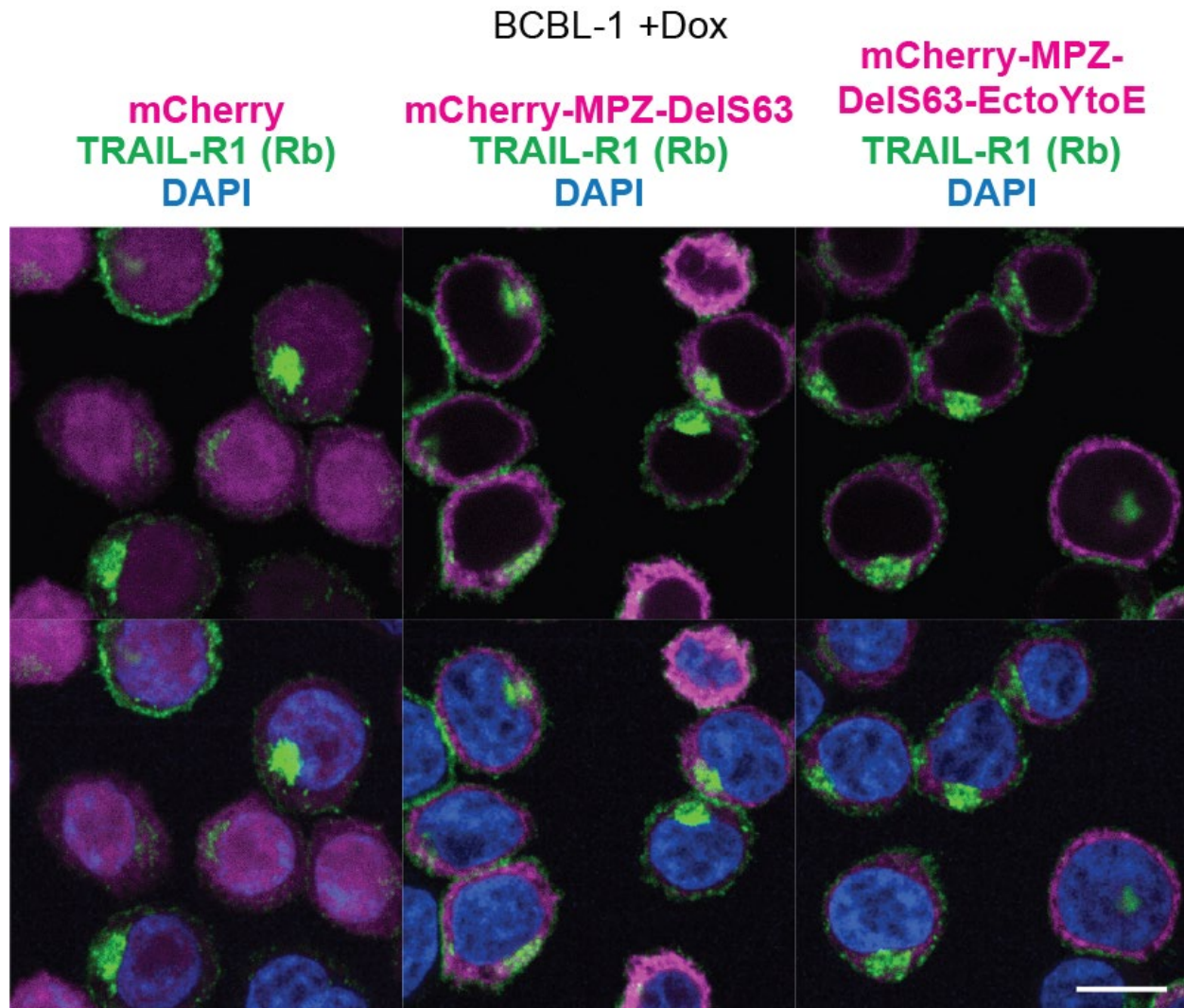


Figure 3.28 TRAIL-R1 does not co-localize with MPZ-DelS63 in BCBL-1 cells.

BCBL-1/Cas9 expressing the indicated Dox-inducible construct (label in magenta) were treated with doxycycline and stained with anti-TRAIL-R1 after 72 hours. Representative images of TRAIL-R1 colocalization with mCherry and mCherry-tagged MPZ mutants are shown. TRAIL-R1 is shown in green with mCherry in magenta to depict overlapping signal as white. Scale bar = 10 μ m. Quantification of co-localization can be found in Fig 3.26.

3.8 UFMylation and JAGN1 promote TRAIL-R1 expression in PEL cells

To extend validation of the resistance screens beyond TRAIL-R1 and CASP8, I chose two hits from the UFMylation pathway (UFM1, DDRGK1), two genes from the chondroitin sulfate proteoglycan synthesis pathway (UGDH, CHST15), JAGN1, and CXCR4 for single gene KO by two independent sgRNAs each. Generation of an SRP68 KO cell line failed due to the essentiality of this gene in PEL cells, which was unsurprising, since all six subunits of the full SRP complex are pan-essential based on data from the Cancer Dependency Map (Table 3.1). Regardless, I speculate that the screens correctly captured a biologically relevant connection to the SRP, due to the functional link between the SRP and UFMylation of RPL26. The essentiality of the SRP complex likely also explains why only 2 of 6 SPR complex members scored in my screen (Fig. 3.15). I did not attempt generating an EHMT2 KO cell pool, since EHMT2 is also pan-essential and likely essential in PEL cells (Table 3.1) [65].

Western Blot analysis confirmed disruption of UFMylation in UFM1 KO pools (Fig. 3.29). Interestingly, DDRGK1 KO did not reduce the most prominent UFM1-modified bands, suggesting that these represent upstream UFMylation pathway intermediates and/or other DDRGK1-independent UFMylation events. I furthermore confirmed robust editing in all cell pools by indel sequencing (Table 3.3).

sgrna	total read pairs	total contigs	pct reads mapped to contigs	indel rate	frame shift rate	synonymous rate	missense rate	nonsense rate	ref peptide length	mean stop loc	median stop loc	mode stop loc	CRISPResso2 pct modified	CRISPResso2 pct frameshift
TNFRSF10B sg1	41015	51	0.9977	0.9575	0.8809704	0.027014507	0	0.9729855	441	150.862745	107	143	0.970334363	0.845779297
TNFSF10 sg1	27226	25	0.9987	1	0.7139866	0	0	1	282	155	155	155	0.980230389	0.617115101
UFM1 sg1	38916	64	0.9969	0.9776	0.5866482	0.018193031	0	0.981807	86	45.78125	30.5	84	0.985050556	0.548352679
UFM1 sg2	38033	73	0.9964	0.9559	0.4742198	0.037677806	0.0148292	0.947493	86	41.3013699	32	41.75	0.970806116	0.517272488
DDRGK1 sg1	36485	62	0.9974	0.9849	0.6733178	0.015074688	0	0.9849253	315	170.048387	141.5	149	0.995845357	0.690051844
DDRGK1 sg2	32946	56	0.9972	1	0.5726947	0	0	1	315	201.5	171	171	0.986851093	0.596539194
JAGN1 sg1	38397	36	0.9984	0.9867	0.8210537	0.013282288	0	0.9867177	184	145.972222	171.5	175	0.989722797	0.779278978
JAGN1 sg2	21476	46	0.9977	0.9844	0.4922239	0.015645372	0.0216986	0.962656	184	56.326087	29	28.5	0.988992986	0.754374159
CXCR4 sg1	59441	18	0.9991	0.9952	0.9884255	0.004777847	0	0.9952222	357	254.722222	279	182	0.995196477	0.957122746
CXCR4 sg2	42258	57	0.9971	0.9914	0.7915424	0.008566425	0	0.9914336	357	126.929825	26	24	0.992296562	0.747795915
UGDH sg1	48337	63	0.9973	1	0.8274407	0	0	1	495	82.0634921	82	82	0.786197246	0.818348166
UGDH sg2	23817	68	0.9971	1	0.6524751	0	0	1	495	343	342.5	344	0.999712205	0.762478409
CHST15 sg1	71679	42	0.9977	0.9912	0.9050628	0.00525956	0	0.9947404	562	408.809524	414	361.333	0.995334857	0.865505711
CHST15 sg2	11329	8	0.9996	1	1	0	0	1	562	396.75	371.5	396.75	0.993563153	0.839571936

Table 3.3 Characterization of CRISPR-target loci by amplicon sequencing

NGS-based validation of CRISPR editing of selected KOs from Figs. 3.23 & 3.30. Displayed is a summary describing each single guide KO pool on a different row. Columns include: 1) summary statistics regarding assembled contigs used for custom variant analysis (total read pairs, total variants/unique contigs, and the percentage of total reads mapping to assembled contigs); 2) rates of different variant classifications (indel, frameshift, synonymous, missense, and nonsense) in custom analysis pipeline as a percentage of all contig-mapped reads; 3) the expected and predicted length of peptides based on stop codon position, provided as three measures of central tendency across all reads mapped to contigs (mean, median, and mode); 4) rates of modified reads and frameshifted reads as predicted by CRISPResso2 (note that CRISPResso2 provides frameshift rates relative to modified reads, not total reads) 86. For more information, see material and methods (section 2.2.12). For detailed, variant-level output, see Electronic Supplementary File 2 (Supplementary Table 4 in [174]).

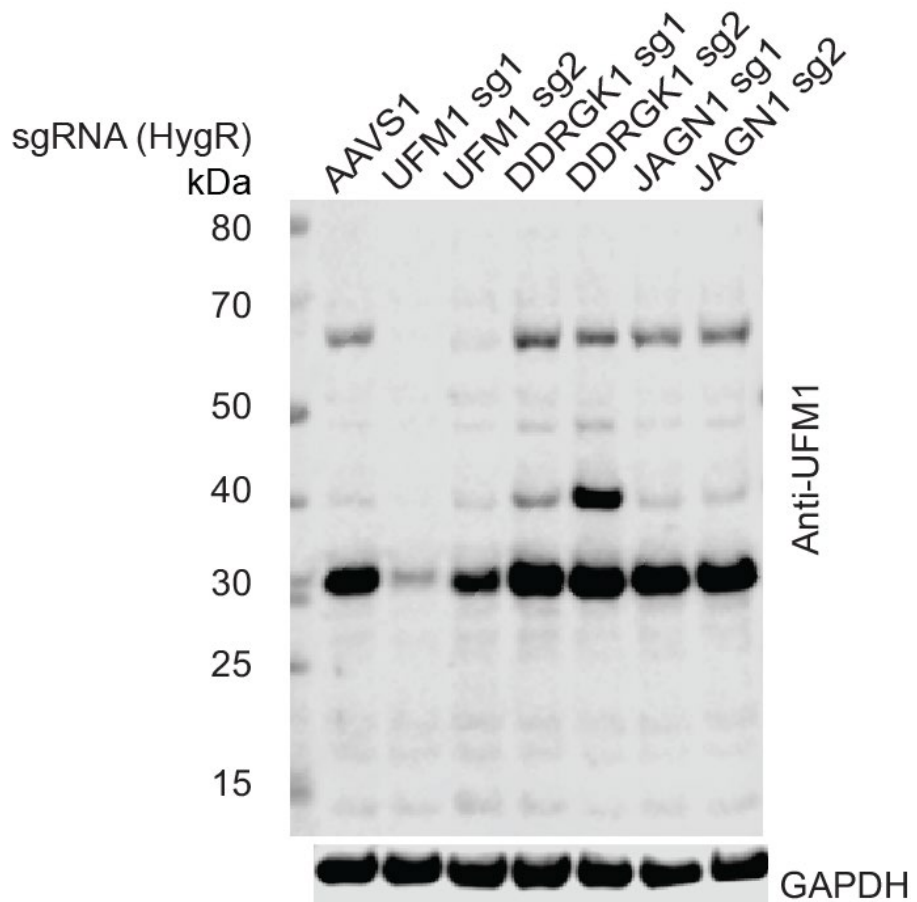


Figure 3.29 Disruption of UFMylation by single gene KOs

Lysates from a subset of single-gene KO pool cell lines (UFM1, DDRGK1, and JAGN1) from Fig. 3.30 were assessed for UFM1-conjugates by Western blot analysis. Unconjugated UFM1 is not shown as its low molecular weight (12 kDa) leads to co-migration with the loading dye front. JAGN1 was included to confirm that it does not impact UFMylation due to downstream functional similarities with UFM1/DDRGK1 presented in Fig. 3.32.

I obtained significant rescue from lethal cFLIP KO challenge for every hit, as predicted by my screens (Fig. 3.30, Fig. 3.31).

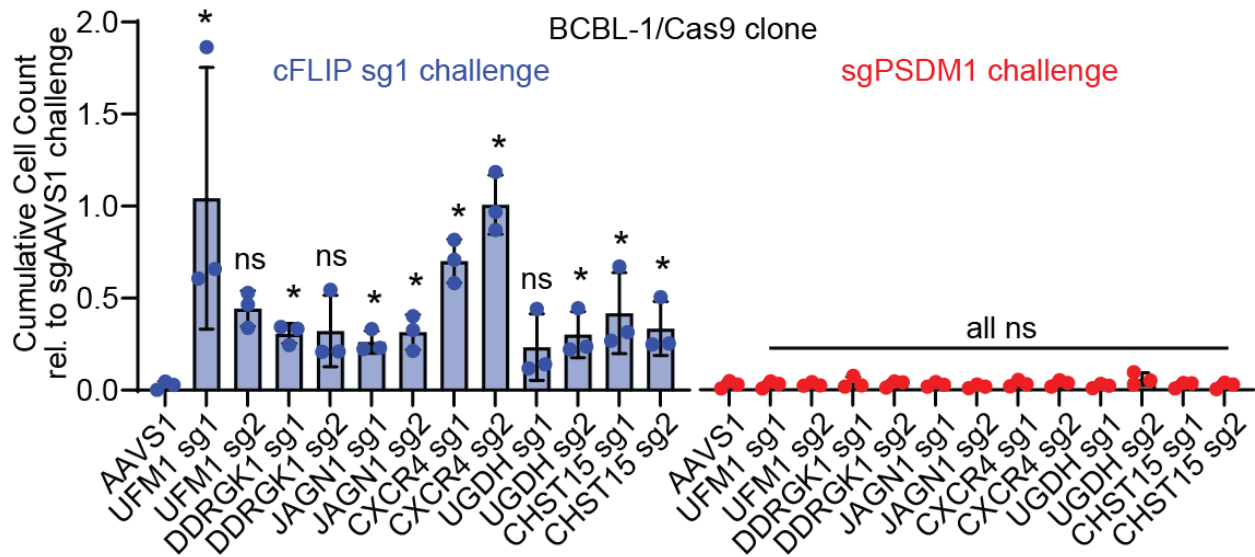


Figure 3.30 KO of genes that participate in UFMylation, the chondroitin sulfate synthesis pathway, or of JAGN1 and CXCR4 overcome cFLIP dependency in PEL cells.

Single-gene KO pools were generated as previously for two genes each in the UFMylation and chondroitin sulfate biosynthesis pathway along with CXCR4 and JAGN1 and these cell lines were used to perform cumulative growth curves following transduction with a second sgRNA as previously. Each bar represents a KO pool containing the pLentiGuide SpBsmBI-HygR sgRNA indicated. All bars are relative to sgAAVS1 (not shown). Statistical significance of rescue from cFLIP sg1 induced cell death was determined using one-sided, independent two-sample t-tests (* denotes FDR-adjusted $p \leq 0.05$). FDR-adjusted p values and statistical significance of loss of viability are listed in Appendix. Western controls are in Fig 3.31.

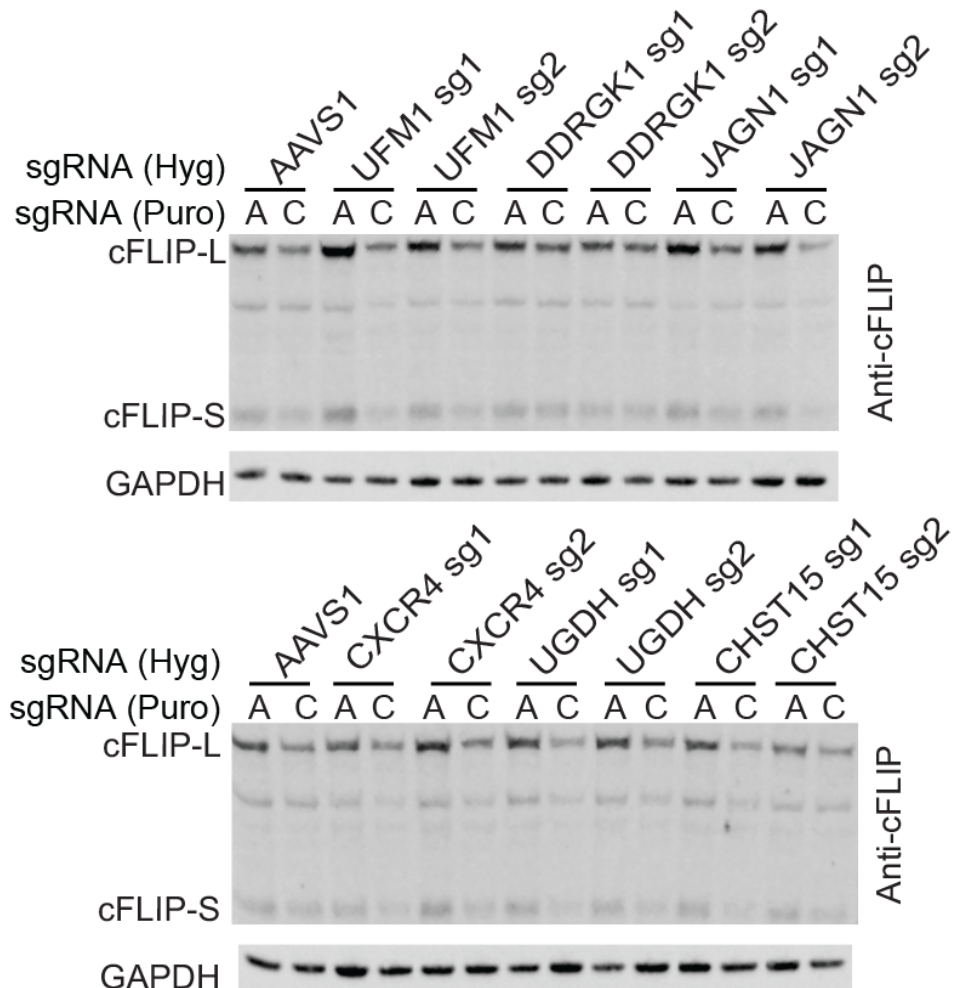


Figure 3.31 cFLIP KO efficiency during validation of additional screen hits.

Lysates were collected 2 days after transduction during the cumulative growth curves shown in Fig. 3.30 and cFLIP KO efficiency was confirmed by Western blot. Incomplete cFLIP KO is due to performing this and similar Westerns before excessive cell death is observed.

Next, I sought to clarify the mechanism(s) by which loss of my screen hits result in cFLIP independence. I noted that UFMylation (UFM1 and DDRGK1) and JAGN1 were required for expression of TRAIL-R1, a type I transmembrane protein that contains an ER signal peptide (Fig. 3.32). In contrast, KO of CXCR4 and chondroitin sulfate proteoglycan synthesis pathway genes (UGDH, CHST15) did not affect total TRAIL-R1 or CASP8 expression (Fig. 3.32).

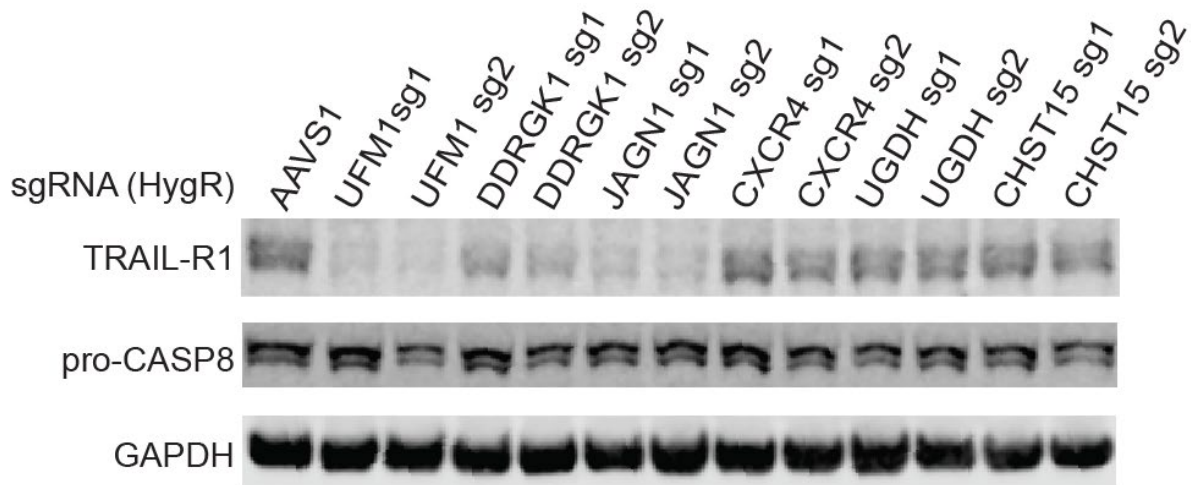


Figure 3.32 UFMylation and JAGN1 expression are required for full expression of TRAIL-R1 in BCBL-1 cells

Single-gene KO pools from 3.30 were analyzed for TRAIL-R1 and pro-caspase 8 expression by Western blot.

Furthermore, none of the KOs I tested led to a redistribution of TRAIL-R1 to the cell surface from its typical intracellular location in PEL cells (Fig 3.33), in contrast to the recently reported redistribution of TNFRSF17 after SEC61A inhibition by others [281]. TRAIL-R1 mRNA levels in the KO cell lines with reduced TRAIL-R1 protein levels were unchanged, indicating that reduced TRAIL-R1 expression is not due to changes in transcription or mRNA abundance (Fig 3.34) but rather due to decreased translation and/or increased degradation.

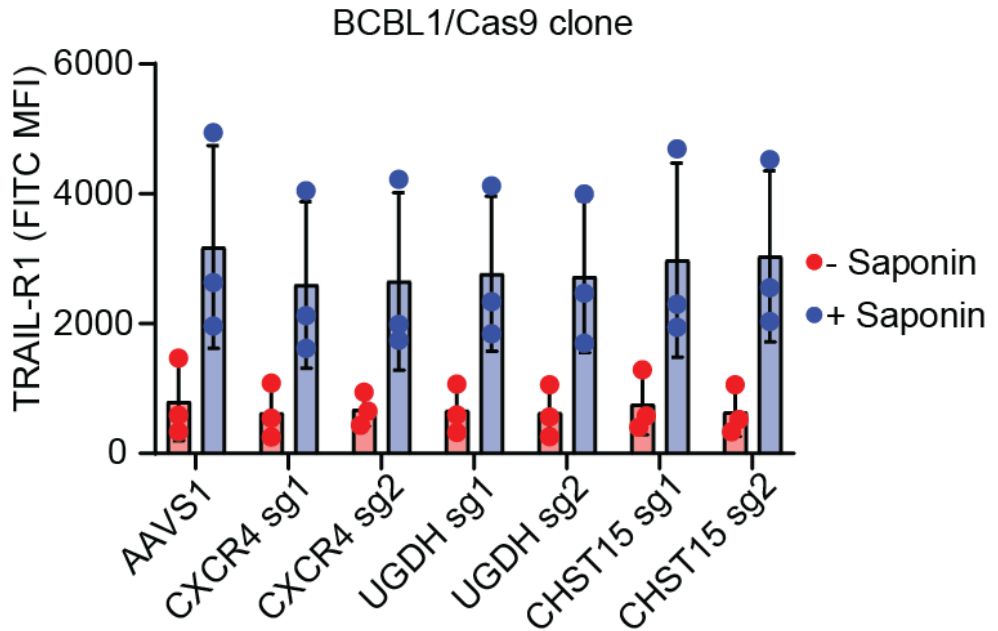


Figure 3.33 TRAIL-R1 is not redistributed to the cell surface in response to KO of any validated screen hits.

The indicated subset of single gene KO cell lines from Fig. 3.30 were stained for TRAIL-R1, and flow cytometry was performed in parallel to the experiments shown in Fig. 3.25. Displayed is the MFI across 3 independent repeats, error bars indicate SD. The lack of significant differences between cell lines within permeabilization groups was tested by one-way ANOVA ($p=0.99$ for both).

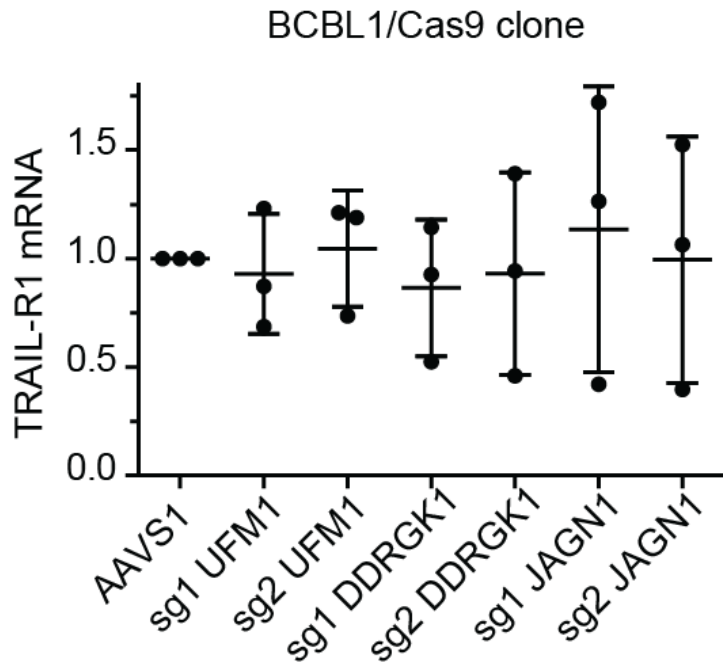


Figure 3.34 TRAIL-R1 mRNA levels are not altered in response to KO of any validated screen hits.

Real-time PCR was performed on cDNA isolated from the indicated single-gene KO pool cell lines. Expression is quantified relative to an endogenous control (B2M) and the sgAAVS1 control. 9 Each point represents the average of 3 technical replicates on a single plate ($n = 3$ independent RNA preparations). Lack of significant differences between cell lines was tested by one-way ANOVA ($p=0.98$).

While CXCR4 is best known for its role as a chemokine receptor and well expressed in PEL RNA-seq data, expression of its ligand, CXCL12, is not detectable in BC-1, BC-3, or BCBL-1 cells (Fig. 3.35). To establish whether CXCR4 signaling is involved in the rescue phenotype, I tested if CXCR4 inhibitor (AMD3100) treatment overcomes the dependency on cFLIP, using BCBL-1 cells with Dox-inducible Cas9 expression [66]. In these experiments, CXCR4 inhibitor treatment failed to recapitulate the genetic CXCR4 KO effect (Fig 3.36). This result and the lack of endogenous CXCL12 expression suggest that the role of CXCR4 in triggering TRAIL-R1-dependent cell death in PEL is unrelated to its normal signaling activity.

In sum, my data suggest that UFMylation and JAGN1 are required for TRAIL-R1 expression, while CXCR4 and the chondroitin sulfate proteoglycan synthesis pathway may promote TRAIL-R1 signaling or affect cFLIP essentiality by other mechanisms.

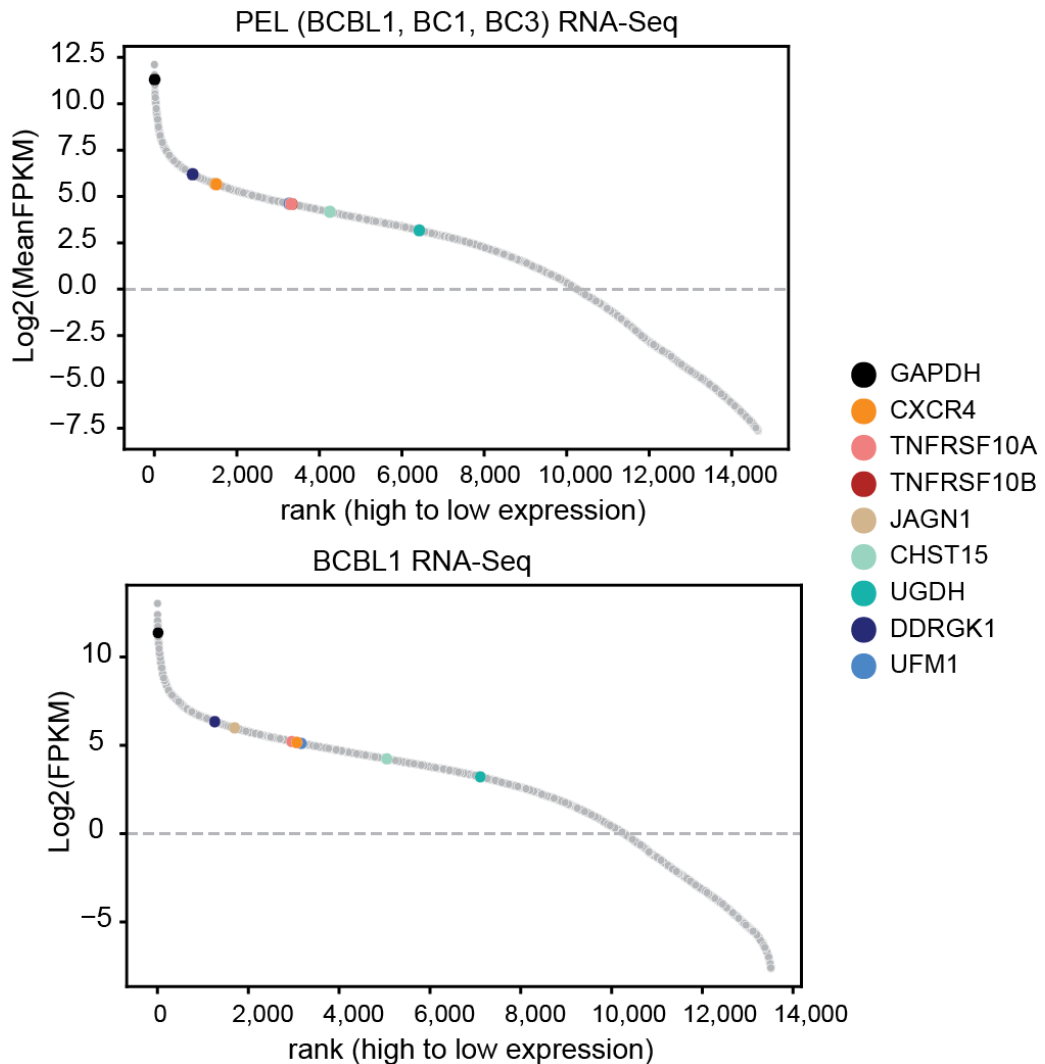


Figure 3.35 Expression of screen hits in PEL cells.

CXCR4 and other genes chosen for validation in Fig. 3.30 are well expressed in the RNA-seq datasets from Fig. 3.12, while CXCL12 expression is not detected (not shown due to lack of detection)

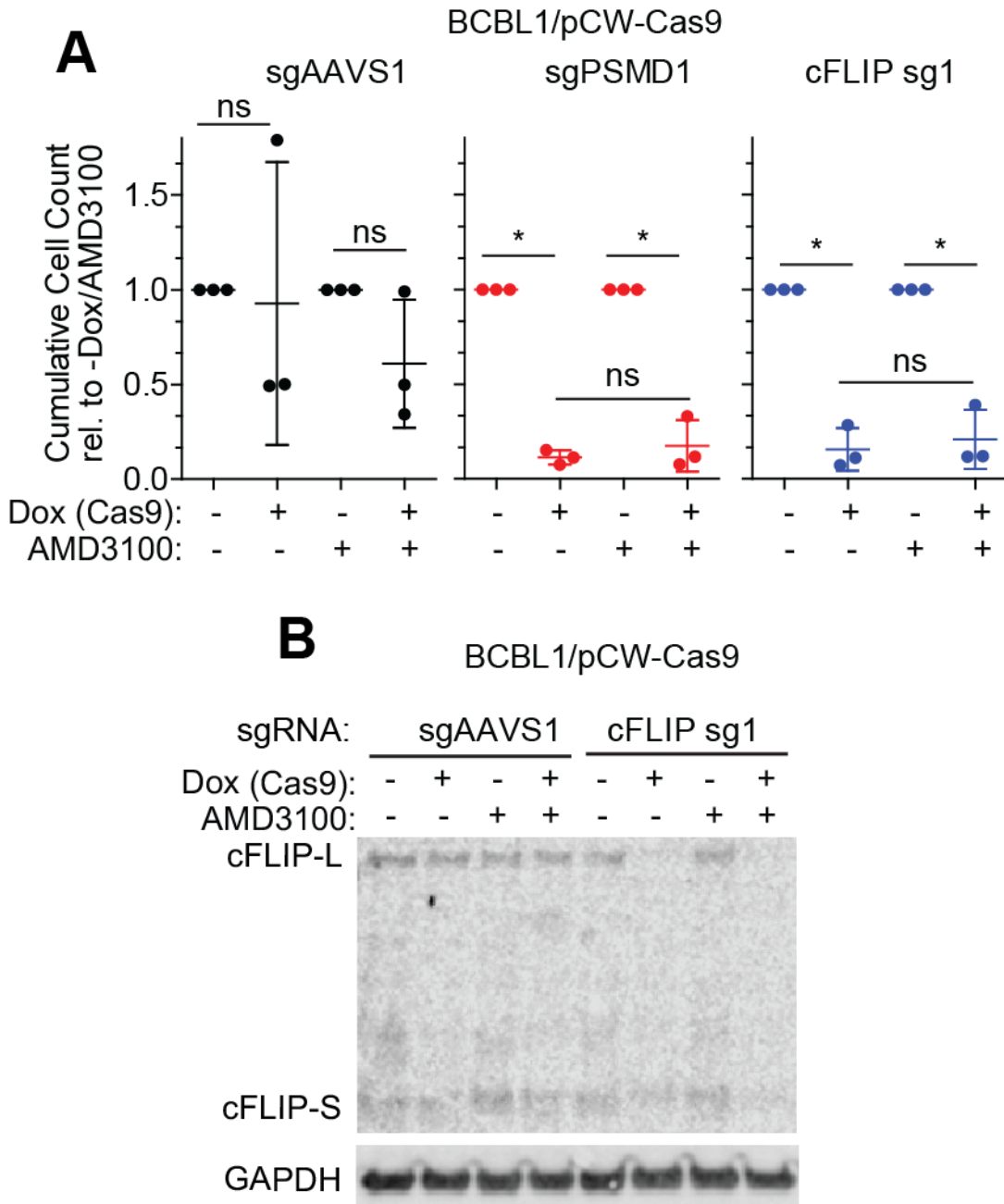


Figure 3.36 Pharmacological inhibition of CXCR4 does not confer resistance to cFLIP loss.

A. BCBL-1 cells with Dox-inducible Cas9 expression (BCBL-1/pCW-Cas9) were transduced with the indicated sgRNAs, selected, and treated with the indicated combinations of Dox and 25 μ M AMD3100. Cumulative cellular growth curves over seven days were performed as described above (n=3 independent repeats). Lack of significant differences was tested by one-tailed, two-sample t-tests, FDR-adjusted p-values are listed in Appendix. **B.** Lysates were collected 5 days after the start of treatment in A) and cFLIP KO efficiency was confirmed by Western blot (n=2)

Chapter 4 Discussion

A partial version of this chapter has been published in Cell Death and Differentiation. CDD 30, 1221–1234 (2023).

CRISPR screens identify novel regulators of cFLIP dependency and ligand-independent, TRAIL-R1-mediated cell death

Neil Kuehnle, Scout Mask Osborne, Ziyan Liang, Mark Manzano & Eva Gottwein

Throughout this dissertation, I have distinguished the roles of KSHV vFLIP and human cFLIP in KSHV-transformed PEL cell lines (for a working model of the role of FLIPs in PEL cells, see Fig 4.1.). While cFLIP is required for its canonical function to inhibit CASP8 downstream of a death receptor signal, vFLIP was surprisingly not detected in all PEL cell lines and could not fully compensate for loss of cFLIP expression. Moreover, detectable vFLIP expression correlated with requirements for NF-κB-related genes, consistent with the well characterized role of KSHV vFLIP as an activator of NF-κB signaling. Thus, my data demonstrate that vFLIP and cFLIP have only limited functional overlap in the most physiologically relevant PEL models available. My results suggest that vFLIP has either low affinity to CASP8 or cannot effectively inhibit CASP8 once bound. Since I achieved very high levels of vFLIP overexpression in my rescue experiments, vFLIP sequestration from CASP8 by NEMO is less likely, although possible. My results with mutated vFLIP indicate that NF-κB activation could plausibly explain this phenotype. However, differences in the level of detection and an inability to establish key controls for the function of this mutant described in the next paragraph preclude conclusive statements or formal publication of this result at the present time.

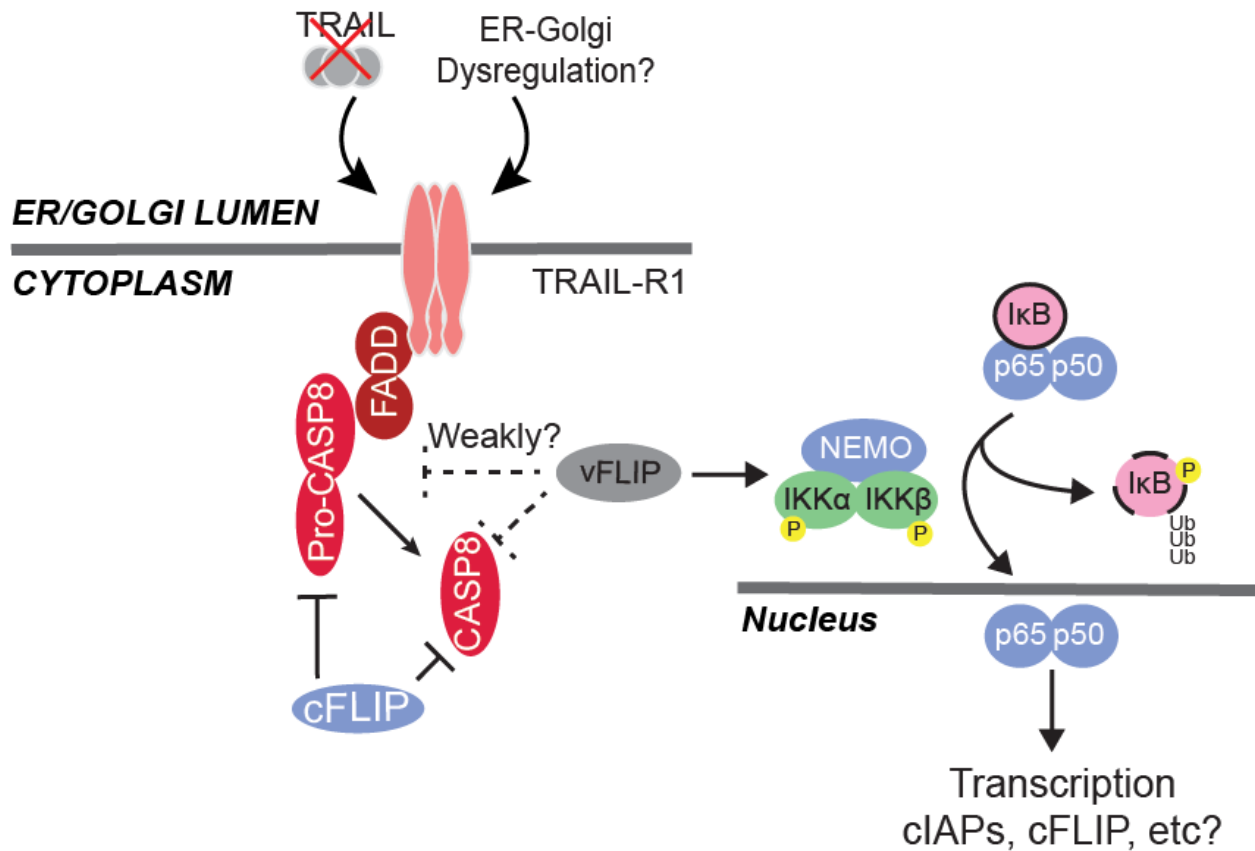


Figure 4.1 Working model of FLIP function in PEL cells.

Left: The recently demonstrated core function of cellular FLIP in PEL, direct inhibition of CASP8-mediated cell death. In this context, CASP8 is activated downstream of TRAIL-R1, but not TRAIL-R2. Further TRAIL-R1 complexes are internally localized (i.e. in the ER/Golgi) and active in the absence of TRAIL. While the nature of this signal is not clear, it is clearly connected to several ER/Golgi resident processes, suggestive of uncharacterized ER/Golgi stress or dysregulation. Right: The known and inferred role(s) of vFLIP in PEL. Though not always detected in cultured PEL cells, vFLIP has a well-established ability to activate NF- κ B signalling and its associated transcriptional targets through direct interactions with the IKK modulator, NEMO. Limited redundancies between cFLIP and vFLIP (i.e. reduced dependence on cFLIP in cell lines ectopically expressing vFLIP) could be explained either by the pro-survival transcriptional activities that have been described for NF- κ B or via weak/limited direct inhibition of CASP8 activity (not tested in this study).

It is worth noting in the context of the viral rescue experiments presented that several limitations apply. Firstly, validation of CASP8 binding (i.e., by co-IP) or NF-κB modulation (e.g., by reporter assay) were not performed. I attempted both assays but was unsuccessful establishing positive and negative controls. I attempted DISC pulldown following previously published protocols which rely on buffers containing weak detergents to solubilize tightly membrane associated DISC complexes [282-287]. In my hands, pulldown of FLAG tagged FLIPs was efficient, but DISC (CASP8) co-IP could not be confirmed even for cFLIP L/S positive controls. Similarly, reporter assays yielded a high degree of background in 293T. Ultimately, I abandoned these experiments in favor of a more productive focus on the role of cFLIP and the mechanism underpinning TRAIL-R1 activity in PEL cells.

Another result presented within this text is that shRNAs targeting the vFLIP/vCyc dicistron often do not result in measurable toxicity in PEL cells. Controversially, this result stands in contrast to a published result [64]. While it seems intuitive that vFLIP/vCyc are not required in PEL cell lines that do not express them well, this experiment has a few conceptual and practical limitations meriting discussion. First, my shRNAs do not produce complete protein KD even in BC-3, where both shRNAs result in significant and large reductions in cumulative growth curves. As vFLIP and vCyc are often not detectable in PEL, it is at the same impossible to verify whether any theoretical “residual” protein is present since the baseline is already undetectable. This experiment also carries considerable conceptual concerns regarding the nature of the vFLIP expression differences in general. Though I tested the earliest available passage of BCBL-1 and found that these neither expressed vFLIP/vCyc nor responded to my shRNA, the possibility that low/absent vFLIP/vCyc expression is an artifact of the use of *in vitro* PEL cell

lines remains. As fresh PEL samples remain rare and difficult to acquire, these experiments were unfeasible for me at present but form an interesting basis for future research.

Further, the use of a higher MOI in these experiments could trigger the same off-target effects that plague other studies of KSHV latency genes (see section 1.5). Indeed, others in our group have observed non-specific toxicity of shRNA expression in PEL that increases with MOI, including shRNA-specific toxicity of my NT-4 control. Thus, my experiments should eventually be repeated at lower MOI, with an empty vector control and updated control shRNAs. A critical experiment necessary to rule out off-target effects in these experiments would be to perform rescue with vCyc and/or vFLIP. Although vFLIP overexpression is achievable in PEL, I was unsuccessful in generating PEL constitutively expressing ectopic vCyc. Cells transduced with vCyc failed to successfully grow out and generally seemed to produce lower titers than FLIP overexpression constructs in the same backbone (data not shown or rigorously tested), consistent with other reports claiming constitutive vCyc overexpression is toxic to cells, particularly when de-coupled from vFLIP expression [152, 288, 289]. Nonetheless, these rescue experiments would address key questions that have resurfaced about the roles of these proteins in PEL cells.

Next, I identified TRAIL-R1, but not TRAIL-R2, as the critical death receptor that triggers CASP8-induced cell death in the absence of cFLIP. Unlike in EBV-transformed LCLs [177], this process appears entirely ligand independent. Interestingly, such a ligand-independent process has been described in response to ER stress-induced cell death, mainly for TRAIL-R2. A ligand-independent role for TRAIL-R1 has also been reported, but primarily in the context of Golgi and/or secretory stressors rather than general ER stress [210, 275-279]. Ligand

independent cell death signaling by TRAIL receptors involves their intracellular accumulation and, similarly, TRAIL-R1 is detected intracellularly in PEL cells within the ER and Golgi.

Additionally, my results were obtained without the use of ER/Golgi stress inducing agents and instead represent a constitutively active TRAIL-R1 death signaling process in robustly growing cells. Importantly, PEL cells are of post-germinal center B cell origin and terminal B cell differentiation is typically accompanied by a broad expansion and alteration of the ER and Golgi. However, PEL cell lines typically lack B cell surface marker and immunoglobulin expression and the status of the ER/Golgi in PEL cell lines has not been investigated in depth. Interestingly, KSHV has been reported to activate the UPR and dampen its downstream transcriptional response during lytic reactivation and ER stress has been shown to trigger KSHV reactivation in latently infected cells [290, 291]. Conversely, I did not detect colocalization of TRAIL-R1 with MPZ-DelS63 as has been reported for TRAIL-R2 in the context of cell death during the UPR [280].

In addition to TRAIL-R1, my work has implicated several other ER/Golgi resident processes in cFLIP dependency. High confidence hits in my cFLIP resistance screens included most genes of the UFMylation pathway. Inactivation of UFM1 or DDRGK1 reduced TRAIL-R1 expression, which is likely to explain their detection in my screens. Compared to ubiquitin, UFM1 modifies only few proteins. The 60S ribosomal subunit RPL26 has been proposed as the primary UFM1 target, where UFM1 modification promotes the processing of translationally stalled polypeptides at the ER [266, 267]. While I did not directly test the role of UFM1 or RPL26 in the translation of TRAIL-R1, UFMylation of RPL26 may explain the requirement for UFM1/DDRGK1 for TRAIL-R1 expression. UFMylation is induced in response to cellular

stressors, directing nascent peptides to the ER for degradation [258, 266, 267, 292, 293] and, accordingly, disruption of UFMylation has been reported to induce ER stress and increase cell death [292, 294, 295]. Of note, genes in the UFMylation pathway do not score as essential in my original PEL screens and their essentiality within the Cancer Dependency Map is mixed [65, 175]. Thus, it is plausible that UFMylation could similarly allow translation of pro-apoptotic proteins, like TRAIL-R1, to proceed. A varied requirement for UFMylation for cellular survival is further supported by findings that deletion of DDRGK1 in mouse plasma cells did not result in increased cell death [296].

Like UFMylation, I observed that JAGN1 promotes expression of TRAIL-R1. While little is known about this gene, JAGN1 has been shown to participate in the secretory pathway in myeloid cells and antibody-producing B cells [269, 297]. As with UFMylation, JAGN1 is increased in response to ER stress and its depletion has been linked to increased apoptosis in granulocytes [269, 298]. Importantly, my PEL CRISPR screens and establishment of a JAGN1 KO cell line suggest that JAGN1 is non-essential in PEL cells. Similarly, the Cancer Dependency Map indicates that JAGN1 is not broadly required for cellular survival [65, 175]. While JAGN1 phenocopies the behavior of UFM1 KO's impact on TRAIL-R1 levels, it does so without any apparent impact on UFMylation. It seems unlikely that JAGN1 is involved in protein co-translation given its known function in endosomal trafficking/secretion. It would be interesting to see if JAGN1 ensures trafficking of TRAIL-R1 beyond the ER, such as to the Golgi. One explanation for why JANG1 KO might negatively impact TRAIL-R1 levels then, is that in its absence TRAIL-R1 traffics in a different manner, such as into the lysosome or proteosome-dependent ERAD pathway (see a hypothetical schematic in Fig 4.2) [299, 300].

In any case, modulation of protein co-translation seems to be the most likely mechanism of action for UFMylation within the context of TRAIL-R1 mediated cell death in PEL cells (see Fig. 4.2 for a working model). However, the question remains whether this requirement for UFMylation is present at homeostasis in most cell types or whether it might be indicative of a grander problem, such as the ER stress/UPR indicated by other studies. It's worth noting that RPL26 was identified as a target in the context of ERAD of nascent cytoplasmic proteins (not typically bound for the ER) [266, 267], though it seems likely UFMylation may function readily as a factor regulating baseline protein co-translation. If this were the case, it would be interesting to determine whether certain nascent peptides (i.e. TRAIL-R1) are preferentially targeted by UFMylation. This possibility is exciting given the unusually bare surface of PEL cells [301-304], though this appears not to be the case during acute, stress induced translational pausing associated with ERAD [266, 267]. Even more exciting is the possibility that KSHV might regulate this process in some form (be it through miRNA targets or transcriptional regulators like vIRF-3 or LANA) [301-304].

My data also suggests that chondroitin sulfate proteoglycan biosynthesis and CXCR4 are involved in the ligand-independent activity of TRAIL-R1. Since inactivation of neither pathway affected TRAIL-R1 expression or caused re-distribution of TRAIL-R1 to the cell surface, the exact mechanism underlying their link to TRAIL-R1 signaling and cFLIP dependency remains unclear. Interestingly, both CXCR4 and its primary ligand, CXCL12, have been identified as targets of chondroitin sulfate moieties, although the roles of these modifications remain unclear [305, 306]. However, CXCL12 is not endogenously expressed in PEL cells and TRAIL-R1-dependent cell death in PEL cells is not overcome by CXCR4 inhibitors. Additionally, there is a report of CXCR4-induced apoptosis, but this process was independent of CASP8 and could not

be inhibited by MC159L, unlike the TRAIL-R1 dependent process that is inhibited by cFLIP in PEL cells [307]. Recent work indicates that misfolded integral membrane proteins, such as MPZ, can act as non-canonical ligands for TRAIL-R2 activity during ER stress-induced cell death [280]. Notably, rhodopsin, a member of the 7-pass transmembrane (7TM) protein family to which CXCR4 belongs, also demonstrated this activity [280]. Future work should therefore test whether misfolding of endogenous CXCR4 serves as a trigger of ligand-independent TRAIL-R1 signaling in PEL cells. This would be particularly interesting in light of observations that PEL cells lack typical surface proteins associated with plasma cells, as misfolded proteins accumulate with the ER/Golgi until they can be degraded [301-304, 308]. Further, it would nicely complement my findings that CXCL12 is not expressed in PEL and that chemical inhibition of CXCR4 fails to recapitulate CXCR4 KO, as misfolding of CXCR4 would be detached from its normal signaling function.

In my original proposal I suggested several lines of experimentation that attempt to dissect the role of ER stress specifically. These include treatment of TRAIL-R1 KO cells with tunicamycin and/or other ER/secretory stressors to assess resistance to these compounds and attempted rescue of cFLIP loss by HSPA5 overexpression. While some groups have reported success with these lines of reasoning, early pilot attempts at establishing these experiments did not produce compelling results in my system (data not shown). Lack of significant differences in the case of ER stressors is complicated by the fact that these drugs not only upregulate TRAIL-R2 and promote cell death in a manner likely orthogonal to the mechanism I observed, but also produce broad toxicity via cell arrest, dysregulation of autophagy, and necrotic cell death. Thus, these experiments were quickly abandoned in favor of more productive experimental aims. One line of reasoning which was pursued to some extent was differential essentiality screens

performed in the context of CASP8 and TRAIL-R1 KO (data not shown). These screens were overall quite poor in quality, in part due to poor sequencing depth. However, they did produce one potentially compelling hit in the form of the prefoldin 6 (PDFN6), a member of the cytoplasmic prefoldin chaperone complex, though this particular subunit may simply be required primarily to assist in the folding of cFLIP which is similarly differentially essential in CASP8 and TRAIL-R1 KO cells. In any case, a deeper understanding of the nature of the ER-Golgi network in PEL cells is of great importance as this organelle system and the ER stress/UPR that act as monitors of their homeostasis are central to plasma cell biology and differentiation.

Several key questions regarding the nature of ligand-independent TRAIL-R1 activation in PEL cells remain for future research. Do PEL cells exhibit endogenous ER/Golgi “stress” or dysregulation? Are there meaningful abnormalities in the functioning of these critical organelles? Does KSHV, perhaps via its transcriptional re-programming or by its nature as a virus trafficking through endosomes impact these processes? For a summary of hypothetical mechanisms and questions involved in the initiation of ligand-independent TRAIL-R1-mediated cell death in PEL cells, see Figs. 4.2 & 4.3. Regardless, my present data strongly support a role for TRAIL-R1 in incorporating multiple ER/Golgi-associated signals in PEL cells into a constitutive, ligand-independent cell death process that must be inhibited by cFLIP to allow for cellular viability.

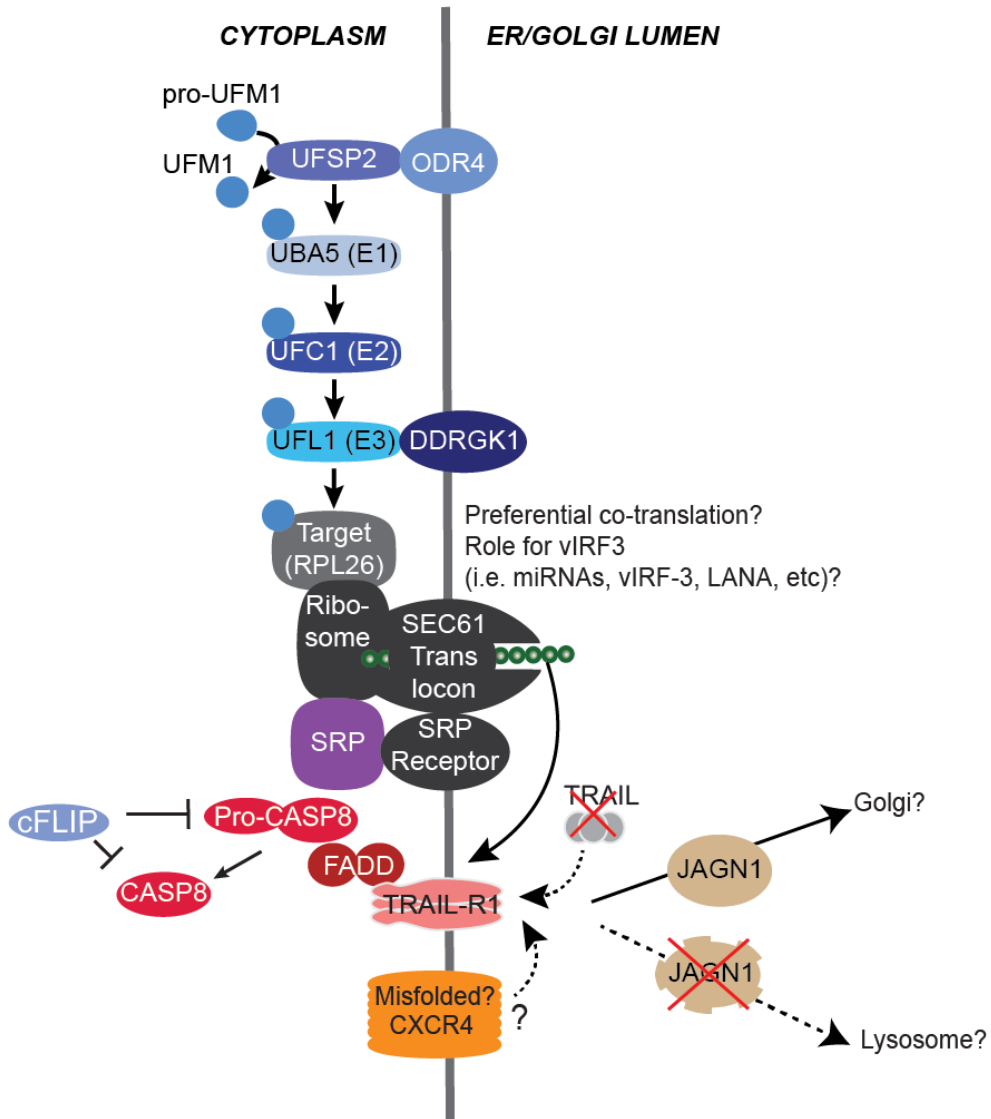


Figure 4.2 Working model of TRAIL-related processes in the ER of PEL cells.

A speculative model of how UFMylation and JAGN1 relate to TRAIL-R1 activity in PEL cells. Work by myself and others point to UFMylation as a modulator of co-translation (see [266, 267], Figs. 3.22 & 3.44), in this case for TRAIL-R1. Whether this process displays a preference for certain ER-bound proteins or is modulated by KSHV remains untested. JAGN1 could possibly alter the trafficking of TRAIL-R1 in the cell, preventing its degradation (untested, though JAGN1 KO reduced TRAIL-R1 levels, see Fig. 3.22). Here JAGN1 is postulated (not shown directly) to direct TRAIL-R1 to the Golgi where it is detected in addition to the ER (Figs.3.26-3.28). Note that chondroitin sulfate biosynthesis (not shown, see Fig. 3.19) is a Golgi-resident process. CXCR4 is a transmembrane protein which undergoes co-translation into the ER, but its localization is not confirmed here. CXCR4 is related to a misfolded protein which binds TRAIL-R2, although this has not been tested for CXCR4 and TRAIL-R1.

Appendices

Statistical Test Outputs Fig 3.4A

Test for loss of viability								
test name	Control CellLine	Control sgRNA	Experimental CellLine	Experimental sgRNA	test type	pvalue	FDR	significant
3.4A BCBL-1 IRF4	BCBL-1	AAVS1	BCBL-1	IRF4	one-sample	7.07E-10	6.27E-09	Y
3.4A BCBL-1 PSMD1	BCBL-1	AAVS1	BCBL-1	PSMD1	one-sample	3.25E-09	1.30E-08	Y
3.4A BCBL-1 cFLIP sg1	BCBL-1	AAVS1	BCBL-1	cFLIP sg1	one-sample	1.86E-09	9.31E-09	Y
3.4A BCBL-1 cFLIP sg2	BCBL-1	AAVS1	BCBL-1	cFLIP sg2	one-sample	1.02E-11	2.03E-10	Y
3.4A BC-1 IRF4	BC-1	AAVS1	BC-1	IRF4	one-sample	8.35E-07	2.09E-06	Y
3.4A BC-1 PSMD1	BC-1	AAVS1	BC-1	PSMD1	one-sample	3.53E-07	1.01E-06	Y
3.4A BC-1 cFLIP sg1	BC-1	AAVS1	BC-1	cFLIP sg1	one-sample	5.50E-04	7.85E-04	Y
3.4A BC-1 cFLIP sg2	BC-1	AAVS1	BC-1	cFLIP sg2	one-sample	7.75E-03	9.12E-03	Y
3.4A BC-2 IRF4	BC-2	AAVS1	BC-2	IRF4	one-sample	9.40E-10	6.27E-09	Y
3.4A BC-2 PSMD1	BC-2	AAVS1	BC-2	PSMD1	one-sample	1.03E-04	1.88E-04	Y
3.4A BC-2 cFLIP sg1	BC-2	AAVS1	BC-2	cFLIP sg1	one-sample	1.97E-04	3.29E-04	Y
3.4A BC-2 cFLIP sg2	BC-2	AAVS1	BC-2	cFLIP sg2	one-sample	4.07E-04	6.26E-04	Y
3.4A BC-3 IRF4	BC-3	AAVS1	BC-3	IRF4	one-sample	6.63E-08	2.21E-07	Y
3.4A BC-3 PSMD1	BC-3	AAVS1	BC-3	PSMD1	one-sample	6.37E-06	1.42E-05	Y
3.4A BC-3 cFLIP sg1	BC-3	AAVS1	BC-3	cFLIP sg1	one-sample	8.45E-02	8.89E-02	N
3.4A BC-3 cFLIP sg2	BC-3	AAVS1	BC-3	cFLIP sg2	one-sample	8.28E-01	8.28E-01	N
3.4A BC-5 IRF4	BC-5	AAVS1	BC-5	IRF4	one-sample	5.82E-03	7.40E-03	Y
3.4A BC-5 PSMD1	BC-5	AAVS1	BC-5	PSMD1	one-sample	5.92E-03	7.40E-03	Y
3.4A BC-5 cFLIP sg1	BC-5	AAVS1	BC-5	cFLIP sg1	one-sample	3.62E-05	7.23E-05	Y
3.4A BC-5 cFLIP sg2	BC-5	AAVS1	BC-5	cFLIP sg2	one-sample	5.10E-02	5.67E-02	N

Statistical Test Outputs Fig 3.5A

Test for loss of viability □								
test name	Control CellLine	Control sgRNA	Experimental CellLine	Experimental sgRNA	test type	pvalue	FDR	significant
3.5A ZsGreen PSMD1	ZsGreen	AAVS1	ZsGreen	PSMD1	one-sample	6.92E-06	2.32E-05	Y
3.5A ZsGreen cFLIP sg1	ZsGreen	AAVS1	ZsGreen	cFLIP sg1	one-sample	7.73E-06	2.32E-05	Y
3.5A ZsGreen cFLIP sg1	ZsGreen	AAVS1	ZsGreen	cFLIP sg2	one-sample	5.44E-03	9.78E-03	Y
3.5A cFLIP-L PSMD1	cFLIP-L	AAVS1	cFLIP-L	PSMD1	one-sample	1.26E-05	2.83E-05	Y
3.5A cFLIP-L cFLIP D1	cFLIP-L	AAVS1	cFLIP-L	cFLIP sg1	one-sample	1.39E-01	2.08E-01	N
3.5A cFLIP-L cFLIP D2	cFLIP-L	AAVS1	cFLIP-L	cFLIP sg2	one-sample	4.57E-01	5.88E-01	N
3.5A cFLIP-S PSMD1	cFLIP-S	AAVS1	cFLIP-S	PSMD1	one-sample	6.42E-06	2.32E-05	Y
3.5A cFLIP-S cFLIP D1	cFLIP-S	AAVS1	cFLIP-S	cFLIP sg1	one-sample	5.45E-01	6.13E-01	N
3.5A cFLIP-S cFLIP D2	cFLIP-S	AAVS1	cFLIP-S	cFLIP sg2	one-sample	8.46E-01	8.46E-01	N

Test for rescue by re-expression of cFLIP-L or cFLIP-S								
test name	Control CellLine	Control sgRNA	Experimental CellLine	Experimental sgRNA	test type	pvalue	FDR	significant
3.5A cFLIP-L Rescue of PSMD1	ZsGreen	PSMD1	cFLIP-L	PSMD1	two-sample	6.94E-01	6.94E-01	N
3.5A cFLIP-L Rescue of cFLIP D1	ZsGreen	cFLIP sg1	cFLIP-L	cFLIP sg1	two-sample	1.48E-03	4.44E-03	Y
3.5A cFLIP-L Rescue of cFLIP D2	ZsGreen	cFLIP sg1	cFLIP-L	cFLIP sg2	two-sample	2.08E-02	3.12E-02	Y
3.5A cFLIP-S Rescue of PSMD1	ZsGreen	PSMD1	cFLIP-S	PSMD1	two-sample	6.60E-01	6.94E-01	N
3.5A cFLIP-S Rescue of cFLIP D1	ZsGreen	cFLIP sg1	cFLIP-S	cFLIP sg1	two-sample	9.21E-05	5.52E-04	Y
3.5A cFLIP-S Rescue of cFLIP D2	ZsGreen	cFLIP sg1	cFLIP-S	cFLIP sg2	two-sample	8.24E-03	1.65E-02	Y

Statistical Test Outputs Fig 3.9A

test_name	Control_CellLine	Control_sgRNA	Experimental_CellLine	Experimental_sgRNA	test_type	pvalue	FDR	significant
3.9A ZsGreen_PSMd1	ZsGreen	AAVS1	ZsGreen	PSMD1	one-sample	6.06E-11	2.44E-10	Y
3.9A ZsGreen_cFLIP_sgl	ZsGreen	AAVS1	ZsGreen	cFLIP_sgl	one-sample	2.70E-12	2.40E-11	Y
3.9A KSHV_vFLIP_PSMd1	KSHV_vFLIP	AAVS1	KSHV_vFLIP	PSMD1	one-sample	6.53E-06	1.74E-05	Y
3.9A KSHV_vFLIP_cFLIP_sgl	KSHV_vFLIP	AAVS1	KSHV_vFLIP	cFLIP_sgl	one-sample	2.51E-05	4.02E-05	Y
3.9A MC159L_PSMd1	MC159L	AAVS1	MC159L	PSMD1	one-sample	1.10E-05	2.20E-05	Y
3.9A MC159L_cFLIP_sgl	MC159L	AAVS1	MC159L	cFLIP_sgl	one-sample	9.53E-01	9.53E-01	N
3.9A MC160L_PSMd1	MC160L	AAVS1	MC160L	PSMD1	one-sample	3.03E-05	4.04E-05	Y
3.9A MC160L_cFLIP_sgl	MC160L	AAVS1	MC160L	cFLIP_sgl	one-sample	1.09E-04	1.25E-04	Y

Test for rescue by expression of KSHV vFLIP, MC159L, or MC160L									
test name	Control CellLine	Control sgRNA	Experimental CellLine	Experimental sgRNA	test type	pvalue	FDR	significant	
3.9A KSHV vFLIP Rel PSMD1	ZsGreen	PSMD1	KSHV vFLIP	PSMD1	two-sample	4.38E-02	8.77E-02	N	
3.9A KSHV vFLIP Rel cFLIP sg1	ZsGreen	cFLIP sg1	KSHV vFLIP	cFLIP sg1	two-sample	2.87E-07	8.60E-07	Y	
3.9A MC159L Rel PSMD1	ZsGreen	PSMD1	MC159L	PSMD1	two-sample	8.63E-01	8.63E-01	N	
3.9A MC159L Rel cFLIP sg1	ZsGreen	cFLIP sg1	MC159L	cFLIP sg1	two-sample	2.50E-09	1.50E-08	Y	
3.9A MC160L Rel PSMD1	ZsGreen	PSMD1	MC160L	PSMD1	two-sample	8.08E-01	8.63E-01	N	
3.9A MC160L Rel cFLIP sg1	ZsGreen	cFLIP sg1	MC160L	cFLIP sg1	two-sample	3.60E-01	5.40E-01	N	

Statistical Test Outputs Fig 3.7

Test for loss of viability								
test name	Control CellLine	Control shRNA	Experimental CellLine	Experimental shRN	test type	pvalue	FDR	significan
3.7 BCBL-1 vCyc	BCBL-1	NT-4	BCBL-1	vCyc sh1	one-sample	2.67E-02	2.14E-01	N
3.7 BCBL-1 vCyc	BCBL-1	NT-4	BCBL-1	vCyc sh2	one-sample	7.93E-01	7.93E-01	N
3.7 BC-1 vCyc sh	BC-1	NT-4	BC-1	vCyc sh1	one-sample	4.26E-02	2.98E-01	N
3.7 BC-1 vCyc sh	BC-1	NT-4	BC-1	vCyc sh2	one-sample	1.12E-01	4.49E-01	N
3.7 BC-2 vCyc sh	BC-2	NT-4	BC-2	vCyc sh1	one-sample	1.04E-01	4.49E-01	N
3.7 BC-2 vCyc sh	BC-2	NT-4	BC-2	vCyc sh2	one-sample	2.12E-01	6.36E-01	N
3.7 BC-3 vCyc sh	BC-3	NT-4	BC-3	vCyc sh1	one-sample	8.23E-06	8.23E-05	Y
3.7 BC-3 vCyc sh	BC-3	NT-4	BC-3	vCyc sh2	one-sample	1.14E-03	1.03E-02	Y
3.7 BC-5 vCyc sh	BC-5	NT-4	BC-5	vCyc sh1	one-sample	4.99E-01	7.93E-01	N
3.7 BC-5 vCyc sh	BC-5	NT-4	BC-5	vCyc sh2	one-sample	7.08E-02	4.25E-01	N

Statistical Test Outputs Fig 3.9B

Test for reduced viability														
test_name	Control_Cell_Line	Control_sgRNA	Experimental_CellLine	Experimental_sgRNA	test_type	numerical_predictor	categorical_predictor	R-squared	tested_coef	coef	std_err	pvalue	FDR	significant
3.9B_ZsGreen_PSM1	ZsGreen	AAVS1	ZsGreen	PSMD1	OLS + t-test	timepoint	None	0.663	day	-0.154938683	0.025368936	3.58E-06	4.77E-06	Y
3.9B_ZsGreen_cFLIP_sg1	ZsGreen	AAVS1	ZsGreen	cFLIP sg1	OLS + t-test	timepoint	None	0.633	day	-0.119768669	0.020940292	8.18E-06	8.18E-06	Y
3.9B_KSHV_vFLIP_PSM1	KSHV vFLIP	AAVS1	KSHV vFLIP	PSMD1	OLS + t-test	timepoint	None	0.708	day	-0.131694075	0.0180506	1.32E-07	2.63E-07	Y
3.9B_KSHV_vFLIP_cFLIP_sg1	KSHV vFLIP	AAVS1	KSHV vFLIP	cFLIP sg1	OLS + t-test	timepoint	None	0.746	day	-0.095803502	0.011931934	2.78E-08	1.11E-07	Y
Test for rescue by expression of KSHV vFLIP														
test_name	Control_Cell_Line	Control_sgRNA	Experimental_CellLine	Experimental_sgRNA	test_type	numerical_predictor	categorical_predictor	R-squared	tested_coef	coef	std_err	pvalue	FDR	significant
3.9B_KSHV_vFLIP_Rescue_PSM1	ZsGreen	PSMD1	KSHV vFLIP	PSMD1	OLS + t-test	timepoint	vFLIP Overexpression[T]	0.727	vFLIP Overexpression[T]	0.077318801	0.067870458	1.31E-01	1.31E-01	N
3.9B_KSHV_vFLIP_Rescue_cFLIP_sg1	ZsGreen	cFLIP sg1	KSHV vFLIP	cFLIP sg1	OLS + t-test	timepoint	vFLIP Overexpression[T]	0.781	vFLIP Overexpression[T]	0.401807015	0.053598033	2.25E-09	4.50E-09	Y

Statistical Test Outputs Fig 3.11

test_name	Control_CellLine	Control_sgRNA	Experimental_CellLine	Experimental_sgRNA	test_type	numerical_predictor	R^2	tested_coef	coef	std_err	pvalue	FDR	significant	
3.11_ZsGreen_PSM1	ZsGreen	AAVS1	ZsGreen	PSMD1	OLS + t-test	timepoint	0.88	day	-0.16	0.02	3.71E-06	1.48E-05	Y	
3.11_ZsGreen_cFLIP_sg1	ZsGreen	AAVS1	ZsGreen	cFLIP sg1	OLS + t-test	timepoint	0.75	day	-0.09	0.02	1.35E-04	1.35E-04	Y	
3.11_KSHV_vFLIP_WT_PSM1	KSHV vFLIP (WT)	AAVS1	KSHV vFLIP (WT)	PSMD1	OLS + t-test	timepoint	0.82	day	-0.12	0.01	1.50E-06	7.50E-06	Y	
3.11_KSHV_vFLIP_WT_cFLIP_sg1	KSHV vFLIP (WT)	AAVS1	KSHV vFLIP (WT)	cFLIP sg1	OLS + t-test	timepoint	0.85	day	-0.08	0.01	5.11E-07	3.07E-06	Y	
3.11_KSHV_vFLIP_Mut_PSM1	KSHV vFLIP (Mut)	AAVS1	KSHV vFLIP (Mut)	PSMD1	OLS + t-test	timepoint	0.78	day	-0.11	0.02	6.96E-06	2.09E-05	Y	
3.11_KSHV_vFLIP_Mut_cFLIP_sg1	KSHV vFLIP (Mut)	AAVS1	KSHV vFLIP (Mut)	cFLIP sg1	OLS + t-test	timepoint	0.73	day	-0.07	0.01	2.51E-05	5.02E-05	Y	

Test for rescue by expression of KSHV vFLIP WT or Mut

test_name	Control_CellLine	Control_sgRNA	Experimental_CellLine	Experimental_sgRNA	test_type	numerical_predictor	categorical_predictor	R^2	tested_coef	coef	std_err	pvalue	FDR	significant
3.11_KSHV_vFLIP_WT_Rescue_PSM1	ZsGreen	PSMD1	KSHV vFLIP (WT)	PSMD1	OLS + t-test	timepoint	vFLIP (WT) Overexpression	0.83	vFLIP (WT) Overexpression	1.02E-01	6.31E-02	5.98E-02	1.63E-01	N
3.11_KSHV_vFLIP_Rescue_cFLIP_sg1	ZsGreen	cFLIP sg	KSHV vFLIP (WT)	cFLIP sg1	OLS + t-test	timepoint	vFLIP (WT) Overexpression	0.86	vFLIP (WT) Overexpression	3.79E-01	4.19E-02	1.71E-09	6.84E-09	Y
3.11_KSHV_vFLIP_Rescue_PSM1	ZsGreen	PSMD1	KSHV vFLIP (Mut)	PSMD1	OLS + t-test	timepoint	vFLIP (Mut) Overexpression	0.80	vFLIP (Mut) Overexpression	5.25E-02	6.79E-02	2.23E-01	2.23E-01	N
3.11_KSHV_vFLIP_Rescue_cFLIP_sg1	ZsGreen	cFLIP sg	KSHV vFLIP (Mut)	cFLIP sg1	OLS + t-test	timepoint	vFLIP (Mut) Overexpression	0.80	vFLIP (Mut) Overexpression	7.23E-02	5.03E-02	8.17E-02	1.63E-01	N

Statistical Test Outputs Fig 3.21A

Test for loss of viability from sgPSMD1 or sg-cFLIP relative to sgAAVS1 after second sgRNA challenge									
test_name	Control_CellLine	Control_sgRNA	Experimental_CellLine	Experimental_sgRNA	test_type	pvalue	FDR	significant	
3.21A_AAVS1_PSMD1	AAVS1	AAVS1	AAVS1	PSMD1	one-sample	6.49E-04	1.95E-03	Y	
3.21A_AAVS1_cFLIP_sg	AAVS1	AAVS1	AAVS1	cFLIP sg1	one-sample	1.15E-05	6.91E-05	Y	
3.21A_CASP8	CASP8 sg1	AAVS1	CASP8 sg1	PSMD1	one-sample	3.17E-03	4.75E-03	Y	
3.21A_CASP8	CASP8 sg1	AAVS1	CASP8 sg1	cFLIP sg1	one-sample	5.41E-01	6.49E-01	N	
3.21A_CASP8	CASP8 sg2	AAVS1	CASP8 sg2	PSMD1	one-sample	1.37E-03	2.75E-03	Y	
3.21A_CASP8	CASP8 sg2	AAVS1	CASP8 sg2	cFLIP sg1	one-sample	9.37E-01	9.37E-01	N	
Test for rescue in CASP8 KO cell lines compared to control cell line after second sgRNA challenge									
test_name	Control_CellLine	Control_sgRNA	Experimental_CellLine	Experimental_sgRNA	test_type	pvalue	FDR	significant	
3.21A_CASP8_sg1_Rescue of PSMD1	AAVS1	PSMD1	CASP8 sg1	PSMD1	two-sample	2.03E-01	2.03E-01	N	
3.21A_CASP8_sg1_Rescue of cFLIP_sg1	AAVS1	cFLIP sg1	CASP8 sg1	cFLIP sg1	two-sample	2.37E-04	4.75E-04	Y	
3.21A_CASP8_sg2_Rescue of PSMD1	AAVS1	PSMD1	CASP8 sg2	PSMD1	two-sample	1.56E-01	2.03E-01	N	
3.21A_CASP8_sg2_Rescue of cFLIP_sg1	AAVS1	cFLIP sg1	CASP8 sg2	cFLIP sg1	two-sample	7.24E-05	2.90E-04	Y	

Statistical Test Outputs Fig 3.23

Test for loss of viability from sgPSMD1 or sg-cFLIP relative to sgAAVS1 after second sgRNA challenge								
test_name	Control_Ce llLine	Control_sgRNA	Experimental_CellLine	Experimental_sgRNA	test_type	pvalue	FDR	significant
3.23_AAVS1_P SMD1	AAVS1	AAVS1	AAVS1	PSMD1	one-sample	5.14E-04	7.34E-04	Y
3.23_AAVS1_c FLIP_sg1	AAVS1	AAVS1	AAVS1	cFLIP sg1	one-sample	2.17E-04	3.88E-04	Y
3.23_TRAIL-R1 sg1_PSMD1	TRAIL-R1 sg1	AAVS1	TRAIL-R1 sg1	PSMD1	one-sample	1.97E-03	2.46E-03	Y
3.23_TRAIL-R1 sg1_cFLIP_sg1	TRAIL-R1 sg1	AAVS1	TRAIL-R1 sg1	cFLIP sg1	one-sample	3.83E-01	3.83E-01	N
3.23_TRAIL-R1 sg2_PSMD1	TRAIL-R1 sg2	AAVS1	TRAIL-R1 sg2	PSMD1	one-sample	3.91E-07	3.91E-06	Y
3.23_TRAIL-R1 sg2_cFLIP_sg1	TRAIL-R1 sg2	AAVS1	TRAIL-R1 sg2	cFLIP sg1	one-sample	8.71E-02	9.68E-02	N
3.23_TRAIL-R2 sg1_PSMD1	TRAIL-R2 sg1	AAVS1	TRAIL-R2 sg1	PSMD1	one-sample	1.67E-04	3.88E-04	Y
3.23_TRAIL-R2 sg1_cFLIP_sg1	TRAIL-R2 sg1	AAVS1	TRAIL-R2 sg1	cFLIP sg1	one-sample	2.33E-04	3.88E-04	Y
3.23_TRAIL sg1_PSMD1	TRAIL sg1	AAVS1	TRAIL sg1	PSMD1	one-sample	7.16E-05	3.58E-04	Y
3.23_TRAIL sg1_cFLIP_sg1	TRAIL sg1	AAVS1	TRAIL sg1	cFLIP sg1	one-sample	2.09E-04	3.88E-04	Y
Test for rescue in TRAILR1 KO cell lines compared to control cell line after second sgRNA challenge								
test_name	Control_Ce llLine	Control_sgRNA	Experimental_CellLine	Experimental_sgRNA	test_type	pvalue	FDR	significant
3.23_TRAIL-R1 sg1_Rescue_of_ PSMD1	AAVS1	PSMD1 s	TRAIL-R1 sg1	PSMD1	two-sample	2.80E-01	7.47E-01	N
3.23_TRAIL-R1 sg1_Rescue_of_c FLIP_sg1	AAVS1	cFLIP sg1	TRAIL-R1 sg1	cFLIP sg1	two-sample	2.26E-02	9.02E-02	N
3.23_TRAIL-R1 sg2_Rescue_of_ PSMD1	AAVS1	PSMD1 s	TRAIL-R1 sg2	PSMD1	two-sample	7.93E-01	7.93E-01	N
3.23_TRAIL-R1 sg2_Rescue_of_c FLIP_sg1	AAVS1	cFLIP sg1	TRAIL-R1 sg2	cFLIP sg1	two-sample	1.40E-03	1.12E-02	Y
3.23_TRAIL-R2 sg1_Rescue_of_ PSMD1	AAVS1	PSMD1 s	TRAIL-R2 sg1	PSMD1	two-sample	5.96E-01	7.58E-01	N
3.23_TRAIL-R2 sg1_Rescue_of_c FLIP_sg1	AAVS1	cFLIP sg1	TRAIL-R2 sg1	cFLIP sg1	two-sample	5.43E-01	7.58E-01	N
3.23_TRAIL sg1_Rescue_of_ PSMD1	AAVS1	PSMD1	TRAIL sg1	PSMD1	two-sample	6.64E-01	7.58E-01	N
3.23_TRAIL sg1_Rescue_of_c FLIP_sg1	AAVS1	cFLIP sg1	TRAIL sg1	cFLIP sg1	two-sample	5.62E-01	7.58E-01	N

Statistical Test Outputs Fig 3.30

Test for loss of viability from experimental sgRNA								
test_name	Control_CellLine	Control_sgRNA	Experimental_CellLine	Experimental_1 sgRNA	test_type	pvalue	FDR	significant
3.30_AAVS1_PSMD1	AAVS1	AAVS1	AAVS1	PSMD1	one-sample	7.36E-05	1.74E-04	Y
3.30_AAVS1_cF	AAVS1	AAVS1	AAVS1	CFLAR sg1	one-sample	9.09E-05	1.97E-04	Y
3.30_UFM1	UFM1 sg1	AAVS1	UFM1 sg1	PSMD1	one-sample	6.49E-05	1.69E-04	Y
3.30_UFM1	UFM1 sg1	AAVS1	UFM1 sg1	CFLAR sg1	one-sample	5.37E-01	5.37E-01	N
3.30_UFM1	UFM1 sg2	AAVS1	UFM1 sg2	PSMD1	one-sample	2.07E-05	1.69E-04	Y
3.30_UFM1	UFM1 sg2	AAVS1	UFM1 sg2	CFLAR sg1	one-sample	5.00E-03	7.17E-03	Y
3.30_DDRGK1	DDRGK1 sg1	AAVS1	DDRGK1 sg1	PSMD1	one-sample	1.85E-04	3.70E-04	Y
3.30_DDRGK1_sg1_cFLIP sg1	DDRGK1 sg1	AAVS1	DDRGK1 sg1	CFLAR sg1	one-sample	1.03E-03	1.79E-03	Y
3.30_DDRGK1_sg2_cFLIP sg1	DDRGK1 sg2	AAVS1	DDRGK1 sg2	CFLAR sg1	one-sample	5.49E-05	1.69E-04	Y
3.30_DDRGK1_sg2_cFLIP sg1	DDRGK1 sg2	AAVS1	DDRGK1 sg2	CFLAR sg1	one-sample	1.31E-02	1.55E-02	Y
3.30_JAGN1	JAGN1 sg1	AAVS1	JAGN1 sg1	PSMD1	one-sample	2.66E-05	1.69E-04	Y
3.30_JAGN1	JAGN1 sg1	AAVS1	JAGN1 sg1	CFLAR sg1	one-sample	1.12E-03	1.82E-03	Y
3.30_JAGN1	JAGN1 sg2	AAVS1	JAGN1 sg2	PSMD1	one-sample	1.67E-05	1.69E-04	Y
3.30_JAGN1	JAGN1 sg2	AAVS1	JAGN1 sg2	CFLAR sg1	one-sample	3.16E-03	4.84E-03	Y
3.30_CXCR4	CXCR4 sg1	AAVS1	CXCR4 sg1	PSMD1	one-sample	5.89E-05	1.69E-04	Y
3.30_CXCR4_sg1_cFLIP sg1	CXCR4 sg1	AAVS1	CXCR4 sg1	CFLAR sg1	one-sample	2.45E-02	2.65E-02	Y
3.30_CXCR4	CXCR4 sg2	AAVS1	CXCR4 sg2	PSMD1	one-sample	5.99E-05	1.69E-04	Y
3.30_CXCR4_sg2_cFLIP sg1	CXCR4 sg2	AAVS1	CXCR4 sg2	CFLAR sg1	one-sample	5.33E-01	5.37E-01	N
3.30_UGDH	UGDH sg1	AAVS1	UGDH sg1	PSMD1	one-sample	2.34E-05	1.69E-04	Y
3.30_UGDH	UGDH sg1	AAVS1	UGDH sg1	CFLAR sg1	one-sample	9.06E-03	1.12E-02	Y
3.30_UGDH	UGDH sg2	AAVS1	UGDH sg2	PSMD1	one-sample	2.21E-04	4.11E-04	Y
3.30_UGDH	UGDH sg2	AAVS1	UGDH sg2	CFLAR sg1	one-sample	5.24E-03	7.17E-03	Y
3.30_CHST15	CHST15 sg1	AAVS1	CHST15 sg1	PSMD1	one-sample	4.90E-05	1.69E-04	Y
3.30_CHST15_sg1_cFLIP sg1	CHST15 sg1	AAVS1	CHST15 sg1	CFLAR sg1	one-sample	2.23E-02	2.52E-02	Y
3.30_CHST15	CHST15 sg2	AAVS1	CHST15 sg2	PSMD1	one-sample	5.75E-05	1.69E-04	Y
3.30_CHST15_sg2_cFLIP sg1	CHST15 sg2	AAVS1	CHST15 sg2	CFLAR sg1	one-sample	7.96E-03	1.04E-02	Y

Statistical Test Outputs Fig 3.30 – continued.

Test for rescue from sg-cFLIP induced cell death								
test_name	Control_CellLine	Control_sgRNA	Experimental_CellLine	Experimental_sgRNA	test_type	pvalue	FDR	significant
3.30_UFM1_sg1_rescue_of_PSMD1	AAVS1	PSMD1	UFM1 sg1	PSMD1	two-sample	4.85E-01	5.82E-01	N
3.30_UFM1_sg1_rescue	AAVS1	CFLAR sg1	UFM1 sg1	CFLAR sg1	two-sample	3.43E-02	7.48E-02	N
3.30_UFM1_sg2_rescue	AAVS1	PSMD1	UFM1 sg2	PSMD1	two-sample	4.40E-01	5.82E-01	N
3.30_UFM1_sg2_rescue	AAVS1	CFLAR sg1	UFM1 sg2	CFLAR sg1	two-sample	9.58E-04	5.75E-03	Y
3.30_DDRGK1_sg1_rescue	AAVS1	PSMD1	DDRGK1 sg1	PSMD1	two-sample	3.20E-01	5.05E-01	N
3.30_DDRGK1_sg1_rescue	AAVS1	CFLAR sg1	DDRGK1 sg1	CFLAR sg1	two-sample	5.94E-04	4.75E-03	Y
3.30_DDRGK1_sg2_rescue	AAVS1	PSMD1	DDRGK1 sg2	PSMD1	two-sample	3.71E-01	5.23E-01	N
3.30_DDRGK1_sg2_rescue	AAVS1	CFLAR sg1	DDRGK1 sg2	CFLAR sg1	two-sample	2.95E-02	7.08E-02	N
3.30_JAGN1_sg1_rescue	AAVS1	PSMD1	JAGN1 sg1	PSMD1	two-sample	4.62E-01	5.82E-01	N
3.30_JAGN1_sg1_rescue	AAVS1	CFLAR sg1	JAGN1 sg1	CFLAR sg1	two-sample	1.64E-03	7.86E-03	Y
3.30_JAGN1_sg2_rescue	AAVS1	PSMD1	JAGN1 sg2	PSMD1	two-sample	7.30E-01	7.30E-01	N
3.30_JAGN1_sg2_rescue	AAVS1	CFLAR sg1	JAGN1 sg2	CFLAR sg1	two-sample	3.45E-03	1.38E-02	Y
3.30_CXCR4_sg1_rescue	AAVS1	PSMD1	CXCR4 sg1	PSMD1	two-sample	3.37E-01	5.05E-01	N
3.30_CXCR4_sg1_rescue	AAVS1	CFLAR sg1	CXCR4 sg1	CFLAR sg1	two-sample	3.13E-04	3.76E-03	Y
3.30_CXCR4_sg2_rescue	AAVS1	PSMD1	CXCR4 sg2	PSMD1	two-sample	3.18E-01	5.05E-01	N
3.30_CXCR4_sg2_rescue	AAVS1	CFLAR sg1	CXCR4 sg2	CFLAR sg1	two-sample	2.35E-04	3.76E-03	Y
3.30_UGDH_sg1_rescue	AAVS1	PSMD1	UGDH sg1	PSMD1	two-sample	6.75E-01	7.04E-01	N
3.30_UGDH_sg1_rescue	AAVS1	CFLAR sg1	UGDH sg1	CFLAR sg1	two-sample	6.00E-02	1.20E-01	N
3.30_UGDH_sg2_rescue	AAVS1	PSMD1	UGDH sg2	PSMD1	two-sample	1.24E-01	2.29E-01	N
3.30_UGDH_sg2_rescue	AAVS1	CFLAR sg1	UGDH sg2	CFLAR sg1	two-sample	9.92E-03	3.39E-02	Y
3.30_CHST15_sg1_rescue	AAVS1	PSMD1	CHST15 sg1	PSMD1	two-sample	5.10E-01	5.82E-01	N
3.30_CHST15_sg1_rescue	AAVS1	CFLAR sg1	CHST15 sg1	CFLAR sg1	two-sample	1.86E-02	4.96E-02	Y
3.30_CHST15_sg2_rescue	AAVS1	PSMD1	CHST15 sg2	PSMD1	two-sample	5.93E-01	6.47E-01	N
3.30_CHST15_sg2_rescue	AAVS1	CFLAR sg1	CHST15 sg2	CFLAR sg1	two-sample	1.13E-02	3.39E-02	Y

Statistical Test Outputs Fig 3.36

Test for loss of viability from +Dox condition by ADM3100 treatment group						
test_name	Guide	Treatment	test_type	pvalue	FDR	significant
3.36_AAVS1_DMSO	AAVS1	DMSO	one-sample	4.41E-01	4.41E-01	N
3.36_AAVS1_AMD3100	AAVS1	25 uM AMD3100	one-sample	9.23E-02	1.11E-01	N
3.36_PSMD1_DMSO	PSMD1	DMSO	one-sample	3.15E-04	1.89E-03	Y
3.36_PSMD1_AMD3100	PSMD1	25 uM AMD3100	one-sample	4.48E-03	8.95E-03	Y
3.36_CFLIP_DMSO	CFLIP sg1	DMSO	one-sample	2.93E-03	8.79E-03	Y
3.36_CFLIP_AMD3100	CFLIP sg1	25 uM AMD3100	one-sample	6.41E-03	9.61E-03	Y

Test for positive rescue versus +Dox treatment by experimental sgRNA						
test_name	Guide	test_type	pvalue	FDR	significant	
3.36_AMD3100_AAVS1_Rescue	AAVS1	two-sample	2.70E-01	7.53E-01	N	
3.36_AMD3100_PSMD1_Rescue	PSMD1	two-sample	7.53E-01	7.53E-01	N	
3.36_AMD3100_CFLIP_sg1_Rescue	CFLIP sg1	two-sample	6.70E-01	7.53E-01	N	

Statistical Test Outputs Figs. 3.24B, 3.33, 3.34D

One-Way analysis of Variance Results				
test_name	Group Variable	Outcome Value	pvalue	significant
3.24B_TRAIL_IC50_sgAAVS1	TRAIL Concentration	Relative cell count	9.996E-01	N
3.24B_TRAIL_IC50_sg1_TRAIL-R1	TRAIL Concentration	Relative cell count	9.886E-01	N
3.33_TRAIL-R1_Non-Perm	sgRNA	Anti-TRAIL-R1 FITC MFI	9.977E-01	N
3.33_TRAIL-R1_Perm	sgRNA	Anti-TRAIL-R1 FITC MFI	9.975E-01	N
3.34D_TRAIL-R1_mRNA	sgRNA	Relative TRAIL-R1 mRNA	9.895E-01	N

Vita

Neil Kuehnle

neilkuehnle2015@u.northwestern.edu – (312)-639-9346 – github.com/nkuehnle

Research Experience

Gottwein Laboratory , Micro-Immuno Department	Northwestern University
PhD Candidate	Dec 2016-Present
Putonti Laboratory , Department of Biology	Loyola University Chicago
Research Assistant	Aug 2013-April 2015
Doering Laboratory , Department of Biology	Loyola University Chicago
Undergraduate Research Fellow	Jan 2012-Aug 2014

Projects

Thesis Project: The Role of FLIPs in KSHV-Transformed PEL Cells (Gottwein Laboratory)

Studied the role of viral and cellular FLIP in primary effusion lymphoma (PEL) cells utilizing targeted and high-throughput synthetic rescue approaches, including CRISPR-based genome-wide synthetic rescue screening. Identified a non-canonical, ligand-independent TRAIL-R1-mediated cell death program in PEL cells and several ER/Golgi-associated processes involved in this. Part of this work resulted in publication #1

Transcriptomic Analysis of KSHV Infected Lymphatic Endothelial Cells (Gottwein Laboratory)

Performed bioinformatic analysis of transcriptional studies in KSHV infected LEC. This included bulk RNA-Seq analysis following infection with both WT and miRNA-deficient viruses as well as single-cell RNA sequencing during a time-course of KSHV infection in LEC. This work is pending publication.

Microbial Diversity in the Nearshore Waters of Lake Michigan (Putonti Laboratory)

Performed sample collection and processing of environmental samples taken from an urban lacustrine ecosystem at different locations and across different seasons to characterize the diversity and community dynamics of phage and bacteria within the water. Also participated in a subset of the bioinformatics analyses. Part of this work resulted in publication #3.

Epigenetic Characterization of Human Satellite III Repeats (Doering Laboratory)

Identified several different subfamilies of the satellite III repeat sequence known to be aberrantly transcribed into RNA in many cancers. Designed primers capable of specifically amplifying these subfamilies. Developed a ChIP-qPCR utilizing these primers to quantify several of their histone modifications in cancerous vs healthy tissue samples with the end goal of identifying new potential cancer biomarkers. This work was

awarded two undergraduate research fellowships, the Outstanding Undergraduate Researcher Award at Loyola, and publication #4.

Publications

1. **Kuehnle N**, Osborne SM, Liang Z, Manzano M, Gottwein E. CRISPR screens identify novel regulators of cFLIP dependency and ligand-independent, TRAIL-R1-mediated cell death. *Cell Death Differ.* 2023 May; 30(5):1221-1234
2. **Kuehnle N** and Gottwein. Druggable Host Gene Dependencies in Primary Effusion Lymphoma. *Curr Opin Virol.* 2022 Sept 28; 56:101270.
3. Watkins SC, **Kuehnle N**, Ruggeri CA, Malki K, Bruder K, Elayyan J, Damisch K, Vahora N, O'Malley P, Ruggles-Sage B, Romer Z and Putonti C. Assessment of a metaviromic dataset generated from nearshore Lake Michigan. *Marine and Freshwater Research.* 2015 Nov 4; 67(11) 1700-1708.
4. **Kuehnle N** and Doering J (2014). Characterization of Satellite III Histone Modifications in Human Cancer. *Scientia.* 2014 Autumn; 4.

Presentations and Posters

Gottwein Laboratory

- 24th International KSHV Conference (2022, Talk)
- 23rd International KSHV Conference (2021, Talk)
- Microbiology Immunology Seminar Series (2019, Talk)
- Chicago Area Virology Association Meeting (2019, Poster)
- International Conference on KSHV and KSHV at University of Wisconsin-Madison (2018, Poster)
- 10+ internal Northwestern poster sessions and/or training grant meetings

Putonti Laboratory

- Great Lakes Bioinformatics Conference at University of Cincinnati (2014, Poster)

Doering Laboratory

- LUROP Symposium at Loyola University Chicago (2014, Poster)
- Chicago Area Undergraduate Research Symposium at Illinois Institute of Technology (2014, Poster)
- St. Albert's Day at Loyola Stritch School of Medicine (2013, Poster)
- LUROP Sympsonium at Loyola University Chicago (2013, Poster)
- Frontiers in Science at Loyola University Chicago (2013, Poster)
- National Conference on Undergraduate Research at University of Wisconsin-LaCrosse (2013, Poster)

Awards, Fellowships & Training Grants

- 2020-2022 Supplemental Training Grant (R01 CA247619-01A1S1)
- 2017-2019 Immunology and Molecular Pathogenesis Training Grant Recipient
- 2013-2014 Loyola University Chicago Outstanding Undergraduate Research Award
- 2013-2014 Mulcahy Scholar through the Loyola Undergraduate Research Opportunity Program.
- 2013-2014 Biology Summer Research Fellow through the Loyola Undergraduate Research Opportunity Program.
- 2013 Best Undergraduate Poster Presentation, St. Albert's Day at Stritch School of Medicine
- 2010-2014 George M. Pullman Foundation Scholar
- 2010-2014 multiple Loyola University Chicago Scholarships/Grants: Damen, Director's, Loyola
- Loyola University Chicago Dean's List

Teaching Experience

- BIOL_SCI_222: Investigate Laboratory (Spring 2018)
 - Served as the primary teaching assistant and ran laboratories to 25-30 undergraduates
 - Taught students techniques and experimental theory as part of a real-life biology research project going on at Northwestern
 - Authored and graded weekly quizzes in addition to student lab reports and literature reviews
 - Received top evaluations from students, emphasizing their appreciation for my thorough review sessions
- DGP 475: Graduate Virology (Spring 2019)
 - Served as an informal teaching assistant
 - Graded regular student reports on primary research articles, ran review sessions for midterm and final exams

Service Work

George M. Pullman Foundation
Scholarship Committee Volunteer

Chicago, IL
2014-2021

- Evaluated >20+ applicants from economically disadvantaged backgrounds based on scholarship essays and one-on-one phone interviews during the annual scholarship application season
- Helped deliver workshops focused on professional networking and resume writing and interview skills for 20+ scholars during an annual new and continuing scholar symposium

Chicago Graduate Student Association

Academic & Professional Development Chair

Chicago, IL

2018-2021

- Directly managed a team of 9 students in collaboration with over 10 campus partners to deliver an array of workshops to a graduate community of 300+ students.
- Organized workshops on: work/life balance skills, grant writing, programming/other technical skills, and a multitude of career planning and networking topics

Student-Assisted Mentoring Program**Chicago, IL**

Student Mentor

2018-2021

- Served as a peer mentor to three PhD students in their first two years of graduate education advising on academic and work-life topics

Techniques and Skills

- PCR, cloning, gel electrophoresis and other basic molecular biology techniques
- Basic cell culture and aseptic techniques
- Lentiviral production, concentration, titration, and transduction
- CRISPR/Cas9-mediated editing
- Flow cytometry/fluorescence activated cell sorting (including intracellular flow cytometry)
- Next-generation sequencing
- Quantitative immunoassays: Western blot, Coomassie staining, dot-blot, ELISA, etc.
- Scientific and statistical programming: R, Python, SQL, Bash
- Statistics, bioinformatics, and machine learning

Coursework

High School:

- General Biology (AP Credit)
- General Chemistry (AP Credit)
- Statistics (AP Credit)
-

Loyola University Chicago:

- Cellular Biology
- Cell Biology Lab
- General Physics I/General Physics Lab I
- Calculus I
- Genetics/Genetics Lab
- General Physics II/General Physics Lab II
- Calculus II
- Freshman Projects (for Physics Majors)
- Organic Chemistry I/Organic Chem Lab I
- Organic Chemistry I/Organic Chem Lab II
- Special Topic: Human Molecular Genetics

- Psychology & Biology of Perception
- Intro to Research (Biology)
- Neurobiology
- Molecular Genetics
- Bioinformatics
- Intro to Research
- Developmental Neurobiology
- Survey in Biochemistry
- Intro to Research
- Ecology
- Special Topic: Metagenomics
- Neuroscience Laboratory
- Undergraduate Research Thesis
- Special Topic: Human Genetics
- Individual Study: Metagenomics
- Brain & Behavior

Northwestern University

- Biochemistry
- Quantitative Biology
- Molecular Biology
- Genetics
- Cell Biology
- Tumor Cell Biology
- Intro to Translational Research
- Virology
- Machine Learning
- Biostatistics I
- Mathematical Statistics I: Probability
- Biostatistics II
- Mathematical Statistics II: Statistical Inference
- Information Management for Data Science
- Northwestern Research Computing Services Workshops
 - Programming Concepts
 - Intro to the Command Line/Bash
 - R Fundamental
 - Python Fundamentals
 - Biopython

References

1. Kaposi, *Idiopathisches multiples Pigmentsarkom der Haut*. Archiv für Dermatologie und Syphilis, 1872. **4**(2): p. 265-273.
2. *Kaposi's sarcoma and Pneumocystis pneumonia among homosexual men--New York City and California*. MMWR Morb Mortal Wkly Rep, 1981. **30**(25): p. 305-8.
3. Gottlieb, G.J., et al., *A preliminary communication on extensively disseminated Kaposi's sarcoma in young homosexual men*. Am J Dermatopathol, 1981. **3**(2): p. 111-4.
4. Friedman-Kien, A.E., *Disseminated Kaposi's sarcoma syndrome in young homosexual men*. J Am Acad Dermatol, 1981. **5**(4): p. 468-71.
5. Safai, B., et al., *The natural history of Kaposi's sarcoma in the acquired immunodeficiency syndrome*. Ann Intern Med, 1985. **103**(5): p. 744-50.
6. Giraldo, G., E. Beth, and F. Haguenau, *Herpes-type virus particles in tissue culture of Kaposi's sarcoma from different geographic regions*. J Natl Cancer Inst, 1972. **49**(6): p. 1509-26.
7. Chang, Y., et al., *Identification of herpesvirus-like DNA sequences in AIDS-associated Kaposi's sarcoma*. Science, 1994. **266**(5192): p. 1865-9.
8. Russo, J.J., et al., *Nucleotide sequence of the Kaposi sarcoma-associated herpesvirus (HHV8)*. Proc Natl Acad Sci U S A, 1996. **93**(25): p. 14862-7.
9. Gorbatenko, A.E., et al., *The new scope of virus taxonomy: partitioning the virosphere into 15 hierarchical ranks*. Nature Microbiology, 2020. **5**(5): p. 668-674.
10. Letunic, I. and P. Bork, *Interactive Tree Of Life (iTOL) v4: recent updates and new developments*. Nucleic Acids Res, 2019. **47**(W1): p. W256-w259.
11. Mortazavi, Y., et al., *The Kaposi's Sarcoma-Associated Herpesvirus (KSHV) gH/gL Complex Is the Predominant Neutralizing Antigenic Determinant in KSHV-Infected Individuals*. Viruses, 2020. **12**(3).
12. Zhu, F.X., et al., *Virion proteins of Kaposi's sarcoma-associated herpesvirus*. J Virol, 2005. **79**(2): p. 800-11.
13. Wingfield, P.T., et al., *Hexon-only binding of VP26 reflects differences between the hexon and penton conformations of VP5, the major capsid protein of herpes simplex virus*. J Virol, 1997. **71**(12): p. 8955-61.
14. Nealon, K., et al., *Lytic replication of Kaposi's sarcoma-associated herpesvirus results in the formation of multiple capsid species: isolation and molecular characterization of A, B, and C capsids from a gammaherpesvirus*. J Virol, 2001. **75**(6): p. 2866-78.
15. Dünn-Kittenplon, D., et al., *The Portal Vertex of KSHV Promotes Docking of Capsids at the Nuclear Pores*. Viruses, 2021. **13**(4).
16. Davidson, A., *Comparative analysis of the genomes*, in *Human Herpesviruses: Biology, Therapy, and Immunoprophylaxis*, G.C.-F. Ann Arvin, Edward Mocarski, Patrick S. Moore, Bernard Roizman, Richard Whitley, Koichi Yamanishi, Editor. 2007, Cambridge University Press.
17. Sathish, N., X. Wang, and Y. Yuan, *Tegument Proteins of Kaposi's Sarcoma-Associated Herpesvirus and Related Gamma-Herpesviruses*. Front Microbiol, 2012. **3**: p. 98.
18. Wu, J.J., et al., *ORF33 and ORF38 of Kaposi's Sarcoma-Associated Herpesvirus Interact and Are Required for Optimal Production of Infectious Progeny Viruses*. J Virol, 2016. **90**(4): p. 1741-56.
19. Dai, X., et al., *Organization of capsid-associated tegument components in Kaposi's sarcoma-associated herpesvirus*. J Virol, 2014. **88**(21): p. 12694-702.
20. Liang, Q. and F. Zhu, *ORF45, a multifunctional immediate early and tegument protein of KSHV*. J Med Virol, 2023. **95**(3): p. e28659.

21. Sun, R., et al., *A viral gene that activates lytic cycle expression of Kaposi's sarcoma-associated herpesvirus*. Proc Natl Acad Sci U S A, 1998. **95**(18): p. 10866-71.
22. Lukac, D.M., et al., *Reactivation of Kaposi's sarcoma-associated herpesvirus infection from latency by expression of the ORF 50 transactivator, a homolog of the EBV R protein*. Virology, 1998. **252**(2): p. 304-12.
23. Li, W., et al., *Kaposi's Sarcoma-Associated Herpesvirus Inhibitor of cGAS (KicGAS), Encoded by ORF52, Is an Abundant Tegument Protein and Is Required for Production of Infectious Progeny Viruses*. J Virol, 2016. **90**(11): p. 5329-5342.
24. Gregory, S.M., et al., *Discovery of a viral NLR homolog that inhibits the inflammasome*. Science, 2011. **331**(6015): p. 330-4.
25. González, C.M., L. Wang, and B. Damania, *Kaposi's sarcoma-associated herpesvirus encodes a viral deubiquitinase*. J Virol, 2009. **83**(19): p. 10224-33.
26. Inn, K.S., et al., *Inhibition of RIG-I-mediated signaling by Kaposi's sarcoma-associated herpesvirus-encoded deubiquitinase ORF64*. J Virol, 2011. **85**(20): p. 10899-904.
27. Full, F., et al., *Kaposi's sarcoma associated herpesvirus tegument protein ORF75 is essential for viral lytic replication and plays a critical role in the antagonization of ND10-instituted intrinsic immunity*. PLoS Pathog, 2014. **10**(1): p. e1003863.
28. Boshoff, C. and R. Weiss, *AIDS-related malignancies*. Nat Rev Cancer, 2002. **2**(5): p. 373-82.
29. Goncalves, P.H., et al., *Kaposi sarcoma herpesvirus-associated cancers and related diseases*. Curr Opin HIV AIDS, 2017. **12**(1): p. 47-56.
30. Orenstein, J.M., *Ultrastructure of Kaposi sarcoma*. Ultrastruct Pathol, 2008. **32**(5): p. 211-20.
31. Roth, W.K., H. Brandstetter, and M. Stürzl, *Cellular and molecular features of HIV-associated Kaposi's sarcoma*. Aids, 1992. **6**(9): p. 895-913.
32. Dupin, N., et al., *Distribution of human herpesvirus-8 latently infected cells in Kaposi's sarcoma, multicentric Castleman's disease, and primary effusion lymphoma*. Proc Natl Acad Sci U S A, 1999. **96**(8): p. 4546-51.
33. Jussila, L., et al., *Lymphatic endothelium and Kaposi's sarcoma spindle cells detected by antibodies against the vascular endothelial growth factor receptor-3*. Cancer Res, 1998. **58**(8): p. 1599-604.
34. Hong, Y.K., et al., *Lymphatic reprogramming of blood vascular endothelium by Kaposi sarcoma-associated herpesvirus*. Nat Genet, 2004. **36**(7): p. 683-5.
35. Wang, H.W., et al., *Kaposi sarcoma herpesvirus-induced cellular reprogramming contributes to the lymphatic endothelial gene expression in Kaposi sarcoma*. Nat Genet, 2004. **36**(7): p. 687-93.
36. Beckstead, J.H., G.S. Wood, and V. Fletcher, *Evidence for the origin of Kaposi's sarcoma from lymphatic endothelium*. Am J Pathol, 1985. **119**(2): p. 294-300.
37. Franceschi, S., et al., *Survival of classic Kaposi's sarcoma and risk of second cancer*. Br J Cancer, 1996. **74**(11): p. 1812-4.
38. Nguyen, H.Q., et al., *Persistent Kaposi sarcoma in the era of highly active antiretroviral therapy: characterizing the predictors of clinical response*. Aids, 2008. **22**(8): p. 937-45.
39. Friedman-Kien, A.E. and B.R. Saltzman, *Clinical manifestations of classical, endemic African, and epidemic AIDS-associated Kaposi's sarcoma*. J Am Acad Dermatol, 1990. **22**(6 Pt 2): p. 1237-50.
40. Mesri, E.A., E. Cesarman, and C. Boshoff, *Kaposi's sarcoma and its associated herpesvirus*. Nat Rev Cancer, 2010. **10**(10): p. 707-19.
41. Indave Ruiz, B.I., et al., *Clonality, Mutation and Kaposi Sarcoma: A Systematic Review*. Cancers (Basel), 2022. **14**(5).

42. Salahuddin, S.Z., et al., *Angiogenic properties of Kaposi's sarcoma-derived cells after long-term culture in vitro*. Science, 1988. **242**(4877): p. 430-3.
43. Lane, H.C. and A.S. Fauci, *Immunologic abnormalities in the acquired immunodeficiency syndrome*. Annu Rev Immunol, 1985. **3**: p. 477-500.
44. Rabkin, C.S., et al., *Monoclonal origin of multicentric Kaposi's sarcoma lesions*. N Engl J Med, 1997. **336**(14): p. 988-93.
45. Gill, P.S., et al., *Evidence for multiclonaity in multicentric Kaposi's sarcoma*. Proc Natl Acad Sci U S A, 1998. **95**(14): p. 8257-61.
46. Duprez, R., et al., *Evidence for a multiclonal origin of multicentric advanced lesions of Kaposi sarcoma*. J Natl Cancer Inst, 2007. **99**(14): p. 1086-94.
47. Hanahan, D. and R.A. Weinberg, *Hallmarks of cancer: the next generation*. Cell, 2011. **144**(5): p. 646-74.
48. Nicolaides, A., et al., *Gene amplification and multiple mutations of the K-ras oncogene in Kaposi's sarcoma*. Anticancer Res, 1994. **14**(3a): p. 921-6.
49. Pillay, P., R. Chetty, and R. Reddy, *Bcl-2 and p53 immunoprofile in Kaposi's sarcoma*. Pathol Oncol Res, 1999. **5**(1): p. 17-20.
50. Pyakurel, P., et al., *CGH of microdissected Kaposi's sarcoma lesions reveals recurrent loss of chromosome Y in early and additional chromosomal changes in late tumour stages*. Aids, 2006. **20**(14): p. 1805-12.
51. Bell, B.M., Jr., et al., *Disseminated Kaposi sarcoma with osseous metastases in an HIV-positive patient*. Proc (Bayl Univ Med Cent), 2016. **29**(1): p. 52-4.
52. Dirweesh, A., et al., *Pulmonary Kaposi Sarcoma with Osseous Metastases in an Human Immunodeficiency Virus (HIV) Patient: A Remarkable Response to Highly Active Antiretroviral Therapy*. Am J Case Rep, 2017. **18**: p. 181-185.
53. Aboulafia, D., G. Mathisen, and R. Mitsuyasu, *Aggressive Kaposi's sarcoma and campylobacter bacteremia in a female with transfusion associated AIDS*. Am J Med Sci, 1991. **301**(4): p. 256-8.
54. Just Sarobé, M., et al., *[Classical Kaposi sarcoma of aggressive course]*. Rev Clin Esp, 1998. **198**(2): p. 95-8.
55. Cesarman, E., et al., *Kaposi's sarcoma-associated herpesvirus-like DNA sequences in AIDS-related body-cavity-based lymphomas*. N Engl J Med, 1995. **332**(18): p. 1186-91.
56. Nador, R.G., et al., *Primary effusion lymphoma: a distinct clinicopathologic entity associated with the Kaposi's sarcoma-associated herpes virus*. Blood, 1996. **88**(2): p. 645-56.
57. Lurain, K., et al., *Viral, immunologic, and clinical features of primary effusion lymphoma*. Blood, 2019. **133**(16): p. 1753-1761.
58. Chen, Y.B., A. Rahemtullah, and E. Hochberg, *Primary effusion lymphoma*. Oncologist, 2007. **12**(5): p. 569-76.
59. Lurain, K., et al., *Use of pembrolizumab with or without pomalidomide in HIV-associated non-Hodgkin's lymphoma*. J Immunother Cancer, 2021. **9**(2).
60. Staudt, M.R., et al., *The tumor microenvironment controls primary effusion lymphoma growth in vivo*. Cancer Res, 2004. **64**(14): p. 4790-9.
61. Chandriani, S. and D. Ganem, *Array-based transcript profiling and limiting-dilution reverse transcription-PCR analysis identify additional latent genes in Kaposi's sarcoma-associated herpesvirus*. J Virol, 2010. **84**(11): p. 5565-73.
62. Thakker, S. and S.C. Verma, *Co-infections and Pathogenesis of KSHV-Associated Malignancies*. Front Microbiol, 2016. **7**: p. 151.
63. Wies, E., et al., *The viral interferon-regulatory factor-3 is required for the survival of KSHV-infected primary effusion lymphoma cells*. Blood, 2008. **111**(1): p. 320-7.

64. Godfrey, A., et al., *Inhibiting primary effusion lymphoma by lentiviral vectors encoding short hairpin RNA*. Blood, 2005. **105**(6): p. 2510-8.
65. Manzano, M., et al., *Gene essentiality landscape and druggable oncogenic dependencies in herpesviral primary effusion lymphoma*. Nat Commun, 2018. **9**(1): p. 3263.
66. Manzano, M., et al., *Kaposi's Sarcoma-Associated Herpesvirus Drives a Super-Enhancer-Mediated Survival Gene Expression Program in Primary Effusion Lymphoma*. mBio, 2020. **11**(4).
67. Kuehnle, N. and E. Gottwein, *Druggable host gene dependencies in primary effusion lymphoma*. Curr Opin Virol, 2022. **56**: p. 101270.
68. Saeed-Abdul-Rahman, I. and A.M. Al-Amri, *Castleman disease*. Korean J Hematol, 2012. **47**(3): p. 163-77.
69. Castleman, B. and V.W. Towne, *Case records of the Massachusetts General Hospital: Case No. 40231*. N Engl J Med, 1954. **250**(23): p. 1001-5.
70. Oksenhendler, E., et al., *Multicentric Castleman's disease in HIV infection: a clinical and pathological study of 20 patients*. Aids, 1996. **10**(1): p. 61-7.
71. Fajgenbaum, D.C., et al., *International, evidence-based consensus diagnostic criteria for HHV-8-negative/idiopathic multicentric Castleman disease*. Blood, 2017. **129**(12): p. 1646-1657.
72. Soulier, J., et al., *Kaposi's sarcoma-associated herpesvirus-like DNA sequences in multicentric Castleman's disease*. Blood, 1995. **86**(4): p. 1276-80.
73. Uldrick, T.S., et al., *Rituximab plus liposomal doxorubicin in HIV-infected patients with KSHV-associated multicentric Castleman disease*. Blood, 2014. **124**(24): p. 3544-52.
74. Bower, M., et al., *Brief communication: rituximab in HIV-associated multicentric Castleman disease*. Ann Intern Med, 2007. **147**(12): p. 836-9.
75. Hoffmann, C., et al., *Improved outcome with rituximab in patients with HIV-associated multicentric Castleman disease*. Blood, 2011. **118**(13): p. 3499-503.
76. Gérard, L., et al., *Rituximab decreases the risk of lymphoma in patients with HIV-associated multicentric Castleman disease*. Blood, 2012. **119**(10): p. 2228-33.
77. Pria, A.D., et al., *Relapse of HHV8-positive multicentric Castleman disease following rituximab-based therapy in HIV-positive patients*. Blood, 2017. **129**(15): p. 2143-2147.
78. Dupin, N., et al., *HHV-8 is associated with a plasmablastic variant of Castleman disease that is linked to HHV-8-positive plasmablastic lymphoma*. Blood, 2000. **95**(4): p. 1406-12.
79. Lurain, K., R. Yarchoan, and T.S. Uldrick, *Treatment of Kaposi Sarcoma Herpesvirus-Associated Multicentric Castleman Disease*. Hematol Oncol Clin North Am, 2018. **32**(1): p. 75-88.
80. Wang, H.W., S. Pittaluga, and E.S. Jaffe, *Multicentric Castleman disease: Where are we now?* Semin Diagn Pathol, 2016. **33**(5): p. 294-306.
81. Du, M.Q., et al., *KSHV- and EBV-associated germinotropic lymphoproliferative disorder*. Blood, 2002. **100**(9): p. 3415-8.
82. Chadburn, A., et al., *Immunophenotypic analysis of the Kaposi sarcoma herpesvirus (KSHV; HHV-8)-infected B cells in HIV+ multicentric Castleman disease (MCD)*. Histopathology, 2008. **53**(5): p. 513-24.
83. Katano, H., et al., *Expression and localization of human herpesvirus 8-encoded proteins in primary effusion lymphoma, Kaposi's sarcoma, and multicentric Castleman's disease*. Virology, 2000. **269**(2): p. 335-44.
84. Parravicini, C., et al., *Differential viral protein expression in Kaposi's sarcoma-associated herpesvirus-infected diseases: Kaposi's sarcoma, primary effusion lymphoma, and multicentric Castleman's disease*. Am J Pathol, 2000. **156**(3): p. 743-9.

85. Oksenhendler, E., et al., *High levels of human herpesvirus 8 viral load, human interleukin-6, interleukin-10, and C reactive protein correlate with exacerbation of multicentric castleman disease in HIV-infected patients*. Blood, 2000. **96**(6): p. 2069-73.
86. Brandt, S.J., et al., *Dysregulated interleukin 6 expression produces a syndrome resembling Castleman's disease in mice*. J Clin Invest, 1990. **86**(2): p. 592-9.
87. Polizzotto, M.N., et al., *Human and viral interleukin-6 and other cytokines in Kaposi sarcoma herpesvirus-associated multicentric Castleman disease*. Blood, 2013. **122**(26): p. 4189-98.
88. Sbihi, Z., et al., *iNKT and memory B-cell alterations in HHV-8 multicentric Castleman disease*. Blood, 2017. **129**(7): p. 855-865.
89. Uldrick, T.S., et al., *An interleukin-6-related systemic inflammatory syndrome in patients co-infected with Kaposi sarcoma-associated herpesvirus and HIV but without Multicentric Castleman disease*. Clin Infect Dis, 2010. **51**(3): p. 350-8.
90. Polizzotto, M.N., et al., *Clinical Manifestations of Kaposi Sarcoma Herpesvirus Lytic Activation: Multicentric Castleman Disease (KSHV-MCD) and the KSHV Inflammatory Cytokine Syndrome*. Front Microbiol, 2012. **3**: p. 73.
91. Polizzotto, M.N., et al., *Clinical Features and Outcomes of Patients With Symptomatic Kaposi Sarcoma Herpesvirus (KSHV)-associated Inflammation: Prospective Characterization of KSHV Inflammatory Cytokine Syndrome (KICS)*. Clin Infect Dis, 2016. **62**(6): p. 730-738.
92. Karass, M., et al., *Kaposi Sarcoma Inflammatory Cytokine Syndrome (KICS): A Rare but Potentially Treatable Condition*. Oncologist, 2017. **22**(5): p. 623-625.
93. Minhas, V. and C. Wood, *Epidemiology and transmission of Kaposi's sarcoma-associated herpesvirus*. Viruses, 2014. **6**(11): p. 4178-94.
94. Slots, J., et al., *Epstein-Barr virus in oral diseases*. J Periodontal Res, 2006. **41**(4): p. 235-44.
95. Pauk, J., et al., *Mucosal shedding of human herpesvirus 8 in men*. N Engl J Med, 2000. **343**(19): p. 1369-77.
96. Johnson, A.S., N. Maronian, and J. Vieira, *Activation of Kaposi's sarcoma-associated herpesvirus lytic gene expression during epithelial differentiation*. J Virol, 2005. **79**(21): p. 13769-77.
97. Bechtel, J.T., et al., *Host range of Kaposi's sarcoma-associated herpesvirus in cultured cells*. J Virol, 2003. **77**(11): p. 6474-81.
98. Myoung, J. and D. Ganem, *Active lytic infection of human primary tonsillar B cells by KSHV and its noncytolytic control by activated CD4+ T cells*. J Clin Invest, 2011. **121**(3): p. 1130-40.
99. Myoung, J. and D. Ganem, *Infection of lymphoblastoid cell lines by Kaposi's sarcoma-associated herpesvirus: critical role of cell-associated virus*. J Virol, 2011. **85**(19): p. 9767-77.
100. Dollery, S.J., et al., *Efficient infection of a human B cell line with cell-free Kaposi's sarcoma-associated herpesvirus*. J Virol, 2014. **88**(3): p. 1748-57.
101. Chakraborty, S., M.V. Veettil, and B. Chandran, *Kaposi's Sarcoma Associated Herpesvirus Entry into Target Cells*. Front Microbiol, 2012. **3**: p. 6.
102. Chen, J., et al., *Ephrin Receptor A4 is a New Kaposi's Sarcoma-Associated Herpesvirus Virus Entry Receptor*. mBio, 2019. **10**(1).
103. Chakraborty, S., et al., *c-Cbl-mediated selective virus-receptor translocations into lipid rafts regulate productive Kaposi's sarcoma-associated herpesvirus infection in endothelial cells*. J Virol, 2011. **85**(23): p. 12410-30.
104. Raghu, H., et al., *Kaposi's sarcoma-associated herpesvirus utilizes an actin polymerization-dependent macropinocytic pathway to enter human dermal microvascular*

- endothelial and human umbilical vein endothelial cells.* J Virol, 2009. **83**(10): p. 4895-911.
105. Akula, S.M., et al., *Kaposi's sarcoma-associated herpesvirus (human herpesvirus 8) infection of human fibroblast cells occurs through endocytosis.* J Virol, 2003. **77**(14): p. 7978-90.
 106. Greene, W. and S.J. Gao, *Actin dynamics regulate multiple endosomal steps during Kaposi's sarcoma-associated herpesvirus entry and trafficking in endothelial cells.* PLoS Pathog, 2009. **5**(7): p. e1000512.
 107. Kerur, N., et al., *Characterization of entry and infection of monocytic THP-1 cells by Kaposi's sarcoma associated herpesvirus (KSHV): role of heparan sulfate, DC-SIGN, integrins and signaling.* Virology, 2010. **406**(1): p. 103-16.
 108. Sharma-Walia, N., et al., *Kaposi's sarcoma-associated herpesvirus/human herpesvirus 8 envelope glycoprotein gB induces the integrin-dependent focal adhesion kinase-Src-phosphatidylinositol 3-kinase-rho GTPase signal pathways and cytoskeletal rearrangements.* J Virol, 2004. **78**(8): p. 4207-23.
 109. Pasdeloup, D., et al., *Herpesvirus capsid association with the nuclear pore complex and viral DNA release involve the nucleoporin CAN/Nup214 and the capsid protein pUL25.* J Virol, 2009. **83**(13): p. 6610-23.
 110. Lieberman, P.M., *Keeping it quiet: chromatin control of gammaherpesvirus latency.* Nat Rev Microbiol, 2013. **11**(12): p. 863-75.
 111. Ballestas, M.E., P.A. Chatis, and K.M. Kaye, *Efficient persistence of extrachromosomal KSHV DNA mediated by latency-associated nuclear antigen.* Science, 1999. **284**(5414): p. 641-4.
 112. Tomaska, L., M.J. McEachern, and J. Nosek, *Alternatives to telomerase: keeping linear chromosomes via telomeric circles.* FEBS Lett, 2004. **567**(1): p. 142-6.
 113. Natarajan, S. and M.J. McEachern, *Recombinational telomere elongation promoted by DNA circles.* Mol Cell Biol, 2002. **22**(13): p. 4512-21.
 114. Aneja, K.K. and Y. Yuan, *Reactivation and Lytic Replication of Kaposi's Sarcoma-Associated Herpesvirus: An Update.* Front Microbiol, 2017. **8**: p. 613.
 115. Toth, Z., K. Brulois, and J.U. Jung, *The chromatin landscape of Kaposi's sarcoma-associated herpesvirus.* Viruses, 2013. **5**(5): p. 1346-73.
 116. Tempera, I. and P.M. Lieberman, *Chromatin organization of gammaherpesvirus latent genomes.* Biochim Biophys Acta, 2010. **1799**(3-4): p. 236-45.
 117. Knipe, D.M. and A. Cliffe, *Chromatin control of herpes simplex virus lytic and latent infection.* Nat Rev Microbiol, 2008. **6**(3): p. 211-21.
 118. Lukac DM, Y.Y., *Reactivation and lytic replication of KSHV, in Human Herpesviruses: Biology, Therapy, and Immunoprophylaxis.*, G.C.-F. Ann Arvin, Edward Mocarski, Patrick S. Moore, Bernard Roizman, Richard Whitley, Koichi Yamanishi, Editor. 2007, Cambridge University Press.
 119. Sun, R., et al., *Kinetics of Kaposi's sarcoma-associated herpesvirus gene expression.* J Virol, 1999. **73**(3): p. 2232-42.
 120. Zhu, F.X., T. Cusano, and Y. Yuan, *Identification of the immediate-early transcripts of Kaposi's sarcoma-associated herpesvirus.* J Virol, 1999. **73**(7): p. 5556-67.
 121. Schulz TF, Y.Y., *KSHV gene expression and regulation, in Human Herpesviruses: Biology, Therapy, and Immunoprophylaxis.*, G.C.-F. Ann Arvin, Edward Mocarski, Patrick S. Moore, Bernard Roizman, Richard Whitley, Koichi Yamanishi, Editor. 2007, Cambridge University Press.
 122. Zacny, V.L., J. Wilson, and J.S. Pagano, *The Epstein-Barr virus immediate-early gene product, BRLF1, interacts with the retinoblastoma protein during the viral lytic cycle.* J Virol, 1998. **72**(10): p. 8043-51.

123. Wang, Y., O.T. Chong, and Y. Yuan, *Differential regulation of K8 gene expression in immediate-early and delayed-early stages of Kaposi's sarcoma-associated herpesvirus*. Virology, 2004. **325**(1): p. 149-63.
124. Izumiya, Y., et al., *Kaposi's sarcoma-associated herpesvirus K-bZIP is a coregulator of K-Rta: physical association and promoter-dependent transcriptional repression*. J Virol, 2003. **77**(2): p. 1441-51.
125. Chen, D., Y. Gao, and J. Nicholas, *Human herpesvirus 8 interleukin-6 contributes to primary effusion lymphoma cell viability via suppression of proapoptotic cathepsin D, a cointeraction partner of vitamin K epoxide reductase complex subunit 1 variant 2*. J Virol, 2014. **88**(2): p. 1025-38.
126. Sun, R., et al., *Epigenetic Landscape of Kaposi's Sarcoma-Associated Herpesvirus Genome in Classic Kaposi's Sarcoma Tissues*. PLoS Pathog, 2017. **13**(1): p. e1006167.
127. Nishimura, M., et al., *Kaposi's sarcoma-associated herpesvirus ORF34 is essential for late gene expression and virus production*. Scientific Reports, 2017. **7**(1): p. 329.
128. Brulois, K., et al., *Association of Kaposi's Sarcoma-Associated Herpesvirus ORF31 with ORF34 and ORF24 Is Critical for Late Gene Expression*. J Virol, 2015. **89**(11): p. 6148-54.
129. Arias, C., et al., *KSHV 2.0: a comprehensive annotation of the Kaposi's sarcoma-associated herpesvirus genome using next-generation sequencing reveals novel genomic and functional features*. PLoS Pathog, 2014. **10**(1): p. e1003847.
130. Kang, M.-S. and E. Kieff, *Epstein-Barr virus latent genes*. Experimental & Molecular Medicine, 2015. **47**(1): p. e131-e131.
131. Hu, J., et al., *LANA binds to multiple active viral and cellular promoters and associates with the H3K4methyltransferase hSET1 complex*. PLoS Pathog, 2014. **10**(7): p. e1004240.
132. Uppal, T., et al., *KSHV LANA--the master regulator of KSHV latency*. Viruses, 2014. **6**(12): p. 4961-98.
133. Jha, H.C., et al., *H2AX phosphorylation is important for LANA-mediated Kaposi's sarcoma-associated herpesvirus episome persistence*. J Virol, 2013. **87**(9): p. 5255-69.
134. Barbera, A.J., et al., *The nucleosomal surface as a docking station for Kaposi's sarcoma herpesvirus LANA*. Science, 2006. **311**(5762): p. 856-61.
135. Toth, Z., et al., *LANA-Mediated Recruitment of Host Polycomb Repressive Complexes onto the KSHV Genome during De Novo Infection*. PLoS Pathog, 2016. **12**(9): p. e1005878.
136. Friborg, J., Jr., et al., *p53 inhibition by the LANA protein of KSHV protects against cell death*. Nature, 1999. **402**(6764): p. 889-94.
137. Si, H. and E.S. Robertson, *Kaposi's sarcoma-associated herpesvirus-encoded latency-associated nuclear antigen induces chromosomal instability through inhibition of p53 function*. J Virol, 2006. **80**(2): p. 697-709.
138. Cai, Q.L., et al., *EC5S ubiquitin complex is recruited by KSHV latent antigen LANA for degradation of the VHL and p53 tumor suppressors*. PLoS Pathog, 2006. **2**(10): p. e116.
139. Radkov, S.A., P. Kellam, and C. Boshoff, *The latent nuclear antigen of Kaposi sarcoma-associated herpesvirus targets the retinoblastoma-E2F pathway and with the oncogene Hras transforms primary rat cells*. Nat Med, 2000. **6**(10): p. 1121-7.
140. Di Bartolo, D.L., et al., *KSHV LANA inhibits TGF-beta signaling through epigenetic silencing of the TGF-beta type II receptor*. Blood, 2008. **111**(9): p. 4731-40.
141. Fujimuro, M. and S.D. Hayward, *The latency-associated nuclear antigen of Kaposi's sarcoma-associated herpesvirus manipulates the activity of glycogen synthase kinase-3beta*. J Virol, 2003. **77**(14): p. 8019-30.

142. Fujimuro, M., et al., *A novel viral mechanism for dysregulation of beta-catenin in Kaposi's sarcoma-associated herpesvirus latency*. Nat Med, 2003. **9**(3): p. 300-6.
143. Chang, Y., et al., *Cyclin encoded by KS herpesvirus*. Nature, 1996. **382**(6590): p. 410.
144. Li, M., et al., *Kaposi's sarcoma-associated herpesvirus encodes a functional cyclin*. J Virol, 1997. **71**(3): p. 1984-91.
145. Godden-Kent, D., et al., *The cyclin encoded by Kaposi's sarcoma-associated herpesvirus stimulates cdk6 to phosphorylate the retinoblastoma protein and histone H1*. J Virol, 1997. **71**(6): p. 4193-8.
146. Sarek, G., A. Järvi, and P.M. Ojala, *KSHV viral cyclin inactivates p27KIP1 through Ser10 and Thr187 phosphorylation in proliferating primary effusion lymphomas*. Blood, 2006. **107**(2): p. 725-32.
147. Chang, P.C. and M. Li, *Kaposi's sarcoma-associated herpesvirus K-cyclin interacts with Cdk9 and stimulates Cdk9-mediated phosphorylation of p53 tumor suppressor*. J Virol, 2008. **82**(1): p. 278-90.
148. Jones, T., et al., *Viral cyclin promotes KSHV-induced cellular transformation and tumorigenesis by overriding contact inhibition*. Cell Cycle, 2014. **13**(5): p. 845-58.
149. Swanton, C., et al., *Herpes viral cyclin/Cdk6 complexes evade inhibition by CDK inhibitor proteins*. Nature, 1997. **390**(6656): p. 184-7.
150. Verschuren, E.W., et al., *The oncogenic potential of Kaposi's sarcoma-associated herpesvirus cyclin is exposed by p53 loss in vitro and in vivo*. Cancer Cell, 2002. **2**(3): p. 229-41.
151. Verschuren, E.W., et al., *The role of p53 in suppression of KSHV cyclin-induced lymphomagenesis*. Cancer Res, 2004. **64**(2): p. 581-9.
152. Koopal, S., et al., *Viral oncogene-induced DNA damage response is activated in Kaposi sarcoma tumorigenesis*. PLoS Pathog, 2007. **3**(9): p. 1348-60.
153. Irmler, M., et al., *Inhibition of death receptor signals by cellular FLIP*. Nature, 1997. **388**(6638): p. 190-5.
154. Thome, M., et al., *Viral FLICE-inhibitory proteins (FLIPs) prevent apoptosis induced by death receptors*. Nature, 1997. **386**(6624): p. 517-21.
155. Sun, Q., S. Zachariah, and P.M. Chaudhary, *The human herpes virus 8-encoded viral FLICE-inhibitory protein induces cellular transformation via NF-kappaB activation*. J Biol Chem, 2003. **278**(52): p. 52437-45.
156. Bielecki, L. and S.J. Talbot, *Kaposi's Sarcoma-Associated Herpesvirus vCyclin Open Reading Frame Contains an Internal Ribosome Entry Site*. Journal of Virology, 2001. **75**(4): p. 1864-1869.
157. Muralidhar, S., et al., *Identification of kaposin (open reading frame K12) as a human herpesvirus 8 (Kaposi's sarcoma-associated herpesvirus) transforming gene*. J Virol, 1998. **72**(6): p. 4980-8.
158. Forte, E., et al., *MicroRNA-mediated transformation by the Kaposi's sarcoma-associated herpesvirus Kaposin locus*. J Virol, 2015. **89**(4): p. 2333-41.
159. Wies, E., et al., *The Kaposi's Sarcoma-associated Herpesvirus-encoded vIRF-3 Inhibits Cellular IRF-5*. J Biol Chem, 2009. **284**(13): p. 8525-38.
160. Schmidt, K., E. Wies, and F. Neipel, *Kaposi's sarcoma-associated herpesvirus viral interferon regulatory factor 3 inhibits gamma interferon and major histocompatibility complex class II expression*. J Virol, 2011. **85**(9): p. 4530-7.
161. Baresova, P., P.M. Pitha, and B. Lubyova, *Kaposi sarcoma-associated herpesvirus vIRF-3 protein binds to F-box of Skp2 protein and acts as a regulator of c-Myc protein function and stability*. J Biol Chem, 2012. **287**(20): p. 16199-208.

162. Joo, C.H., et al., *Inhibition of interferon regulatory factor 7 (IRF7)-mediated interferon signal transduction by the Kaposi's sarcoma-associated herpesvirus viral IRF homolog vIRF3*. J Virol, 2007. **81**(15): p. 8282-92.
163. Zuo, J., et al., *Kaposi's sarcoma-associated herpesvirus-encoded viral IRF3 modulates major histocompatibility complex class II (MHC-II) antigen presentation through MHC-II transactivator-dependent and -independent mechanisms: implications for oncogenesis*. J Virol, 2013. **87**(10): p. 5340-50.
164. Chang, H., et al., *Role of Notch signal transduction in Kaposi's sarcoma-associated herpesvirus gene expression*. J Virol, 2005. **79**(22): p. 14371-82.
165. Osborne, J., P.S. Moore, and Y. Chang, *KSHV-encoded viral IL-6 activates multiple human IL-6 signaling pathways*. Hum Immunol, 1999. **60**(10): p. 921-7.
166. Cai, X., et al., *Kaposi's sarcoma-associated herpesvirus expresses an array of viral microRNAs in latently infected cells*. Proc Natl Acad Sci U S A, 2005. **102**(15): p. 5570-5.
167. Manzano, M., et al., *Kaposi's sarcoma-associated herpesvirus encodes a mimic of cellular miR-23*. J Virol, 2013. **87**(21): p. 11821-30.
168. Skalsky, R.L., et al., *Kaposi's sarcoma-associated herpesvirus encodes an ortholog of miR-155*. J Virol, 2007. **81**(23): p. 12836-45.
169. Morrison, K., et al., *The Oncogenic Kaposi's Sarcoma-Associated Herpesvirus Encodes a Mimic of the Tumor-Suppressive miR-15/16 miRNA Family*. Cell Rep, 2019. **29**(10): p. 2961-2969.e6.
170. Linnstaedt, S.D., et al., *Virally induced cellular microRNA miR-155 plays a key role in B-cell immortalization by Epstein-Barr virus*. J Virol, 2010. **84**(22): p. 11670-8.
171. Gottwein, E., et al., *Viral microRNA targetome of KSHV-infected primary effusion lymphoma cell lines*. Cell Host Microbe, 2011. **10**(5): p. 515-26.
172. Gottwein, E., *Kaposi's Sarcoma-Associated Herpesvirus microRNAs*. Front Microbiol, 2012. **3**: p. 165.
173. Patil, A., M. Manzano, and E. Gottwein, *CK1 α and IRF4 are essential and independent effectors of immunomodulatory drugs in primary effusion lymphoma*. Blood, 2018. **132**(6): p. 577-586.
174. Kuehnle, N., et al., *CRISPR screens identify novel regulators of cFLIP dependency and ligand-independent, TRAIL-R1-mediated cell death*. Cell Death Differ, 2023. **30**(5): p. 1221-1234.
175. Tsherniak, A., et al., *Defining a Cancer Dependency Map*. Cell, 2017. **170**(3): p. 564-576.e16.
176. Dempster, J.M., et al., *Agreement between two large pan-cancer CRISPR-Cas9 gene dependency data sets*. Nat Commun, 2019. **10**(1): p. 5817.
177. Ma, Y., et al., *CRISPR/Cas9 Screens Reveal Epstein-Barr Virus-Transformed B Cell Host Dependency Factors*. Cell Host Microbe, 2017. **21**(5): p. 580-591.e7.
178. Nakagawa, M., et al., *Targeting the HTLV-I-Regulated BATF3/IRF4 Transcriptional Network in Adult T Cell Leukemia/Lymphoma*. Cancer Cell, 2018. **34**(2): p. 286-297.e10.
179. Nakagawa, M., et al., *Targeting the HTLV-I-Regulated BATF3/IRF4 Transcriptional Network in Adult T-Cell Leukemia/Lymphoma*. Blood, 2017. **130**: p. 731.
180. Jiang, S., et al., *The Epstein-Barr Virus Regulome in Lymphoblastoid Cells*. Cell Host Microbe, 2017. **22**(4): p. 561-573.e4.
181. Schmidt, S.C.S., et al., *Epstein-Barr virus nuclear antigen 3A partially coincides with EBNA3C genome-wide and is tethered to DNA through BATF complexes*. Proceedings of the National Academy of Sciences, 2015. **112**(2): p. 554-559.
182. Jiang, S., et al., *Epstein-Barr Virus Nuclear Antigen 3C binds to BATF/IRF4 or SPI1/IRF4 composite sites and recruits Sin3A to repress CDKN2A*. Proceedings of the National Academy of Sciences, 2014. **111**(1): p. 421-426.

183. Zhou, H., et al., *Epstein-Barr virus oncoprotein super-enhancers control B cell growth*. Cell Host Microbe, 2015. **17**(2): p. 205-16.
184. Wang, C., et al., *Primary effusion lymphoma enhancer connectome links super-enhancers to dependency factors*. Nature Communications, 2020. **11**(1): p. 6318.
185. Tang, T.F., et al., *Regulatory network of BLIMP1, IRF4, and XBP1 triad in plasmacytic differentiation and multiple myeloma pathogenesis*. Cell Immunol, 2022. **380**: p. 104594.
186. Low, M.S.Y., et al., *IRF4 Activity Is Required in Established Plasma Cells to Regulate Gene Transcription and Mitochondrial Homeostasis*. Cell Rep, 2019. **29**(9): p. 2634-2645.e5.
187. Sciammas, R., et al., *Graded Expression of Interferon Regulatory Factor-4 Coordinates Isotype Switching with Plasma Cell Differentiation*. Immunity, 2006. **25**(2): p. 225-236.
188. Klein, U., et al., *Transcription factor IRF4 controls plasma cell differentiation and class-switch recombination*. Nat Immunol, 2006. **7**(7): p. 773-82.
189. Hamada, M., N. Satoh, and K. Khalturin, *A Reference Genome from the Symbiotic Hydrozoan, Hydra viridissima*. G3 (Bethesda), 2020. **10**(11): p. 3883-3895.
190. Cikala, M., et al., *Identification of caspases and apoptosis in the simple metazoan Hydra*. Curr Biol, 1999. **9**(17): p. 959-62.
191. Hu, S., et al., *A novel family of viral death effector domain-containing molecules that inhibit both CD-95- and tumor necrosis factor receptor-1-induced apoptosis*. J Biol Chem, 1997. **272**(15): p. 9621-4.
192. Krueger, A., et al., *Cellular FLICE-inhibitory protein splice variants inhibit different steps of caspase-8 activation at the CD95 death-inducing signaling complex*. J Biol Chem, 2001. **276**(23): p. 20633-40.
193. Kavuri, S.M., et al., *Cellular FLICE-inhibitory protein (cFLIP) isoforms block CD95- and TRAIL death receptor-induced gene induction irrespective of processing of caspase-8 or cFLIP in the death-inducing signaling complex*. J Biol Chem, 2011. **286**(19): p. 16631-46.
194. Chang, D.W., et al., *c-FLIP(L) is a dual function regulator for caspase-8 activation and CD95-mediated apoptosis*. Embo j, 2002. **21**(14): p. 3704-14.
195. Shisler, J.L. and B. Moss, *Molluscum contagiosum virus inhibitors of apoptosis: The MC159 v-FLIP protein blocks Fas-induced activation of procaspases and degradation of the related MC160 protein*. Virology, 2001. **282**(1): p. 14-25.
196. Gil, J., et al., *MC159L protein from the poxvirus molluscum contagiosum virus inhibits NF-kappaB activation and apoptosis induced by PKR*. J Gen Virol, 2001. **82**(Pt 12): p. 3027-34.
197. Bertin, J., et al., *Death effector domain-containing herpesvirus and poxvirus proteins inhibit both Fas- and TNFR1-induced apoptosis*. Proc Natl Acad Sci U S A, 1997. **94**(4): p. 1172-6.
198. Chugh, P., et al., *Constitutive NF- κ B activation, normal Fas-induced apoptosis, and increased incidence of lymphoma in human herpes virus 8 K13 transgenic mice*. Proceedings of the National Academy of Sciences of the United States of America, 2005. **102**(36): p. 12885-12890.
199. Bagneris, C., et al., *Probing the Solution Structure of I κ B Kinase (IKK) Subunit gamma and Its Interaction with Kaposi Sarcoma-associated Herpes Virus Flc-Interacting Protein and IKK Subunit beta by EPR Spectroscopy*. J Biol Chem, 2015. **290**(27): p. 16539-49.
200. Galluzzi, L., et al., *Molecular mechanisms of cell death: recommendations of the Nomenclature Committee on Cell Death 2018*. Cell Death Differ, 2018. **25**(3): p. 486-541.

201. McStay, G.P., G.S. Salvesen, and D.R. Green, *Overlapping cleavage motif selectivity of caspases: implications for analysis of apoptotic pathways*. Cell Death & Differentiation, 2008. **15**(2): p. 322-331.
202. Julien, O. and J.A. Wells, *Caspases and their substrates*. Cell Death & Differentiation, 2017. **24**(8): p. 1380-1389.
203. Donepudi, M., et al., *Insights into the regulatory mechanism for caspase-8 activation*. Mol Cell, 2003. **11**(2): p. 543-9.
204. Oberst, A., et al., *Catalytic activity of the caspase-8-FLIP(L) complex inhibits RIPK3-dependent necrosis*. Nature, 2011. **471**(7338): p. 363-7.
205. Fritsch, M., et al., *Caspase-8 is the molecular switch for apoptosis, necroptosis and pyroptosis*. Nature, 2019. **575**(7784): p. 683-687.
206. Newton, K., et al., *Activity of caspase-8 determines plasticity between cell death pathways*. Nature, 2019. **575**(7784): p. 679-682.
207. Yu, L., et al., *Regulation of an ATG7-beclin 1 program of autophagic cell death by caspase-8*. Science, 2004. **304**(5676): p. 1500-2.
208. Bell, B.D., et al., *FADD and caspase-8 control the outcome of autophagic signaling in proliferating T cells*. Proc Natl Acad Sci U S A, 2008. **105**(43): p. 16677-82.
209. Jimbo, A., et al., *ER stress induces caspase-8 activation, stimulating cytochrome c release and caspase-9 activation*. Exp Cell Res, 2003. **283**(2): p. 156-66.
210. Munoz-Pinedo, C. and A. Lopez-Rivas, *A role for caspase-8 and TRAIL-R2/DR5 in ER-stress-induced apoptosis*. Cell Death Differ, 2018. **25**(1): p. 226.
211. Chaudhary, P.M., et al., *Modulation of the NF-kappa B pathway by virally encoded death effector domains-containing proteins*. Oncogene, 1999. **18**(42): p. 5738-46.
212. Kataoka, T., et al., *The caspase-8 inhibitor FLIP promotes activation of NF-kappaB and Erk signaling pathways*. Curr Biol, 2000. **10**(11): p. 640-8.
213. Tolani, B., et al., *NEMO is essential for Kaposi's sarcoma-associated herpesvirus-encoded vFLIP K13-induced gene expression and protection against death receptor-induced cell death, and its N-terminal 251 residues are sufficient for this process*. J Virol, 2014. **88**(11): p. 6345-54.
214. Hu, W.H., H. Johnson, and H.B. Shu, *Activation of NF-kappaB by FADD, Casper, and caspase-8*. J Biol Chem, 2000. **275**(15): p. 10838-44.
215. Kataoka, T. and J. Tschoopp, *N-terminal fragment of c-FLIP(L) processed by caspase 8 specifically interacts with TRAF2 and induces activation of the NF-kappaB signaling pathway*. Mol Cell Biol, 2004. **24**(7): p. 2627-36.
216. Baratchian, M., et al., *Distinct Activation Mechanisms of NF-kappaB Regulator Inhibitor of NF-kappaB Kinase (IKK) by Isoforms of the Cell Death Regulator Cellular FLICE-like Inhibitory Protein (cFLIP)*. J Biol Chem, 2016. **291**(14): p. 7608-20.
217. Liu, L., et al., *The human herpes virus 8-encoded viral FLICE inhibitory protein physically associates with and persistently activates the Ikappa B kinase complex*. J Biol Chem, 2002. **277**(16): p. 13745-51.
218. Nichols, D.B. and J.L. Shisler, *The MC160 protein expressed by the dermatotropic poxvirus molluscum contagiosum virus prevents tumor necrosis factor alpha-induced NF-kappaB activation via inhibition of I kappa kinase complex formation*. J Virol, 2006. **80**(2): p. 578-86.
219. Biswas, S., et al., *A comparison of the effect of molluscum contagiosum virus MC159 and MC160 proteins on vaccinia virus virulence in intranasal and intradermal infection routes*. J Gen Virol, 2018. **99**(2): p. 246-252.
220. Pobezinskaya, Y.L. and Z. Liu, *The role of TRADD in death receptor signaling*. Cell Cycle, 2012. **11**(5): p. 871-6.

221. Challal, S., et al., *Viral cell death inhibitor MC159 enhances innate immunity against vaccinia virus infection*. J Virol, 2010. **84**(20): p. 10467-76.
222. Iyer, A.K., et al., *Antioxidant c-FLIP inhibits Fas ligand-induced NF-kappaB activation in a phosphatidylinositol 3-kinase/Akt-dependent manner*. J Immunol, 2011. **187**(6): p. 3256-66.
223. Quintavalle, C., et al., *c-FLIPL enhances anti-apoptotic Akt functions by modulation of Gsk3 β activity*. Cell Death Differ, 2017. **24**(6): p. 1134.
224. Nakajima, A., et al., *An antiapoptotic protein, c-FLIPL, directly binds to MKK7 and inhibits the JNK pathway*. Embo j, 2006. **25**(23): p. 5549-59.
225. Kim, Y.Y., et al., *Long form of cellular FLICE-inhibitory protein interacts with Daxx and prevents Fas-induced JNK activation*. Biochem Biophys Res Commun, 2003. **312**(2): p. 426-33.
226. Naito, M., et al., *Cellular FLIP inhibits beta-catenin ubiquitylation and enhances Wnt signaling*. Mol Cell Biol, 2004. **24**(19): p. 8418-27.
227. Katayama, R., et al., *Modulation of Wnt signaling by the nuclear localization of cellular FLIP-L*. J Cell Sci, 2010. **123**(Pt 1): p. 23-8.
228. Lee, J.S., et al., *FLIP-mediated autophagy regulation in cell death control*. Nat Cell Biol, 2009. **11**(11): p. 1355-62.
229. Randall, C.M.H., et al., *Inhibition of interferon gene activation by death-effector domain-containing proteins from the molluscum contagiosum virus*. Proceedings of the National Academy of Sciences, 2014. **111**(2): p. E265-E272.
230. Edgar, R.C., *MUSCLE: multiple sequence alignment with high accuracy and high throughput*. Nucleic Acids Res, 2004. **32**(5): p. 1792-7.
231. Guindon, S., et al., *New algorithms and methods to estimate maximum-likelihood phylogenies: assessing the performance of PhyML 3.0*. Syst Biol, 2010. **59**(3): p. 307-21.
232. Yu, G., et al., *ggtree: an r package for visualization and annotation of phylogenetic trees with their covariates and other associated data*. Methods in Ecology and Evolution, 2017. **8**(1): p. 28-36.
233. Pelossof, R., et al., *Prediction of potent shRNAs with a sequential classification algorithm*. Nat Biotechnol, 2017. **35**(4): p. 350-353.
234. Knott, S.R.V., et al., *A computational algorithm to predict shRNA potency*. Mol Cell, 2014. **56**(6): p. 796-807.
235. Pham, H., N.A. Kearns, and R. Maehr, *Transcriptional Regulation with CRISPR/Cas9 Effectors in Mammalian Cells*. Methods Mol Biol, 2016. **1358**: p. 43-57.
236. Bogerd, H.P., et al., *Derivation and characterization of Dicer- and microRNA-deficient human cells*. Rna, 2014. **20**(6): p. 923-37.
237. Martin, M., *CUTADAPT removes adapter sequences from high-throughput sequencing reads*. EMBnet.journal, 2011. **17**.
238. Langmead, B., et al., *Ultrafast and memory-efficient alignment of short DNA sequences to the human genome*. Genome Biology, 2009. **10**(3): p. R25.
239. Li, W., et al., *MAGECK enables robust identification of essential genes from genome-scale CRISPR/Cas9 knockout screens*. Genome Biol, 2014. **15**(12): p. 554.
240. Colic, M., et al., *Identifying chemogenetic interactions from CRISPR screens with drugZ*. Genome Medicine, 2019. **11**(1): p. 52.
241. Cock, P.J.A., et al., *Biopython: freely available Python tools for computational molecular biology and bioinformatics*. Bioinformatics, 2009. **25**(11): p. 1422-1423.
242. Clement, K., et al., *CRISPResso2 provides accurate and rapid genome editing sequence analysis*. Nature Biotechnology, 2019. **37**(3): p. 224-226.

243. Livak, K.J. and T.D. Schmittgen, *Analysis of relative gene expression data using real-time quantitative PCR and the 2(-Delta Delta C(T)) Method*. Methods, 2001. **25**(4): p. 402-8.
244. Seabold, S. and J. Perktold. *Statsmodels: Econometric and statistical modeling with python*. in *Proceedings of the 9th Python in Science Conference*. 2010. Austin, TX.
245. Virtanen, P., et al., *SciPy 1.0: fundamental algorithms for scientific computing in Python*. Nature Methods, 2020. **17**(3): p. 261-272.
246. Waskom, M.L., *Seaborn: statistical data visualization*. Journal of Open Source Software, 2021. **6**(60): p. 3021.
247. Grundhoff, A. and D. Ganem, *Mechanisms governing expression of the v-FLIP gene of Kaposi's sarcoma-associated herpesvirus*. J Virol, 2001. **75**(4): p. 1857-63.
248. Field, N., et al., *KSHV vFLIP binds to IKK-gamma to activate IKK*. J Cell Sci, 2003. **116**(Pt 18): p. 3721-8.
249. Sun, Q., H. Matta, and P.M. Chaudhary, *The human herpes virus 8-encoded viral FLICE inhibitory protein protects against growth factor withdrawal-induced apoptosis via NF-kappa B activation*. Blood, 2003. **101**(5): p. 1956-61.
250. Kreuz, S., et al., *NF-kappaB inducers upregulate cFLIP, a cycloheximide-sensitive inhibitor of death receptor signaling*. Mol Cell Biol, 2001. **21**(12): p. 3964-73.
251. Micheau, O., et al., *NF-kappaB signals induce the expression of c-FLIP*. Mol Cell Biol, 2001. **21**(16): p. 5299-305.
252. Lee, R.T. and T. Collins, *Nuclear Factor- κ B and Cell Survival*. Circulation Research, 2001. **88**(3): p. 262-264.
253. Doench, J.G., et al., *Optimized sgRNA design to maximize activity and minimize off-target effects of CRISPR-Cas9*. Nat Biotechnol, 2016. **34**(2): p. 184-191.
254. Sherman, B.T., et al., *DAVID: a web server for functional enrichment analysis and functional annotation of gene lists (2021 update)*. Nucleic Acids Res, 2022. **50**(W1): p. W216-21.
255. Komatsu, M., et al., *A novel protein-conjugating system for Ufm1, a ubiquitin-fold modifier*. Embo j, 2004. **23**(9): p. 1977-86.
256. Kang, S.H., et al., *Two novel ubiquitin-fold modifier 1 (Ufm1)-specific proteases, UfSP1 and UfSP2*. J Biol Chem, 2007. **282**(8): p. 5256-62.
257. Tatsumi, K., et al., *A novel type of E3 ligase for the Ufm1 conjugation system*. J Biol Chem, 2010. **285**(8): p. 5417-27.
258. Lemaire, K., et al., *Ubiquitin fold modifier 1 (UFM1) and its target UFBP1 protect pancreatic beta cells from ER stress-induced apoptosis*. PLoS One, 2011. **6**(4): p. e18517.
259. Chen, C., et al., *An ER complex of ODR-4 and ODR-8/Ufm1 specific protease 2 promotes GPCR maturation by a Ufm1-independent mechanism*. PLoS Genet, 2014. **10**(3): p. e1004082.
260. Cai, Y., et al., *UFBP1, a Key Component of the Ufm1 Conjugation System, Is Essential for Ufmylation-Mediated Regulation of Erythroid Development*. PLoS Genet, 2015. **11**(11): p. e1005643.
261. Wu, J., et al., *A novel C53/LZAP-interacting protein regulates stability of C53/LZAP and DDRGK domain-containing Protein 1 (DDRGK1) and modulates NF-kappaB signaling*. J Biol Chem, 2010. **285**(20): p. 15126-15136.
262. Jiang, Y., et al., *An interaction between the SRP receptor and the translocon is critical during cotranslational protein translocation*. J Cell Biol, 2008. **180**(6): p. 1149-61.
263. Song, W., et al., *Role of Sec61alpha in the regulated transfer of the ribosome-nascent chain complex from the signal recognition particle to the translocation channel*. Cell, 2000. **100**(3): p. 333-43.

264. Mason, N., L.F. Ciufo, and J.D. Brown, *Elongation arrest is a physiologically important function of signal recognition particle*. *Embo j*, 2000. **19**(15): p. 4164-74.
265. Walter, P. and G. Blobel, *Translocation of proteins across the endoplasmic reticulum III. Signal recognition protein (SRP) causes signal sequence-dependent and site-specific arrest of chain elongation that is released by microsomal membranes*. *J Cell Biol*, 1981. **91**(2 Pt 1): p. 557-61.
266. Walczak, C.P., et al., *Ribosomal protein RPL26 is the principal target of UFMylation*. *Proc Natl Acad Sci U S A*, 2019. **116**(4): p. 1299-1308.
267. Wang, L., et al., *UFMylation of RPL26 links translocation-associated quality control to endoplasmic reticulum protein homeostasis*. *Cell Res*, 2020. **30**(1): p. 5-20.
268. García-Suárez, O., et al., *Neuroendocrine tumors show altered expression of chondroitin sulfate, glypican 1, glypican 5, and syndecan 2 depending on their differentiation grade*. *Front Oncol*, 2014. **4**: p. 15.
269. Boztug, K., et al., *JAGN1 deficiency causes aberrant myeloid cell homeostasis and congenital neutropenia*. *Nat Genet*, 2014. **46**(9): p. 1021-7.
270. Hwang, S., et al., *Euchromatin histone methyltransferase II (EHMT2) regulates the expression of ras-related GTP binding C (RRAGC) protein*. *BMB Rep*, 2020. **53**(11): p. 576-581.
271. Xu, L., et al., *EHMT2 inhibitor BIX-01294 induces endoplasmic reticulum stress mediated apoptosis and autophagy in diffuse large B-cell lymphoma cells*. *J Cancer*, 2021. **12**(4): p. 1011-1022.
272. Sheard, M.A., et al., *Membrane-bound TRAIL supplements natural killer cell cytotoxicity against neuroblastoma cells*. *J Immunother*, 2013. **36**(5): p. 319-29.
273. Mirandola, P., et al., *Activated human NK and CD8+ T cells express both TNF-related apoptosis-inducing ligand (TRAIL) and TRAIL receptors but are resistant to TRAIL-mediated cytotoxicity*. *Blood*, 2004. **104**(8): p. 2418-2424.
274. Chen, J.J., et al., *A 71-gene signature of TRAIL sensitivity in cancer cells*. *Mol Cancer Ther*, 2012. **11**(1): p. 34-44.
275. Sullivan, G.P., et al., *TRAIL Receptors Serve as Stress-Associated Molecular Patterns to Promote ER-Stress-Induced Inflammation*. *Developmental Cell*, 2020. **52**(6): p. 714-730.e5.
276. Dufour, F., et al., *TRAIL receptor gene editing unveils TRAIL-R1 as a master player of apoptosis induced by TRAIL and ER stress*. *Oncotarget*, 2017. **8**(6): p. 9974-9985.
277. Lu, M., et al., *Opposing unfolded-protein-response signals converge on death receptor 5 to control apoptosis*. *Science*, 2014. **345**(6192): p. 98-101.
278. Iurlaro, R., et al., *Glucose Deprivation Induces ATF4-Mediated Apoptosis through TRAIL Death Receptors*. *Mol Cell Biol*, 2017. **37**(10).
279. van Raam, B.J., et al., *Secretory stressors induce intracellular death receptor accumulation to control apoptosis*. *Cell Death Dis*, 2017. **8**(10): p. e3069.
280. Lam, M., et al., *Misfolded proteins bind and activate death receptor 5 to trigger apoptosis during unresolved endoplasmic reticulum stress*. *Elife*, 2020. **9**.
281. Ramkumar, P., et al., *CRISPR-based screens uncover determinants of immunotherapy response in multiple myeloma*. *Blood Adv*, 2020. **4**(13): p. 2899-2911.
282. Kischkel, F.C., et al., *Apo2L/TRAIL-dependent recruitment of endogenous FADD and caspase-8 to death receptors 4 and 5*. *Immunity*, 2000. **12**(6): p. 611-20.
283. Constantinescu, A.A., A. Morlé, and O. Micheau, *Immunoprecipitation of Death Inducing Signaling Complex by Caspase-8*. *Methods Mol Biol*, 2017. **1557**: p. 19-31.
284. Bodmer, J.L., et al., *TRAIL receptor-2 signals apoptosis through FADD and caspase-8*. *Nat Cell Biol*, 2000. **2**(4): p. 241-3.

285. Xiao, C., et al., *Tumor necrosis factor-related apoptosis-inducing ligand-induced death-inducing signaling complex and its modulation by c-FLIP and PED/PEA-15 in glioma cells*. J Biol Chem, 2002. **277**(28): p. 25020-5.
286. Bellail, A.C., et al., *DR5-mediated DISC controls caspase-8 cleavage and initiation of apoptosis in human glioblastomas*. J Cell Mol Med, 2010. **14**(6a): p. 1303-17.
287. Humphreys, L.M., et al., *A revised model of TRAIL-R2 DISC assembly explains how FLIP(L) can inhibit or promote apoptosis*. EMBO Rep, 2020. **21**(3): p. e49254.
288. Leidal, A.M., et al., *Subversion of autophagy by Kaposi's sarcoma-associated herpesvirus impairs oncogene-induced senescence*. Cell Host Microbe, 2012. **11**(2): p. 167-80.
289. Ojala, P.M., et al., *The apoptotic v-cyclin-CDK6 complex phosphorylates and inactivates Bcl-2*. Nat Cell Biol, 2000. **2**(11): p. 819-25.
290. De Leo, A., et al., *Deregulation of KSHV latency conformation by ER-stress and caspase-dependent RAD21-cleavage*. PLoS Pathog, 2017. **13**(8): p. e1006596.
291. Johnston, B.P., E.S. Pringle, and C. McCormick, *KSHV activates unfolded protein response sensors but suppresses downstream transcriptional responses to support lytic replication*. PLoS Pathog, 2019. **15**(12): p. e1008185.
292. Azfer, A., et al., *Activation of endoplasmic reticulum stress response during the development of ischemic heart disease*. Am J Physiol Heart Circ Physiol, 2006. **291**(3): p. H1411-20.
293. Zhang, Y., et al., *Transcriptional regulation of the Ufm1 conjugation system in response to disturbance of the endoplasmic reticulum homeostasis and inhibition of vesicle trafficking*. PLoS One, 2012. **7**(11): p. e48587.
294. Liu, J., et al., *A critical role of DDRGK1 in endoplasmic reticulum homoeostasis via regulation of IRE1 α stability*. Nature Communications, 2017. **8**(1): p. 14186.
295. Hu, X., et al., *Ubiquitin-fold modifier 1 inhibits apoptosis by suppressing the endoplasmic reticulum stress response in Raw264.7 cells*. Int J Mol Med, 2014. **33**(6): p. 1539-46.
296. Zhu, H., et al., *Ufbp1 promotes plasma cell development and ER expansion by modulating distinct branches of UPR*. Nature Communications, 2019. **10**(1): p. 1084.
297. Hagelkruys, A., et al., *A crucial role for Jag1 homolog 1 in humoral immunity and antibody glycosylation in mice and humans*. J Exp Med, 2021. **218**(1).
298. Nosak, C., et al., *Jagn1 Is Induced in Response to ER Stress and Regulates Proinsulin Biosynthesis*. PLoS One, 2016. **11**(2): p. e0149177.
299. Werner, E.D., J.L. Brodsky, and A.A. McCracken, *Proteasome-dependent endoplasmic reticulum-associated protein degradation: an unconventional route to a familiar fate*. Proc Natl Acad Sci U S A, 1996. **93**(24): p. 13797-801.
300. Fregno, I. and M. Molinari, *Proteasomal and lysosomal clearance of faulty secretory proteins: ER-associated degradation (ERAD) and ER-to-lysosome-associated degradation (ERLAD) pathways*. Crit Rev Biochem Mol Biol, 2019. **54**(2): p. 153-163.
301. Alkhasawneh, A., et al., *Flow Cytometric Findings in Primary Effusion Lymphoma: A Report of Two Cases*. Cureus, 2022. **14**(6): p. e25637.
302. Gathers, D.A., et al., *Primary Effusion Lymphoma: A Clinicopathologic Perspective*. Cancers (Basel), 2022. **14**(3).
303. Klein, U., et al., *Gene expression profile analysis of AIDS-related primary effusion lymphoma (PEL) suggests a plasmablastic derivation and identifies PEL-specific transcripts*. Blood, 2003. **101**(10): p. 4115-21.
304. Carbone, A., et al., *Expression profile of MUM1/IRF4, BCL-6, and CD138/syndecan-1 defines novel histogenetic subsets of human immunodeficiency virus-related lymphomas*. Blood, 2001. **97**(3): p. 744-51.

305. Charnaux, N., et al., *Syndecan-4 is a signaling molecule for stromal cell-derived factor-1 (SDF-1)/ CXCL12*. Febs j, 2005. **272**(8): p. 1937-51.
306. Farzan, M., et al., *The Role of Post-translational Modifications of the CXCR4 Amino Terminus in Stromal-derived Factor 1 α Association and HIV-1 Entry**. Journal of Biological Chemistry, 2002. **277**(33): p. 29484-29489.
307. Kremer, K.N., et al., *CXCR4 chemokine receptor signaling induces apoptosis in acute myeloid leukemia cells via regulation of the Bcl-2 family members Bcl-XL, Noxa, and Bak*. J Biol Chem, 2013. **288**(32): p. 22899-914.
308. Read, A. and M. Schröder, *The Unfolded Protein Response: An Overview*. Biology, 2021. **10**(5).